# INVESTIGATIONS ON THE EQUATORIAL IONOSPHERIC PHENOMENA

A THESIS
SUBMITTED FOR THE DEGREE OF
DOCTOR OF PHILOSOPHY
TO THE

GUJARAT UNIVERSITY
AHMEDABAD



PRABHAKAR SHARMA

AUGUST 1976

PHYSICAL RESEARCH LABORATORY
AHMEDABAD 380009
INDIA

# C E R T I F I C A T E

I hereby declare that the work presented in this thesis is original and has not formed the basis for award of any degree by any University or Institution.

( P.SHARMA )
Author

Certified

R.RAGHAVARAO
(Professor-in-Charge)

## STATEMENT

The work presented in this thesis was carried out by the author at the Physical Research Laboratory (PRL), Ahmedabad under the guidance of Prof.R.Raghavarao.

The sounding of the topside ionosphere by means of satellites is one of the established techniques for studying the F2 region and the topside ionosphere. An experimental set up has been established at PRL for receiving the telemetry data from the ISIS (International Satellites for Ionospheric Studies) satellites at 136.08 and 136.59 MHz frequencies. The 136.08 MHz telemetry signal contains the video data (in the FM mode) of the ionospheric sounder experiment, in the range of 0.1 to 20 MHz frequency, on board the ISIS satellites. The topside sounder data are retrieved from the telemetry signal and recorded on a magnetic tape. The data signals are later processed through a locally built signal analysing unit to produce the ionograms on 35 mm film.

The location of Ahmedabad ($+18^{\circ}.6$ dip latitude, $72^{\circ}.3$ E geog.longitude) is suitable for studying the low latitude ionospheric phenomena, for example the equatorial anomaly. The establishment of a satellite telemetry station at Thumba ($-0^{\circ}.3$ dip latitude, $76^{\circ}.9$E geog.longitude) provides the much needed information about the F2 region on

the southern side of the magnetic equator where there is no ground station in the Indian zone.

The author has actively participated in the recording as well as reproducing the topside data. The reduction of the topside ionogram data to N(h) profiles was carried out by the author by using the IBM 360 Computer at PRL. The present thesis describes the results obtained from the topside sounder data recorded at PRL, Ahmedabad during 1972-1975. The study concerns the equatorial ionospheric phenomena: the ionisation ledge, the ionisation and the neutral anomalies, the electrojet, the spread F, and their interrelationship.

A Chapterwise break up of the thesis is as follows:-

Chapter I

The first chapter describes the present knowledge of the equatorial ionosphere. The composition and the dynamical processes in the ionosphere are briefly discussed.

A brief description of the earlier work on the equatorial ionisation anomaly, especially its behaviour in sunspot minimum and maximum periods, is presented. The dynamical interaction of the ionisation anomaly with the neutral atmosphere, through the ion drag force, is known to produce a similar anomaly in the neutral temperature and density at the F2 region altitudes known as "neutral anomaly".

The neutral anomaly in turn modifies the distribution of ionisation through partial inhibition of the diffusion of plasma that is lifted up at the magnetic equator due to the $\underline{E}X\underline{B}$ force, thus leading to the formation of the ionisation ledge. The high crest to trough ratio of the ionisation anomaly in the forenoon hours in solar minimum period helps to build up the neutral anomaly and consequently the ionisation ledge.

Chapter II

Two ionospheric phenomena occurring at the equatorial magnetic latitudes and caused by the eastward electric field ($\underline{E}$) interacting with the horizontal magnetic field ($\underline{B}$) of the earth, are: (1) the ionisation anomaly in the F region extending into the topside ionosphere and (2) the electrojet in the E region. Both these phenomena are understood to be caused by the $\underline{E} \times \underline{B}$ force on the plasma. In the E region, only the electrons move under the influence of this force giving rise to an upward Hall polarisation electric field that in turn causes the eastward electrojet current. In the F region, however, both the electrons and the ions drift upward under the influence of the $\underline{E} \times \underline{B}$ force and the subsequent plasma diffusion along the magnetic field lines creates the crests of ionisation on either side of the magnetic equator. The correlation between

the two phenomena has been investigated by a number of authors using different parameters for representing the electrojet and the ionisation anomaly strengths. A discussion of the earlier work is given and a new method of analysis, that takes into account the time integrated strength of the electrojet intensity, is shown to exhibit better correlation between the two phenomena than obtained by other workers. It is shown that this method of approach shown here for evaluating the electrojet strength provides more clear insight in understanding the basic process responsible for the formation of ionisation anomaly.

Chapter III

The observations and interpretations of ledge formation in the topside ionosphere by earlier authors are critically discussed in view of several new characteristics revealed by our observations on the ledge formation. A brief discussion of the new mechanism for the formation ledge, due to Raghavarao and Sivaraman (1974), is given. The mechanism invokes the presence of neutral anomaly in the neutral temperature and density. A method for calculating the neutral anomaly is described and the anomaly in the neutral atomic oxygen is calculated on a few occasions. The diurnal variation of the neutral anomaly appears to be similar to the observed diurnal behaviour of the ionisation anomaly.

Chapter IV

The procedure for delineating the spatial structure of ionisation ledge is described. It is seen that the structures during equinoxes are symmetric in their latitude extent in the two hemispheres around the magnetic equator. However, during solstices the spatial structures are physically shifted to the winter hemisphere. These observations reveal the presence of neutral wind across the magnetic equator from summer to winter hemisphere. The magnitudes of these winds are calculated from the excess length of the ledge in the winter hemisphere over that in the summer hemisphere. The wind magnitudes obtained in this manner represent average winds and are found to be of the same order as hypothesised for explaining the observed solstice asymmetry of the ionisation anomaly crests (in the topside as well as bottomside ionosphere) in the numerical simulations by various workers.

Chapter V

The occurrence and intensity distribution of more than 200 ledge occurrences (during 1972-75) when plotted against lunar age, shows two broad peaks around 0300 and 1500 hours lunar age. This behaviour is explained on the basis of modulation of the diurnal Sq electric field (due to solar tide) by the semidiurnal L electric field (due to lunar tide).

The modulation enhances the electric field in the forenoon hours for the above lunar ages. The effect of the enhancement in the electric field is to create strong ionisation anomaly around the noon hours by which time the neutral flow reverses its direction of motion from west to east at F region altitudes. The ion drag force thus becomes effective around noon and the existence of strong ionisation anomaly provides resistance to neutral flow in proportion to the ionisation density, leading to the formation of neutral anomaly. The occurrence of ledge is thus related to the strength of the ionisation anomaly by the time the neutral wind reverses its direction around noon. The modulation of L field at 0300 and 1500 lunar ages, on Sq field is shown to provide the explanation for the observed results.

Chapter VI

The results of comparison of the occurrence of two phenomena in the equatorial ionosphere, (1) the ionisation ledge in the topside ionosphere and (2) the counter electrojet in the E region, are presented. About 170 ionisation ledge observations on magnetically undisturbed days when compared with the diurnal variation of $(\triangle H_T - \triangle H_A)$, $\triangle H_T$ and $\triangle H_A$ are increments from the night time base level in the horizontal components of earth's magnetic field at Trivandrum and Alibag respectively during the days of ledge observation, reveal that

the counter electrojet, either partial or full, during the afternoon hours occurred on 70 per cent of these days. The other morphological features which the ionisation ledge exhibits are: (1) more frequent occurrence in solar minimum than solar maximum period, (2) two maxima in the occurrence and intensity distribution around 0300 and 1500 hours lunar age, (3) tendency to occur on a series of days in succession and (4) occurrence in a narrow longitude belt on certain occasions. The counter electrojet was known to exhibit the same morphological features in its occurrence, as shown by a number of authors.

All these similarities in the morphological features of both ledge and counter electrojet together with the high correlation (70%) in their occurrence on a day to day basis indicate that the two phenomena could have been caused by the same source. As neutral anomaly is now known to be the cause for the ionisation ledge formation, it is suggested that the same anomaly might also cause the counter electrojet at the at the E region heights. A brief description of the mechanism for causing the counter electrojet by the vertical winds, in a narrow region ($\pm$ 2$^{o}$ dip latitude) on either side of the magnetic equator, generated by the pressure bulges associated with the neutral anomaly crest formations (around $\pm$ 15$^{o}$ dip latitudes), on the basis of the work of Raghavarao (1976) is given.

Chapter VII

Analysis of topside ionograms for the year 1969, obtained from ISIS-1 satellite, reveals the presence of spread F below the satellite altitude on a number of nighttime passes. The minimum range of the spread F echoes from the satellite altitude delineates the upper boundary of spread F irregularities across the latitudes around the magnetic equator. When the spread F is fully developed, the boundary is found to be aligned to a particular geomagnetic field line. In the early part of the night, when the spread F is in the formative stage the boundary is, however, found to be non field aligned. On this basis it is suggested that the origin of spread F could be due to a disturbance in the neutral atmosphere.

The source of the disturbance is identified as the internal atmospheric gravity waves which are likely to be generated by the neutral pressure bulges associated with intense ionisation anomaly formation in the premidnight hours of solar maximum period.

Thus the present thesis provides the observational evidence for the dynamical interaction between the ionisation anomaly and the neutral atmosphere at the F region altitudes, which leads to the geomagnetic control of the neutral atmosphere, resulting in the formation of the neutral anomaly.

The consequences of the excess pressure bulges associated with the neutral anomaly have a significant role in producing the counter electrojet in the E region and in triggering the irregularities in the F region responsible for spread F phenomenon.

## ACKNOWLEDGEMENTS

The author expresses his deep gratitude and indebtness to Prof.Raghavarao for his invaluable guidance, encouragement in the course of this study and reviewing the thesis critically. He also thanks him for bringing it into a presentable form.

The author expresses his thanks to Mr.Dave Boulding, the satellite controller, CRC, Canada for scheduling the passes and to Dr.J.H.Whitteker of CRC, Canada and Mr.R.Sanford, NASA, USA for help in providing the look angles of the ISIS satellites regularly.

The author's thanks are due to Mr.D.V.Subhedar, Mr.R.K.Swami and other members of the telemetry group for their help in recording and reproducing the topside data. The scaling of the ionograms was done by Miss R.Patel and Mrs.M.Pandya and the author is thankful to them. The author's thanks are due to Prof.B.N.Bhargava and Dr.A.R.Jain of IIG, Bombay and Prof.R.G.Rastogi for providing the ground magnetic field data used in this study. The author is thankful to Dr.B.V.Krishnamurthy of SSTC, Trivandrum for making available the topside ionogram data recorded at Thumba telemetry station.

The author wishes to record his grateful thanks to Dr.(Mrs)Suhasini R.Rao for many useful suggestions at various stages of the work and help in the statistical analysis of the

data. The author expresses his sincere thanks to Dr.M.R.Sivaraman for his invaluable help and discussions throughout the course of the work.

It is a pleasure to acknowledge the useful discussions with the members of my advisory committee, Profs.A.C.Das and B.H.Subbaraya. The useful discussions with Prof.R.P.Kane and Prof.Satya Prakash are also greatfully acknowledged. The author is thankful to Dr.G.Subramanian for his help and encouragement during the course of the work.

The author sincerely thanks Mr.B.G.Anandarao and Dr.V.H.Kulkarni for careful reading of the manuscript of the thesis, The discussions and help of Drs.A.G.Ananth and P.Muralikrishna and Messrs P.K.Chaturvedi, R.K.Jain and H.S.S.Sinha are greatfully acknowledged.

The author is thankful to Dr.Dinesh Patel and his colleagues of the Computer Centre, Dr.P.D.Angreji and his colleagues of the drafting and the photography section and Mrs.R.R.Bharucha and the library staff for providing excellent facilities during the course of the work.

The author expresses his sincere thanks to Mr.M.Narayanan Kutty who typed the manuscript excellently within a very short time. The help of Mr.K.Ravi and Mr.M.Arvindnath in typing the figure captions and references is greatfully acknowledged.

The author wishes to record an appreciation of the cooperation and moral support of his parents. My wife, Pramila and daughter, Priti, deserve a special mention of thanks for their remarkable patience and bearing my odd behaviour during the execution of the work and preparation of the thesis.

Finally, the author acknowledges the financial support provided by the Department of Space and the Ministry of Education, Govt. of India for this study.

CONTENTS

# C H A P T E R - I

## MORPHOLOGY AND DYNAMICS OF THE UPPER ATMOSPHERE

### I.1 INTRODUCTION

In this chapter the composition and processes occurring in the earth's upper atmosphere are described. The upper atmosphere consists of neutral as well as charged species of gases. The behaviour of the neutrals as well as the charged particles is different in different height regions of the atmosphere and thus provides means to classify the various altitude ranges.

One of the schemes to classify the various altitude ranges is based on the variation of the neutral temperature with height. The temperature ($\sim 300^{\circ}K$ at the surface of the earth) declines rapidly with altitude to a value of about $200^{\circ}K$ at about 20 km altitude. The region in which the decrease takes place is called the 'troposphere' and the region of minimum temperature is termed as the 'tropopause'. After the tropopause level the temperature rises through the 'stratosphere' until the 'stratopause' is reached at about 50 km altitude. After the stratopause the gas temperature declines through the 'mesosphere' to a minimum value (of about $150^{\circ}K$) at the 'mesopause' level at about 80-85 km altitude. Above the mesopause level the neutral temperature increases in the 'thermosphere' and reaches a nearly constant value above 400 km. The constant value of the neutral temperature in the uppermost levels of the atmosphere is called the "exospheric temperature".

The mean free path of the neutral gas particles is large at the exospheric altitudes and therefore these particles follow ballistic trajectories under the influence of gravity alone. The concept of isotropic pressure and temperature based on the collisional interactions of the particles is not valid and, in fact, the fluid dynamics is no longer applicable in the exosphere.

Another method to classify various altitude ranges in the upper atmosphere is based on the behaviour of the charged particles. The charged particles (viz. free electrons and ions) are produced mainly by the action of the ionising radiations of the sun on the neutral gases in the atmosphere. The ionisation distributed into various layers, therefore, provides another means of categorizing the various altitude ranges.

The lowest of the ionospheric regions is the D region between 60-90 km altitude. The altitude region 90-140 km is termed as the E region and that above 140 km altitude is termed as the F region. The F layer usually splits into two layers during daytime, the F1 and the F2 layer, which merge into a single layer during the nighttime. The maximum ionisation density occurs in the F2 peak, the height of which varies between 250-450 km depending on place, time of day, sunspot cycle and magnetic activity. The ionisation density decreases gradually above the F2 peak altitude. The ionosphere is broadly classified into the 'bottomside' and the 'topside'.

This division is based on the radio wave sounding for studying the various ionised layers. The 'bottomside' ionosphere upto the F2 peak is amenable to exploration from the ground based ionosondes and hence the name. The 'topside' ionosphere cannot be investigated from the groundbased ionosonde because the underlying bottomside ionosphere shields the topside ionosphere.

## I.2 COMPOSITION AND PROCESSES

The averege daytime composition of neutral and ionised constituents in the altitude range 80-1000 km for sunspot minimum activity condition is shown in Fig. 1.1 (after C.Y. Johnson, 1969). The ion and neutral composition distribution below 250 km are from two daytime rocket measurements above White Sands, New Mexico ($32^{o}$N geog. lat., $106^{o}$W long). Distributions above 250 km are from satellite measurements. The helium distribution is from a nighttime measurement. The bars show the variation of the respective neutral constituents within the atmosphere due to latitudinal, diurnal and storm effects. The figure very well demonstrates the preponderance of neutral gases over ionic constituents in the upper atmosphere. In the topside ionosphere the predominant ion is $O^{+}$ with $He^{+}$ as minor constituent. The transition from $O^{+}$ to $H^{+}$ ion occurs around 950 km altitude and above this altitude $H^{+}$ remains the dominant ion.

The D region ionisation is produced mainly due to the photoionisation of molecular oxygen and molecular nitrogen by solar X rays in the wavelength range 1-10 Å and also due to

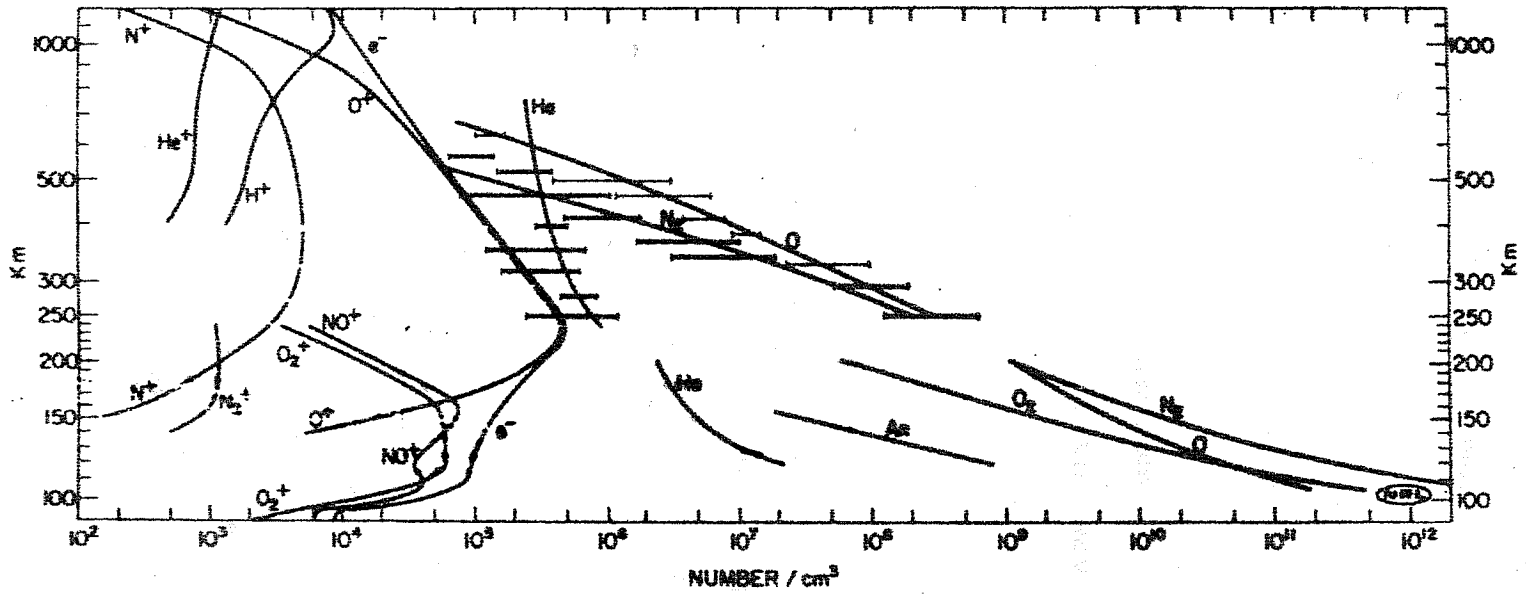


Fig.1.1 :- Daytime ionospheric and atmospheric composition above White Sands, New Mexico (32°N, 106°W). (After C.Y. Johnson, 1969).

the photoionisation of nitric oxide by solar Lyman alpha radiation (1216 Å). The free electrons and ions thus produced are lost through the dissociative recombination reaction

$$XY^+ + e \longrightarrow X^* + Y^* \qquad - - - - - \qquad (1)$$

where $XY^+$ is the ionised molecule and $X^*$ and $Y^*$ are atoms in excited state. In the E region (90-140 km) the ionisation is mainly produced by the photoionisation of molecular oxygen and molecular nitrogen by the EUV in the range 911-1027 Å. A small contribution comes from the X rays in the wavelength range 10-170 Å. The loss of ionisation in the E region is also through the dissociate recombination scheme shown in eq.(1).

The lower boundary of the F region is usually taken to be around 140 km altitude. The chief neutral constituents in the altitude range 150-600 km are atomic oxygen (O) and molecular nitrogen ($N_2$). The source of ionisation is solar UV radiation in the range of wavelengths 200 Å upto 911 Å (the latter wavelength being the ionisation limit of atomic oxygen). The production of the F region ionisation results mainly through the photoionisation of atomic oxygen, although, at high latitudes energetic particle precipitation also plays an important role. The free electrons are lost through a two stage process, viz. (a) formation of molecular ions by ion-atom interchange and (b) dissociative recombination. If $X_2$ denotes either $O_2$ or $N_2$, the loss scheme may be written as

$$O^+ + X_2 \longrightarrow XO^+ + X$$

$$XO^+ + e \longrightarrow X + O$$

It is well known (e.g. Ratcliff, 1956) that the above processes lead to a loss rate of electrons approximating in the form $L = \alpha N^2$ in the lower F region and $L = \beta N$ higher up, N represents the electron concentration. The change over from the quadratic rate of loss of electrons in the lower F region to a linear loss rate higher up takes place at a transition level where

$$\alpha N = \beta$$

The transition defined above is shown to cause the occasional splitting of F region into F1 and F2 regions during midday hours (Ratcliff, 1956).

Above the F1 layer, the loss rate is linear and hence the electron concentration increases rapidly towards the F2 peak. The formation of the peak is because of two competing processes (1) the recombination, decreasing exponentially with altitude and (2) the plasma diffusion, increasing exponentially with altitude. The F2 peak occurs at a level where diffusion and loss are of comparable importance, i.e. where $\beta \sim D / H^2$ where D represents the diffusion coefficient at the peak and H is the plasma scale height (Rishbeth and Barron, 1960). $\beta^{-1}$ and $H^2 / D$ are usually referred to as the chemical and the diffusion time constant respectively. At the peak, the electron concentration is given by $N_m = q_m / \beta_m$ (the subscript 'm' refers to the peak) just as it would be in the absence of diffusion. Well above the F2

peak the plasma assumes a diffusive equilibrium distribution, with a plasma scale height $H_p$ (Rishbeth, 1968) given by

$$-\frac{d}{dh}(\ln N T_p) = \frac{1}{H_p} = \frac{m_i g}{2 k T_p}$$

where $m_i$ is mean ion mass, g is acceleration due to earth's gravity, k is the Boltzmann constant and $T_p = \frac{T_e + T_i}{2}$. If it is assumed that the plasma temperature, $T_p$, is independent of altitude, the electron concentration decreases exponentially with height in the form exp ( $-h/H_p$).

Fig. 1.2 gives a series of profiles of electron and ion temperatures in the F region obtained by Farley et al. (1967) by means of Jicamarca incoherent scatter radar for low solar and magnetic activity conditions. It is observed that during daytime $T_e > T_i$ below 300-350 km altitude (i.e. near $h_{max}F2$ level); the difference $T_e - T_i$ is 1000°K at 200-220 km. In the uppermost levels, $T_e = T_i$ implying good thermal contact between electrons and ions and also the electron (or ion) temperature attains a nearly constant value with altitude. In this isothermal region the charged particle temperature is much higher than the neutral gas temperature. At sunset the electron temperature peak in the lower F region disappears rapidly with time and the ions and electrons reach equilibrium. The time constant for heat exchange between the electrons and ions in the F region is a few seconds and therefore $T_e - T_i$ drops to zero as the heat source disappears. At night the

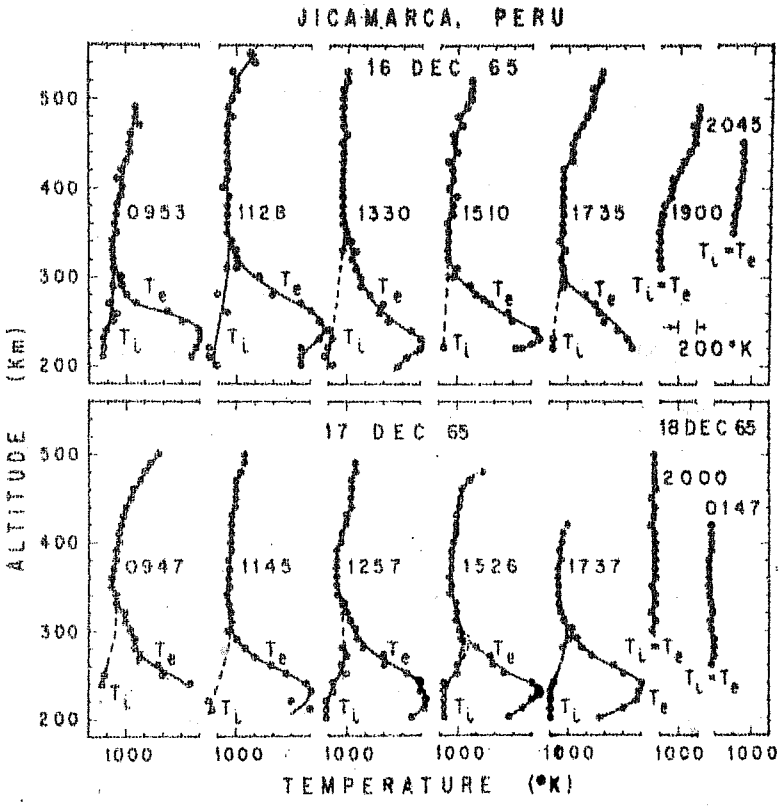


Fig. 1.2 :- A series of profiles of electron and ion temperatures obtained by means of Jicamarca incoherent scatter radar for a period of low solar activity. (After Farley et al, 1967).

ionosphere is observed to be isothermal, with $T_e = T_i$. After an initial fairly rapid decrease after sunset (of about 200°K), the temperature decreases much more slowly throughout the night.

The model behaviour of F region in terms of production, loss and diffusion does not explain a number of 'anomalies' of ionisation both at low and high latitudes. The word 'anomaly' was initially used to describe a particular feature which does not fit with the idea of the layer formation predicted by the simple Chapman theory (Chapman, 1931) obeyed by E and F1 layers. For instance, the simple Chapman theory predicts that the maximum electron concentration ($N_{max}F2$) at any location should be higher during summer than during winter, because of its dependence on the solar zenith angle. However, it was found (e.g. Thomas et al. 1958) that the noon $N_{max}F2$ at the same location tends to be greater in winter than in summer. This behaviour cannot be explained by the Chapman theory and is called as the "seasonal anomaly". The anomaly in the latitudinal distribution of the F region ionisation, the equatorial anomaly, is relevant to the present study. The equatorial anomaly, first discovered by Appleton (1946), refers to the distribution of $N_{max}F2$ revealing a minimum (trough) at the magnetic equator with a prominent crest on either side at about $\pm$ 15° dip latitude. The simple Chapman theory predicts the ionisation density to be maximum at the location of the subsolar latitude, decreasing smoothly on either side.

The existence of these anomalies reveals that the distribution of ionisation in the low latitude F region is controlled by dynamical processes rather than the static processes of photoionisation and recombination. The dynamical effects are brought about mainly by (1) the electric fields (2) the neutral winds and (3) the waves. These effects are briefly described below.

1) The electric fields:

The equatorial anomaly in the F2 region was explained by Martyn (1947) by invoking the vertical drift of the ionisation at the magnetic equator caused by the daytime eastward electric field. The electric fields are generated by the dynamo action in the E region of the ionosphere and communicated to higher altitudes along the geomagnetic field lines. A number of workers (e.g. Matsushita, 1969; Tarpley 1970) have estimated the electric fields generated by the action of solar and lunar tidal winds. The calculated magnitudes range from one to few millivolt/m. The electric fields are communicated to F region altitudes along the equipotential geomagnetic field lines. Direct measurements of electric fields in the upper E and F regions have been made by barium releases but they are limited to twilight hours only. The vertical drift velocity of plasma by the incoherent scatter technique has been measured at equatorial station Jicamarca (e.g. Balsley and Woodman, 1969). The F region vertical drift velocity at Jicamarca has been interpreted as $\underline{E} \times \underline{B}$ drift caused by the E-W electric field

associated with the electrojet. Balsley and Woodman (1969) showed that the F region vertical velocity shows good correlation with the E-W velocity of the E region irregularities embedded in the electrojet. The vertical F region velocities at Jicamarca during daytime are upward with values $\sim$ 20 m/s (corresponding to an E-W electric field $\sim$ 0.5 mv/m) and downward at night with comparable magnitude (Woodman, 1970). Thus the incoherent scatter observations appear to support Martyn's theory of anomaly formation, which invokes the electrodynamic lifting of the F region plasma at the equator.

In the equatorial F region, vertical lifting of the ionisation by the electric fields is shown to be more important than the neutral winds in controlling the diurnal variation of foF2 and $h_{max}F2$ (e.g. Sterling et al. 1969).

2) Neutral winds:

Ionospheric F layer is much influenced by vertical plasma motion; the height of the F2 peak ($h_{max}F2$) increases by upward plasma motion. Rishbeth (1968) has shown that if a vertical drift W is imposed on the plasma in the F region then the height of the peak is shifted by an amount $\Delta h_m$ given by

$$\Delta h_m \simeq W H_i^2 / D(h_m)$$

where $H_i$ is the ionisation scale height, and $D(h_m)$ is the plasma diffusion coefficient at the altitude of the peak. Collisions

between neutral particles and ions cause the plasma to be driven along the geomagnetic field lines at a speed equal to the component of the wind velocity in that direction. A horizontal wind velocity U in the magnetic meridian produces a vertical drift, W = U sin I Cos I (King and Kohl, 1965) at a location where the dip angle is'I'.

It is mentioned earlier that the behaviour of the equatorial F region is controlled by the electrodynamic processes. However, the neutral winds substantially modify the distribution of ionisation. For example, it is necesary to invoke the cross equatorial winds blowing from summer to winter hemisphere to explain the solstice asymmetry of the equatorial ionisation anomaly (e.g. Bramley and Young, 1968). The "super cooling" of nighttime plasma in the equatorial topside ionosphere observed by Hanson et al. (1973) has also been explained by invoking the cross equatorial winds (Bailey et al. 1973). Thus it is clear that the neutral winds play an important role in the dynamics of the equatorial F region.

There are few direct methods of measuring neutral winds at F region altitudes. A number of wind models have been proposed on the basis of the pressure differences at F region heights inferred from the satellite drag data. In the initial models (e.g. Kohl and King, 1967), the winds were computed by using Jacchia (1965) model atmosphere pressure variations and a fixed profile for the electron density distribution for all latitudes and local times. Recently, more elaborate

calculations for the estimation of winds, with better atmospheric pressure models (Jacchia, 1970, 1971), realistic ionisation density profiles and also including non-linear terms in the equation of motion (Blum and Harris, 1975a,b) have been made.

Neutral winds have been inferred from incoherent scatter observations at midlatitude stations. The velocity with which the F region plasma, diffuses downward along the magnetic field line is measured by this technique. The electron density and the ion and electron temperatures as a function of height are also measured, from which the pressure variations in the plasma and hence the expected diffusion velocity is calculated. Any difference between the measured and the calculated diffusion velocity of plasma is attributed to the action of neutral winds (Evans, 1972). The wind magnitude obtained from this method is in agreement with the general wind pattern calculated from the static model atmospheres of Jachia.

3) Wave phenomena in F region:

A number of wave phenomena has been found in the lower thermosphere from observations on the deformation of meteor trails, chemical releases by means of rockets, and incoherent scatter observations of plasma temperature and horizontal ionisation drifts in the E region.

The stratification of the atmosphere in the presence of gravity causes a parcel of air that is displaced in height to be subjected to a restoring force known as the buoyancy force. This restoring force causes oscillations with a characteristic frequency (the Brunt-Vaisala frequency) with a period $\sim$ 10 min in the thermosphere. Waves with the periods longer than the Brunt-Vaisala period are known as the internal atmospheric gravity waves and those with shorter periods are known as acoustic gravity waves. The internal atmospheric gravity waves are transverse waves except near acoustic limit. Their smaller scale sizes and shorter periods render them less affected by the curvature of the earth and the coriolis force but somewhat more dependent on the acceleration due to gravity.

The basic equations governing the propagation of gravity waves in the atmosphere are given by Hines (1960). The asymptotic relation which applies to the parameters that describes these waves is given by

$$\frac{\lambda_x}{\lambda_z} \simeq \frac{u_x}{u_z} \simeq \frac{\tau}{\tau_g}$$

where $\lambda_x$ and $\lambda_z$ are the horizontal and the vertical wavelengths, $u_x$ and $u_z$ are the velocities, $\tau$ is the wave period and $\tau_g$ is the Brunt-Vaisala period. As $\tau$ is greater than $\tau_g$ for internal atmospheric gravity waves, $U_x > U_z$ and $\lambda_x > \lambda_z$.

The amplitude of the internal atmospheric gravity waves increases exponentially with altitude. This behaviour can be interpreted in terms of energy flux, since the increase

in amplitude just compensates for the upward decrease of atmospheric density in maintaining the flux constant (Hines, 1960). However, the dissipative processes namely kinematic viscosity, thermal conduction and ion drag, damp the wave amplitudes in the thermosphere. Yeh et al. (1975) have discussed the relative importance of these three processes with altitude for different wavelengths. They conclude that the dissipative forces of viscosity and thermal conduction have strong control on the waves beyond 300 km altitude. The dissipation due to ion drag is complex. The ion drag force (because of its dependence on ion number density) is large during daytime. They show that the ion drag will compete with viscosity and thermal conduction in daytime and will not be important in night when the ionisation density is low. Waves with a frequency above $10^{-2}$ rad/s (corresponding to Brunt-Vaisala period of about 10 min) and below about $2 \times 10^{-3}$ rad/s (period about 60 min) will be filtered out in the thermosphere by damping.

Another mechanism which affects the propagation of gravity waves is their reflection at a thermal barrier (Hines, 1960). Temperature fluctuations in the stratosphere and mesosphere reflect the long wavelengths of gravity waves propagating upwards from the tropospheric level.

The origin of internal atmospheric waves remains uncertain. Weather disturbances in the tropospheric and stratospheric regions and non-linear tidal wave interaction appear to provide the most likely sources in the lower atmosphere.

As the waves propagate upward, some of the energy is partially reflected. The dominant modes that escape reflection attain maximum amplitude in the E region. At higher altitudes the energy is dissipated by thermal conduction, kinematic viscosity and ion drag. By the time the waves reach the F region only a minor portion (in the long wavelength range) of the original spectrum remains.

The amplitudes of gravity waves in the F region are nevertheless large, for there is continual increase of amplitude with height in all modes free from severe dissipation. Some of the wave energy reaches the F region does so, only after suffering a partial ducting at the stratosphere - mesosphere level due to the varying temperature. The ducted energy can be carried over very great distances with little loss. The other source of gravity waves is the supersonic motion of the earth's terminator with respect to the neutral atmosphere at altitudes upto about 200 km (Beer, 1973). The condition for generation of a shock wave by the terminator as given by Cole (1974) is

$$V_T + V_{nE} > V_S \qquad - - - \quad - \qquad (3)$$

where $V_T$ = speed of terminator with respect to the rotating earth coordinate frame, $V_{nE}$ = wind speed, positive towards east, and $V_S$ = speed of sound. $V_{nE}$ may be as large as 200 m/s at F region altitudes and thus the supersonic terminator launches gravity waves directly at F region altitudes. Beer (1973)

assumed the atmosphere to be rotating with the earth and so has restricted the possibility of generation internal gravity waves to altitudes less than 100 km. However, Cole's (1974) works shows that with modest winds the shock condition can exist upto the altitudes of the dynamo region.

Blumen and Hendl (1969) proposed that the joule heating of the neutral atmosphere caused by the dissipation of the current flowing in the auroral arc as the source of gravity waves. Chimonas and Hines (1970) compared the effectiveness of this mechanism with the Lorentz coupling (due to $\underline{J} \times \underline{B}$ force) of the auroral electrojet to the neutrals via collisions. From their study it appears probable that both mechanisms can contribute to the generation of gravity waves.

The internal atmospheric gravity waves affect the ionisation through the collisions between the charged and the neutral particles and also from the changes induced by the gravity waves in the production as well as loss rate of ionisation (Hooke, 1968). The former process is dominant in F2 region where the component of the neutral velocity parallel to the magnetic field moves the ions through collisional interaction. In the lower regions (E and F1) the main effect of the gravity waves is to modify the production as well as the loss rate of ionisation. The change in the photoionisation rate occurs because of changes in the local values of 1) the neutral gas number density and 2) the ionising radiation flux.

However, more recent work (Anandarao, 1976) shows that the electrodynamic effect $\underline{W} \times \underline{B}$, where $\underline{W}$ represents the gravity wave wind velocity, could also be important at the E region heights. Fluctuations in the F region electron and ion temperatures have also been observed and are attributed to gravity waves (e.g. Klostermeyer, 1972).

In conclusion, the plasma density distribution at F region altitudes is strongly influenced by the neutral motions in the meridional plane. At low latitudes the electromagnetic drift in addition to the meridional winds controls the distribution of the ionisation.

## I.3 THE EQUATORIAL IONISATION ANOMALY AND ITS INTERACTION WITH NEUTRAL ATMOSPHERE

### I.3.1 BACK GROUND

The equatorial anomaly in the F region of the ionosphere was first reported by Appleton (1946) and is subsequently studied by many workers. The initial results showed the existence of two crests on either side of the magnetic equator around $\pm 15^{o}$ dip latitude with the trough occurring at the magnetic equator. The study of anomaly required the knowledge of electron concentration over a wide range of latitudes and hence analysis of a large amount of ionogram data. For this reason, the initial studies were made by using the plot of the critical frequency, foF2, of the F2 layer at different latitudes.

Croom et al. (1959) obtained the latitudinal distribution of electron concentration at fixed altitudes from the bottomside ionograms by evaluating the altitude distribution of the electron concentration, known as N(h) profiles. They showed that the anomaly extends from about 180 km upto the $h_{max}F2$ altitude. The field alignment of the anomaly peaks in the bottomside ionosphere is also evident from their work.

The launching of the polar orbiting satellite Alouette-1 in 1962, having an onboard topside sounder, greatly helped in detailed study of the anomaly. King et al. (1964) and Lockwood and Nelms (1964) showed that the anomaly extends beyond the peak of the F2 layer into the topside ionosphere upto the altitudes 1000-1200 km. Polar orbiting satellites are especially suitable for studying the anomaly because of wide range of latitude coverage at the same local time. For instance, Alouette-1 moving in a circular path at 1000 km altitude having orbital inclination of $80^{\circ}$ covers a latitude range of $+80^{\circ}$ to $-80^{\circ}$ in each of its orbit. During a pass of the satellite at a low latitude station the longitude of the subsatellite point changes by less than $5^{\circ}$ and the local time by about 20 minutes. Therefore, this eliminates any longitudinal effects that could not be avoided in the case of bottomside data as the location of different stations are widely separated in longitude.

King et al. (1964) and Eccles and King (1969) presented latitudinal distribution of electron concentration, at a series of fixed altitudes on several occasions and

at different local times, obtained from Alouette-1 topside sounder data. The results show that the peaks of the anomaly at different heights fall on a magnetic field line, usually referred to as the "anomaly field line".

Fig. 1.3(a,b) shows a typical plot for representing the anomaly obtained by means of ISIS-2 satellite topside sounder data recorded at Ahmedabad on Jan. 18, 1974 at 1250 hr LT at a mean longitude of 68°E. The ISIS-2 is a polar orbiting satellite of inclination 88°, with the result that the change of its longitude during the pass at a low latitude station (e.g. Ahmedabad) is about 2° and hence the change in local time of the pass of about 8 minutes. The local time and the longitude for a particular pass in the work described in this thesis refer to the position of the satellite when it is nearly overhead to the observing station.

Fig. 1.3(a) shows the latitudinal distribution of electron concentration at a number of fixed altitudes in the topside. Fig. 1.3(b) shows the latitudinal variation of the altitude of various constant electron concentrations. The anomaly peaks in Fig. 1.3(a,b) are field aligned, in this case two magnetic field lines with their equatorial heights about 1000 km and 900 km are seen to pass through the summer and the winter peaks respectively. The anomaly shows the solstice asymmetry, the summer peak of electron concentration at any altitude being of higher strength than the corresponding winter peak (Fig. 1.3a).

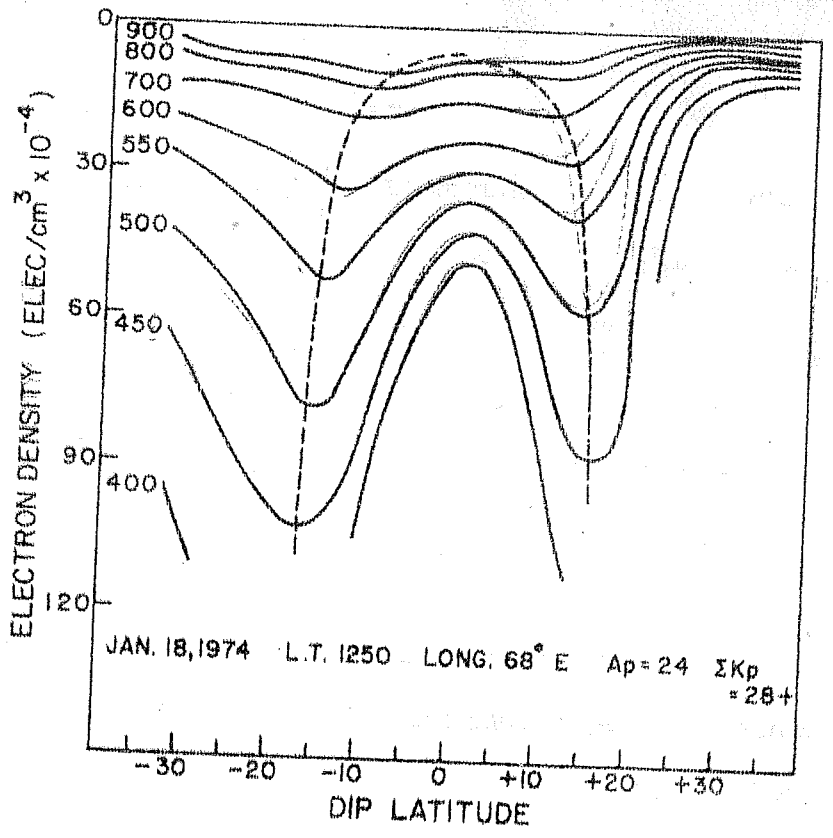


(a)

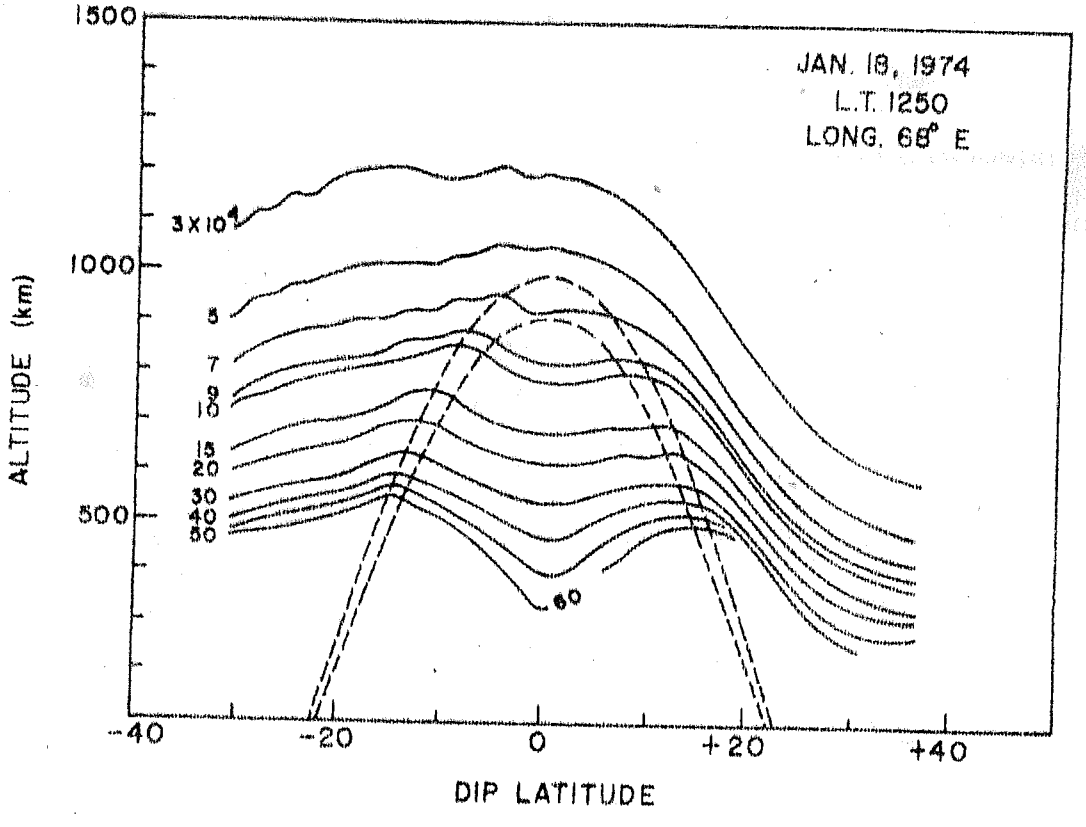


(b)

Fig. 1.3 (a, b):- Latitudinal distribution of (a) electron concentration at constant altitudes and (b) constant electron concen-

Fig. 1.3(b) reveals that the height at which a particular electron concentration occurs is higher in the summer hemisphere than in the winter hemisphere.

In literature both the words 'crest' and 'peak' are used to denote the regions of high electron concentration on either side of the magnetic equator. However, in this thesis the author has used the word 'crest' to denote the maximum electron concentration enhancements on either side of the magnetic equator at the $h_{max}F2$ altitude. At all other altitudes the word 'peak' would denote the regions of high electron concentration on either side of the magnetic equator.

A comparison of Fig.1.3(a) with Fig.1.3(b) reveals that the former representation of anomaly provides more resolution at the lower altitudes in the topside ionosphere. Fig.1.3(b) provides more resolution near the top of the anomaly field line. In order to ascertain the magnitude of the anomaly strength, the representation shown in Fig.1.3(a) is often used for the reason that one can directly obtain the strength of the anomaly (denoted by S) at any altitude, by calculating the ratio of electron concentration at the peak to that at the trough (denoted by R). Some authors use the dip latitude, $\phi$, of the crest to denote the anomaly strength. However, most of the workers in this field represent the anomaly strength at any altitude by the product of the ratio R with $\phi$, the dip latitude of the anomaly peak at that altitude. A detailed discussion of this point is given in Sec. II.2 of Chapter 2.

## I.3.2 MORPHOLOGICAL FEATURES OF THE EQUATORIAL ANOMALY

The equatorial ionisation anomaly, henceforth denoted by 'IA' for brevity, has been found to depend strongly on solar activity, longitude, season and magnetic activity. Appleton (1954), H. Maeda (1955) and Rastogi (1959 ) studied the diurnal development of anomaly during sunspot minimum period. Rastogi showed the diurnal variation of IA during the equinox months of 1953-1954 by using the published foF2 data from a worldwide network of ionosondes in the northern hemisphere. He found that the anomaly crest begins to develop close to the dip equator around 0900 hr LT and thenafter the crest moves to higher latitudes rapidly with time. The maximum development of the anomaly occurs around 1400 hr LT; the location of the crest being around $15^{o}$ dip latitude. After the maximum development the crest begins to loose its prominence and moves towards the equator. The anomaly disappears around 2100 hr LT.

A causative mechanism for the anomaly was first suggested by Mitra (1946). He proposed that the ionisation produced near the equator would diffuse along magnetic field lines causing enhancement on the north and south of the magnetic equator. However, low electron production rates in the upper F region led a number of authors (e.g. Hirono and Maeda, 1954) to speculate that the origin of such particles might arise from electrodynamic lifting near the

equator (Martyn, 1947) rather than from direct solar ionisation. This "fountain effect" was discussed quantitatively by Duncan (1960) and later by several authors.

On the theoretical side a number of authors (e.g. Bramley and Peart, 1965; Hanson and Moffett, 1966) attempted to explain the anomaly by solving the steady state continuity equation for electrons in the F2 region. The equation of continuity for the electron concentration (N) in general takes the form

$$\frac{\partial N}{\partial t} = q - L - \text{div}\,(N\underline{v})$$

in which the terms on the right-hand side stand for production, loss and diverging movement of ionisation respectively. The electron velocity '$\underline{v}$' is the vector sum of $\underline{v}_{||}$ and $\underline{v}_{\perp}$, where the subscripts refer to directions parallelor perpendicular to a magnetic field line. The component $\underline{v}_{||}$ is dominated by diffusion under the gravity (Chandra and Goldberg, 1964) and $\underline{v}_{\perp}$ is caused by the $\underline{E}$ X $\underline{B}$ force (being upwards during daytime) at the equatorial latitudes. The steady state analysis ($\partial N/\partial t = 0$) of Bramley and Young and Hanson and Moffett, mentioned above, showed that an upward drift ($\underline{v}_{\perp}$) $\sim$ 20 m/s is sufficient to produce the observed crest to trough ratio of the anomaly. Subsequently a number of authors obtained time dependent solution of the continuity equation, following the method given by Baxter and Kendal (1968). Sterling et al. (1969), D.N. Anderson (1973) and Sivaraman et al. (1976) have attempted to explain several observed features of the equatorial anomaly in this manner

Rastogi (1966) compared the diurnal development of the anomaly in sunspot minimum ($S_{min}$) and sunspot maximum ($S_{max}$) epochs. Fig. 1.4 reproduced from his paper clearly shows that the diurnal development of the anomaly in the two epochs is different. Although the time at which the anomaly first develops is the same (viz. 1000 hr) in $S_{min}$ and $S_{max}$, the strength of the anomaly (as given by the crest to trough ratio of foF2) is significantly higher in the forenoon and early afternoon hours in $S_{min}$ than $S_{max}$ epoch. Also the time at which the anomaly attains its maximum development is different in the two epochs; being around 2000 hr in $S_{max}$ and 1400 hr in $S_{min}$. The anomaly disappears after 2000 hr in $S_{min}$ while it persists until 0300 hr in $S_{max}$. Although, Rastogi's work reveals many a detail of the diurnal development of the anomaly, the data used by him was obtained at a number of stations widely distributed in longitude. To the extent the anomaly development shows longitudinal differences (e.g. Eccles and King, 1969) the conclusions regarding the time development could be different from those mentioned above on the basis of his work.

Brown (1973) studied the diurnal development of anomaly by means of the foF2 data obtained from a chain of ground based ionosondes located in a narrow longitude zone during IQSY (1964-65) and IGY (1957-58). Fig. 1.5 reproduced from his work shows the diurnal development of anomaly at three hours 1000, 1200 and 1400 LT for the two epochs.

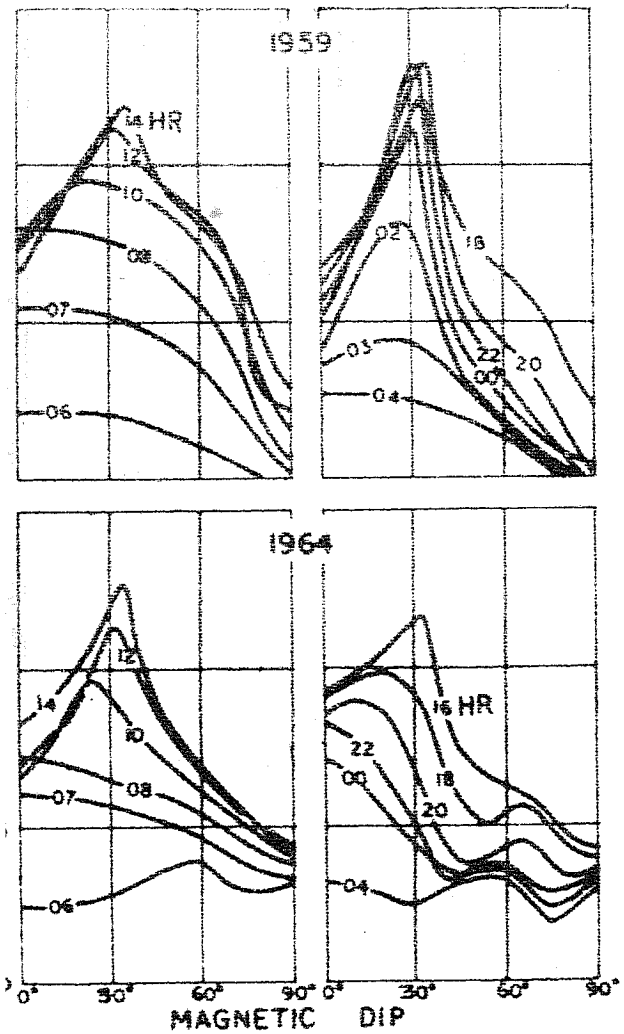


:- Variation of foF2 with magnetic dip for different hours of the day during March of a low sunspot year and a high sunspot year. (After Rastogi, 1966)

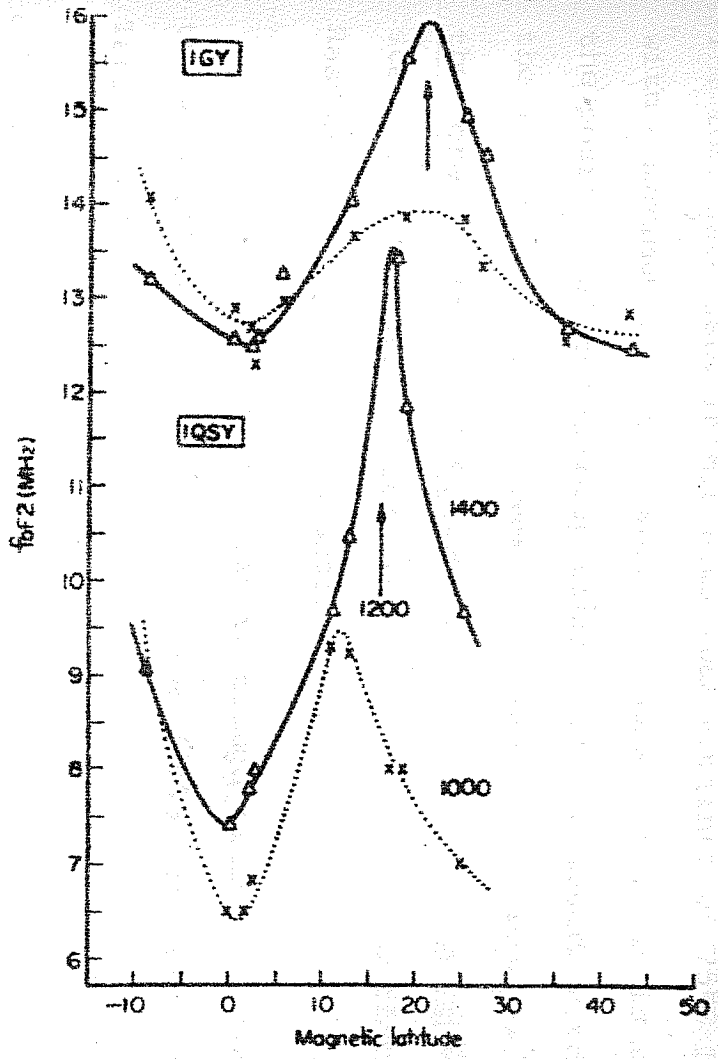


Fig.1.5 :- Variation of foF2 at 1000 hr (dotted) and 1400 hr (full line) at 75°E for IGY and IQSY, equinox, noon. Vertical arrows indicate the position of the anomaly crests at 1200 hr. (After Brown, 1975).

The foF2 data used in his study was obtained at 75°E longitude, with a maximum longitude spread of about 15°. It is seen that the position of the anomaly crest shifts poleward with time for the IQSY period, in agreement with Rastogi's (1966) work. However, the crests at 1000, 1200 and 1400 hrs remain approximately stationary in position for the IGY period, thus differing with Rastogi's findings corresponding to $S_{max}$ period (Fig. 1.4).

The results of crest to trough ratio inferred from the work of Rastogi (1966) and Brown (1973) are summarised in Table 1 (after Sivaraman, 1974).

TABLE 1

| Local time | $R_{IA}$ $S_{max}$ (1959) | $S_{min}$ (1964) |
|---|---|---|
| 1000 | 1.37 (1.20) | 2.01 (2.20) |
| 1200 | 2.04 (1.71) | 2.61 (3.32) |
| 1400 | 1.85 (1.64) | 2.18 (3.38) |
| 1600 | 1.81 | 1.58 |
| 1800 | 2.1 | 1.15 |
| 2000 | 3.9 | 1.14 |
| 2200 | 2.64 | - |

The values given within the brackets are from the foF2 plots by Brown (1973) for epochs 1957-58 and 1964-65.

The parameter $R_{IA}$ denotes the crest to trough ratio of electron concentration and therefore $(R_{IA} - 1) \times 100$ denotes the percentage enhancement of ionisation at the anomaly crest. It is clear from the table that the anomaly strength upto 1400 hr LT is higher in $S_{min}$ period than in $S_{max}$ period; after 1400 hr the anomaly strength in $S_{min}$ decreases rapidly with time and collapses after 2000 hr. The anomaly development in $S_{max}$ period occurs in a different manner. The initial increase in its strength by noon hour is followed by a small decrease in the afternoon hours. In the late evening hours around 2000 LT, however, the anomaly strength goes up and reaches about 300% excess at the crest. This feature of enhancement of the anomaly has been explained by Huang (1974) on the basis of the post-sunset enhancement of the vertical upward drift velocity observed at equatorial station Jicamarca in $S_{max}$ period (Woodman, 1970). The postsunset enhancement of the vertical drift velocity is observed conspicuously in $S_{max}$ period. On the basis of the observations (Huang, 1960) that the post-sunset peak of foF2 at the station Taipei ($19^{o}$ dip latitude) is less prominent and less frequent in low sunspot years, Huang (1974) suggests that the sunset peak of drift velocity also becomes small with decrease in the solar activity.

Raghavarao and Sivaraman (1975) explain the higher strength of IA in $S_{min}$ period on the basis of higher diffusion of the plasma in $S_{min}$ than in $S_{max}$ period. The ambipolar diffusion velocity of the plasma parallel to the magnetic field

is given by (e.g. Rishbeth and Garriott, 1969, p.146)

$$V_{||} = \frac{-D_a}{H} \left( \frac{1}{N} \frac{dN}{ds} - \tfrac{1}{2} \operatorname{Sin} I \right)$$

Where $D_a$ denotes the ambipolar plasma diffusion coefficient; H, the scale height of the neutral density and N, the electron concentration. 's' denotes the distance along a magnetic field line in terms of the scale height, H, and I denotes the dip angle. Thus $V_{||}$ varies directly as the ambipolar diffusion coefficient $D_a$ and inversely as the scale height H. The ambipolar diffusion coefficient $D_a$ is given by (Rishbeth, 1966)

$$D_a = \frac{6.9 \times 10^{18}}{n(O)} \frac{T_e + T_i}{T_i} \left[ \frac{T_n}{1000} \right]^{\frac{1}{2}}$$

where n(O) is the concentration of neutral atomic oxygen; $T_e$, $T_i$ and $T_n$ refer to temperature of electron, ion and neutral particles respectively. Therefore, the plasma diffusion is inversely proportional to the concentration of neutral atomic oxygen. The noon values of $D_a$ amd neutral temperature $T_n$ at 300 km altitude are given in Table 2 (after Rishbeth and Garriott, 1969 p. 171).

TABLE 2

| Parameter | $S_{min}$ | $S_{max}$ | Units | Ratio($S_{min}$ / $S_{max}$) |
|---|---|---|---|---|
| $D_a$ | 7 | 2 | $10^{10}$ $cm^2$ $sec^{-1}$ | 3.5 |
| $T_n$ | 900 | 1700 | $^oK$ | 0.53 |

The ambipolar diffusion velocity is about 7 times higher in $S_{min}$ than $S_{max}$ due to its dependence on the ratio of D and H (the latter varies directly as the neutral temperature $T_n$). The higher diffusion velocity of plasma enhances the "fountain effect" by increasing the supply of ionisation that is responsible for forming stronger IA peaks at the noon hour of $S_{min}$ as compared to $S_{max}$.

Recently, Sivaraman et al. (1976) solved the time dependent continuity equation of electrons in the equatorial F2 region. Their results show that the IA forms at 0800 hr LT in $S_{min}$ period and 1000 hr in $S_{max}$ period. They confirm the result previously obtained (Raghavarao and Sivaraman, 1975) on the basis of preliminary calculations that the crest to trough ratio of electron concentration is higher in the forenoon hours of $S_{min}$ than $S_{max}$.

D.N. Anderson (1973) suggested that the solar cycle variation of the IA could have been caused by different commencement times of the upward drift in $S_{max}$ and $S_{min}$ epochs. He suggested that the commencement time of the upward drift should be progressively later with increasing solar activity,

in order to account for late development IA in $S_{max}$ period. However, there is no experimental evidence to support this argument.

A striking feature noticed on the topside ionograms recorded at equatorial stations is the appearance of 'V' shaped cusp on occasion on both the ordinary and the extraordinary echo traces. The cusp formation is associated with excess electron concentration, known as 'ledge' of ionisation, that occurs in a certain altitude range of the topside ionosphere (King et al. 1964; Lockwood and Nelms, 1964). The phenomenon is found to occur more frequently in $S_{min}$ than $S_{max}$ period (Van Zandt et al. 1972). Raghavarao and Sivaraman (1974, 1975) examined the phenomenon in more details and proposed a new mechanism for the ledge formation which explained satisfactorily its more frequent occurrence in $S_{min}$ period than $S_{max}$ period.

### I.3.3 INTERACTION OF IONISATION ANOMALY WITH THE NEUTRAL ATMOSPHERE

Chandra and Goldberg (1964) postulated that the ion drag force, which the ions exert on the neutrals due to collisions, would distort the hydrostatic distribution of the neutral atmosphere thus, leading to geomagnetic control of the neutral atmosphere at the F region heights. Such a geomagnetic control of the neutrals was first reported by Philbrick and McIssac (1970). They observed a minimum near

the magnetic equator in the distribution of neutral constituents $N_2$ , O , $O_2$ and NO at about 400 km altitude by means of OV3-6 satellite. Hedin and Mayr (1973) observed two maxima with a minimum in between, in the distribution of $N_2$ and O at 450 km altitude around 1700 LT at a number of longitudes. The minima at various longitudes occur at the magnetic equator thus revealing the control of the geomagnetic field. Fig. 1.6 (a) reproduced from their work shows the anomaly in the distribution of $N_2$ on September 22, 1969 at 1700 hr LT at 450 km altitude. They solved the quasi-three dimensional energy and continuity equation for neutrals taking into account the ion drag force on the neutrals and could explain their observations.

It is well known that the neutral motions in the F region are governed by the ion drag force (e.g. King and Kohl, 1965). The force due to ion drag in the east-west direction is given as

$$F_x = - \frac{N \nu_{in} (U_x - V_{ix})}{n}$$

where $\nu_{in}$ is the ion neutral collision frequency, n is the neutral density (of atomic oxygen in the F region) and $V_{ix}$ and $U_x$ are the ion and the neutral velocities in the eastward (x) direction. At the F region altitudes $\nu_{in}/n$ , the number of collisions per second an oxygen ion makes with one oxygen atom, is nearly constant with altitude (being about $7 \times 10^{-10}$) and therefore the ion drag force is proportional to 1) the ion number density and 2) the differential velocity between the ions and the neutrals. If the ionisation density (N) were

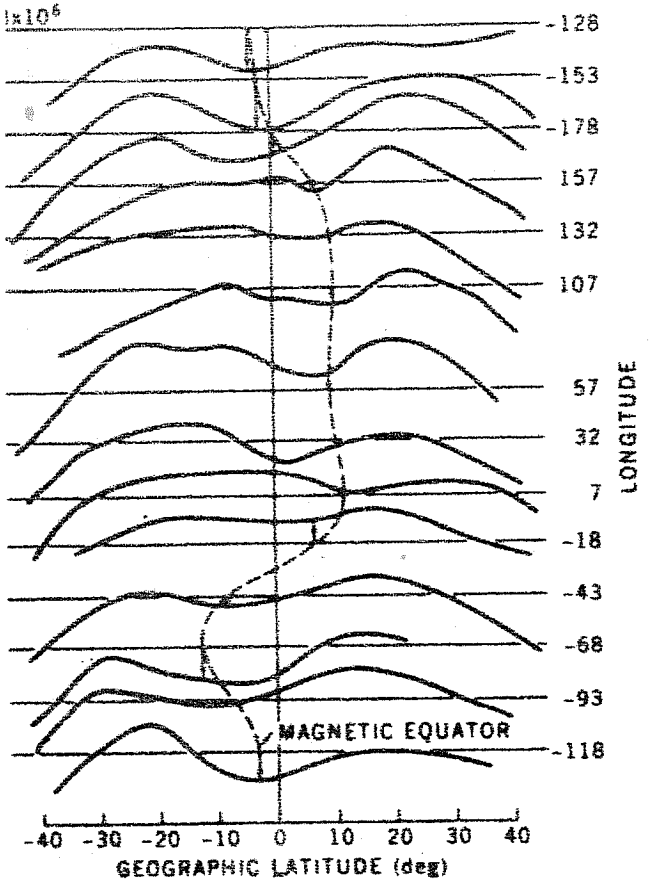


(a)

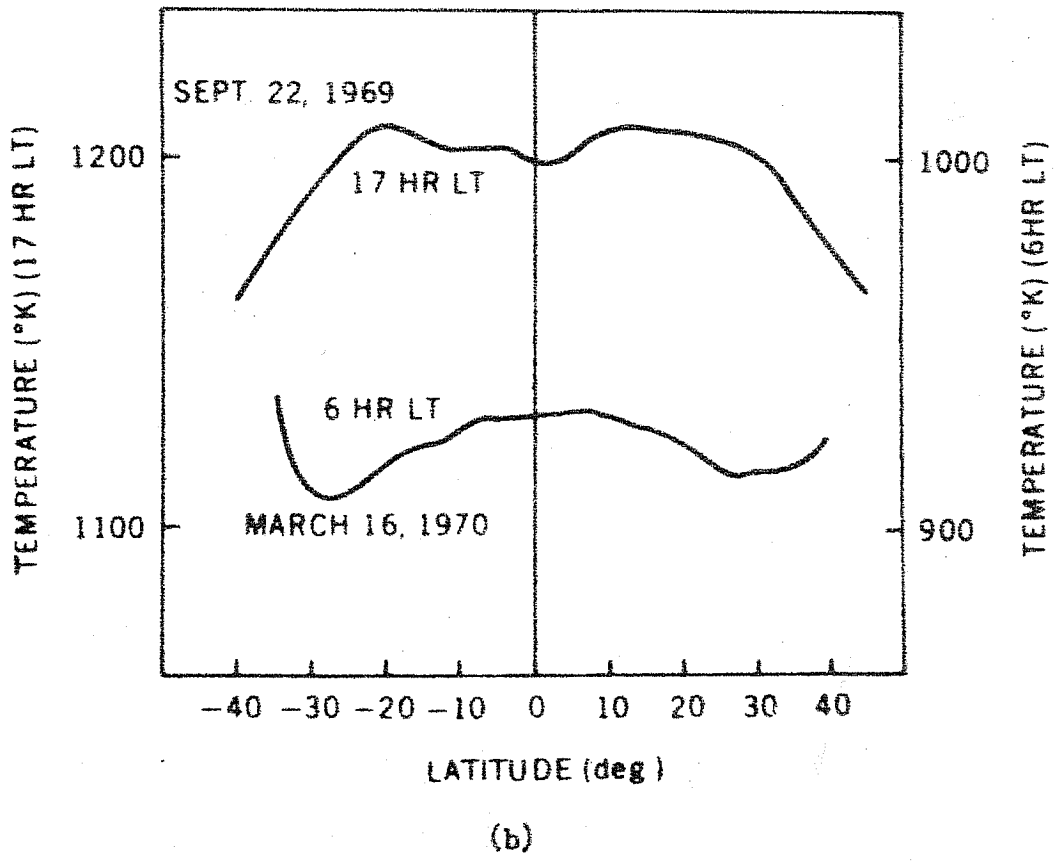


(b)

Fig.1.6 (a,b):- (a) $N_2$ densities at 450 km altitude on Sept. 22, 1969 at 1700 hr LT at various longitudes obtained by means of OGO-6 satellite and (b) latitudinal variation of exospheric temperature for 1700 and 0600 hr. (After Hedin and Mayr, 1973)

constant in the low latitude region around the magnetic equator, the ion drag force to the extent of its dependence on N would also be constant with latitude. However, the higher electron concentration at the latitudes of the ionisation anomaly crest than at the magnetic equator, would inhibit the neutral flow (from dayside to the nightside) more at the latitudesof anomaly crest than at the trough. This would lead to retention of the kinetic energy of the neutrals at the anomaly crest latitudes, thus leading to higher exospheric temperatures and hence the higher neutral densities at the creststhan at the trough. This process therefore leads to geomagnetic control in the latitudinal distribution of neutrals, similar to that observed in the ionisation. The distribution of neutrals at the F region altitudes would also show the anomaly, henceforth called as the neutral anomaly (NA).

In addition, to the ion drag of the ionisation anomaly on the neutral motion based on the effect caused by N alone, Raghavarao and Sivaraman (1975) discussed the effect of the term $(U_x - V_{ix})$ in the expression for the ion drag. It is known that the ion motions are westward throughout the day (e.g. Woodman, 1972) whereas the neutral motion is westward in the forenoon hours and eastward in the afternoon hours, as given by the wind models based on the Jacchia's models of the neutral atmosphere. The reversal of the zonal motion of the neutrals occurs around 1300 hr LT as given by

the latest wind model of Blum and Harris (1975). The ion drag force becomes significant one or two hours before the neutral wind reversal time when the neutral speed becomes minimum, and hence the $(U_x - V_{ix})$ term is large. Therefore, the presence of a strong ionisation anomaly, around noon hours, which imposes higher drag force on the neutral motion at the latitudes of the anomaly crest than at the latitude of the trough (i.e. equator) would assist the formation of NA.

The ambipolar diffusion coefficient of the plasma, $D_a$, because of its inverse relationship with the neutral concentration, would be reduced due to presence of the NA crests along the ionisation anomaly field line. This leads to reduction in the ambipolar diffusion velocity, $V_{||}$, because of its direct dependence on the ambipolar diffusion coefficient. The partial inhibition of diffusion caused by the presence of the NA would cause accretion of the plasma near the top of the magnetic field line, thus causing the ionisation ledge (Raghavarao and Sivaraman, 1974). Raghavarao and Sivaraman (1975) and Sivaraman et al. (1976) have shown that the NA formation would occur more frequently in $S_{min}$ (due to strong IA formation in the forenoon hours) than $S_{max}$ period. On this basis they have explained more frequent occurrence of the ionisation ledge in the topside ionosphere in $S_{min}$ period than $S_{max}$ period.

## I.4 DEFINITION OF THE PROBLEM

The main topic of the thesis is on understanding the phenomenon of ledge formation in the topside ionosphere. A number of its morphological features, e.g. the lunar age dependence, correlation in the day to day occurrence of the ledge and the counter electrojet (in the equatorial E region) are discussed in detail in the Chapters 5 and 6. The origin of the counter electrojet phenomenon is still puzzling. On the basis of observational features presented in Chapter 6 it is suggested that the neutral anomaly is responsible for causing the counter electrojet event.

The study of the spatial distribution of ledge intensity discussed in the Chapter 4 provides much needed evidence for the existence of cross equatorial winds at the F region altitudes. Therefore, the study presented here is important and provides many a useful information on the dynamical interaction of the bottomside and the topside ionosphere. This will also be helpful in the clear understanding of the dynamics of ledge formation, counter electrojet and the cross equatorial winds in the F region of the ionosphere.

# C H A P T E R - II

## CORRELATION BETWEEN THE IONISATION ANOMALY STRENGTH AND THE ELECTROJET STRENGTH

### II.1 INTRODUCTION

Two ionospheric phenomena occurring at the equatorial magnetic latitudes are 1) the ionisation anomaly and 2) the electrojet. The equatorial ionisation anomaly is the name given to a feature of the latitudinal distribution of electron concentration in the F-region showing two well defined peaks at 15-20$^{o}$ dip latitudes with a prominent trough at the magnetic equator. The anomaly was discovered in the latitudinal distribution of foF2 by Appleton (1946). King et al. (1964), and Eccles and King (1969) found the phenomenon to extend into the topside ionosphere as well.

The equatorial electrojet is a strong eastward current in the E-region (at about 100 km altitude) within a narrow zone of $\pm$ 3$^{o}$ dip latitude during the daylight hours (Chapman, 1951, 1956). The strong electrojet current is shown to be responsible for the observed large diurnal range of the geomagnetic H field at stations near the magnetic equator (Egedal 1947, 1948; Pramanik and Hariharan 1953).

The common cause for the existence of both the ionisation anomaly and the electrojet is understood to be the eastward electric field ($\underline{E}$) which interacts with approximately horizontal magnetic field ($\underline{B}$) and exerts $\underline{E}$ X $\underline{B}$

force on the plasma. In the F-region as well as the topside ionosphere, the ion and the electron gyrofrequencies are greater than their respective collision frequencies with the neutral particles with the result that ions and electrons drift together with the Hall drift velocity, $(\underline{E} \times \underline{B})/B^2$. The plasma thus lifted up, diffuses downward along the earth's magnetic field lines giving rise to the peaks of anomaly on either side of the equator (Martyn, 1947; Rastogi, 1959 ; Duncan, 1960). This process termed as "Martyn's Fountain Theory" explains satisfactorily most of the observed features of the ionisation anomaly (Bramley and Peart, 1965; Hanson and Moffett, 1966).

In the E-region, around 100 km altitude, the electron gyrofrequency greatly exceeds the electron-neutral collision frequency but the ion gyrofrequency is less than the ion-neutral collision frequency. Under these circumstances the electrons move under the influence of $\underline{E} \times \underline{B}$ force whereas the ions remain unaffected. For a location at a dip angle $I \simeq \pm 5^{\circ}$ the vertical Hall currents are greatly inhibited, and more so at the magnetic equator ($I = 0$). The inhibition of vertical Hall current leads to vertical Hall polarisation electric field which is $\sigma_2/\sigma_1$ ($\simeq 30$ at 100 km altitude at the equator; Sugiura and Cain, 1966) times the primary eastward electric field (E), $\sigma_1$ and $\sigma_2$ are the Pedersen and the Hall conductivities respectively. More recently

Anandarao et al. (1975) have shown observationally that the vertical polarisation electric field is $\left[\int \sigma_2 \, ds / \int \sigma_1 \, ds\right]$ times the primary electric field, where 'ds' is the line element along the earth's magnetic field line. The vertical polarisation electric field interacting with the northward horizontal B field produces westward motion of the electrons causing the eastward electrojet current. The current is given by $j = \sigma_3 . E$, where $\sigma_3 = (\sigma_2^2 / \sigma_1 + \sigma_1)$ is termed as the "Cowling conductivity", which greatly exceeds the Pedersen conductivity ($\sigma_1$) in the equatorial E region (Baker and Martyn, 1952, 1953). From the above description it is apparent that the electric field is the cause for the ionisation anomaly in the F region/topside and the electrojet in the E region. One would naturally expect a close relation between the phenomena caused by the same agency.

## II.2 SUMMARY OF EARLIER WORK

The close relation between the electrojet current and the F2 layer ionisation near the magnetic equator was pointed out by Rastogi (1963, 1965). He showed that at an equatorial station the seasonal, the latitudinal and the solar cycle variations in the amplitude of lunar tidal variations in the foF2 and the geomagnetic H field are very similar to each other and the phases between the two are almost opposite in all the cases. Thus an increase of the electrojet current strength causes a decrease of the F2 layer ionisation at the magnetic equator and vice versa.

A quantitative relationship between the two phenomena was first shown by Dunford (1967). He argued that if the Martyn's fountain effect were the cause for the ionisation anomaly, there should be some relationship between the anomaly and the current in the E region (at which level the electric field is impressed). Dunford normalised the published foF2 data at 1300 hr. LT for different stations in the Asian zone by the respective monthly mean foF2 at the same local time. He plotted the normalised foF2 data against the maximum daily range of H field ($\triangle$H) at equatorial station. At Trivandrum (equatorial station) the foF2 showed decreasing trend with increase in the maximum range of $\triangle H_T$ (suffix 'T' represents "Trivandrum"), whereas the foF2 at stations Delhi and Ahmedabad (stations near the anomaly crest) showed increasing trend with increase in maximum daily range of $\triangle H_T$. Dunford estimated the eastward electric field from the magnetic range $\triangle$H at the equatorial station and concluded that the higher the vertical ($\underline{E}$ X $\underline{B}$) drift over the magnetic equator the lower the values of foF2 over the magnetic equator and the higher the values of foF2 at the anomaly crest, in agreement with Martyn's concept of anomaly formation.

Dunford defined a parameter S, given by S = W X D to represent the anomalystrength at a fixed altitude (450 km) in the ionosphere. The parameter W denotes the separation between the latitudes of the anomaly peak and the trough.

The parameter D represents $(N_p - N_t)/N_t$, where $N_p$ and $N_t$ are the electron concentrations at the anomaly peak and trough respectively. The parameters W and D are called the 'width' and the 'depth' of the anomaly, and the quantity S is called the "anomaly product". The quantities used for calculating W and D were obtained from latitudinal distribution of electron concentration at 450 km altitude obtained from Alouette - 1 topside sounder data. Dunford found that the latitudinal structure as well as the crest to trough ratio of the anomaly shows large variations. On some days, D is small while W is large and vice versa. The parameter S minimizes the effect of these variations and hence is a better measure of the anomaly strength instead of either W or D separately. He showed that the anomaly product S obtained on a number of days shows linear relationship with magnetic range at equatorial station Muntinlupa.

Mao Fu Wu (1970) presented a few individual examples of anomaly formation using Alouette-1 satellite data recorded at equatorial station Huancayo and compared the strength of anomaly with the maximum amplitude of the $\triangle$H field at Huancayo. She found that the days on which the maximum range of $\triangle$ H at Huancayo is large, the anomaly develops prominently and vice versa.

Rastogi and Rajaram (1971) showed that foF2 at the equatorial station Kodaikanal decreases while foF2 at Ahmedabad increases steadily with the increase of equatorial electrojet strength estimated by the difference in the maximum daily range of $\triangle$ H at equatorial station Trivandrum and that at the low latitude station Alibag.

The work of Mao Fu Wu and Rastogi and Rajaram supplemented Dunford's work and provided support to the Martyn's fountain theory of ionisation anomaly formation.

Rush and Richmond (1973) made quantitative investigation of the relationship between the anomaly strength and the electrojet strength using the published foF2 data for American, African, Indian, and Japanese sectors for the year 1958. They defined six parameters for representing anomaly strength: $R_N$ , $\phi_N$ , $R_N \times \phi_N$ , $R_S$ , $\phi_S$ and $R_S \times \phi_S$ . The parameters are calculated from the latitudinal distribution profiles of foF2. The parameter R denotes the crest to trough ratio of electron concentration and $\phi$ denotes the latitude of the anomaly crest. The suffixes 'N' and 'S' denote the 'northern' and the 'southern' crest of the anomaly respectively. The parameter $\phi$ is same as the parameter W of Dunford (1967) and R is related to the parameter D as R = (1 + D).

Rush and Richmond compared the anomaly strength S with the maximum midday electrojet strength defined by two parameters, $\triangle H_I$ and $\triangle H_{II}$ . The parameter $\triangle H_I$ was defined as

$$\triangle H_I = \frac{H_{10} + 2H_{11} + 2H_{12} + H_{13}}{6} - \frac{H_{00} + H_{01} + H_{02} + H_{22} + H_{23} + H_{24}}{6} \quad \ldots\ldots(1)$$

where $H_{10}$ , $H_{11}$ ------- , say $H_i$ represents the average value of H between i and (i + 1) hr LT at an equatorial station. $\triangle H_{II}$ was obtained by subtracting similar $\triangle H_I$ at a low latitude station outside the influence of electrojet belt from the $\triangle H_I$ at the equatorial station as calculated by using eq.(1). $\triangle H_I$ and $\triangle H_{II}$ represent the midday electrojet strength. According to these authors $\triangle H_{II}$ represents the midday electrojet strength more closely than $\triangle H_I$ especially during magnetically disturbed period.

Rush and Richmond calculated correlation coefficients between the midday electrojet strength and the anomaly strength and showed that the correlation coefficients tend to maximise in the early afternoon between 1300-1600 hr LT. They pointed out that this time interval is about 2-3 hours after the mean local time at which the midday electrojet strength is calculated and thus this result is consistent with the results obtained by solving the continuity equation for electrons in the F2 region (Sterling et al. 1969; Anderson, 1973), showing

the response of the anomaly to lag about 2-3 hrs behind the changes in the electric field. Fig. 2.1 reproduced from their work shows the diurnal variation of the correlation coefficient between the six anomaly parameters and the electrojet parameter $\triangle H_I$ for the American sector for Oct. 1958. It is seen from the figure that the correlation coefficients decrease in the evening hours and become insignificant after 2000 hr LT. It is also seen that the correlation coefficients decrease steeply between 1400 and 1200 hr LT. At 1200 hr, the correlation coefficients of the electrojet strength with the anomaly parameters $\Phi_N$ and $\Phi_S$ show negative values; with the anomaly products $(R_N \times \Phi_N)$ and $(R_S \times \Phi_S)$ the correlation coefficients are nearly zero. From the trend of the variation of the correlation coefficients with local time we conclude that the correlation of the anomaly strength with the midday electrojet strength prior to 1200 hr LT would either be zero or negative.

We feel that the choice of the electrojet parameter, the midday electrojet strength, taken for comparison with the anomaly strength at all hours of the day by the authors mentioned above, is not proper. The equatorial anomaly develops usually around 08-10 hr LT and thereafter its strength increases with time until about 1400 hr LT in sunspot minimum period and until 2000 hr LT in sunspot maximum period (Rastogi, 1966). The crest to trough ratio of electron

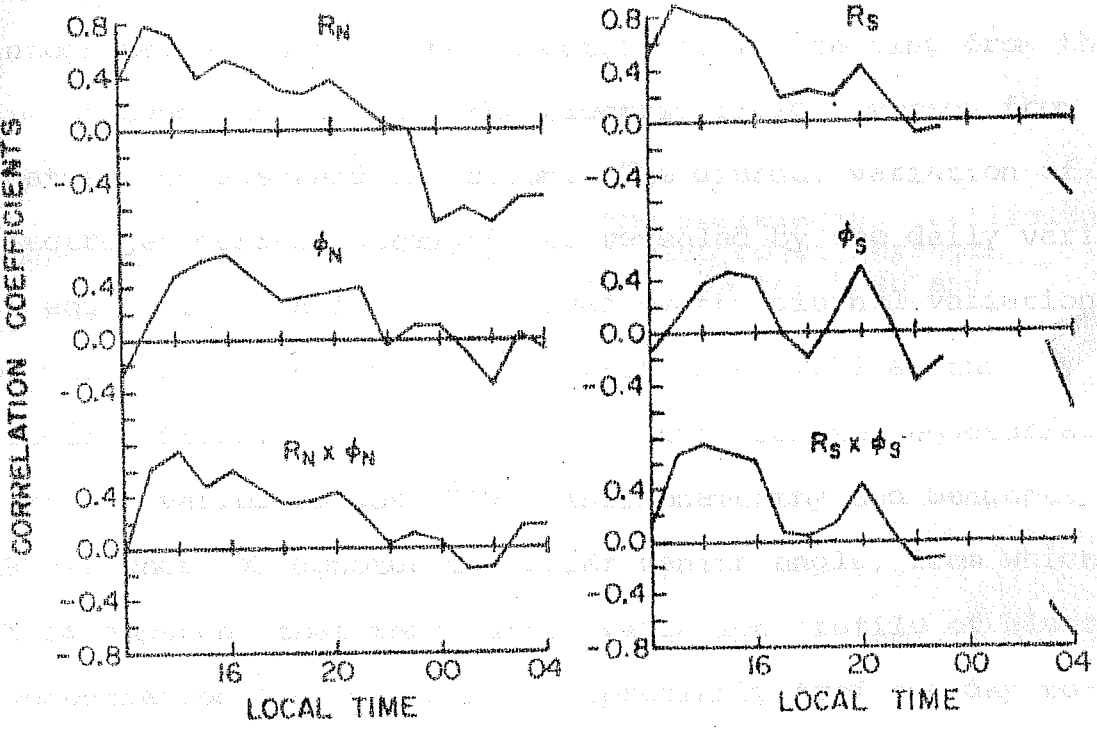


Fig. 2.1 : Diurnal variation of the correlation coefficients between six anomaly parameters and electrojet strength ($\Delta H_T$) for Oct. 1958, American sector (after Rush and Richmond, 1973).

concentration as well as the dip latitude of the crest increase continuously, although not monotonically, from the time the anomaly first appears until its maximum development. The continuous build-up of the anomaly suggests that its strength at any particular time should depend upon the time-integrated strength of the electric field starting from the time (around sunrise) when the electric field reverses from westward to eastward direction. The diurnal variation of the electrojet current strength, as revealed by the daily variation of equatorial $\triangle$H field, is caused by the diurnal variation of the E region electron concentration as well as the electric field. The electron concentration the equatorial E region varies as $\mathrm{Cos}^{0.33}\chi$ (Krishnamurthy and Sengupta, 1972), where $\chi$ denotes the solar zenith angle, from which it is apparent that the diurnal variation profile of electron concentration does not change appreciably from one day to the other. However, the diurnal variation profile of the equatorial H field reveals substantial day to day changes which cannot be attributed to electron concentration alone. This suggests that the E region electric field varies differently on different days in order to account for the observed day to day changes in the daily variation profile of the equatorial H field. The time integrated area of the $\triangle$H curve, although gives the integrated product of the electric field and the electron concentration, it essentially represents the

integrated electric field only, on the basis of above arguments. The results presented in the following pages support our choice of the integrated electric field in the electrojet for comparing with the anomaly strength.

The work of Rastogi and Rajaram (1971), Rush and Richmond (1973) and Chandra and Rastogi (1974) shows that the difference of $\triangle$ H field between an equatorial station (say Trivandrum, $-0^{\circ}.3$ diplatitude) and a low latitude station just outside the effect of the electrojet (say Alibag, $+12^{\circ}.9$ dip latitude) is a better measure of the electrojet current as compared to $\triangle$ H field at Trivandrum only. The $\triangle$ H field at Trivandrum represents the combined effect of the Sq current, the electrojet current and the magnetospheric current. The magnetospheric contribution to $\triangle$ H is negligible on magnetically quiet days. The $\triangle$H field at Alibag is caused by the Sq current and the magnetospheric current. As Alibag is not too far away from Trivandrum, the Sq contribution to the $\triangle$ H field can be taken approximately the same at both the stations, on the basis of the latitudinal profile of the Sq given by Onwumechilli (1967). The magnetospheric contribution to $\triangle$ H field is very nearly the same at both

the stations (Kane, 1973b). The subtraction of Alibag $\triangle H$ from Trivandrum $\triangle H$ removes the magnetospheric as well as the Sq contribution and thus $(\triangle H_T - \triangle H_A)$, where suffixes 'T' and 'A' denote Trivandrum and Alibag respectively, represents the contribution of only the electrojet current on quiet as well as disturbed days.

## II.3 DATA ANALYSIS AND RESULTS

We correlate the observed anomaly strength on a particular day with the electrojet strength represented in two ways : 1) the area under the $\triangle H_T$ curve measured from the time when the H field rises above the nighttime base level upto the time of anomaly observation, and 2) the area under the $(\triangle H_T - \triangle H_A)$ curve measured in the same manner as for the $\triangle H_T$ curve. In addition, we study the correlation between the anomaly strength and the midday ranges of $\triangle H_T$ and $(\triangle H_T - \triangle H_A)$ curves, these two parameters being same as $\triangle H_I$ and $\triangle H_{II}$ respectively of Rush and Richmond (1973). The parameter S $(= R \times \Phi)$ taken to represent the anomaly strength in the present study is the same parameter as used by Rush and Richmond. For the present study R is evaluated at 600 km altitude. The choice of 600 km altitude (rather than the $h_{max}$ F2 altitude taken by Rush and Richmond) is made on the basis that the latitudinal profiles of electron concentration are available at this altitude for all the 116 passes of ISIS-1 and 2 satellites used in this study.

To obtain latitudinal distribution of electron concentration at $h_{max}F2$ altitude it is necessary to have good quality ionograms, on which the echo traces are seen upto the penetration frequencies, throughout the entire duration of a satellite pass.

The parameters defined above for representing the anomaly and the electrojet strengths are illustrated in Fig. 2.2(a,b). Fig.2.2(a) gives the constant height plot obtained from an ISIS-2 pass, showing ionisation anomaly at 1330 hr LT on April 20, 1972. The values of the electron concentration at the anomaly peak at 600 km altitude and that at the trough are $1.30 \times 10^{6} cm^{-3}$ and $6.60 \times 10^{5} cm^{-3}$ respectively. The crest to trough ratio (R) of electron concentration is 1.97. The dip latitude of the anomaly peak at 600 km altitude is $14.0^{\circ}$ and the trough being at the magnetic equator, $\phi = 14.0^{\circ}$. The anomaly strength S ( $= R \times \phi$ ) is 27.6.

Fig. 2.2(b) gives the diurnal variation of $\triangle H_T$ and $(\triangle H_T - \triangle H_A)$ curves on April 20, 1972. The nighttime base levels, represented by $\triangle H_T = 0$ and $(\triangle H_T - \triangle H_A) = 0$, have been obtained by the method followed by Rush and Richmond. The two vertical arrows CD and IJ mark the time of anomaly observation on $\triangle H_T$ and $(\triangle H_T - \triangle H_A)$ curves resepctively. The areas ABCDEA and GHIJKG under the $\triangle H_T$ and $(\triangle H_T - \triangle H_A)$ curves respectively, taken to represent the electrojet strength in the present

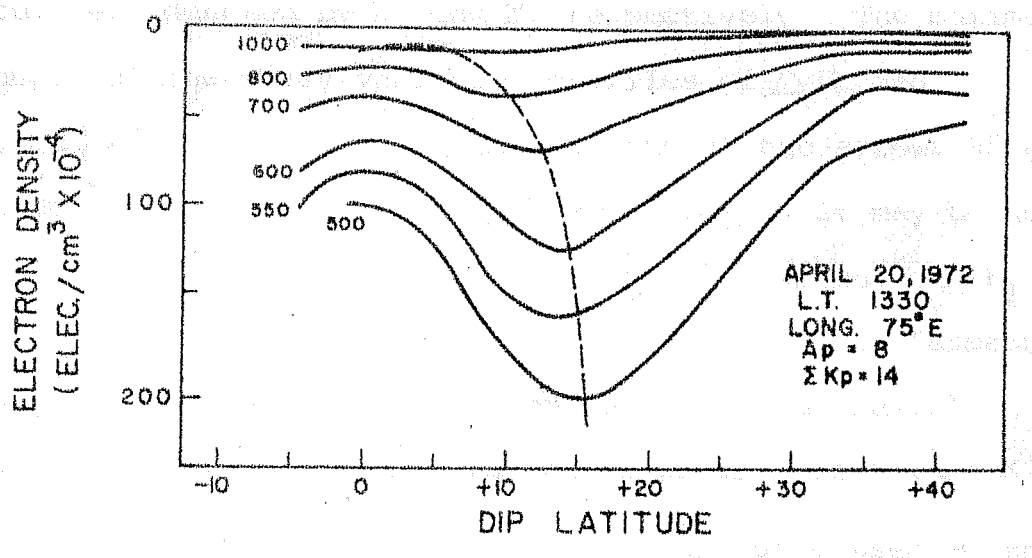


(a)

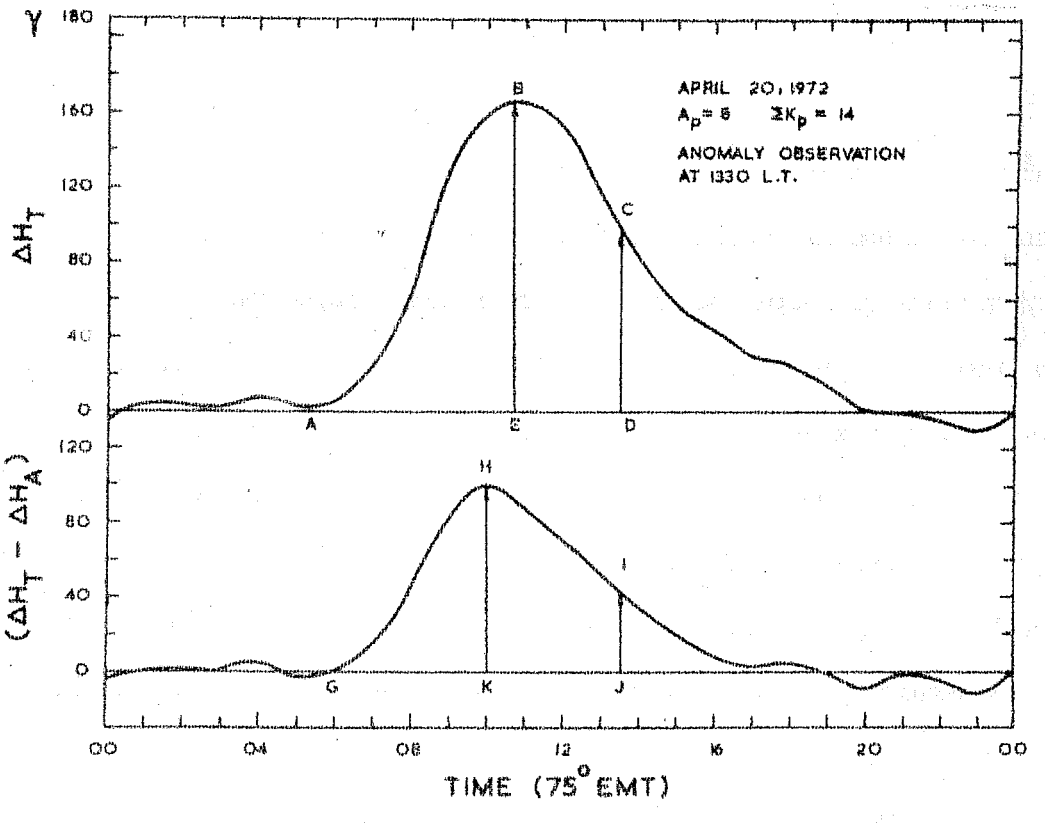


(b)

Fig. 2.2(a,b):- (a) Latitudinal distribution of electron concentration at various fixed altitudes on April 20, 1972 at 1330 hr LT and (b) diurnal variation of $\Delta H_T$ and $(\Delta H_T - \Delta H_A)$ on the same day.

study are denoted by $X_A$ and $Y_A$ respectively. The maximum ranges of the daily variation profiles of $\triangle H_T$ and $(\triangle H_T - \triangle H_A)$, given by the lengths of the arrows BE and HK, are denoted by $X_R$ and $Y_R$ respectively. It may be noted that the symbols 'X' and 'Y' represent '$\triangle H_T$' and '$(\triangle H_T - \triangle H_A)$' respectively. The subscripts 'A' and 'R' denote "area upto the time of anomaly observation" and "maximum range" respectively of the daily variation profile of either 'X' or 'Y'.

Most of the ionisation anomaly data used in the present study is selected from the ISIS satellite passes recorded at Ahmedabad during the equinoctial months (March-April and September-October) of 1972-1974. During equinox period the two peaks of ionisation anomaly at any altitude are of equal strength and also equally distant (in latitude) from the magnetic equator, hence any one of the two peaks can be taken for evaluating the anomaly strength. During the solstice period, however, the summer peak of the anomaly at any altitude in the topside ionosphere is of higher strength than the corresponding winter peak. The satellite passes recorded at Ahmedabad usually cover only the northern peak of the anomaly. Thus the anomaly strength would be overestimated if evaluated from the northern peak during local summer and would be underestimated if the same peak is taken during local winter months.

Magnetically disturbed days ($A_p > 15$) are omitted from the present study for the reason that the anomaly is shown to be either depleted or enhanced (Sato, 1968; Raghavarao and Sivaraman, 1973) because of storm induced changes in the electric field or in the neutral composition (namely the $[O]/[N_2]$ ratio at the F region altitudes; Prolss and Von Zahn, 1974). The storm-time equatorward wind ($\sim$ 50 m/s) has also been suggested as a possible cause for the observed changes in the ionisation anomaly (Burge et al. 1973). The storm induced changes in the anomaly are therefore not due to the changes in the electrojet and hence it was considered desirable to confine the scope of the present correlative study of the two phenomena to quiet days only.

The anomaly data is grouped in hourly interval between 1000-1600 hr LT, the upper limit of the time interval as 1600 hr is due to the absence of sufficient number of anomaly data after this local time during the period under study.

The correlation coefficients between the anomaly and the electrojet parameters are calculated by the method of linear correlation (e.g. Young, 1962, p 126). The standard error ( $\sigma$ ) in the correlation coefficient ( r ) is given as

$$\sigma = (1 - r^2) \cdot (n - 1)^{-\frac{1}{2}}$$

where 'n' represents the number of pair of data points on which the correlation is based (Fisher and Yates, 1957; p 3).

Three representative plots of the correlation between the anomaly and the electrojet are shown in Fig. 2.3 (I - III). Each one of the plots is divided into parts (a), (b), (c), and (d) showing the correlation of the anomaly strength S with the four electrojet parameters $X_A$, $Y_A$, $X_R$ and $Y_R$ respectively. The straight lines drawn through the data points in parts (a) and (b) are regression lines obtained by the least square fitting.

Referring to Fig. 2.3 (I - III), at 1000 LT the correlation coefficients between the anomaly parameter S and the electrojet parameters $X_A$ and $Y_A$ are (0.83 $\pm$ 0.09) and (0.89 $\pm$ 0.06) respectively, whereas the correlation coefficients between S and the parameters $X_R$ and $Y_R$ are (0.48 $\pm$ 0.21) and (0.52 $\pm$ 0.20) respectively. At 1400 LT the correlation coefficients of the anomaly with the electrojet parameters $X_A$ and $Y_A$ are (0.90 $\pm$ 0.04) and (0.94 $\pm$ 0.03) respectively, whereas with the electrojet parameters $X_R$ and $Y_R$ the correlation coefficients are (0.78 $\pm$ 0.09) and (0.82 $\pm$ 0.07) respectively. At 1600 LT, the correlation coefficients between S and the electrojet parameters $X_A$, $Y_A$, $X_R$ and $Y_R$ (0.83 $\pm$ 0.08), (0.90 $\pm$ 0.05), (0.65 $\pm$ 0.15) and (0.71 $\pm$ 0.13) respectively.

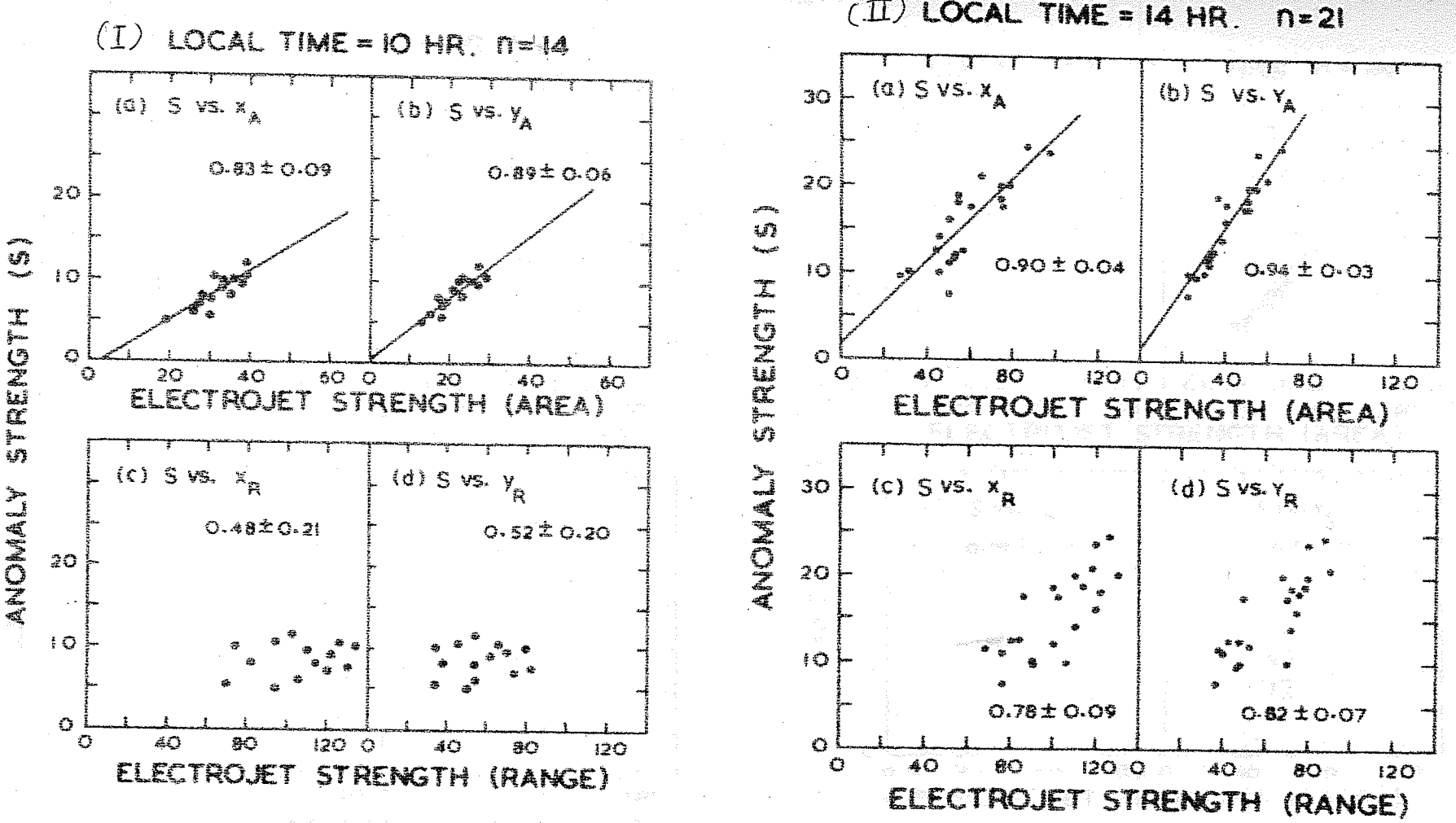


Fig. 2.3(I, II):- Scatter plots of correlation between the anomaly strength and the electrojet strength at 1000 hr and 1400 hr IT respectively. The two parameters correlated and the correlation coefficients obtained are mentioned in each of the compartments (a), (b), (c) and (d).

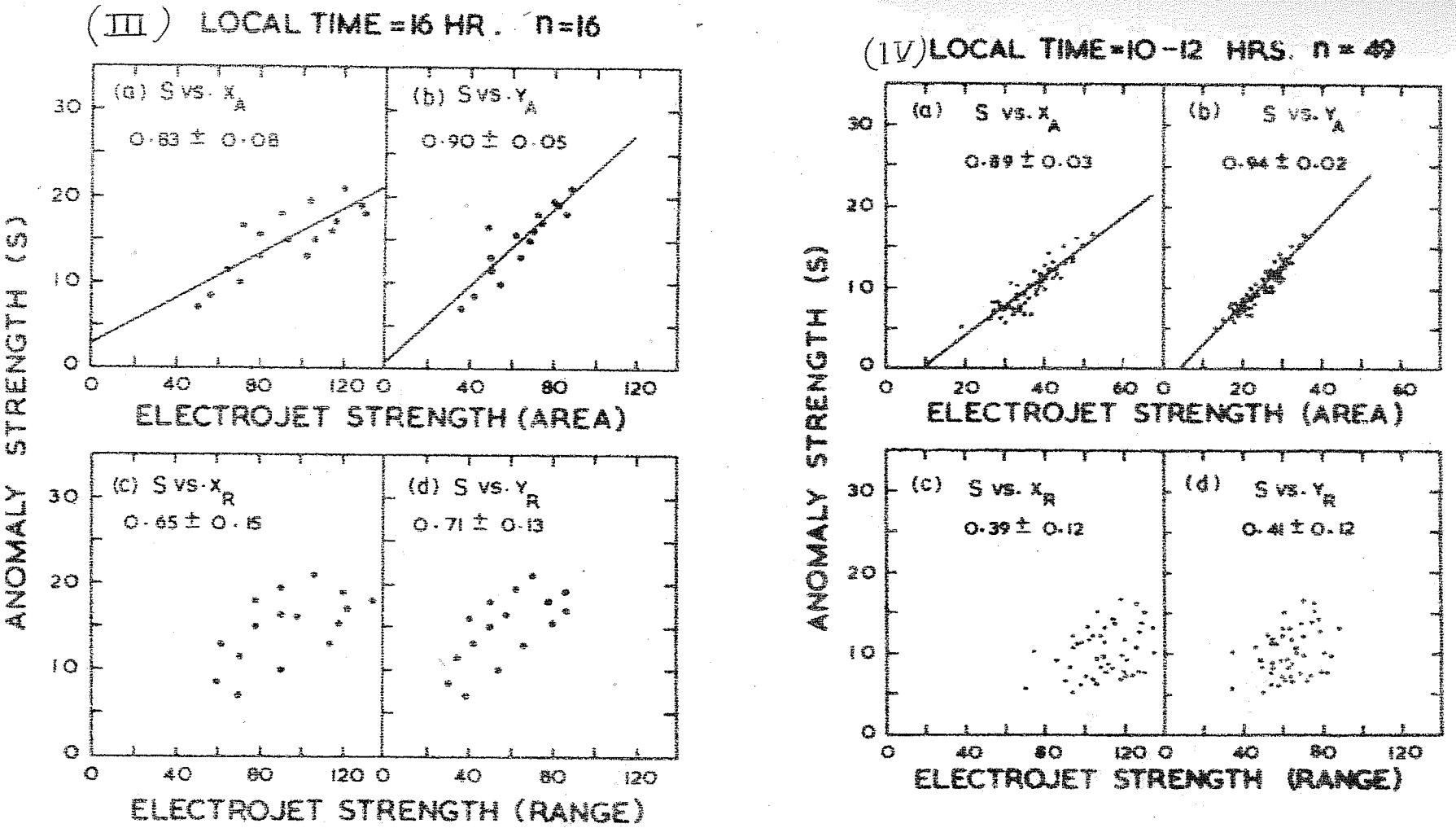


Fig. 2.3(III, IV):- Same as in Fig. 2.5(I, II) at 1600 hr and 1000-1200 hr LT respectively.

However, it should be pointed out that small number of data points (average being about 16) for each individual hour makes the correlation less significant especially when it is low. For instance, corresponding to 16 pairs of independent data points the 95% significance level of the correlation coefficient, as given by Fisher and Yates (1957, Table VII), is about 0.47. This means that any value of 'r' greater than 0.47 can be taken as significant correlation. In order to ascertain whether the time integrated area of the electrojet strength is really a better parameter for comparing with the anomaly strength, we combine the data for three forenoon hours 1000, 1100 and 1200 LT. The total number of data points for these three hours is 49. From Fisher and Yates' table, the 95% significance level of the correlation coefficient for n = 50 is 0.27. Fig. 2.3 (IV) shows that the correlation coefficients of the anomaly strength S with the electrojet parameters $X_A$, $Y_A$, $X_R$ and $Y_R$ are $(0.89 \pm 0.03)$, $(0.94 \pm 0.02)$, $(0.39 \pm 0.12)$ and $(0.41 \pm 0.12)$ respectively. These values are above the statistically significant value of the correlation coefficient (0.27). The high correlation of the anomaly with the electrojet parameters $X_A$ and $Y_A$ and low correlation with parameters $X_R$ and $Y_R$ substantiates our suggestion that the time-integrated electrojet strength rather than its instantaneous midday strength should be compared with the observed anomaly strength at any local time.

Fig. 2.4 shows the diurnal variation of the correlation coefficient of S with $X_A$, $Y_A$, $X_R$ and $Y_R$ in the curves marked 'a', 'b', 'c' and 'd' respectively. The comparison of 'a' with 'b' shows that the integrated electrojet strength, $X_A$, shows higher correlation, at any hour between 1000-1600 LT, than the maximum electrojet range, $X_R$. Similarly the parameter $Y_A$ shows higher correlation than $Y_R$ with the anomaly strength S, as apparent by comparing the curve 'c' with 'd'. It may be recalled that the parameters $X_R$ and $Y_R$ are the same as the parameters $\triangle H_I$ and $\triangle H_{II}$ of Rush and Richmond (1973). The daily variation of the correlation coefficient obtained by taking these parameters of the electrojet, shown by the curves 'b' and 'd', reveal low correlation especially in the forenoon hours similar to their results (reproduced in Fig.2.1 for the parameter $\triangle H_I$).

It is also interesting to note from curves 'a' and 'c' of Fig. 2.4 that the correlation coefficient remains fairly constant (in the range 0.80 - 0.96) between the local times 1000-1600 hr, whereas the curves 'b' and 'd' reveal that the correlation varies appreciably (in the range 0.48 - 0.82) with time. This further shows that it is physically more meaningful to compare the time-integrated electrojet strength with the anomaly strength. Out of the two parameters $X_A$ and $Y_A$, the latter shows consistently

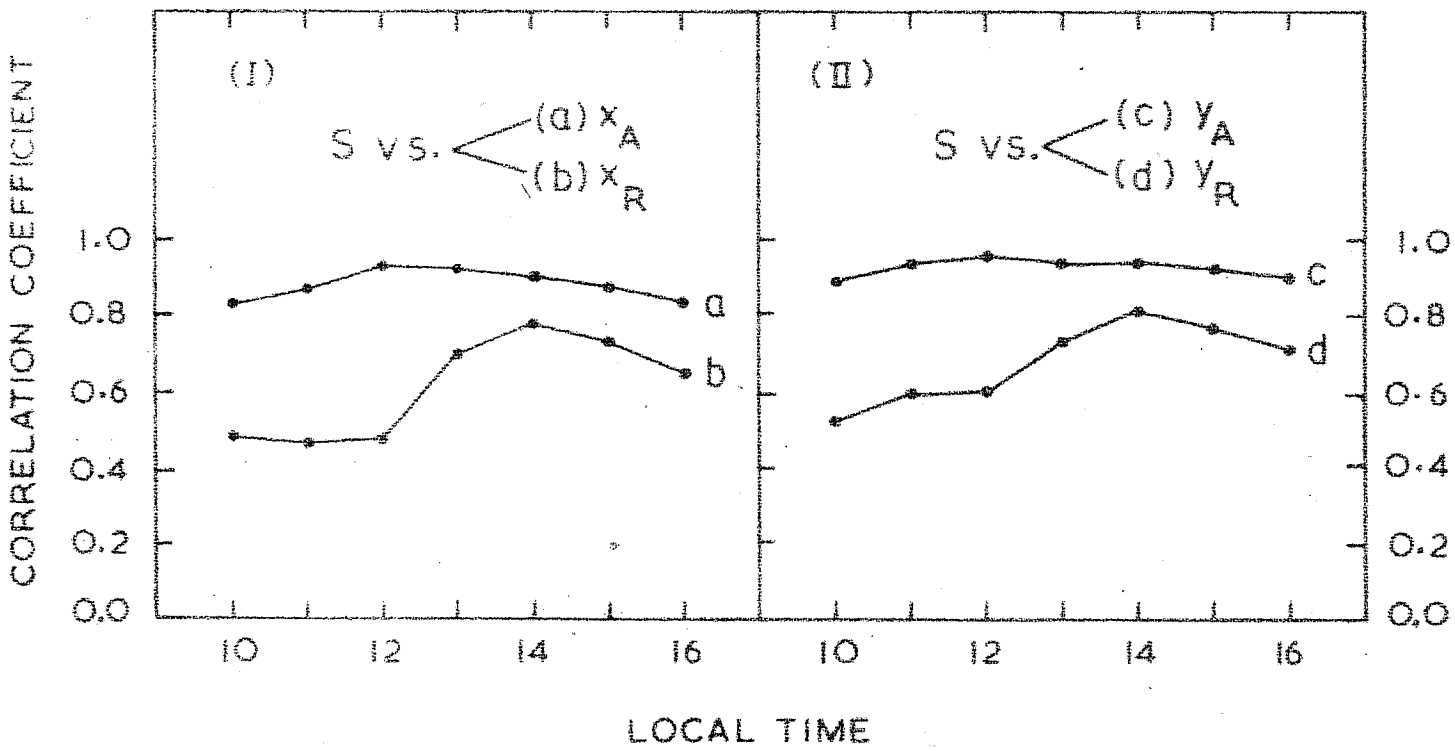


Fig.2.4:- Local time variation of the correlation coefficient between the anomaly strength S and the electrojet parameters $X_A$, $X_R$, $Y_A$ and $Y_R$.

higher correlation with the anomaly strength than the former, as is apparent by comparing the curve 'a' with 'c'. This confirms the suggestion of earlier workers that the difference of the $\triangle H$ field between the equatorial and a low latitude station just outside the electrojet belt should give a better estimate of the electrojet strength at any time than the $\triangle H$ field at the equatorial station alone.

## II.4 CONCLUSIONS AND DISCUSSION

We have shown that the time integrated area of the $\triangle H$ field at equatorial station ($\triangle H_T$) and the difference in the $\triangle H$ field at an equatorial station and a non-equatorial station ($\triangle H_T - \triangle H_A$) correlate very well with the anomaly strength at any hour of the day. This can be understood in terms of the 'fountain theory' of the ionisation anomaly formation. The equatorial anomaly strength at any hour depends on the time integrated strength of the eastward electric field upto that hour rather than just the instantaneous midday value of the electric field.

Out of the two methods followed by the author for representing the electrojet strength, by the areas under the daily variation of $\triangle H_T$ curve and the ($\triangle H_T - \triangle H_A$) curve, the latter shows higher correlation at any local time with the anomaly strength. This suggests that the electric field in the electrojet is more closely related to the parameter ($\triangle H_T - \triangle H_A$) rather than to $\triangle H_T$. The electric field in

the E-region has been estimated by various authors (e.g. Dunford, 1967; Tarpley and Balsley, 1972; Krishnamurthy and Sengupta, 1972) using the $\triangle$H field at the equatorial station only. However, our results confirm the suggestion of the earlier workers that the difference in the $\triangle$H field at an equatorial station and that at a low latitude station is a better parameter for evaluating the electric field in the electrojet, and hence this quantity should be taken for evaluating the electric field in the electrojet region from the observed geomagnetic H field variations.

# C H A P T E R - III

## OBSERVATIONS AND INTERPRETATIONS OF LEDGE FORMATION

### III.1 INTRODUCTION

In this chapter the author describes some new features of the ionisation ledge in the equatorial topside ionosphere as revealed by the ISIS-1 and 2 satellite topside sounder data recorded at Ahmedabad. The ionisation ledge manifests itself in the form of a 'V' shaped cusp on the echo traces on the topside ionograms, similar to those observed on the bottomside ionograms corresponding to the 'F1' ledge.

The ledge is found to be present on more than 200 days between 1100 and 2200 hrs LT during the period 1972-75. The time at which the ledge is usually present is around 1200 hr. However, on rare occasions the ledge is present around 1000 hr LT.

King et al. (1964) and Lockwood and Nelms (1964) observed the ionisation ledge in the topside ionosphere, by means of Alouette-1 satellite, in the Asian zone ($105^{o}$E) and the American zone ($75^{o}$W) respectively. These authors showed that the presence of the ledge is revealed through cusp formations on the topside ionograms. Subsequently, Rishbeth et al. (1966), Rush et al. (1969) and Van Zandt et al. (1972) studied this phenomenon. Although the ledge has been investigated for over a decade, there was no

mechanism which could explain its various observational features satisfactorily. Raghavarao and Sivaraman (1974), henceforth referred to as RS1, proposed a new mechanism for the ledge formation by invoking the presence of the neutral anomaly (NA), similar to the equatorial ionisation anomaly (IA). The observational evidence for the neutral anomaly at the F region altitude was provided by Hedin and Mayr (1973) by means of the mass spectrometer on-board OGO-6 satellite. Subsequent work by Raghavarao and Sivaraman (1975), henceforth referred to as 'RS2', showed that the mechanism proposed by them is consistent with many of the observed features of the ledge.

In this chapter the author presents a number of new features of the ionisation ledge. A brief description of the observational features and the interpretations of the ledge by the earlier workers is presented in view of his own observations.

## III.2 OBSERVATIONAL FEATURES OF THE IONISATION LEDGE

Fig. 3.1(a) shows a topside ionogram obtained from the ISIS-2 satellite pass on March 19, 1974 at 14.54.07 U.T. at $80^{\circ}.9$E longitude (local time 2018 hr). The presence of the cusps on the ordinary (O) and extraordinary (X) echo trace is apparent; the cusp tip frequencies being 1.40 and 1.80 MHz respectively. The apparent range (p'), of the X trace is read at 0.05 MHz interval in the frequency range 1.30-3.0 MHz, during which the apparent range changes

(a) (b)

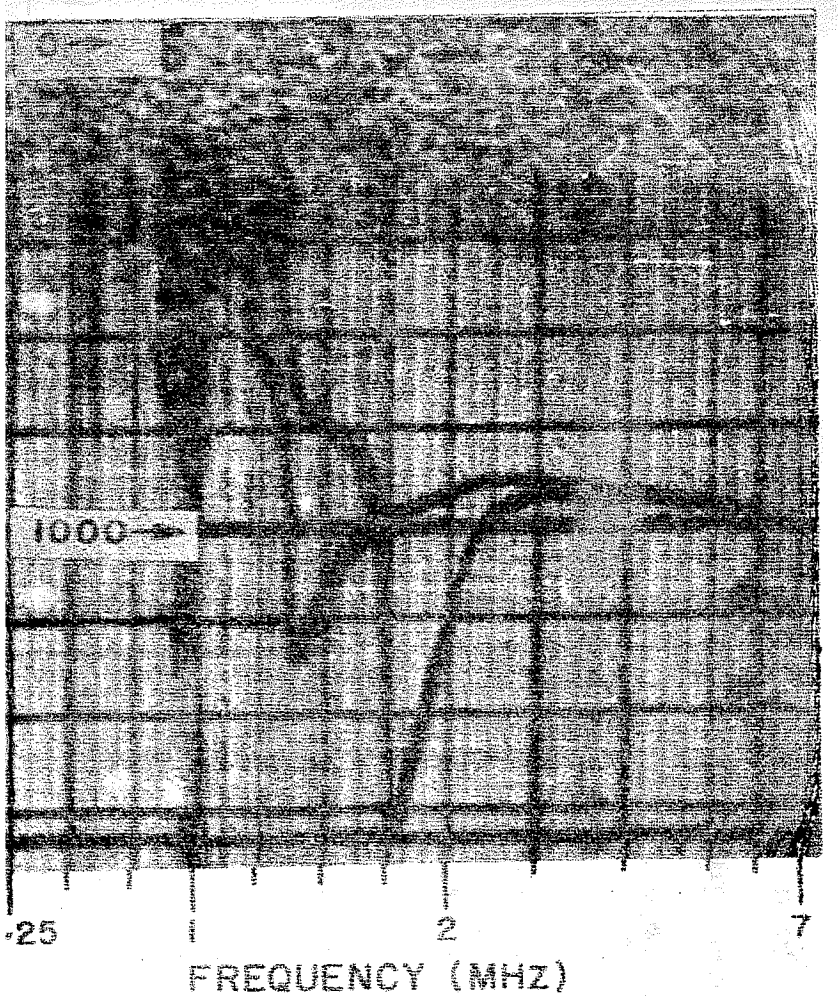


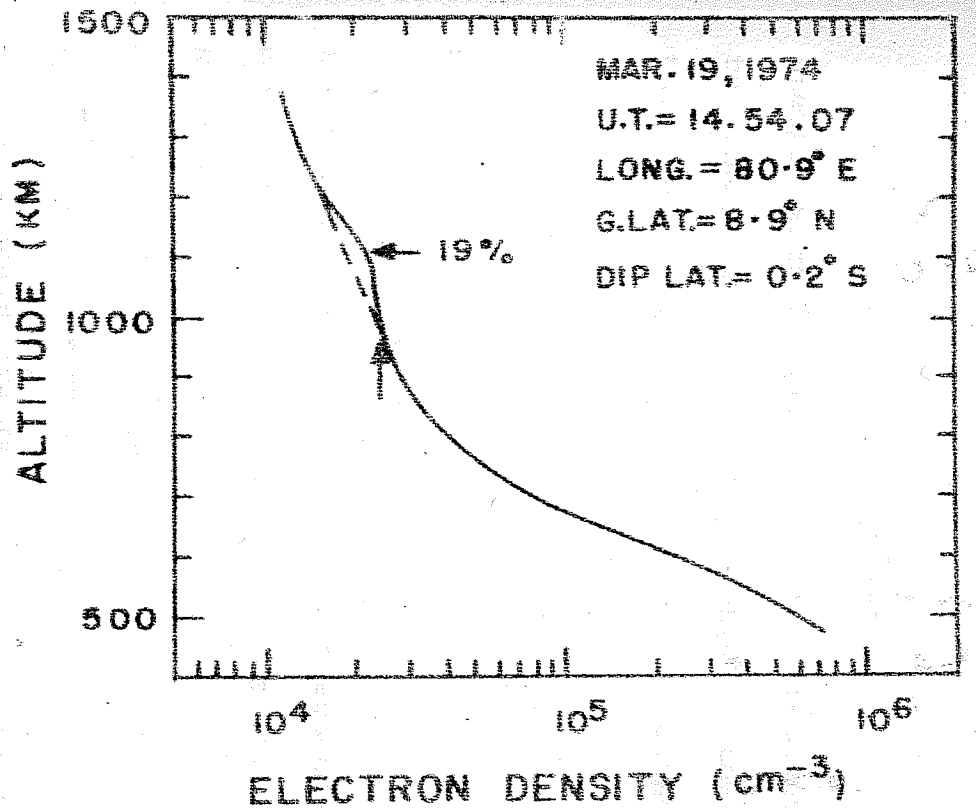


Fig.3.1(a,b):- (a) An ISIS-2 ionogram on March 19, 1974 at 2018 hr IT showing prominent cusp formation and (b) the corresponding computed N(h) profile. The vertical and the horizontal arrows denote the altitudes corresponding to the cusp tip and the maximum electron concentration in the ledge respectively.

steeply with frequency. In the frequency range 3.0-7.0 MHz, the change in the apparent range of the X echo is small and therefore it is read at 0.5 MHz frequency interval.

The reduction of the p'-f data is done by the "parabolic-in log N" method given by Jackson (1969). The method gives fairly accurate N(h) profiles corresponding to the ionograms showing cusp formation, provided the p'-f data are read at sufficiently close frequency intervals. This method has been adopted by RS1 and RS2 for computing the N(h) profiles from the ionograms showing cusp formations. The computed N(h) profile corresponding to the ionogram in Fig.3.1(a) is shown in Fig. 3.1(b). The enhancement of electron concentration in the altitude range 970-1220 km is apparent. The dashed portion of the N(h) profile represents the normal profile of ionisation that would have been obtained in the absence of the ledge by assuming the diffusive equilibrium in the topside ionosphere (e.g. Bauer, 1969). This procedure has been adopted on the basis of the work presented in RS1 and RS2. The tip of the vertical arrow denotes the true height corresponding to the frequency of the cusp tip on the X trace. The excess percentage electron concentration in the ledge with respect to the dashed profile is calculated at each 10 km altitude interval. The horizontal arrow denotes the altitude (1110 km) at which the excess ionisation in the ledge is maximum (19%). It may be noted

that the ledge occurs above the ion transition ($O^+ - H^+$) altitude, the latter being seen as broad curvature of the N(h) profile around 800 km altitude.

Fig. 3.2(a) shows an ionogram obtained from an ISIS-1 satellite pass on May 8, 1973 at 10.55.31 UT at 65°E longitude (1704 hr LT), showing cusp formation on the O and the X echo traces. The cusps are less prominent than those shown in Fig.3.1(a). The N(h) profile computed from the X echo trace of Fig.3.2(a) is shown in Fig. 3.2(b). The maximum excess electron concentration in the ledge is 13% at 875 km altitude. The $O^+ - H^+$ transition is estimated to be around 750 km altitude from the shape of the N(h) profile.

Fig. 3.3 shows the N(h) profile computed from an ionogram obtained on May 24, 1974 at 10.55.31 UT at 65°E longitude (approximate LT 1515 hr) with prominent cusp formation. The excess electron concentration in the ledge is 42% at 520 km altitude. The ledge in this case occurs between the F2 peak (not seen) and the $O^+ - H^+$ transition altitude, the latter estimated to be around 700 km.

It may be noted that the ledge shown in Fig. 3.3, which is nearest to the F2 peak, of the three examples shown in Figs. 3.1 - 3.3, is the strongest. The higher intensity of the ledge when it occurs near the $h_{max}F2$ altitude is probably significant, as this behaviour is found to be true on a number of occasions of the ledge formation around midday

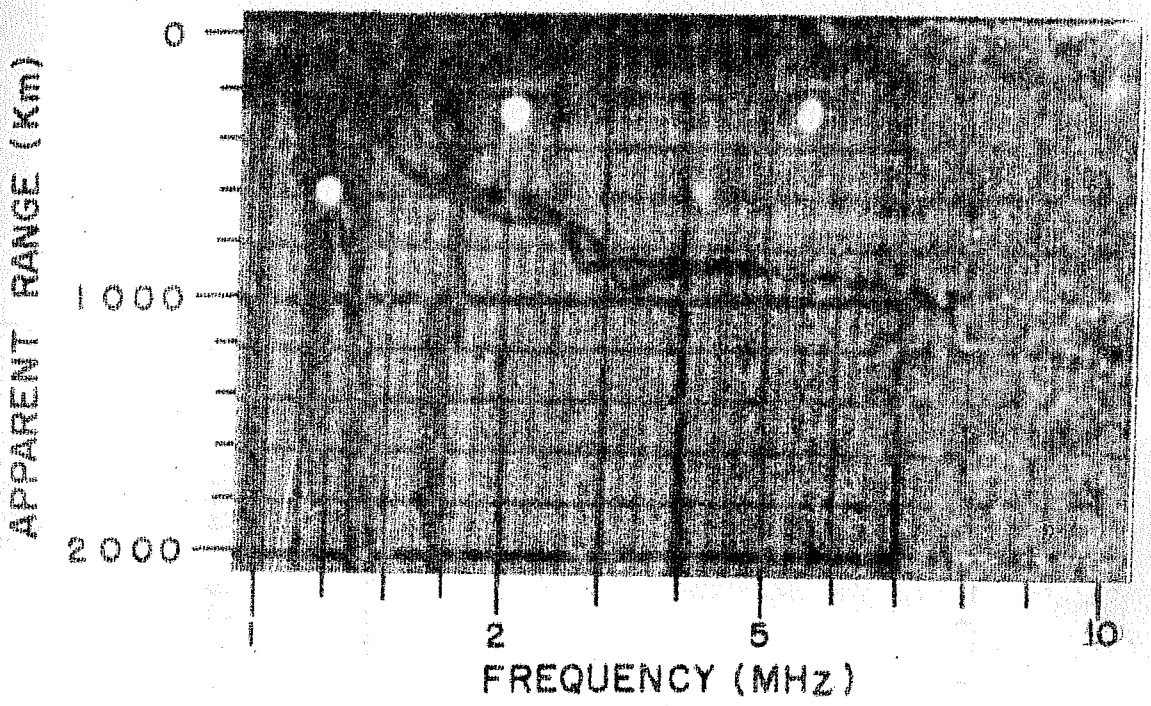


(a)

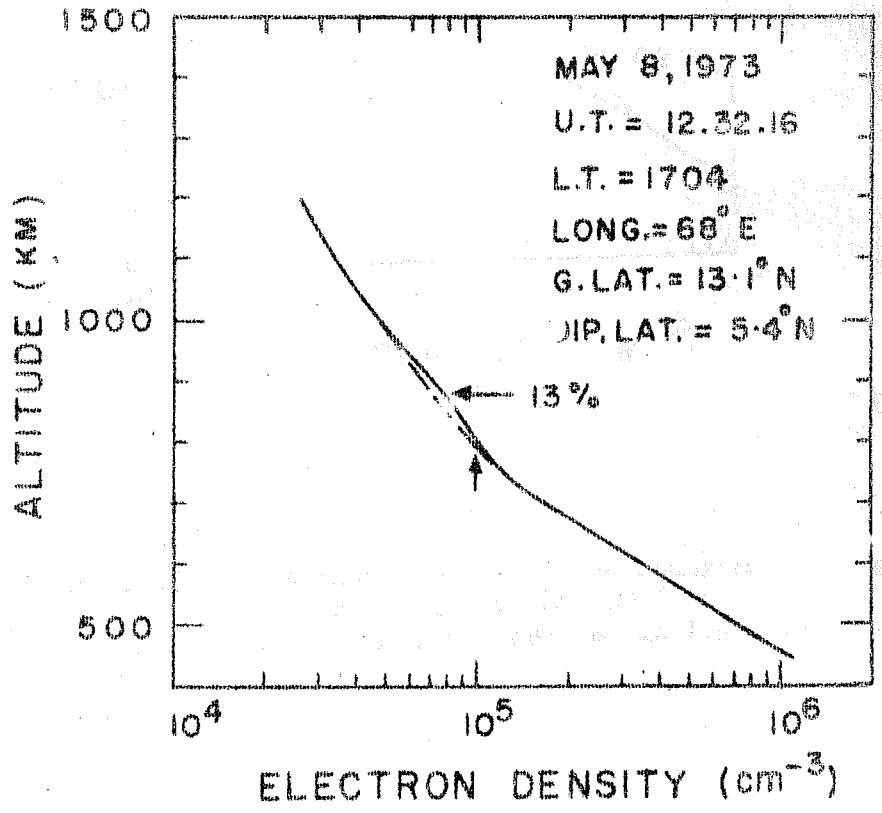


(b)

Fig. 5.2(a,b):- Same as in Fig. 5.1(a,b) obtained on May 8, 1973 at 1704 hr LT by means of ISIS-1 satellite.

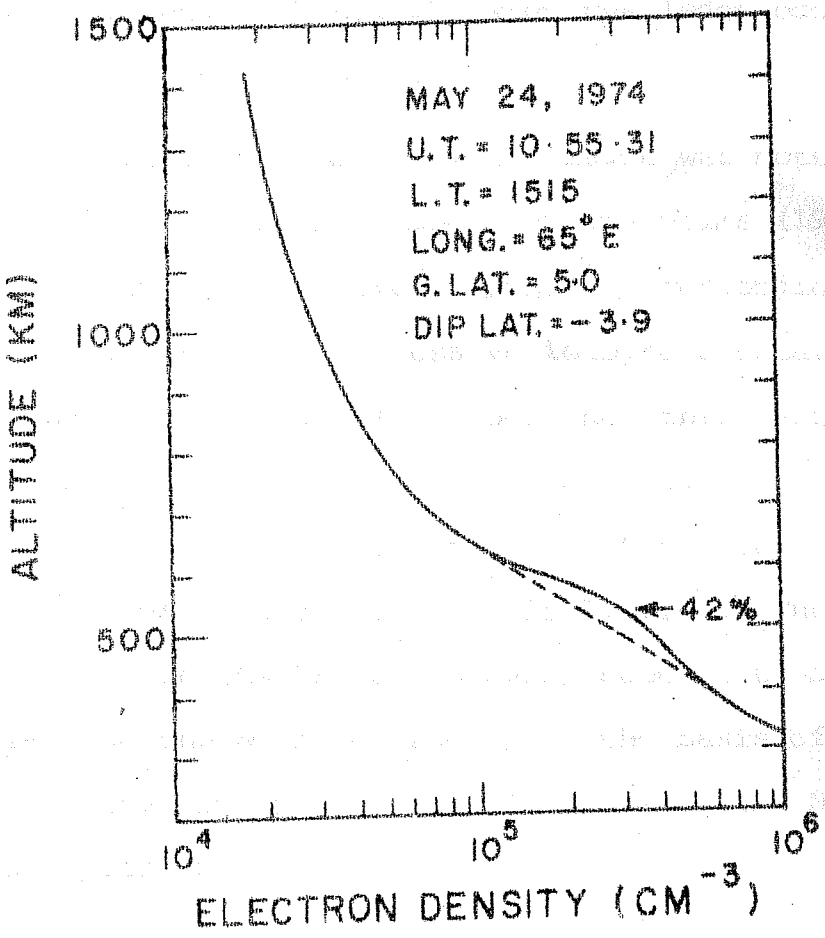


Fig.3.5:- N(h) profile obtained from an ISIS-2 ionogram with the cusp formation on May 24, 1974 at 1515 hr LT. The details are same as in Fig.1(b).

hours. The N(h) profiles presented in Fig. 3.4 showing ionisation ledges at different local times also reveal this feature (at 10.0 and 10.7 hrs LT) when the ledge occurs nearest to the altitude of the F2 peak.

The field alignment of the ledge was noted by King et al. (1964) as well as Lockwood and Nelms (1964). These authors computed the true heights corresponding to the frequency of cusp tips on successive ionograms obtained during individual satellite passes and found that these altitudes lie on a magnetic field line, henceforth referred to as "cusp-tip field line". These authors found that the cusp-tip field line is coincident with the anomaly field line. The diurnal behaviour of the IA itself is, however, seen to be different in the Asian and the American zones, on the basis of the examples presented by King et al. and Lockwood and Nelms for the same year (1962).

King et al. showed that the IA usually develops around 1000 hr LT. The height of the top of the anomaly field line increases until about 1500 hr and then decreases with local time until the IA collapses around 2200 hr LT. The magnetic field line passing through the cusp-tip altitudes (being coincident with the anomaly field line) also shows the same diurnal behaviour as the anomaly field line. They presented (in Fig. 40 of their paper) the cusp-tip field lines on four occasions at 1545, 1930, 2030 and 2045 hrs LT,

which shows that the altitude of the top of the field line decreases with increasing time.

Lockwood and Nelms (1964) however, observed the diurnal behaviours of the IA and the ledge in the American zone to be different than that in the Asian zone shown by King et al. The diurnal development of IA as well as the ledge, according to Lockwood and Nelms, depends upon the magnetic activity. On quiet days ($K_p \leq 2^+$) the IA formed around 1100 hr and persisted until about 2200 hr LT. The anomaly moved to higher magnetic field lines with increasing local time. The location of the ledge was found to be on the anomaly field line and therefore the altitude variation of the ledge followed the same diurnal behaviour as that of the IA. On disturbed days ($K_p > 2^+$), however, the IA as well as the ledge was not observed until 1730 hr LT. The ledge was located on the anomaly field line and the altitude of the top of the field line increased with local time between 1730 and 2200 hrs. Thus the movement of the ledge to the higher field lines until about 2200 hr LT in the American zone is strikingly different than the behaviour observed by King et al. in the Asian zone.

On the basis of the ledge observations revealing its presence between 1730 and 2200 hrs LT, Lockwood and Nelms suggested that the longitudinal extent of the ledge is about $70^o$ centered near 2000 hr LT. The observed increase in the height of the ledge at the equator with increasing time of

day, reveals that the ledge exists along higher field lines at 2200 hr than at 1730 hr LT. On the basis of these features, they suggested: "the ledge defines a surface or shell of ionisation whose north-south locus is a magnetic field line and whose east-west locus is a series of field lines that reach successively higher field lines".

Rishbeth et al. (1966) also investigated the ledge formation in the topside ionosphere by using Alouette-1 ionogram data in the American zone. They found that the ledge occurs in the altitude region dominated by the light ions, $He^+$ and $H^+$.

Van Zandt et al. (1972) observed enhancement in the electron concentration on the N(h) profiles obtained by means of the incoherent scatter radar at the equatorial station, Jicamarca. Fig. 3.4 reproduced from their work shows the diurnal development of the ionisation ledge on a single day in the year 1964. This example is perhaps the only one reported in literature regarding the diurnal development of the ledge on a single day. The ledge is seen to form at 10.0 hr near the $h_{max}F2$ altitude subsequently moving up with time until 13.1 hr, and then onwards maintains itself at nearly constant altitude until 16.1 hr.

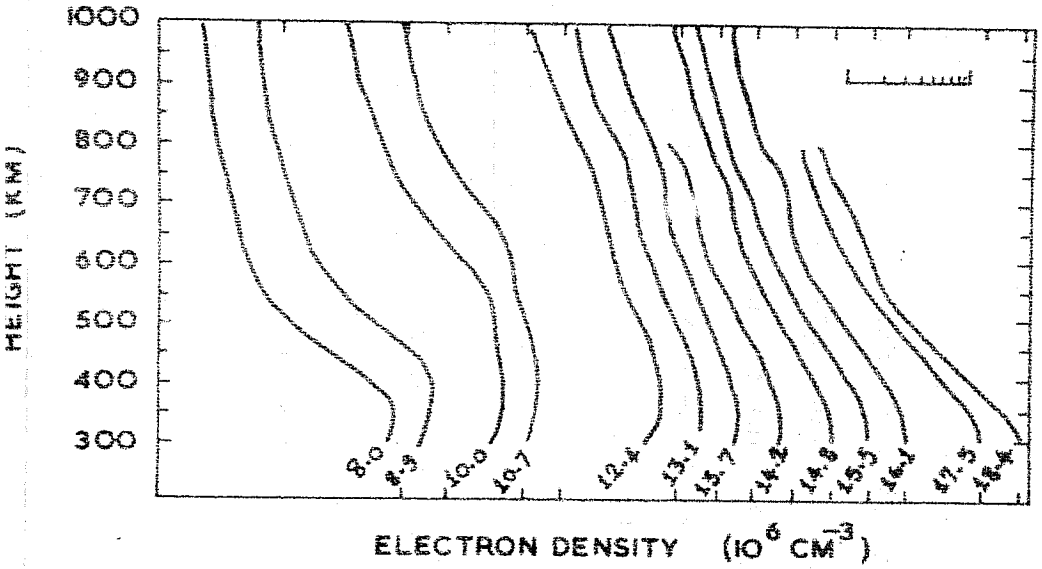


Fig.3.4

Fig.3.4:- Diurnal variation of the ledge during the course of a single day in 1964 obtained by means of Jicamarca radar. The numbers marked against the individual N(h) profiles are the local times.

Fig.3.5:- The diurnal development of the ledge for periods of low and high solar activity as obtained from Alouette-1 ionograms. The details are given in the text.

(Both reproduced from Van Zandt et al, 1972)

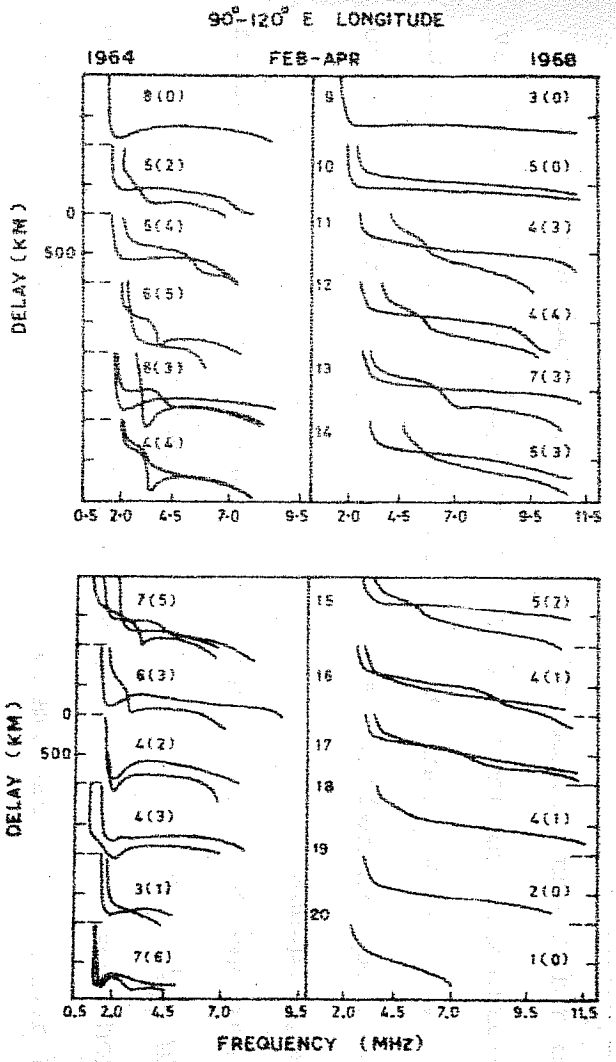


Fig.3.5

Van Zandt et al. also presented the solar cycle variations of the ledge in the Asian zone on Alouette-1 ionograms. Fig. 3.5 reproduced from their work shows the occurrence frequency of the cusps at different local hours for the years 1964 and 1968 (low and higher sunspot years respectively). The figure gives the copies of the ionogram echo traces at different local hours; 9-14 hrs in the upper half and 15-20 hrs in the lower half part. For each hour, the number of passes with usable ionograms and the number of passes with ledges (the latter written inside the parentheses) are mentioned. In 1964, the ledge is first observed between 10 hr and 11 hr LT and is seen to be present until 2000 hr LT. In 1968 the ledge first forms between 11 hr and 12 hr LT, the occurrence decreases after 1500 hr LT and it disappears after sunset. Van Zandt et al. state that the difference in diurnal behaviour of the ledge does not necessarily indicate that the causative mechanism of the ledge is different in the two epochs. However, they mention that the absence of the ledge after sunset in the high sunspot year 1968 is probably significant.

Raghavarao and Sivaraman (1974, 1975) investigated the phenomenon of ledge formation in the topside ionosphere by means of the ISIS-1 and 2 topside data recorded at Ahmedabad during 1972-73 revealing prominent cusp formation on the ionograms. They calculated the excess percentage electron concentrations in the ledge from the N(h) profiles obtained in a satellite pass and showed that the altitudes of

ledge maxima at different latitudes lie on a magnetic field line, henceforth referred to as the "ledge field line". By definition, the "ledge field line" would be higher than the "cusp-tip field line" by the altitude equal to half the vertical extent of the ledge on the N(h) profile at the magnetic equator.

Fig. 3.6, reproduced from RS1, shows the latitudinal plot of constant electron concentration in the topside ionosphere, from an ISIS-2 pass on Oct. 6, 1972 at 1240 hr ($70^{\circ}$ EMT). The 'squares' denote the location of the ledge maxima and the magnetic field line passing through these is seen to be the same as the anomaly field line. The open circles denote the true heights corresponding to the frequency of the cusp tips at various latitudes. The apex of the cusp-tip field line is about 90 km lower than the anomaly field line. This observation thus differs from that of King et al. (1964) which showed the cusp tip field line to be coincident with the anomaly field line.

Fig. 3.7, reproduced from RS2, shows the constant electron concentration plot obtained from an ISIS-2 pass on Oct. 7, 1973 at 2040 hr ($77^{\circ}$ EMT). The equatorial heights of the ledge field line and the cusp-tip field line are 1075 km and 960 km respectively. The presence of the ionisation anomaly is doubtful. If at all it occurs, the crest to trough

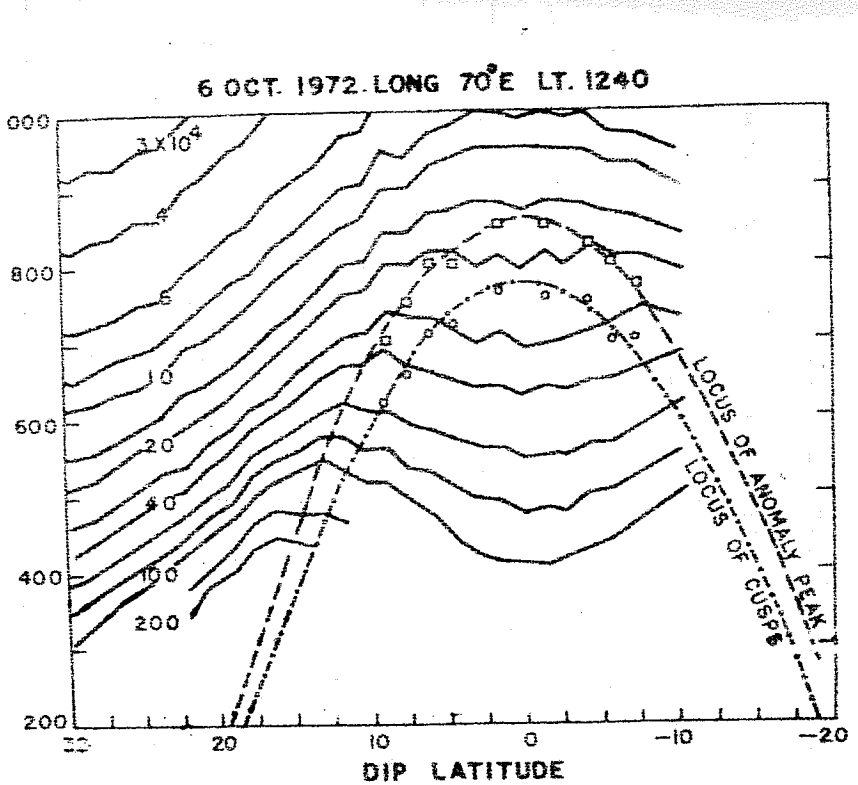


Fig. 3.6

Fig.3.6:- Latitudinal variation of the height of the constant electron concentration on Oct. 6,1972 at 1240 hr at 70°E longitude (after Raghavarao and Sivaraman, 1974).

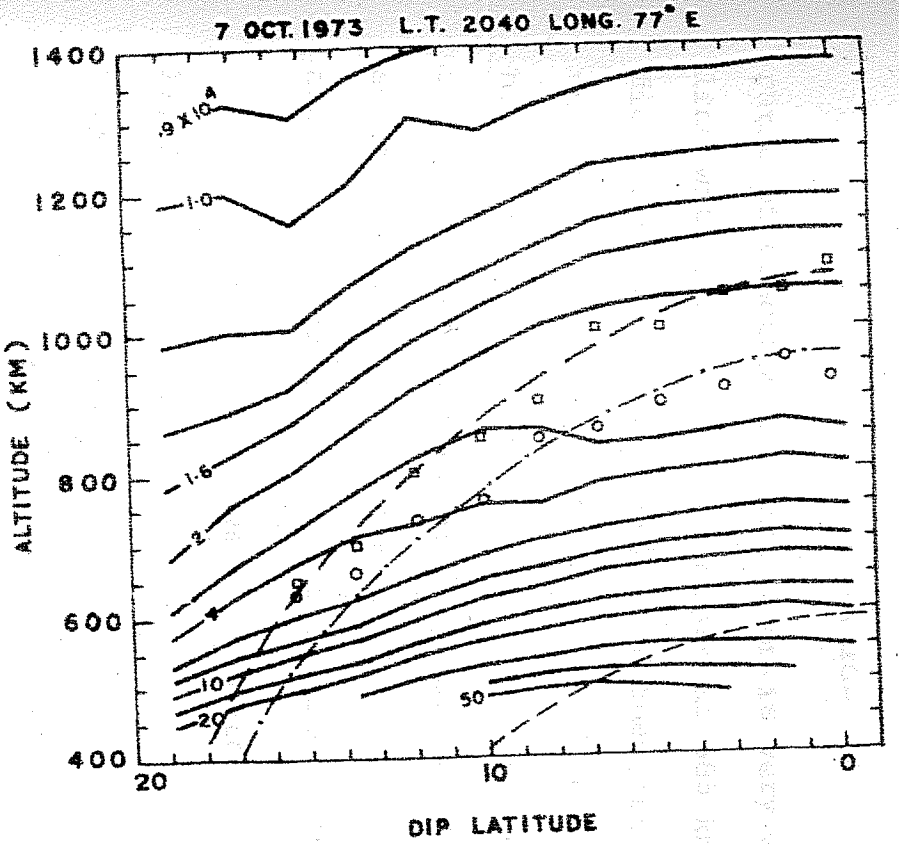


Fig. 3.7

Fig. 3.7:- Same as in Fig. 3.6 on Oct. 7, 1973 at 2040 hr at 77°E longitude (after Raghavarao and Sivaraman, 1975).

ratio of electron concentration is very small and magnetic field line with its equatorial height as 585 km would be the anomaly field line. Thus the work of Raghavarao and Sivaraman shows that the ionisation ledge can be present at the premidnight hour, even though the IA becomes very weak. This result differs from that presented by King et al. (1964) and Lockwood and Nelms (1964) which showed the ionisation ledge to be associated with intense IA formation only.

Fig. 3.8 shows the constant height plot on March 19, 1974 at 2015 hr corresponding to the ledge observation shown in Fig. 3.1(a,b). The electron concentration at any altitude is maximum at the magnetic equator thus showing the absence of IA. This result supplements the result of RS2 (shown in Fig. 3.7) in that the ledge could be present in the premidnight hours when the IA completely disappears.

The daily variation of the altitudes of the top of the ledge field line and the corresponding anomaly field line are shown in Fig. 3.9(a) and 3.9(b) respectively, in which a pair of corresponding data points represents the observations on one day. The altitudes of the two field lines are estimated from the same satellite pass in the manner illustrated in Figs.3.6 and 3.7. The error in estimating the altitude of the ledge field line is about $\pm$25 km and is due to the subjectivity in delineating the magnetic field line due to the scatter of the ledge maxima points.

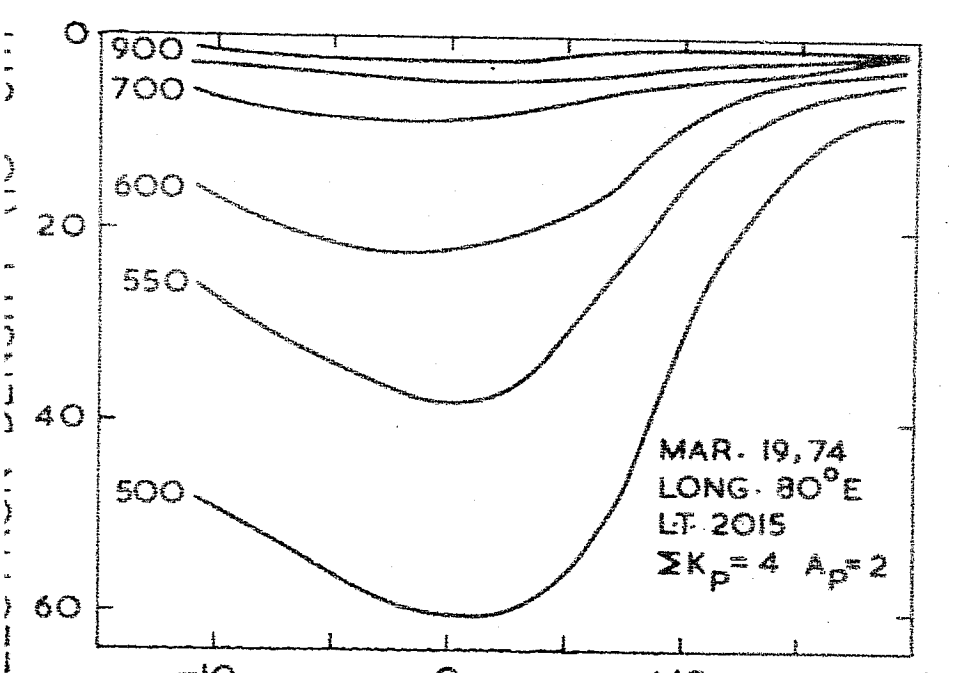


Fig. 3.8

Fig. 3.8:- Latitudinal variation of electron concentration at constant altitudes on March 19, 1974 at 2015 hr LT at 80°E long.

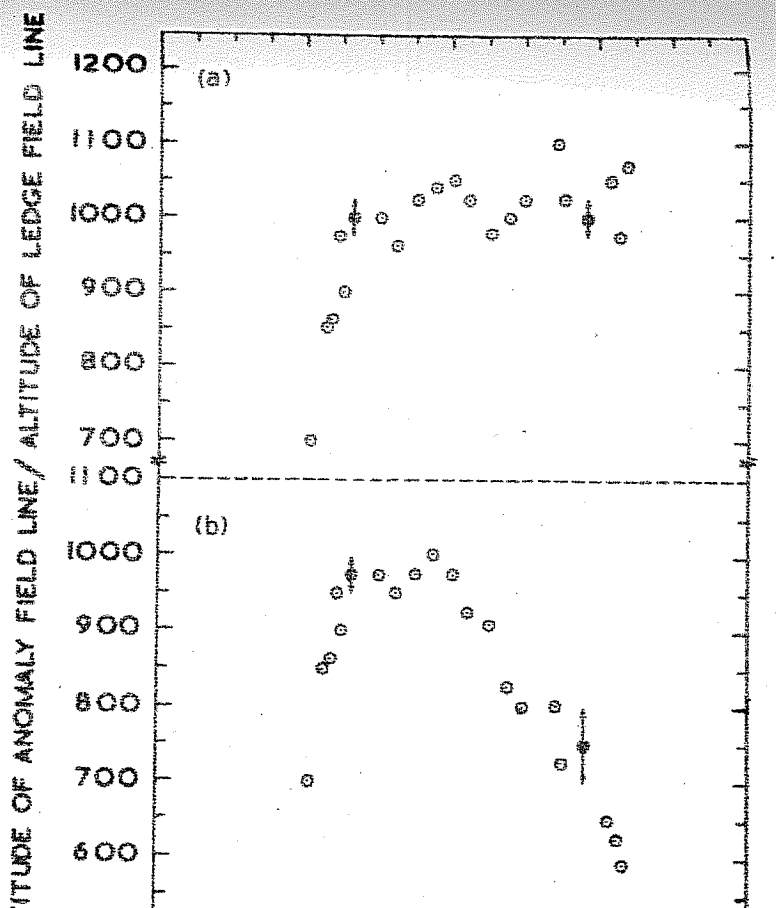


Fig.3.9(a,b)

Fig.3.9(a,b):- Daily variation of the altitudes of the top of the ledge field line and anomaly field line. The pair of data points in (a) and (b) at any particular LT are obtained from a single satellite pass.

The subjectivity in delineating the altitude of the anomaly field line is about ±25 km when the anomaly is strong (i.e. the peaks are well defined, e.g. shown in Fig. 3.6). However, in the evening hours, when the anomaly is very weak (e.g. Fig. 3.7) the subjective error in delineating the field line, due to the poorly defined peaks, could be upto ±50 km. The comparison of the corresponding data points of Fig. 3.9(a) and 3.9(b) reveals that the two field lines are the same until about 1530 hr LT. The pair of data points at 1600 hr LT shows that the ledge field line is higher than the anomaly field line by about 100 km. After 1600 hr, the difference in the equatorial heights of the two field lines increases with time. The top of the ledge field line goes up in altitude between 1700-2100 hrs LT, after the slight dip between 1600 and 1700 hrs. However, the altitude of the anomaly field line decreases rapidly with time due to the decay of the anomaly in the evening hours.

The diurnal variation of the altitude of the ledge field line, shown in Fig. 3.9(a), differs from the result of King et al. (1964) mentioned earlier. However, the daily variation of the altitude of the anomaly field line shown in Fig. 3.9(b) is consistent with the observations of King et al. showing that the anomaly field line altitude increasesuntil about 1500 hr LT and decreases smoothly in the evening hours.

The diurnal variation of the top of the ledge field line shown in Fig. 3.9(a) is consistent with the result of Lockwood and Nelms described earlier.

Fig. 3.9(a,b) reveals a very interesting feature of the ionisation ledges viz., until about 1530 hr LT the ionisation ledge seems to be coupled to the anomaly field line. Around 1600 hr LT, however, the ledge detaches itself from the IA and moves onto higher magnetic field lines with increasing local time. In the evening hours, although, the IA collapses, the ledge remains virtually unaffected.

## III.3 SOME NEW FEATURES OF THE IONISATION LEDGE

The author now presents some interesting morphological features of the ionisation ledges observed in the longitude zone $50^{o}$ - $100^{o}$E covered by the ISIS-1 and 2 passes recorded at Ahmedabad.

1) The ledge formation is observed on the satellite passes recorded around midday when the IA is fairly well developed. Fig. 3.10(a,b,c) illustrates this point. The figure shows the latitudinal distribution of electron concentration at constant altitudes on three consecutive days, Oct. 12-14, 1972, obtained from the ISIS-2 satellite data. Fig. 3.10(a) shows that on Oct. 12, the IA is not formed at 1209 hr LT. None of the ionograms for this pass shows cusp formation. On Oct. 13, the constant height plot

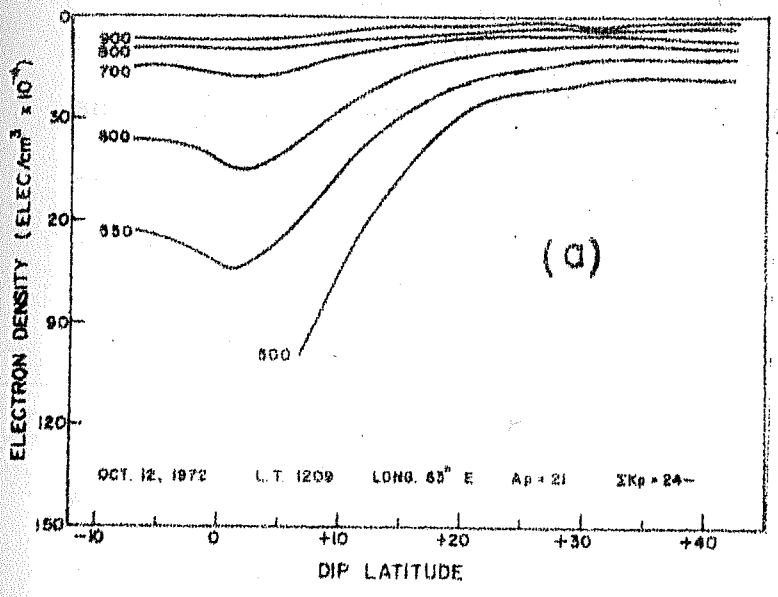


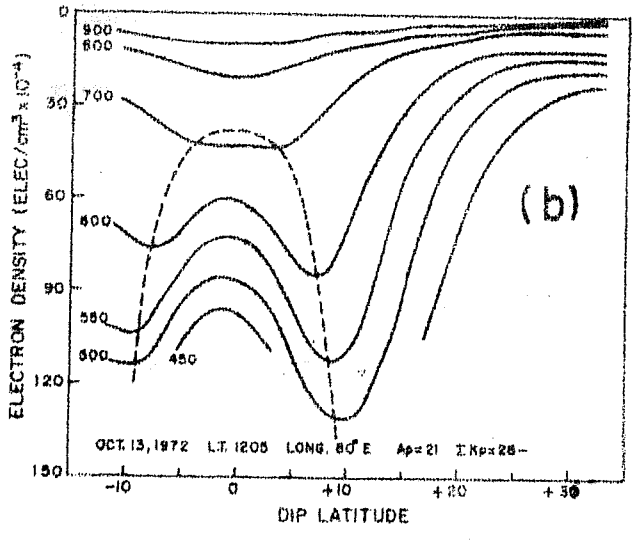


Fig. 3.10(a, b, c):- Latitudinal distribution of electron concentration at constant altitudes on Oct. 12-14, 1972 by means of ISIS-2 satellite.

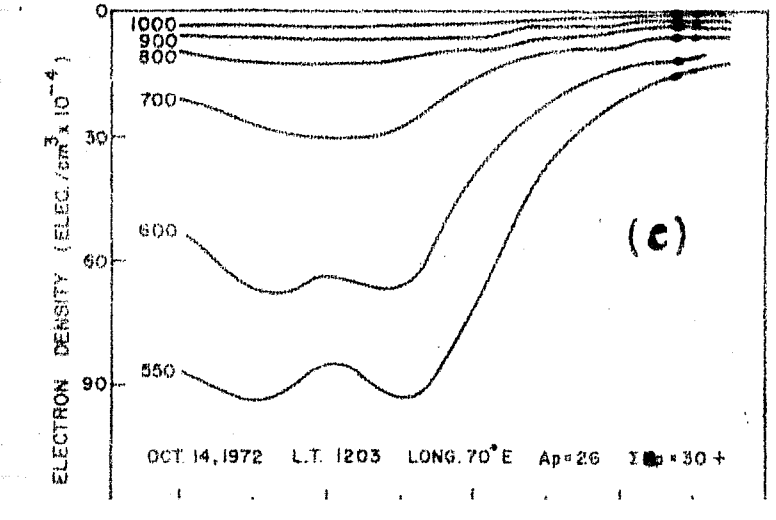

shown in Fig. 3.10(b) reveals the presence of prominently developed anomaly peaks at 1205 hr LT. The ionograms corresponding to this pass show cusp formation; the maximum excess electron concentration in the ledge being about 13%. Fig. 3.10(c) shows that the IA is very weakly developed on Oct.14 at 1203 hr LT. The ionograms obtained during this pass do not show cusp formation. From these examples it is apparent that the ledge formation necessitates the presence of well developed IA peaks around midday hours. The significance of this feature is discussed in the Sec. III.4 in view of the explanation of the ledge proposed by Raghavarao and Sivaraman (1974).

2) Two consecutive passes of the polar orbiting satellites ISIS-1 and ISIS-2, differing in U.T. by 2 hours, occur at two longitudes about $30^{\circ}$ apart and hence the local time of the two passes is nearly the same. It is interesting to compare the occurrence and intensity of the ledge at two longitudes $30^{\circ}$ apart at the same local time.

Fig. 3.11 shows two N(h) profiles, marked A and B, obtained from two consecutive passes of ISIS-2 on Oct. 5, 1972. These two passes at 0721 UT at $80^{\circ}$E longitude (pass 07007) and the next pass at 0917 UT at $51^{\circ}$E longitude (pass 07008) are at nearly the same local time, 1245 hr. The two N(h) profiles A and B showing the presence of the ledge are computed from two ionograms at nearly the same dip latitude ($7^{\circ}$) at

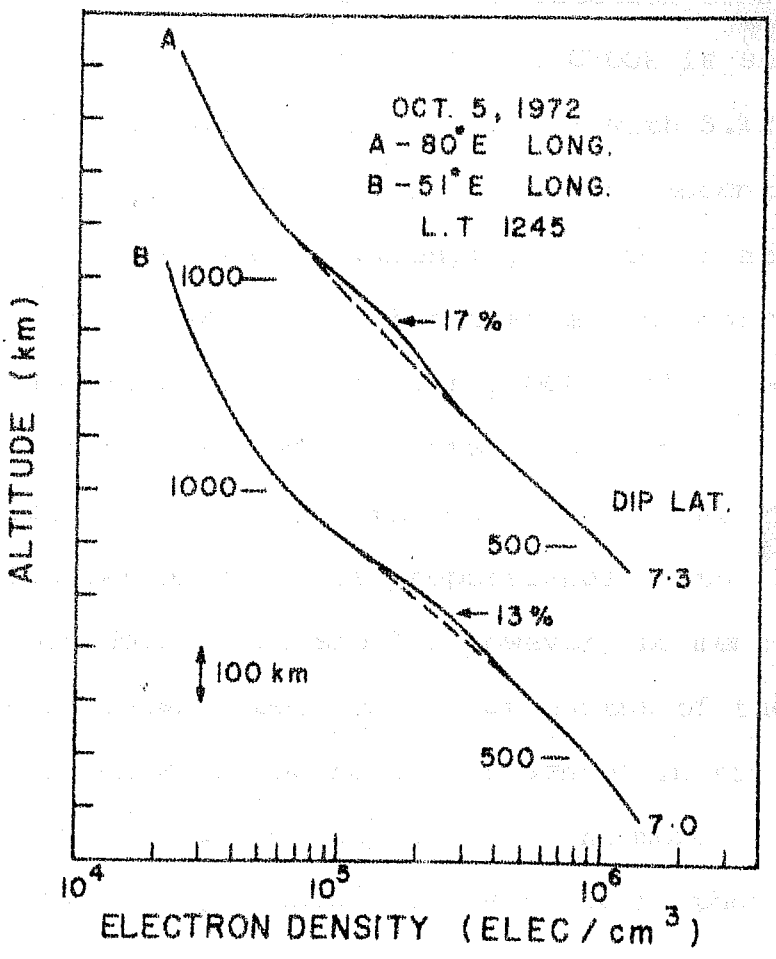


Fig.5.11:- Two N(h) profiles (marked A and B) showing ledges of ionisation on Oct. 5, 1972 at 1245 hr LT obtained from two consecutive ISIS-2 passes 07007 and 07008 respectively.

07.25.11 and 09.18.32 hrs UT respectively. The maximum excess electron concentrations in the ledge on the profiles A and B are 17% and 13% respectively.

The latitudinal distribution of electron concentration at constant heights for the passes 07007 and 07008 is shown in Fig. 3.12(a,b). The comparison of Fig.3.12(a) with 3.12(b) shows that the crest to trough ratio of electron concentration at any altitude, revealing the IA strength, is higher at the longitude 80°E (of pass 07007) than that at the corresponding altitude for the longitude 51°E (of pass 07008). The comparison of the ledge strengths at the two longitudes with the corresponding IA strength leads to the conclusion that the strength of the ionisation ledge is proportional to the IA strength around noon hours. It should, however, be mentioned that the linear relationship between the strengths of the ledge and the IA, in view of the result presented in Fig. 3.9(a,b), is true only around midday hours. The more important feature revealed by these observations is that the ionisation ledge as well as the IA are present at two closeby longitudes with different intensities at the same local time.

Fig. 3.13 shows two N(h) profiles, marked A and B, at about 3° dip latitude obtained from two consecutive ISIS-2 passes 16901 and 16902 respectively, recorded on Nov. 25, 1974. The passes 16901 and 16902 were recorded at 0645 UT

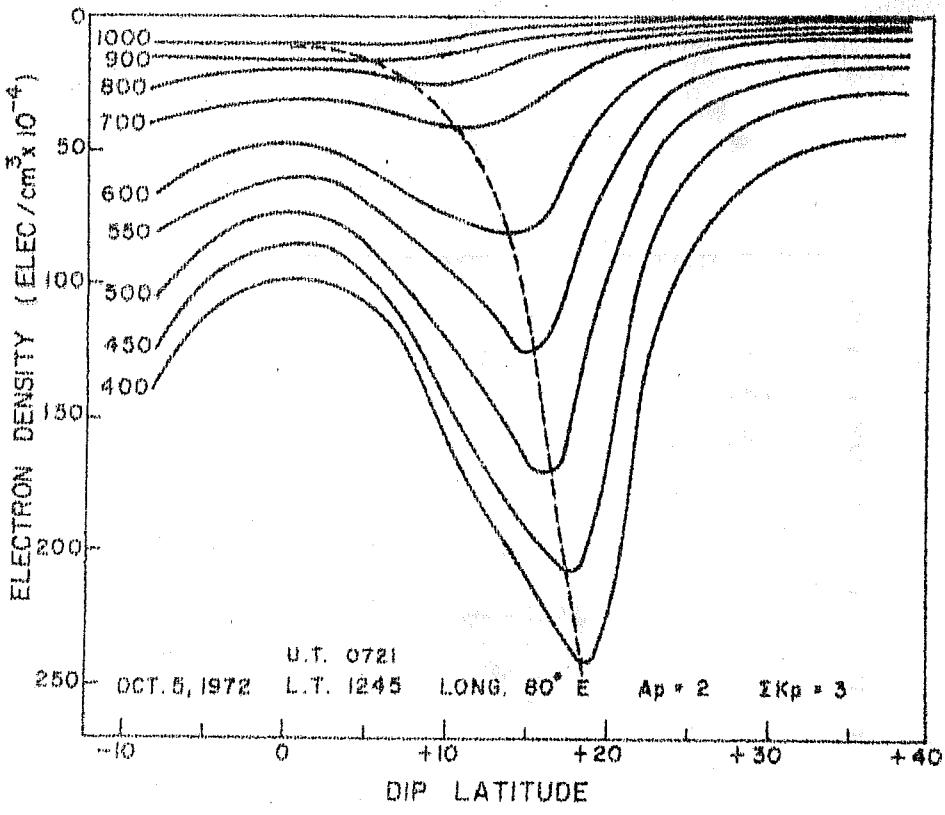


(a)

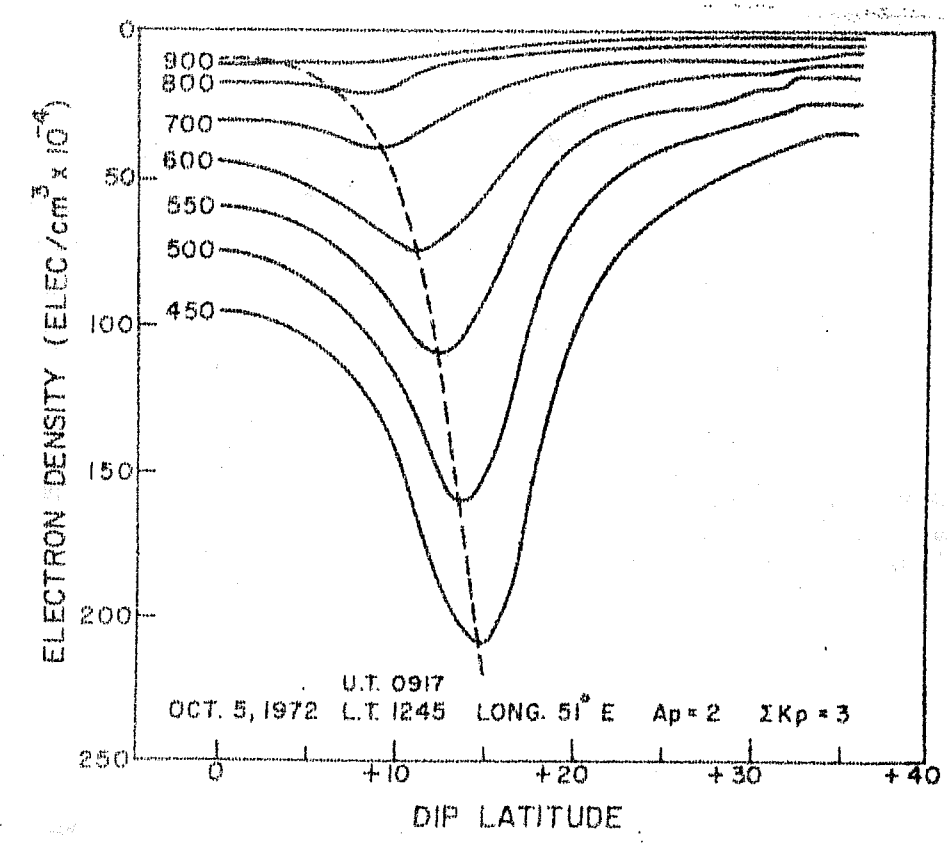


(b)

Fig.5.12(a,b):- Latitudinal distribution of electron concentration

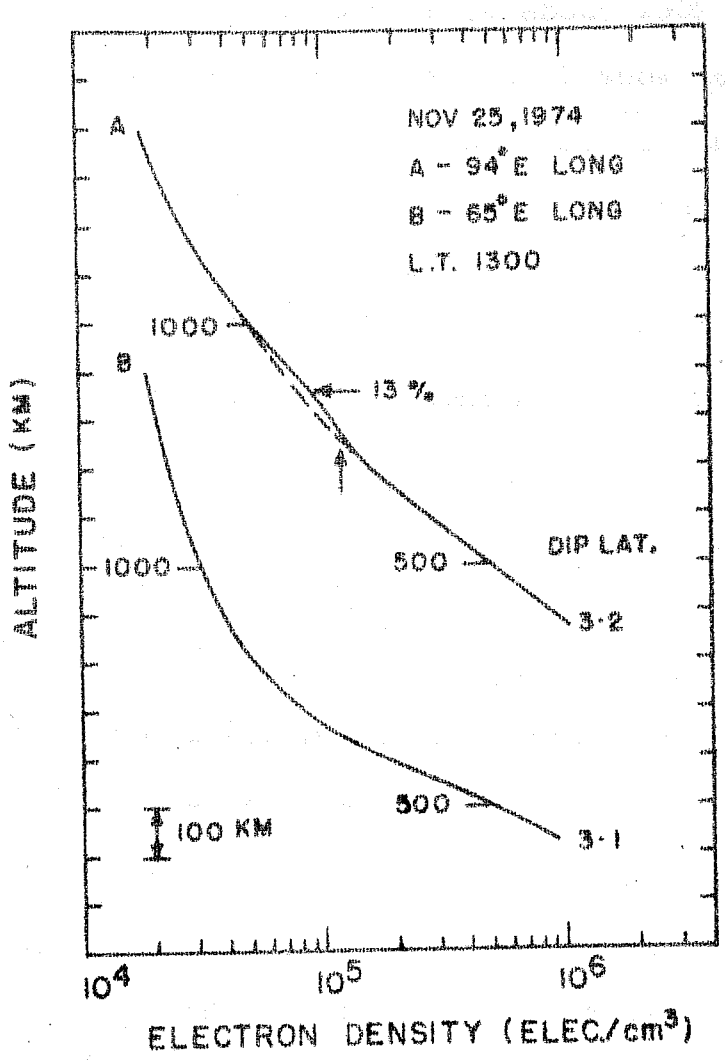


Fig.3.13:- The N(h) profiles (marked A and B)at nearly the same dip latitude obtained from the ISIS-2 passes 16901 and 16902 respectively on Nov. 25, 1974 at about 1300 hr LT.

($94^{o}$E longitude) and 0840 UT ($65^{o}$E longitude) respectively. The local time for both the passes is about 1300 hr. The ionograms corresponding to the pass 16901 show cusp formation whereas none of the ionograms corresponding to the pass 16902 shows cusp formation. The profile 'A' shows the presence of the ionisation ledge, with maximum intensity 13% at 860 km altitude. The profile 'B' derived from a normal ionogram shows a smooth decrease of electron concentration in the topside ionosphere.

Fig. 3.14(a,b) shows the latitudinal distribution of electron concentration at various fixed altitudes obtained from the passes 16901 and 16902 respectively. It is apparent from this figure that the IA is prominently developed at $94^{o}$E longitude at 1300 hr LT and is not developed at $65^{o}$E longitude at the same local time.

The observations presented in Figs. 3.11 - 3.14 are very interesting in that they bring out two new features of the ionisation ledge as well as the ionisation anomaly.

a) They occur, on occasion, in a narrow longitude zone as revealed by the examples presented in Fig. 3.13 and 3.14. Both are present at $94^{o}$E longitude and absent at $65^{o}$E longitude.

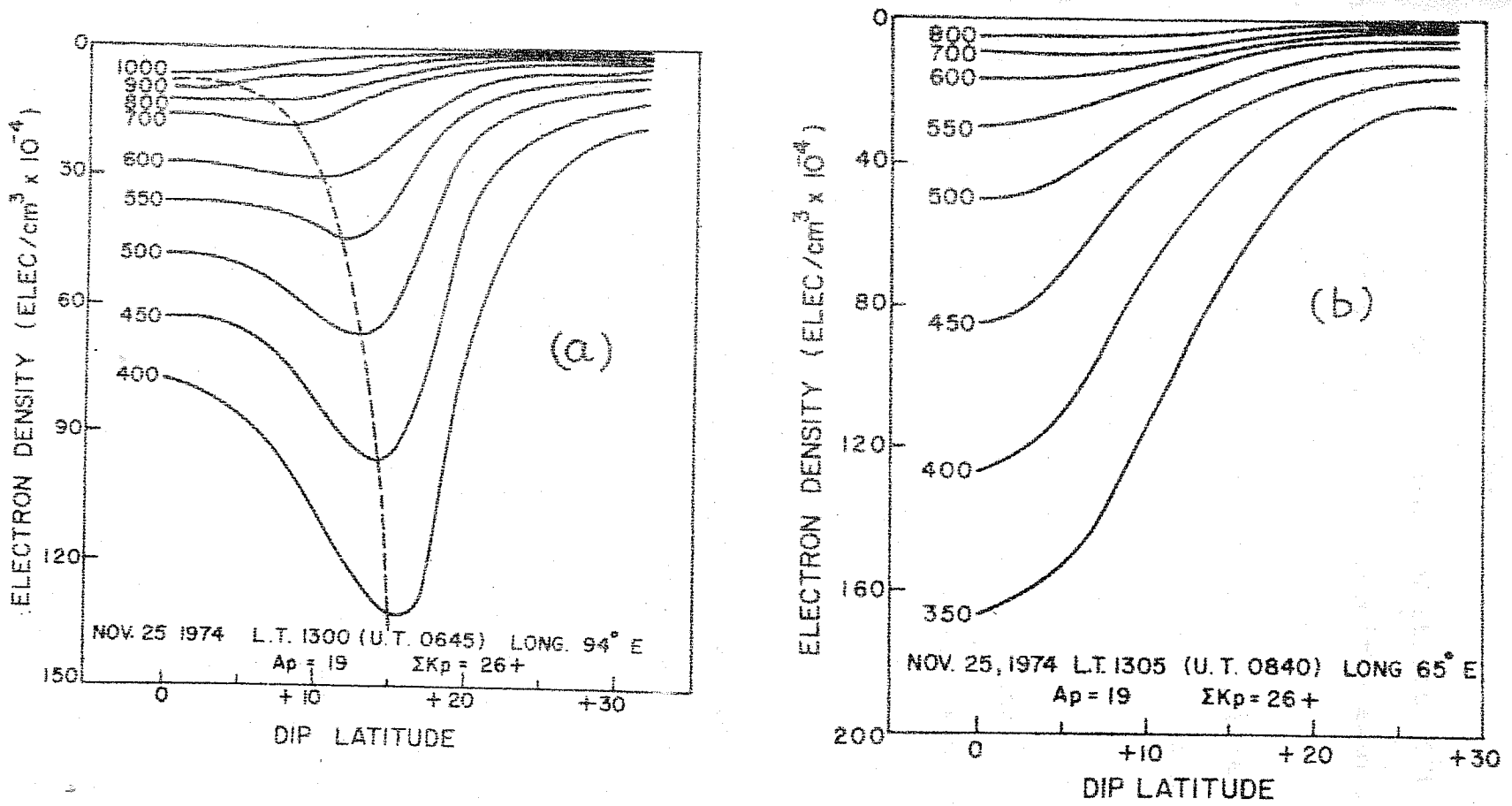


**Fig.5.14(a,b):-** **Latitudinal distribution of electron concentration at constant altitudes obtained from the ISIS-2 passes 16901 and 16902 respectively.**

b) They occur at the longitudes 80°E and 51°E but with different strengths, as seen from the examples in Figs. 3.11 and 3.12.

It may be noted that the features (a) and (b) have been reported in the counter-electrojet phenomenon in the E region (Gouin and Mayaud, 1967; Kane 1973a ; Rastogi 1973a, 1974 ). It should also be mentioned that these features of the IA have not been reported in literature so far.

3) It is found that the ledge usually occurs on a sequence of days in succession although there are some exceptions. An evidence for its occurrence on a sequence of days is presented in Fig. 3.15. The figure shows the spatial distribution of excess electron concentration in the ledge on 5 days between Oct. 4-9, 1972 obtained by means of ISIS-2 satellite. On Oct. 8, the ionogram data are not good due to local interference caused by noise. However, cusp formations are seen on the ionograms. The contours represent excess percentage electron concentrations in the ledge over the ambient level, the outermost contour represents 0% excess ionisation and thus delineates the boundary of the ledge. The inner contours represent excess concentrations in increasing steps of 5% on Oct. 4-7 and in steps of 10% on Oct. 9. The dashed lines represent the earth's magnetic field lines. The position of the magnetic equator is approximately at 9° geographic latitude for the longitude zone 60° - 90°E.

It may be noted that the ledge on Oct. 9, 1972 is the lowest in altitude and the highest in intensity, of the sequence of observations shown in Fig. 3.15. The individual N(h) profiles at different latitudes from which the spatial structure on Oct. 9 is obtained, reveal that the ledge occurs below the $O^+ - H^+$ transition altitude. This observation supports the conclusion stated in Sec. 3.2 that the ledge is more intense when it occurs near the F2 layer peak than in the case when it occurs higher up. An explanation for this behaviour of the ledge is given in Sec. III.4 on the basis of the mechanism proposed by RS1.

The spatial structures of the ledge (such as shown in Fig. 3.15) are described in Chapter 4. It is shown that the spatial distribution of the ledge intensity reveals some interesting features of the interaction between the ionised and the neutral atmosphere at the F region altitudes.

## III.4 INTERPRETATIONS OF THE IONISATION LEDGE

King et al. (1964) considered the ionisation ledge as a natural manifestation of the presence of the IA on the N(h) distribution in the topside ionosphere. According to these authors, the presence of IA, having enhanced ionisation concentration along the anomaly field line, would reveal a distortion on the N(h) profiles when the column investigated intersects the enhanced arch of ionisation on which the anomaly peaks lie. In particular, at the locations where the

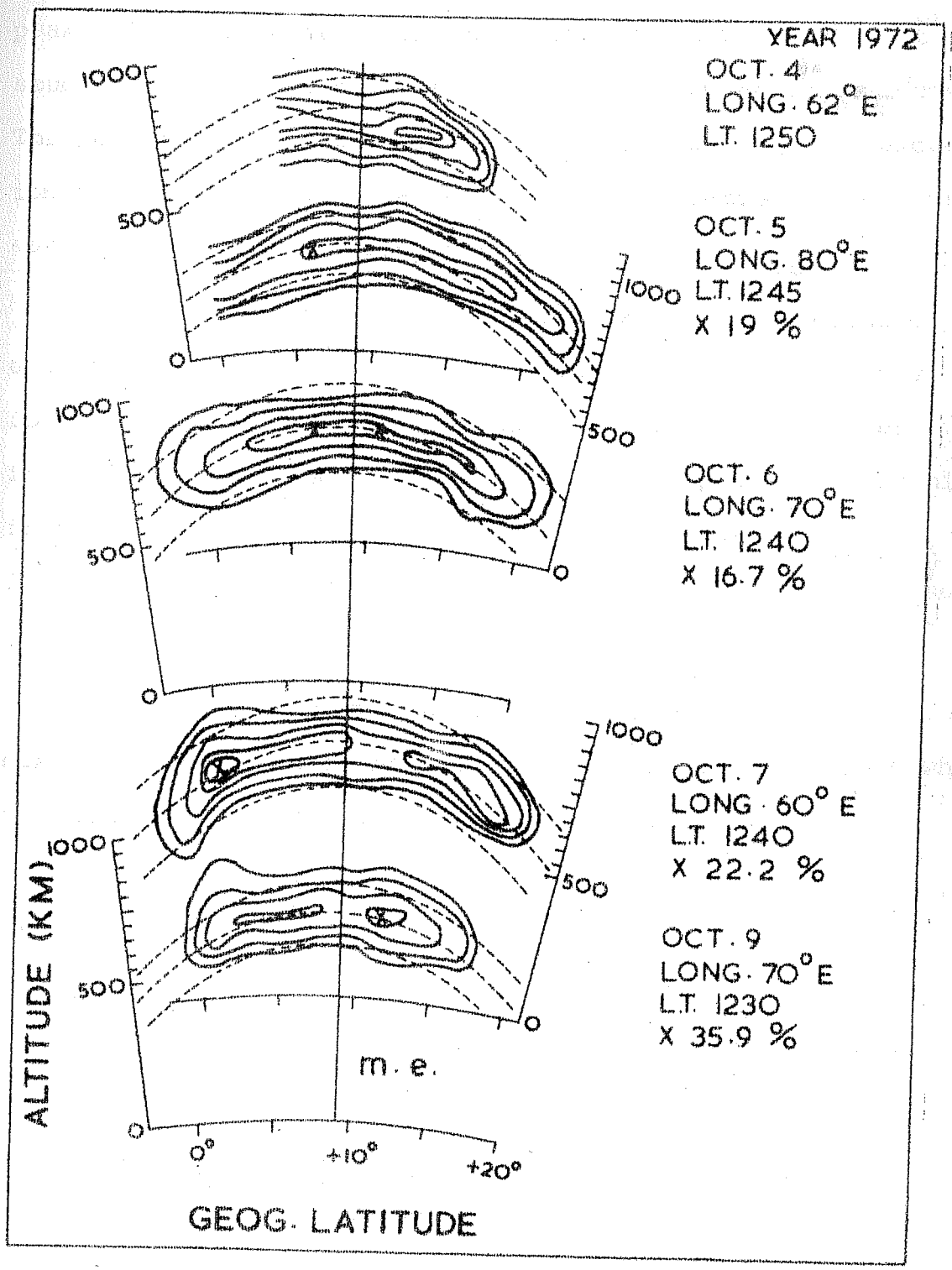


Fig.3.15:- Contours of excess percentage electron concentration in the ledge on Oct. 4-7 and Oct. 9, 1972 as described in the text.

peaks of the IA occur along the anomaly field line, the topside sounder will experience more ionisation than at other locations. Thus, according to the explanation of King et al., the excess ionisation in the ledge at a particular location is just that associated with the relevant anomaly peak.

The explanation offered by King et al. could explain one of the features by which the ledge manifests itself on the ionograms, namely, the cusps usually occur at the lowest frequency over the magnetic equator and at progressively higher frequencies towards either crest of IA. However, the following features of the ionisation ledge cannot be explained on the basis of their explanation.

1) The formation of IA is almost an everyday phenomenon but the ledge is not observed on all the occasions when the anomaly is present.

2) If the explanation of King et al. were correct, there should be no ledge formation at the magnetic equator where the trough of the IA occurs. However, King et al. did observe the ledge at the magnetic equator. Our observations of the spatial distribution of the ledge intensity shown in Fig. 3.15 and a number of spatial structures shown in Chapter 4, reveal that the ledge is always present at the magnetic equator. In fact, on most occasions in the equinoctial period, the ledge at or near the equator is found to be stronger than at the latitudes of the IA crest. For instance, on all the

five occasions during Oct. 72 presented in Fig. 3.15, the ledge maxima occur within $\pm$ 10$^{o}$ latitude of the magnetic equator, whereas the anomaly crests occur farther away. More specifically, on Oct. 6, 1972 the ledge maxima occur within $\pm$2$^{o}$ geographic latitude ($\pm$1.5$^{o}$ dip lat.) of the magnetic equator (at 9$^{o}$ geog. lat.) as seen from Fig. 3.15. The dip latitude of the northern crest of the anomaly on the same day is found to occur at about 18$^{o}$ dip latitude, as apparent from Fig. 3.6.

(3) According to the mechanism of King et al., the magnetic field line passing through the ledge should be the same as the anomaly field line, and also that the ledge should not be observed when the IA is absent. However, the observations presented in Fig. 3.9(a,b) reveal that the ledge field line is distinctly higher than the anomaly field line after 1600 hr LT. Figs. 3.7 and 3.8 reveal that the ledge is present even though the IA is either very weak or absent.

Lockwood and Nelms (1964) studied the ledge formation in the American zone using Alouette-1 ionograms. The location of the ledge was found to be along the anomaly field line. They found that the ledge developed earlier on magnetically quiet days than on disturbed days. A qualitative interpretation of the ledge was suggested by Lockwood and Nelms on the basis of their observations in the following manner.

The upward movement of ionisation caused by the eastward electric field produces an increased concentration (dome) over the magnetic equator. This process starts after sunrise and continues until mid-afternoon. In the afternoon, the upward drift is reduced and the ionisation begins to fall, first along the low and then along successively higher field lines. The redistribution of ionisation along a particular field line causes the contours of fixed electron concentration to appear flat below and dome shaped above the field line (e.g. see Fig. 3.6). The apparent excess ionisation above the field line is observed as the ledge.

The explanation of Lockwood and Nelms can be best summarised in the following sentences reproduced from their paper : "The redistribution of ionisation below the field line leaves an apparent excess of ionisation above, causing the field-aligned ledge observed by the topside sounder. The ledge represents the transition between elevated ionisation at higher heights and redistributed ionisation below".

The explanation of Lockwood and Nelms for the ledge formation is similar to that of King et al. (1964), except that they describe it by the physical process responsible for giving rise to an apparent excess ionisation along the anomaly field line. Hence the same discrepancies, which are pointed out for King et al.'s explanation also arise for the mechanism of Lockwood and Nelms.

Rishbeth et al. (1966) also investigated the phenomenon of the ledge formation from the Alouette-1 satellite data for the American zone. They noted that the ledge occurred in the altitude region dominated by light ions, $He^+$ and $H^+$. They derived the vertical distribution profiles of the ions, $O^+$, $He^+$ and $H^+$, by assuming the diffusive equilibrium in the topside ionosphere. Their results showed that the ledge in the electron concentration profile occurs at the altitude where the ion transition $O^+ - He^+$ occurs. On the basis of their results, Rishbeth et al. suggested that the ionisation ledge at the equator is merely a manifestation of the $He^+$ profile.

Recently Bauer and Hartle (1974) showed that the F2 ledge in the ionosphere of Venus occurs at the altitude where the ion transition, $O^+ - He^+$, takes place.

Although, the author agrees with the importance of the role of ion transition in causing the ionisation ledge, the suggestion of Rishbeth et al. (1966) that the ledge in the earth's topside ionosphere is due to $O^+ - He^+$ transition is not consistent with the following facts and features of the ionisation ledge:

1) It is now known that $He^+$ is a minor constituent at the equator in the altitude range 600-1000 km during daytime, as shown by Farley et al. (1967) by means of Jicamarca back-scatter radar. The mass spectrometer measurements (Taylor, 1971) also showed that in the low latitude region $He^+$ is a

minor ion in the afternoon hour. Thus, the ion transition $O^+$ - $He^+$ considered by Rishbeth et al. is now known to be $O^+$ - $H^+$ transition. Therefore, we would compare the diurnal variation of the altitude of the ledge with the observed daily variation of the $O^+$ - $H^+$ transition altitude, in the subsequent discussion.

2) The latitudinal variation of the $O^+$ - $H^+$ ion transition height, derived by Titheride (1976) from Alouette-1 electron density profiles, shows that the transition height is practically constant within $\pm 30^o$ geomagnetic latitude and increases with increasing latitude on either side. The latitudinal variation of the ledge (e.g. shown in Figs. 3.6 and 3.7) follows a magnetic field line very precisely. Thus the latitudinal variations of the ion transition height and the altitude of the ledge are different, indicating that the two are really uncorrelated.

3) The diurnal variation of the ion transition altitude, as given by Farley et al. (1967) at the equator and Titheridge (1976) for the low latitudes, shows that these heights are lower in the evening and the premidnight hours than during daytime. The diurnal behaviour of the ion transition height at the equator cannot thus explain the local time variation of the altitude of the ionisation ledge at the equator, given in Fig. 3.9(a), which shows that the ledge occurs at higher altitudes in the evening than during daytime hours.

Van Zandt et al. (1972) sought an explanation for the ledge formation by a pulse-like sudden enhancement on the diurnal variation of the eastward electric field to produce corresponding increase in the upward $\underline{E} \times \underline{B}$ drift of ionisation at the magnetic equator. They solved the continuity equation with an enhanced vertical drift, from 12.5 m/s at 08 hr to 50 m/s at 09 hr LT followed by a symmetrical decrease. In that manner they could generate a ledge at 10.4 hr LT by the numerical simulation. However, they pointed out that there is no experimental evidence of such a spike in the vertical drift velocity at Jicamarca in the morning hours on the day when the ledge of ionisation is observed. There is no a priori physical reasoning to expect such large changes in the electric field in the morning hours in solar-minimum period when the ionisation ledges are observed. However, the most serious problem with a mechanism involving a pulse type transient causative source, would be to explain the maintenance (against diffusion) of the ledge throughout the day in the topside ionosphere, where the diffusion time constant ( $= H^2/D$, as defined in Chapter 1) is a few seconds only.

Raghavarao and Sivaraman (1974) proposed a new mechanism for the ledge formation by invoking the presence of an equatorial anomaly in the distribution of the neutrals (atomic oxygen and molecular nitrogen) similar to that observed in the ionisation. They suggested that the existence of the NA would partially inhibit the ambipolar diffusion of plasma

that is lifted at the F region altitudes at the magnetic equator due to the $\underline{E} \times \underline{B}$ force. The partial inhibition of the plasma diffusion would thus cause a 'pile-up' of the ionisation near the top of magnetic field line passing through the NA crests, thus leading to the formation of ledge.

The experimental evidence for the presence of the NA and the physical process for the ledge formation are discussed in Chapter 1. It is also mentioned there that the NA formation on a particular day requires the presence of strong IA around noon hours at which time the differential motion between the ions and the neutrals starts becoming significant, thus causing the neutral motion to be subjected to a large ion drag force. We now examine the above arguments for explaining the NA and hence the ledge formation on Oct. 6, 1972 at 1240 hr LT (Shown in Fig. 3.15).

Fig. 3.16 shows the latitudinal distribution of electron concentration on Oct. 6, 1972 at 1240 hr at a number of fixed altitudes obtained from the same pass from which the ledge structure is delineated. The contours show the presence of well developed IA; the crest to trough ratio of electron concentration (at the $h_{max}F2$ level) being 1.711. From the electron concentration contour at a fixed height, the excess percentage concentration at each $2^{o}.5$ latitude over the value at the magnetic equator is calculated. In this manner the excess percentage electron concentrations associated with

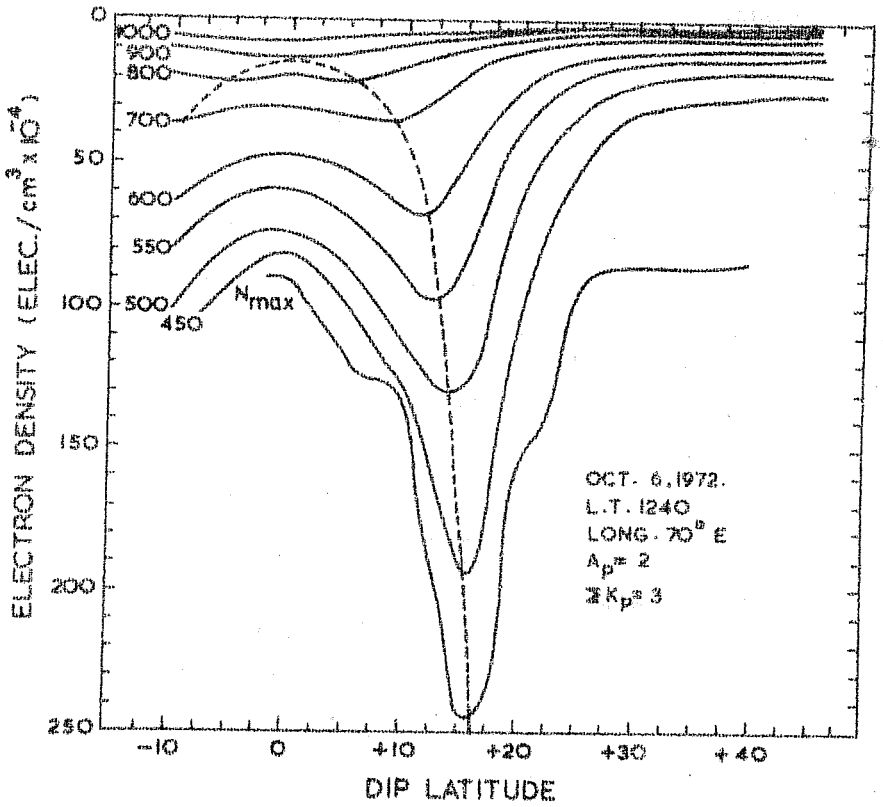


Fig. 5.16:- Latitudinal distribution of electron concentration at constant altitudes on Oct. 6, 1972 at 1240 hr($70^{0}$EMT).

the anomaly peaks are calculated for each of the constant height contours and from these values the altitudes where the excess concentrations are 20%, and in steps of 20% thereafter, are interpolated for each one of the latitudes mentioned above. These contours are shown in Fig. 3.17; the outermost being 20% and increasing in steps of 20% towards the centre, the maximum value being 170%. The dashed portions of the contours are drawn on the basis of the field aligned behaviour of the IA in the bottomside ionosphere (Croom et al. 1959). The contours on the southern side of the magnetic equator (denoted by m.e.) are drawn by the assumed symmetry of the IA in the two hemispheres during the equinoctial period. Thus Fig. 3.17 essentially gives the distribution of the excess ionisation associated with the IA peaks in the F region and the topside ionosphere. Such intense ionisation crest formations on either side of the magnetic equator would offer higher resistance to the zonal motion of the neutrals from the dayside to the nightside, thus retaining their kinetic energy leading to higher exospheric temperature at the latitudes of the IA crests than at the magnetic equator, as shown by Hedin and Mayr (1973). The higher exospheric temperatures at the latitudes of the IA crests would give rise to higher concentration of the neutrals at the F region altitudes, characterising the NA. This process of NA formation is described in Chapter 1. The method to calculate the anomaly in the neutral concentration is described in Sec. III.5.

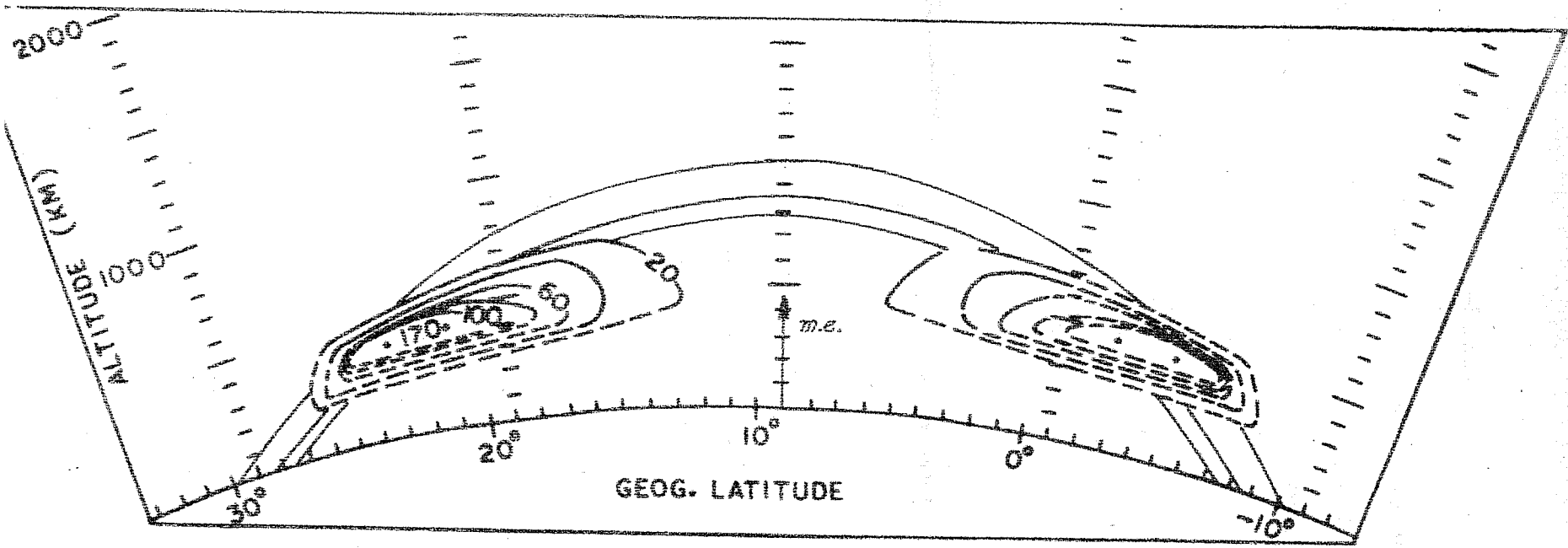


Fig.5.17:- Contours of excess percentage electron concentration on Oct. 6, 1972 at 1240 hr LT obtained from the constant height plot shown in Fig. 3.16 as described in the text.

The calculated magnitudes of the anomaly at the $h_{max}F2$ altitude on Oct. 6, 1972 at 1240 hr LT are 12.5% in the neutral temperature and, 91.6% and 37.6% in $N_2$ and O concentrations respectively.

It is also mentioned in Chapter 1 that the NA formation would occur more frequently in sunspot minimum ($S_{min}$) than in sunspot maximum ($S_{max}$) period, due to higher crest to trough ratio of electron concentration in the IA during forenoon hours of $S_{min}$ period. On this basis Raghavarao and Sivaraman (1975) explained the more frequent occurrence of the ledge in $S_{min}$ period. The IA during $S_{min}$ period, however, starts weakening after 1400 hr and disappears around 2000 hr LT (Rastogi, 1966). Thus it appears that the IA would not be able to maintain the NA in the evening hours during $S_{min}$ period. The observations presented in Fig. 3.9(a,b), however, suggest that the ledge in the evening and premidnight hours is maintained at a higher field line than the IA field line. Raghavarao and Sivaraman (1975) suggested that the maintenance of the ledge at a higher magnetic field line than the anomaly field line in the premidnight period could be explained on the basis of the equatorward winds generated due to the excess pressure bulges, characterising the NA, on either side of the magnetic equator. The magnitudes of the pressure bulges is calculated by Raghavarao (1976) and is shown in Fig. 6.9

of Chapter 6. The equatorward wind velocities, as shown by the horizontal arrows in Fig. 6.9, at about 10-15$^{o}$ dip latitudes would help in maintaining the ionisation ledge against diffusion in the evening period.

The work of Lindzen (1967) shows that the ion drag is also governed by the vertical distribution of plasma density and the height $h_{max}F2$ of the layer peak. Lindzen solved the equation of motion of the neutrals by considering the east-west pressure acceleration and included the effects of inertia and ion drag. Fig. 3.18(a) reproduced from his work shows four N(h) distributions N1, N2, N3 and N4. The distributions N1 and N2 have the same $N_{max}F2$ as well as $h_{max}F2$. The two ionisation distributions N3 and N4 have the same $h_{max}F2$, which is about 200 km lower than that of the distribution N1 or N2. The $N_{max}F2$ for the profile N3 is about 5 times higher than that of the profile N4. Fig. 3.18(b) shows the diurnal velocity oscillation of the zonal wind with the ion drags corresponding to the N(h) distributions N1, N2, N3 and N4 and also in the absence of the ion drag (shown by D = 0). A comparison of the profiles N1 and N2 of the velocity oscillation with the corresponding ionisation distribution in Fig. 3.18(a) brings out an interesting result that the oscillation of the zonal wind not only depends upon the $N_{max}F2$ but also on, 1) the altitude at which the maximum occurs and 2) the shape of the N(h) distribution. In the absence of the ion drag, D = 0, the zonal wind has large

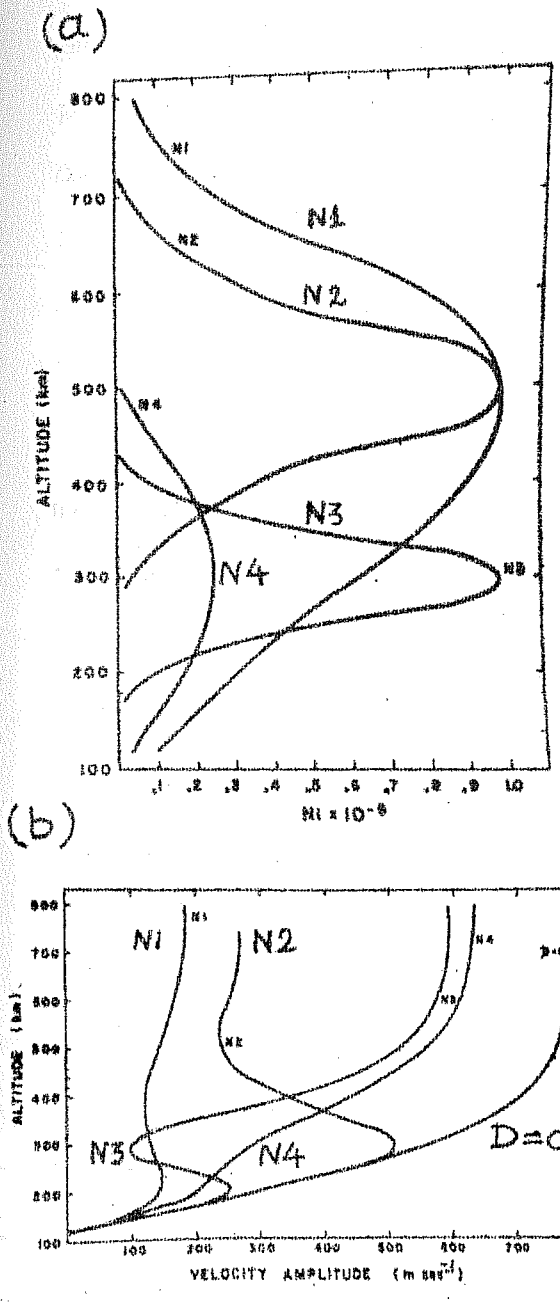


Fig.5.18(a,b)

Fig.5.18(a,b):- (a) Various distributions of ionizations used in calculation of ion drag and (b) amplitude of zonal wind velocity oscillation as a function of altitude without ion drag (D = 0) and with ion drag corresponding to the various ion distributions shown in (a).
(After Lindsen, 1967)

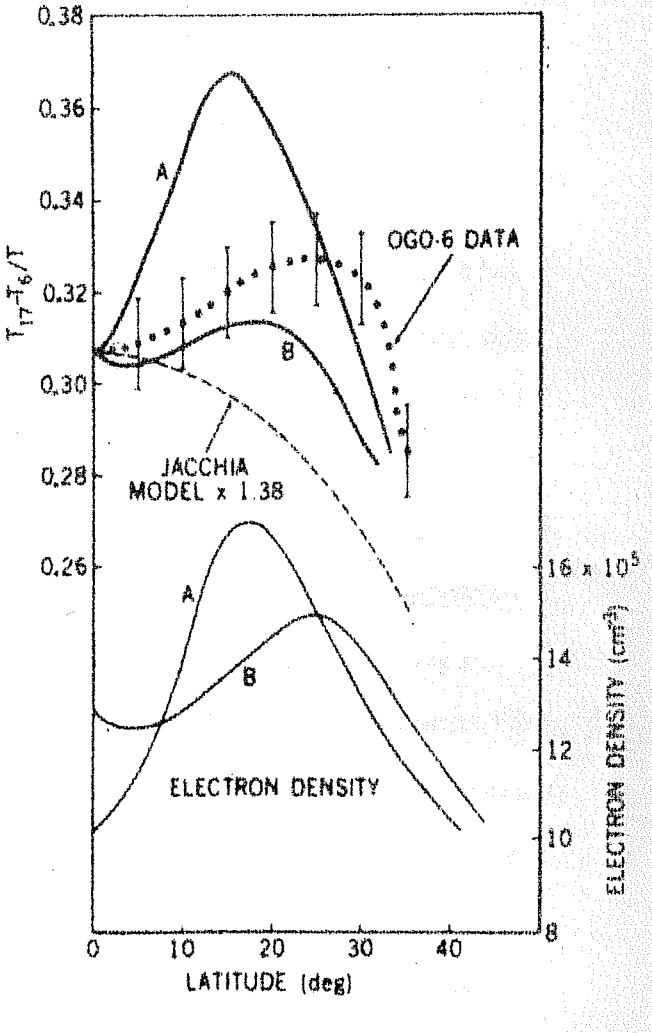


Fig.5.19

Fig.5.19:- Diurnal temperature amplitude, $(T_{17} - T_6)/\bar{T}$, for two representative latitudinal distributions of electron concentrations.
(After Hedin and Mayr, 1973).

amplitude which increases with altitude. However, in the presence of the ion drag the amplitude of the wind oscillation decreases; the maximum decrease being near the $h_{max}F2$ level for individual distributions. The decrease in the wind amplitude is more for the ionization distribution N3 having the lower $h_{max}F2$ and the sharper profile than the distribution N2.

Lindzen's work is of relevance for explaining the maintenance of the NA until the premidnight hours even though the IA becomes very weak (or even collapses) around 2000 hr LT in $S_{min}$ period. The electron concentration below the F2 peak decreases rapidly with time after the sunset, causing the N(h) profile to become sharp in the evening hours. Rastogi (1971) showed that the $h_{max}F2$ level is higher (by about 100 km) at the latitude of IA crest than at the magnetic equator until 2100 hr LT. Under these circumstances, following Lindzen's work, the neutral wind oscillation amplitude will be reduced more at the locations of the IA crests than at the trough. The retention of the kinetic energy per unit volume ( $= \frac{1}{2}\rho v^2$) of the neutrals would be more at the location of the IA crests where the mass density, $\rho$, is higher, by virtue of the lower value of $h_{max}F2$, than at the trough. This process would help to maintain the NA in the premidnight hours even though the IA collapses.

It should be mentioned that Raghavarao and Sivaraman (1974, 1975) considered the NA formation because of the ion drag effect of the IA on the neutral motion. However, the neutral density peaks in the low latitude region could exist due to other reasons as well. A.D. Anderson (1973), for example, has shown latitudinal plots of neutral mass density at 406 km altitude, obtained from the Lockheed microphone density gauge onboard the OGO-6 satellite, on four successive days, Sept. 27-30, 1969, at 1600 hr LT. The $K_p$ index on these four occasions was 0, 4+, 6 and 8 respectively. It is seen from Anderson's work (Fig. 1 of his paper) that marked density variation occurs at low latitudes during geomagnetic storms. The average density from $10^{o}$N to $20^{o}$N geomagnetic latitude is over twice as great for $K_p = 8$ than for $K_p = 0$. The density distribution for $K_p = 8$ showed three peaks between $15^{o}$ - $35^{o}$N lat.; for $K_p = 4^{+}$, a sharp peak around $15^{o}$N was observed. Although the magnetic field alignment of these peaks was not examined by Anderson, the density minima occurred near the geomagnetic equator, indicating that the peaks would probably be field aligned. Such field aligned peaks of neutral density in the F-region would partially inhibit the plasma diffusion, leading to the ionisation ledge formation on magnetically disturbed days. The ledge observed on Jan. 8, 1975 at 0945 hr LT (the spatial structure shown in Fig. 4.4 in Chapter 4) could be due to the effect of the disturbance in causing the NA. The day is magnetically disturbed, the $K_p$ value being 4

corresponding to the period of the ledge observation. The occurrence of the ledge on this day at 0945 hr LT is one of the rare occasions showing its formation before 1200 hr LT in the present study.

The higher intensity of the ionisation ledge when it occurs lower in altitude around the midday hours, can be explained on the basis of the mechanism proposed by Raghavarao and Sivaraman in the following manner.

During the midday hours altitude of the top of the IA field line is low and therefore the NA would form very strongly due to more effectiveness of the ion drag in controlling the zonal flow of the neutrals, on the basis of the work of Lindzen described above. The ambipolar diffusion of ionisation lifted up at the magnetic equator due to the $\underline{E} \times \underline{B}$ force, would be inhibited more due to the presence of strong NA crests. Thus the ledge, during midday hours, being located on the same field line which passes through the strong NA crests, would be of higher strength.

## III.5 CALCULATION OF NEUTRAL ANOMALY FROM IONISATION ANOMALY

We now describe a method to calculate the neutral anomaly, based on the work of Hedin and Mayr (1973). These authors solved the energy and continuity equations for neutrals taking into account the ion drag force. They obtained the latitudinal distribution of neutral temperature for a given distribution of $N_{max}F2$. The computed latitudinal exospheric

temperature profile shows enhancement in the neutral temperature at the IA crest, in proportion to the excess electron concentration at the crest with respect to that at the trough. Fig. 3.19 reproduced from the work of Hedin and Mayr shows the amplitude of the diurnal temperature variation, $(T_{17} - T_{06}) / T_{av}$ (hereafter referred to as "temperature amplitude"), as a function of dip latitude; $T_{17}$ and $T_6$ are the neutral temperatures at 1700 and 0600 hrs LT and $T_{av}$ is the average diurnal temperature. The two curves A and B showing the temperature amplitude correspond to the electron density distributions A and B respectively. It is easy to see that the excess temperature amplitude at any latitude over that at the equator is linearly proportional to the excess electron concentration at that latitude over that at the magnetic equator. In other words, if $T_L$ and $T_O$ represent the value of the temperature amplitude, $(T_{17} - T_6) / T_{av}$, at a latitude L and the equator respectively and if $N_L$ and $N_O$ denote the electron concentrations at the latitude L and the equator, then $(T_L - T_O) / T_O$ should be linearly related to $(N_L - N_O) / N_O$. This is shown in Fig. 3.20 in which the solid and the dashed line show the linear relationship between the rising and the falling portions respectively of the two curves A in Fig. 3.19.

The procedure for calculating the neutral anomaly strength is illustrated below for the case Oct. 6, 1972. The value of $(N_L - N_O) / N_O$ on this day at 1240 hr LT, as calculated from the constant height plot at $h_{max}F2$

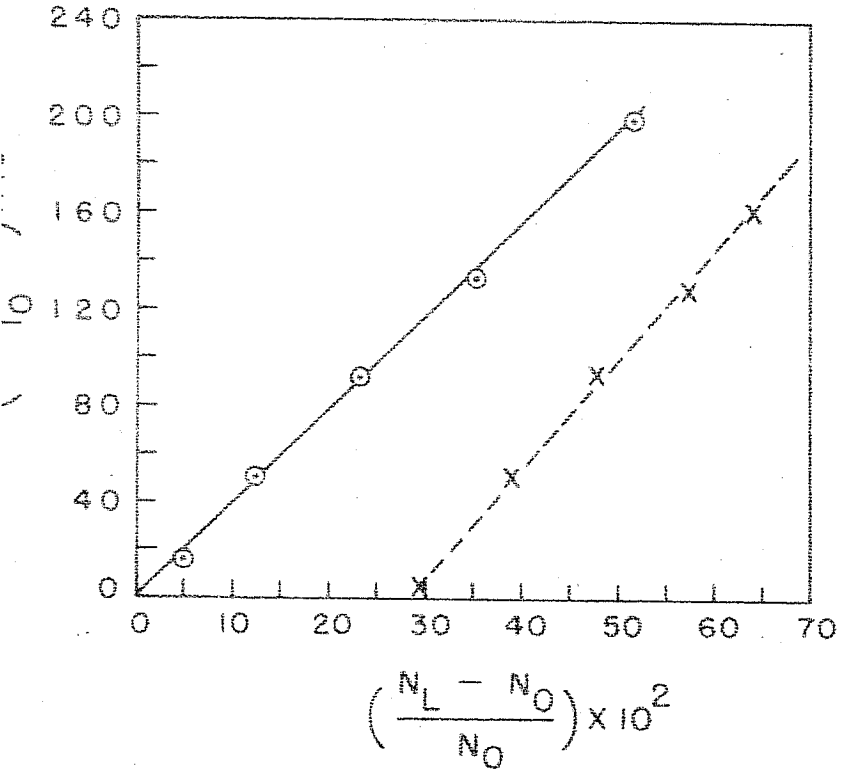


Fig.3.20

.20:- Relation between excess temperature amplitude and excess electron concentration obtained from Fig. 5.19 in the manner described in the text.

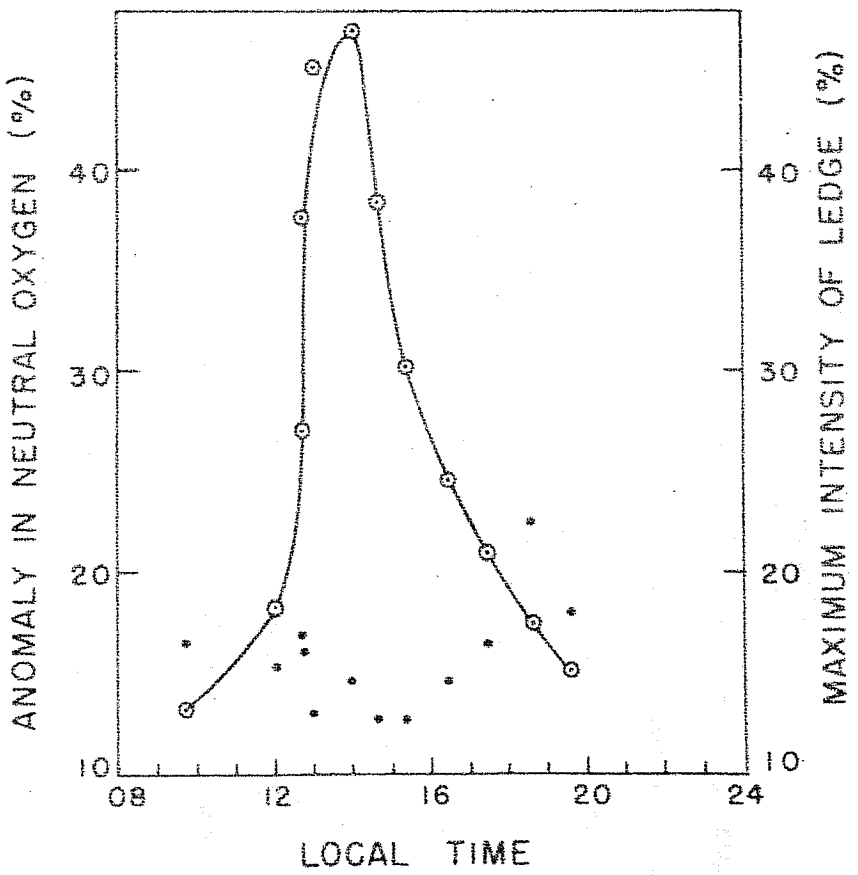


Fig. 3.21

Fig.3.21:- Daily variation of the computed anomaly in neutral atomic oxygen (open circles) and the corresponding observed maximum intensity of the ledge (thick dots).

altitude in Fig. 3.16, is 1.711; $N_L$ and $N_O$ represent the electron concentrations at the IA crest and the trough respectively. The 10.7 cm solar flux is 98 units on Oct. 6 and the day is magnetically quiet, the value of $A_p$ being 2. Using Jacchia (1970) model, the calculated values of the neutral temperature at the $h_{max}F2$ altitude at the equator (350 km in this case) at 0600 and 1240 hrs LT are 789.3°K and 983.6°K respectively. The value of the average temperature, $T_{av}$, on this day is 866.9°K. By making use of the linear relationship between the parameters $(N_L - N_O) / N_O$ and $(T_L - T_O) / T_O$, given by the solid line in Fig. 3.20, the value of the neutral temperature at the IA crest corresponding to the value $(N_L - N_O) / N_O$ equal to 1.711 can be calculated in the following way :

$$T_{crest} = 0.37 \times 1.711 \times (983.6 - 783.9) + 983.6 = 1106.6^{\circ}K$$

where 0.37 is the slope of the solid straight line in Fig. 3.20. Thus the excess temperature at the latitude of the IA crest with respect to that at the trough is $\frac{1106.6 - 983.6}{983.6} \times 100 = 12.5\%$.

The excess concentrations of $N_2$ and O at the IA crest over their respective values at the trough, calculated from the Jacchia (1970) model corresponding to the exospheric temperature 1106.6°K at the crest, are 91.6% and 37.6% respectively. It may be noted that these calculated values of neutral anomaly strength in $N_2$ and O are considerably higher than

their respective observed values (25% and 11%) by Hedin and Mayr (1973) on Sept. 22, 1969 during sunspot maximum period. The calculated magnitudes of the NA on Oct. 6, 1972 confirm the preliminary calculations of RS2 which show that the NA is expected to form more prominently in $S_{min}$ as compared to the $S_{max}$ period.

In a similar manner as descibed above for Oct. 6, 1972, the magnitudes of the NA are calculated on a number of days (on which the ionisation ledge is present) at different local times, from the experimentally observed values of the electron concentrations at the IA crest and the trough, by means of the ISIS satellite data recorded at Ahmedabad. Fig. 3.21 shows the plot of the calculated anomaly in atomic oxygen (the continuous curve joining the open circles) against local time. The number of data points is rather small, due to the fact that the calculation of the NA necessitates the latitudinal distribution of electron concentration at the $h_{max}F2$ altitude, that in turn requires good quality ionograms throughout the pass duration (and especially at the latitude of the IA crest and the trough) on which the X and O echoes are seen upto the penetration frequencies. The NA is seen to maximise around 1400 LT; this behaviour being same as that of the IA in $S_{min}$ period.

The solid points in Fig. 3.21 represent the observed maximum excess percentage ionisation in the ledge. The diurnal behaviour of the ledge is seen as a decrease in its intensity during the afternoon hours and an increase during the evening hours. Raghavarao et al. (1976a) proposed an explanation for this on the basis that the meridional winds generated by the NA in the lower thermosphere (as shown in Fig. 6.9 of Chapter 6) decrease the eastward electric field in dip latitude region $\sim 4^{o} - 12^{o}$ on both sides of the equator. The effective eastward field communicated to 150 km and upto 600 km would then be reduced and hence the supply of ionisation to the ledge is weakened when the NA ridge is strongest.

## III.6 DISCUSSION AND CONCLUSION

We have presented a number of new features of the ionisation ledge in the longitude zone $50^{o}E - 100^{o}E$. The observations of earlier workers are also presented and the explanations put forth by them are critically discussed in view of our own observations. It is found that the mechanism of the ledge formation proposed by Raghavarao and Sivaraman (1974), which invokes the presence of the neutral anomaly, explains many of its observed features.

A method to calculate the strength of the anomaly in the neutral temperature as well as the constituents $N_2$ and O, is described. It is shown that the strength of the NA in sunspot minimum period is much higher than that observed

experimentally by Hedin and Mayr (1973) for the solar maximum period. Thus the occurrence of the ledge during sunspot minimum period is explainable on the basis of the mechanism proposed by Raghavarao and Sivaraman which invokes the presence of the neutral anomaly. The observation of the ledge and the ionisation anomaly in a narrow longitude zone, on occasion, reveals that the ion drag, caused by the ionisation anomaly, acting over a limited longitude zone can effectively quench the neutral motion thereby causing the neutral anomaly in the limited longitude zone.

# C H A P T E R - IV

## IONISATION LEDGE - A TRACER FOR THE CROSS EQUATORIAL WIND

### IV.1 INTRODUCTION

In this chapter the author describes a method for delineating the "spatial structure" of the ionisation ledge. The spatial structure gives the distribution of the excess ionisation characterising the ledge. These are found to be aligned to the magnetic field lines of the earth and thus appear as arch-shaped over the magnetic equator.

It is found that the latitudinal extents of the ledge structure in the two hemispheres around the magnetic equator, are equal during the equinoctial period. In the solstitial period, however, the ledge length in the winter hemisphere is found to be longer than that in the summer hemisphere revealing that the ledge is bodily shifted into the winter hemisphere. The bodily displacement of the ledge into the winter hemisphere provides an evidence for the existence of the cross-equatorial wind from summer to winter hemisphere. The average speeds of the winds calculated from the displacement of the ledge at different local times are in the range 30-80 m/s and thus agree with the theoretical values shown to be required for explaining the observed solstice asymmetry of the equatorial ionisation anomaly.

## IV.2 METHOD FOR OBTAINING SPATIAL STRUCTURE OF THE LEDGE

Fig. 4.1(a) gives a sequence of ionograms obtained by means of ISIS-2 satellite on March 19, 1974 at 80°E mean longitude (mean local time of the pass 2015 hr). The ionograms are obtained at intervals of approximately 28 seconds during which the dip and the geographic latitudes of the satellite position changed by about 1°.8 and 1°.5 respectively. The ionograms, with the exception of the last one (at +15°.8 dip lat.), show prominent cusp formation. The cusp gradually grows in prominence from the beginning of the northbound pass until the satellite crosses the equator and thereafter gradually weakens, finally disappearing at +15°.8 dip latitude. It may also be noted that the frequency at which the cusp tip occurs in either X or O trace undergoes a systematic change; being the lowest for the cusp occurring at the magnetic equator and increases gradually on either side.

Fig. 4.1(b) shows the sequence of N(h) profiles computed from the ionograms shown in Fig. 4.1(a). The vertical arrow on each profile shows the lower boundary of the ledge, being the true height corresponding to the frequency of the cusp tip on the X trace. The excess percentage electron concentration is calculated at each 10 km interval in the altitude range of the upper and the lower boundary of the ledge on the individual N(h) profiles. The two altitudes where the excess concentrations are 5%, 10%, 15% etc. (in steps of 5%) which occur on either side of the maximum of

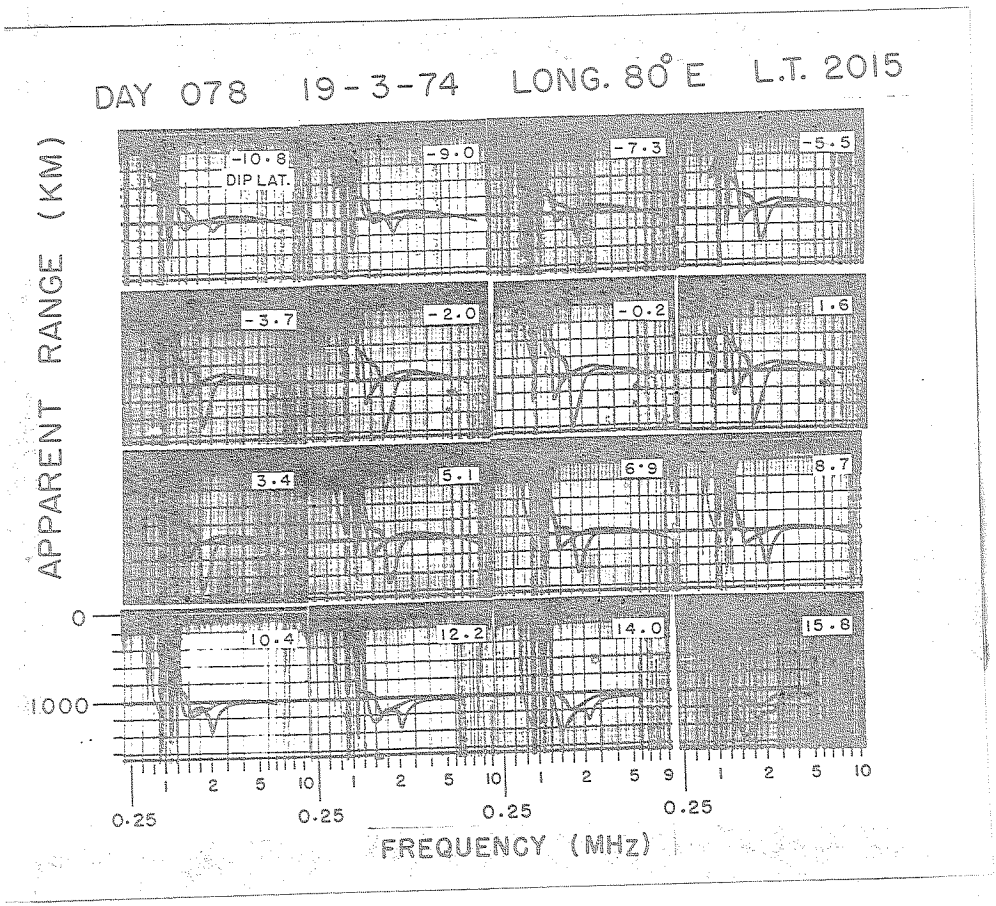


(a)

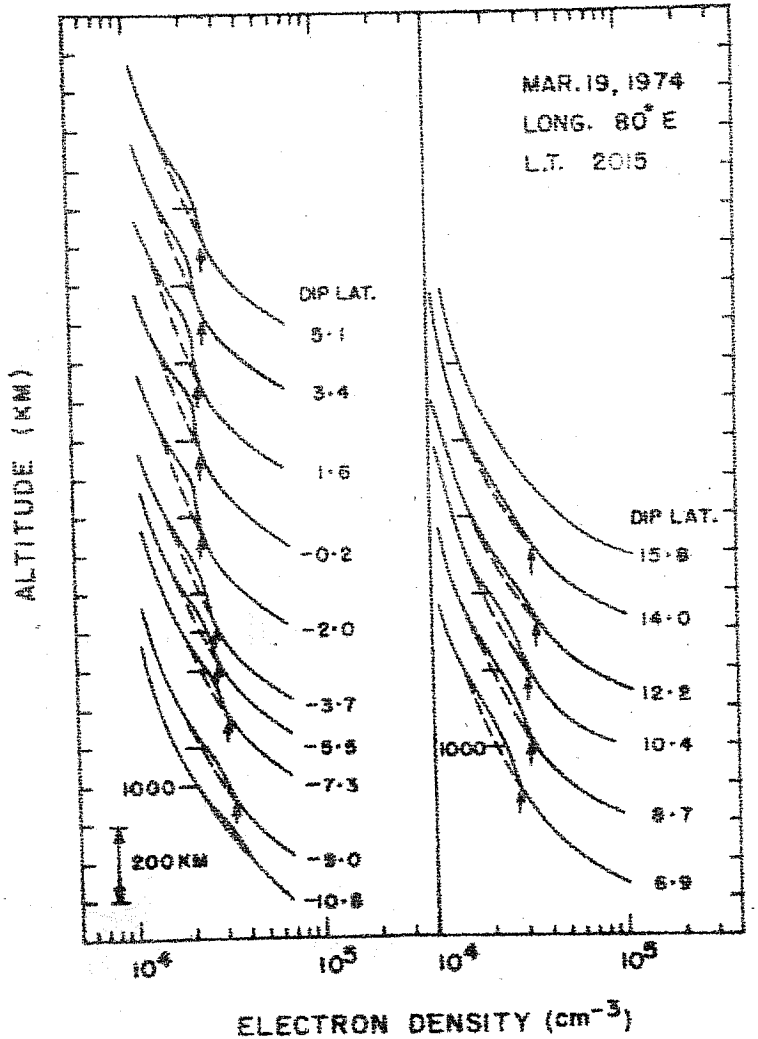


(b)

Fig. 4.1(a,b):- (a) A sequence of cusps on ISIS-2 ionograms on March 19, 1974 at 2015 hr ($80^{\circ}$ GMT) and (b) the corresponding N(h) profiles.

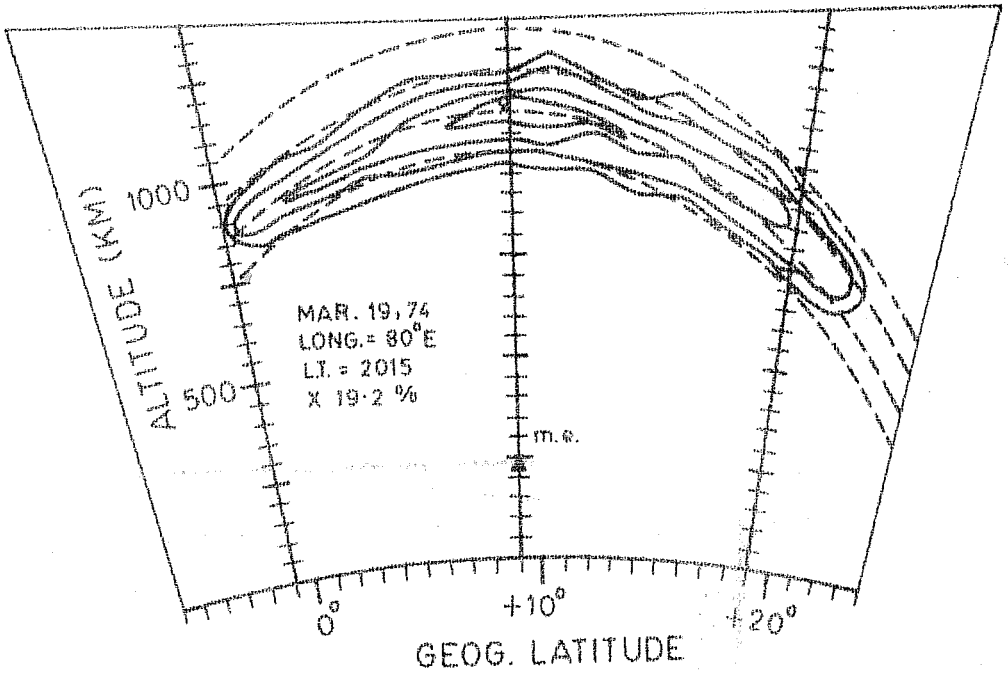


Fig. 4.1(c):- The contours of excess percentage electron concentration in the ledge obtained from Fig. 4.1(a,b) as described in the text. The dashed lines represent the earth's magnetic field lines and 'm.e.' denotes the position of the magnetic equator.

the ledge are interpolated from each one of the N(h) profiles. These altitudes are plotted on an altitude versus geographic latitude diagram on which the earth's magnetic field lines are also drawn. The altitudes corresponding to the same excess percentage concentration at various latitudes are joined by a smooth curve, which represents the "intensity contour" of the ledge. The contour diagram obtained from the N(h) profiles of Fig. 4.1(b) is shown in Fig. 4.1(c). The outermost contour, representing the zero percent excess ionisation gives the vertical and the latitudinal boundary of the ledge.

The uncertainty in determining the vertical boundary of the ledge structure is about $\pm$10 km when the ledge is prominent (as defined in Chapter 3). However, when the ledge is weak, its vertical boundary cannot be ascertained very accurately; the error being typically about $\pm$20 km. The extremity of the latitudinal boundary of the spatial structure in either hemisphere is obtained by closing the outermost contour midway between the latitudes of two successive N(h) profiles, one showing the ledge and the other showing no ledge formation. From the N(h) profiles shown in Fig. 4.1(b), it may be noted that the profile at 14.0 dip latitude ($21^{\circ}.0$ geog. lat.) shows the ledge while the profile at $15^{\circ}.8$ dip latitude ($22^{\circ}.5$ geog. lat.) does not show the ledge.

In the absence of an ionogram between the above two latitudes, it is reasonable to assume that the ledge could have disappeared midway between the two latitudes and on this basis the outermost contour in Fig. 4.1(c) is symmetrically closed at $14^{o}.9$ dip latitude ($21^{o}.7$ geog. lat.). In the same manner, the extremity of the ledge boundary on the southern side of the magnetic equator is at $-11^{o}.6$ dip latitude ($-1^{o}.0$ geog. lat.); midway between $-10^{o}.8$ dip latitude ($-0^{o}.2$ geog. lat.) and $-12^{o}.6$ dip latitude ($-1^{o}.7$ geog. lat.). The accuracy in delineating the latitudinal extent of the ledge in either hemisphere is estimated to be about one fourth of the latitude interval between the successive ionograms; in this case it is about $0^{o}.4$ geog. latitude. The vertical extent of the ledge (at the magnetic equator) is about 225 km and its total horizontal extent is $23^{o}.2$ latitude (about 3000 km), $10^{o}.5$ on the northern side and $12^{o}.7$ on the southern side of the magnetic equator. The latitudinal extent of the spatial structure measured from the magnetic equator in either hemisphere will henceforth be called as the "ledge length".

For the reason that the contour plot of the intensity, such as one shown in Fig. 4.1(c) represents the horizontal and the vertical extent of the ionisation ledge, we will henceforth refer to such a plot as 'spatial structure' of the ionisation ledge.

The accuracy in delineating the vertical boundary of the spatial structure is approximately same for the ISIS-1 as well as the ISIS-2 satellite data. However, the accuracy in delineating the latitudinal boundary is different for the two satellites (because of the difference in their orbital parameters), as discussed below.

The normal mode of the sounder sweep (covering 0.1 to 20.0 MHz frequency range) requires about 11 seconds in case of ISIS-2 and 15 seconds in case of ISIS-1 satellite. The extended sweep mode (covering 0.1 to 20.0 MHz frequency range) requires about 17 and 25 seconds respectively for ISIS-2 and 1 satellites. Following the transmitter sweep, the fixed frequency sounding (on any one of the five preselected frequencies) occurs either for about 3 seconds duration (corresponding to the sweep fly-back) or else for the same time duration as that of the sounder frame (a frame denotes the sweep plus the fly-back). The different modes of the sweep and fixed frequency transmissions yield one to five ionograms in each one minute interval of the satellite pass. The geographic latitude covered by the ISIS-2 satellite in one minute of its orbit is about $3^{o}.2$. The ISIS-1 covers approximately $2^{o}$ latitude while the satellite is near the apogee and $4^{o}$ latitude near the perigee. Thus the latitudinal interval between the successive ionograms depends upon the mode of operation of the sounder transmitter as well as on the orbit of the satellite. For plotting the spatial

structure, however, only those passes of ISIS-1 and 2 are considered for which at least one ionogram is available for each $1^{o}$ - $1^{o}.5$ of latitude. The closer the latitude interval between two successive ionograms, the higher is the accuracy in delineating the latitudinal boundary of the ledge spatial structure.

## IV.3 DETECTION OF CROSS-EQUATORIAL WINDS

The spatial structures of the ionisation ledges are found to be symmetric in their latitudinal extent in the two hemispheres around the magnetic equator during the equinoctial months. This is apparent from the spatial structures on Oct. 6-7 and Oct. 9, 1972 around noon hour presented in Fig. 3.15 of Chapter 3. A typical example showing the same feature in the evening period is presented in Fig. 4.2(a) which is obtained by means of an ISIS-2 pass on Oct. 21, 1973 at 1934 hr ($73^{o}$ EMT). The ledge length on either side of the magnetic equator is $12^{o}.5$ latitude. The electron concentration contours at fixed altitudes in the topside ionosphere revealing the presence of ionisation anomaly (IA) are shown in Fig. 4.2(b). It is seen that the two peaks of the IA are of equal strength at any altitude. The symmetry of the IA during equinoctial months has been explained by Bramley and Young (1968) by hypothesising that the cross-equatorial winds are absent during this period.

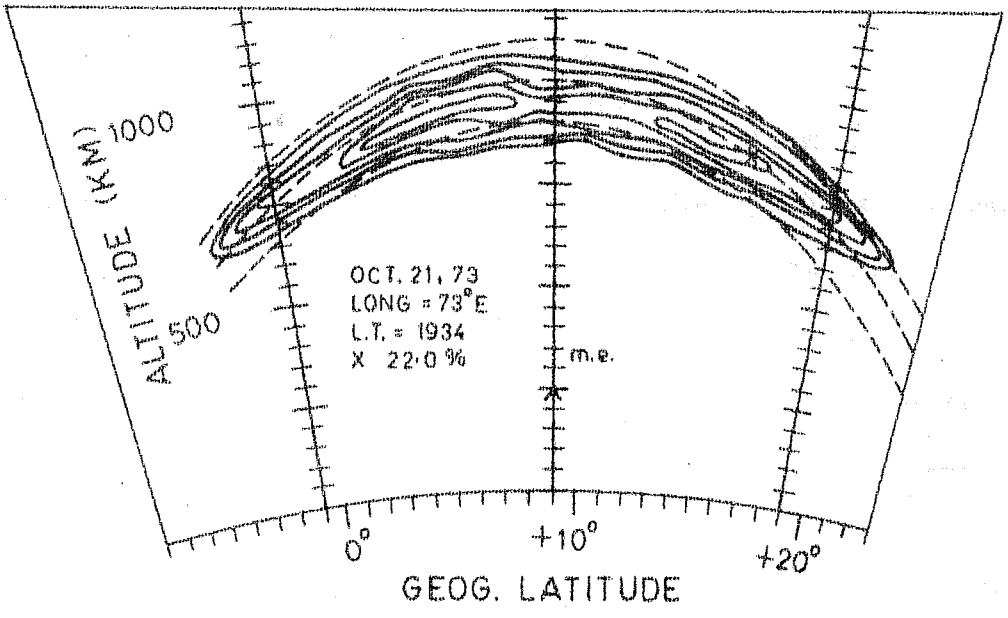


(a)

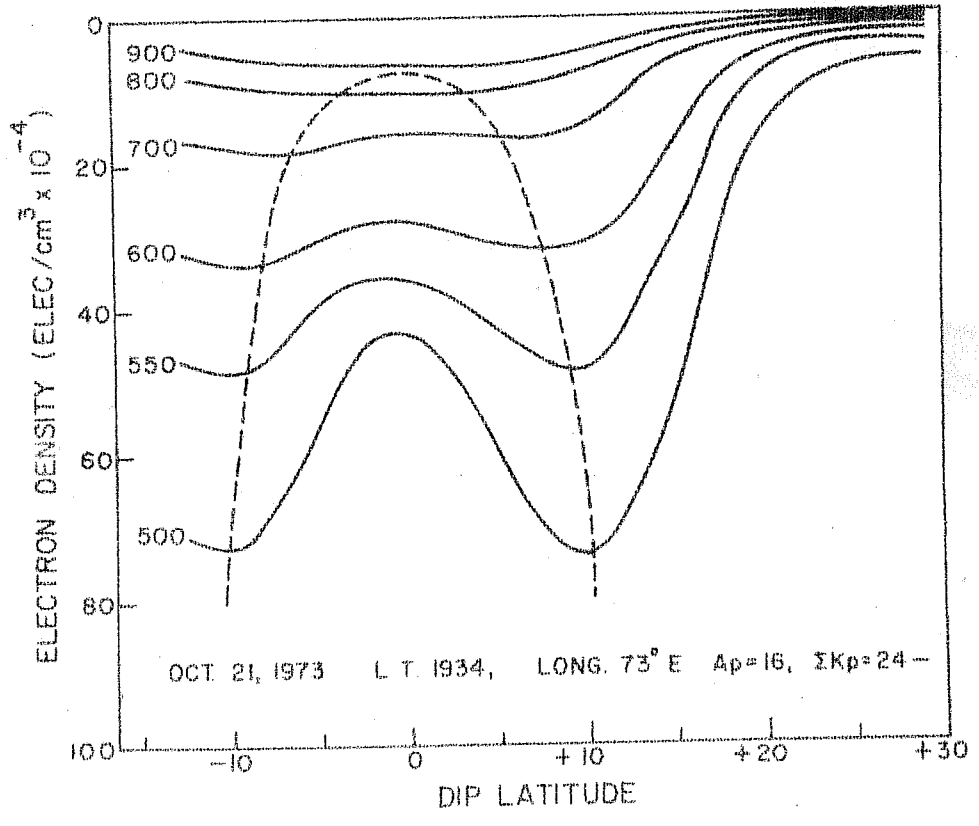


(b)

Fig. 4.2(a,b):- (a) Spatial structure of the ionisation ledge on Oct. 21, 1973 at 1934 hr (73°EMT) from an ISIS-2 pass and (b) latitudinal distribution of electron concentration at constant altitudes obtained from the same pass.

Fig. 4.3(a) shows the spatial structure of the ionisation ledge obtained from an ISIS-2 pass on November 2, 1973 at 1842 hr ($87^{o}$ EMT). The ledge lengths are $3^{o}.5$ and $12^{o}$ latitude in the summer and winter hemispheres respectively, thus giving $8^{o}.5$ latitudinal displacement of the ledge into the winter hemisphere. Fig. 4.3(b) gives the latitudinal distribution of electron concentration at fixed altitudes obtained from the same satellite pass from which the ledge structure in Fig. 4.3(a) is delineated. The asymmetry of the IA peaks in the two hemispheres is clearly apparent in Fig. 4.3(b); the summer peak (at the southern dip latitudes) of the anomaly at any altitude is higher in strength than the corresponding winter peak.

The solstice asymmetry of the IA at the F2 layer altitude, first reported by Lyon and Thomas (1963), shows the winter crest of the anomaly to be stronger than the summer crest. Subsequently, King et al. (1964) found the solstice asymmetry to occur in the topside ionosphere as well, with the sense of the asymmetry being reversed with respect to that in bottomside.

The explanation for the solstice asymmetry was attempted by many workers (e.g. Hanson and Moffett, 1966; Bramley and Young, 1968) by solving the steady state continuity equation for the electrons in the F2 region. Hanson and Moffett showed that a transequatorial wind of 60 m/s can

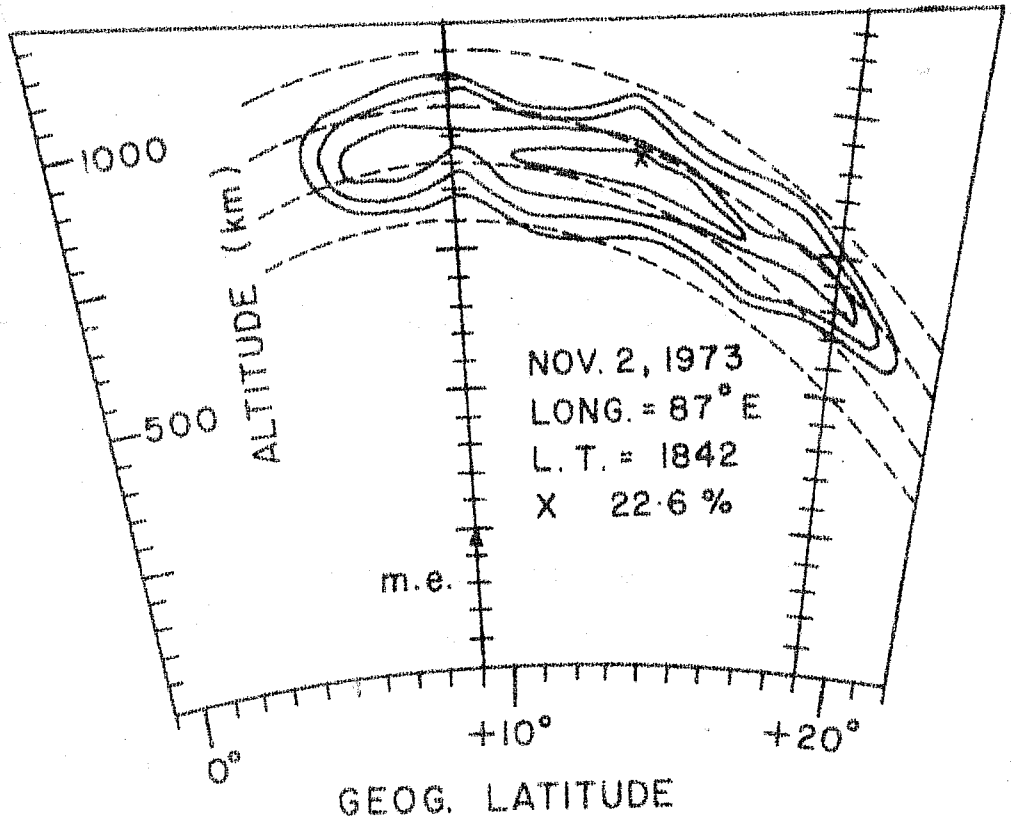


(a)

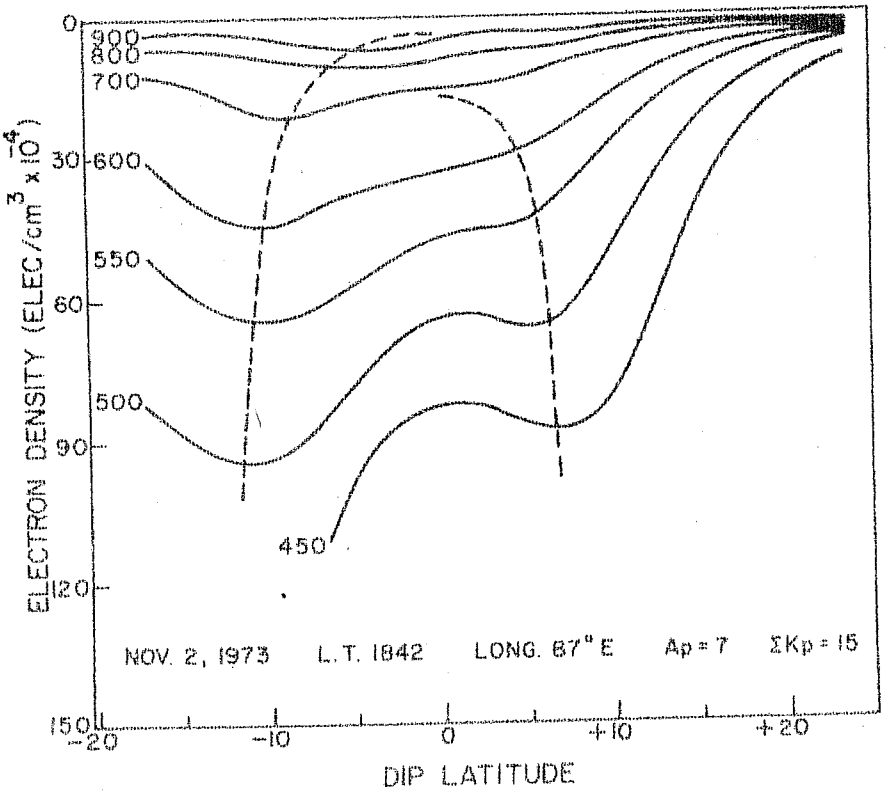


(b)

Fig. 4.3(a,b):- Same as in Fig. 4.2(a,b) on Nov. 2, 1973

produce 15% interhemisphere asymmetry in the electron concentration at the IA crests (at the $h_{max}$ F2 altitude). Bramley and Young considered the effect of such factors as asymmetrical production rates of ionisation, asymmetrical electrodynamic drifts and different atmospheric conditions (in particular the neutral temperature) in the summer and the winter hemispheres, as possible causes for the solstice asymmetry of the IA. However, none of the above factors could explain the observed magnitude of the asymmetry. These authors then invoked the presence of the winds blowing from summer to winter hemisphere across the magnetic equator and showed that such winds in the range 40-80 m/s produce the asymmetric IA peaks (at the $h_{max}$F2 altitude as well as in the topside) in quantitative agreement with the observations.

In addition to the solstice asymmetry of the IA, there are some other phenomena occurring in the F region/ topside ionosphere which have been explained by invoking the presence of the cross-equatorial winds. A brief description of these phenomena is given below.

The asymmetrical distributions of OI (6300 Å) night airglow emission by means of OGO-6 satellite (Chandra et al. 1973) as well as of the Mg II (2796-2803 Å)dayglow emission observed by means of TD1-A satellite (Gerard and Monfils, 1974), with higher intensities occurring on the winter side of the magnetic equator, were explained on the basis of the

winds assumed to be blowing from summer to winter hemisphere. Such a wind raises the $h_{max}F2$ in the summer hemisphere and lowers the $h_{max}F2$ in the winter hemisphere (as shown in Sec. I.2, Chapter 1), thereby giving rise to the asymmetric distribution of the airglow emission rates in the two hemispheres.

Hanson et al. (1973), by means of retarding potential analyser data from OGO-6 satellite, presented evidence that on occasion the nighttime plasma temperatures at 800-1000 km altitude range in the vicinity of the magnetic equator are below the expected neutral gas temperature. The minima in electron and ion temperatures occur at 3-4$^{o}$ latitude on the summer side of the equator. Bailey et al. (1973) explained this 'super cooling' on the basis of the inter-hemisphere transport of plasma caused by summer to winter wind across the magnetic equator, producing expansion cooling of the plasma when it is moved upwards along the magnetic field lines in the summer hemisphere.

Recent satellite measurement of the neutral helium concentration (Reber, 1975) revealing higher concentration in the winter hemisphere than in the summer hemisphere, is also attributed to the presence of the wind across the equator, transporting the neutral helium from summer to winter hemisphere.

The phenomena mentioned above were explained by invoking the presence of cross-equatorial winds. However, there is no evidence to show the existence of such winds. The observations presented in Figs. 3.15, 4.2(a) and 4.2(b) provide observational evidence for the absence of the cross-equatorial wind during equinoctial period and for its presence during the solstitial period, as discussed below.

A neutral wind $\underline{U}$ moves the ionisation along a magnetic field line with the velocity component $(\underline{U} \cdot \underline{B})\ \underline{B}/B^2$, where $\underline{B}$ represents the earth's magnetic induction. Thus the cross-equatorial wind $\underline{U}$ blowing from the summer to winter hemisphere, would disturb the initial symmetry of the "cloud" of the excess ionisation characterising the ledge. If the excess ledge length $\triangle L$ is attributed to the effect of the wind, operative for time interval $\triangle t$, we have

$$\triangle L = \left| \frac{(\underline{U} \cdot \underline{B})\ \underline{B}}{B^2} \right| \times \triangle t = U \cos I \times \triangle t \quad ---(1)$$

wherein it is taken that the cross equatorial wind magnitude 'U' is at the $h_{max}F2$ altitude, and 'I' represents dip angle corresponding to the location where the ledge field line (as defined in Chapter 3) intersects the $h_{max}F2$ altitude in the summer hemisphere. In order to obtain the magnitude of the cross equatorial wind from eq.(1), it is necessary to know the time interval, $\triangle t$, for which the wind is operative in causing the observed shift, $\triangle L$, of the spatial structure.

No observational evidence has been reported in literature regarding the diurnal variation in addition to the possible day to day variation of the cross equatorial wind. In the absence of any information on the time of the day at which significant cross equatorial wind starts blowing, we reckon it to be effective at 1100 hr LT on the basis of the following examples on the hemispherical displacement of the ledge structures.

Figs. 4.4 and 4.5 show the ledge spatial structure on Jan. 8, 1975 and Feb. 4, 1974 at 0945 hr and 1130 hr LT respectively, obtained by means of ISIS-2 satellite. The spatial structure in Fig. 4.4 shows that the ledge is nearly symmetric around the magnetic equator at 0945 hr whereas the spatial structure in Fig. 4.5 shows that the ledge length is $1^{o}.5$ more in the winter hemisphere than that in the summer hemisphere at 1130 hr LT. Fig. 4.6, showing the spatial structure of the ledge observed on Jan. 18, 1974 by means of ISIS-2 satellite, reveals that the structure is displaced about $3^{o}$ latitude into the winter hemisphere at 1250 hr LT. On the basis of the examples shown in Figs. 4.4 - 4.6 and a number of other observations (not shown here) in solstice period revealing $2^{o}$ - $3^{o}$ latitudinal shift of the ledge structure between 1200 - 1300 hr LT, we reckon the time at which the cross-equatorial wind becomes significant, to be around 1100 hr LT.

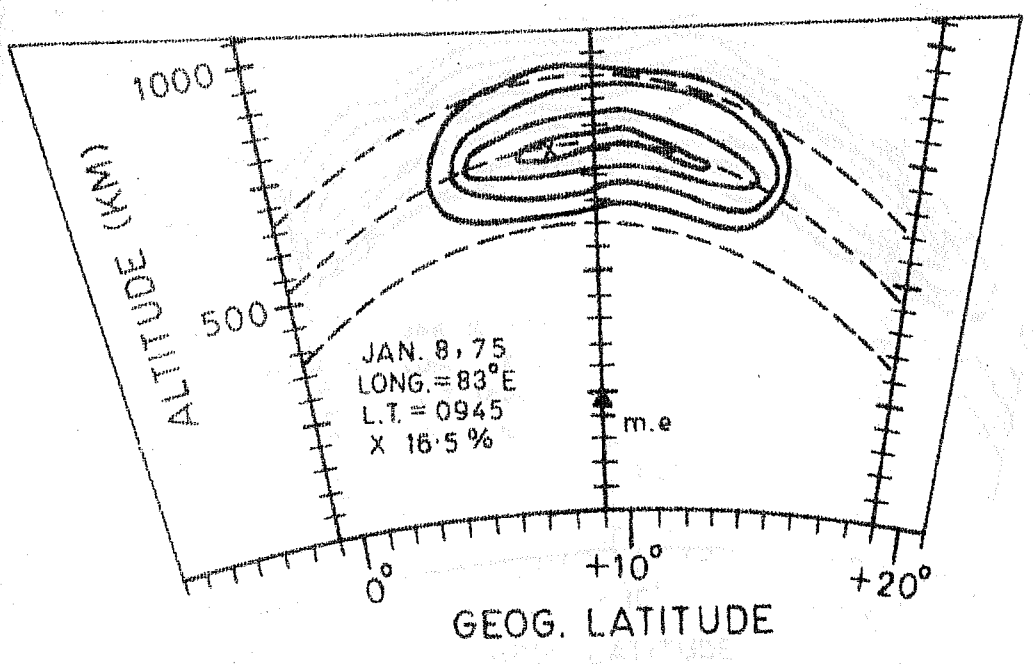


Fig.4.4

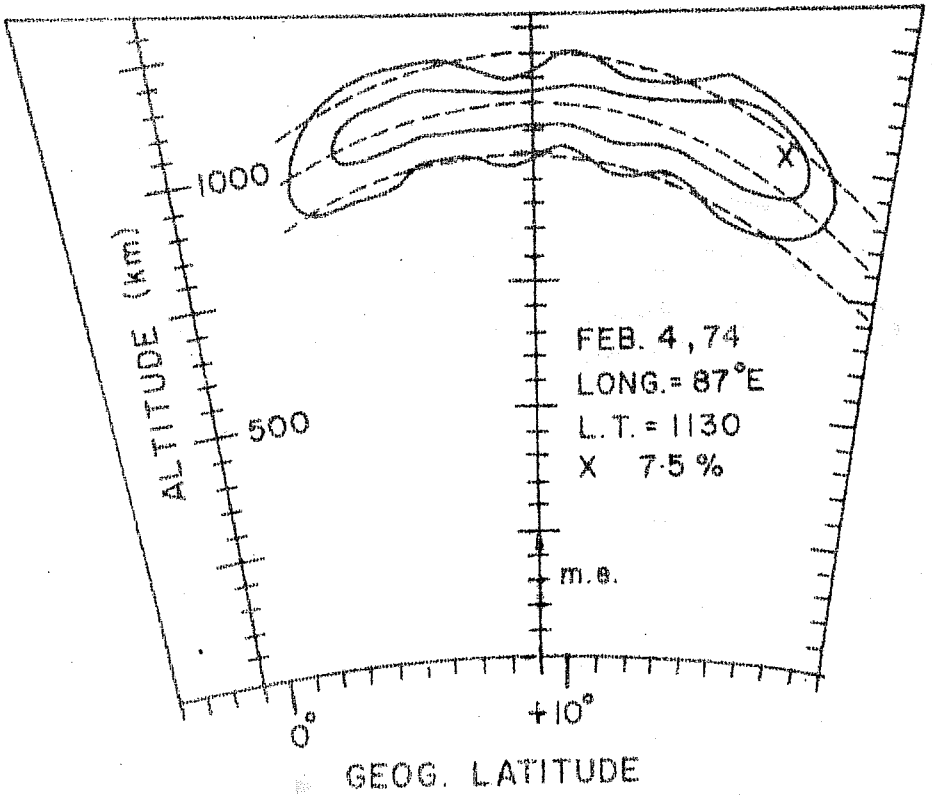


Fig.4.5

Figs. 4.4 and 4.5:- Spatial structures of the ledge on Jan. 8, 1975 at 0945 hr (83°EMT) and on Feb. 4, 1974 at 1130 hr (87°EMT) respectively obtained by means of ISIS-2 satellite.

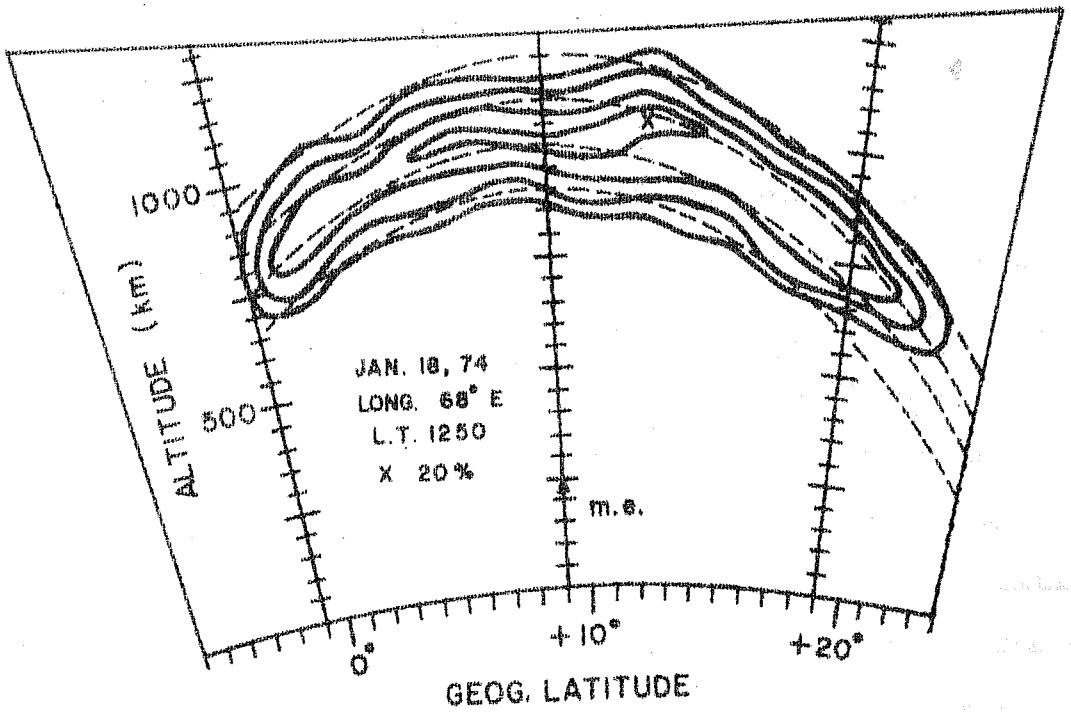


Fig. 4.6.- Spatial structure of the ledge on Jan. 18, 1974 at 1250 hr (68°EMT) by means of ISIS-2 satellite.

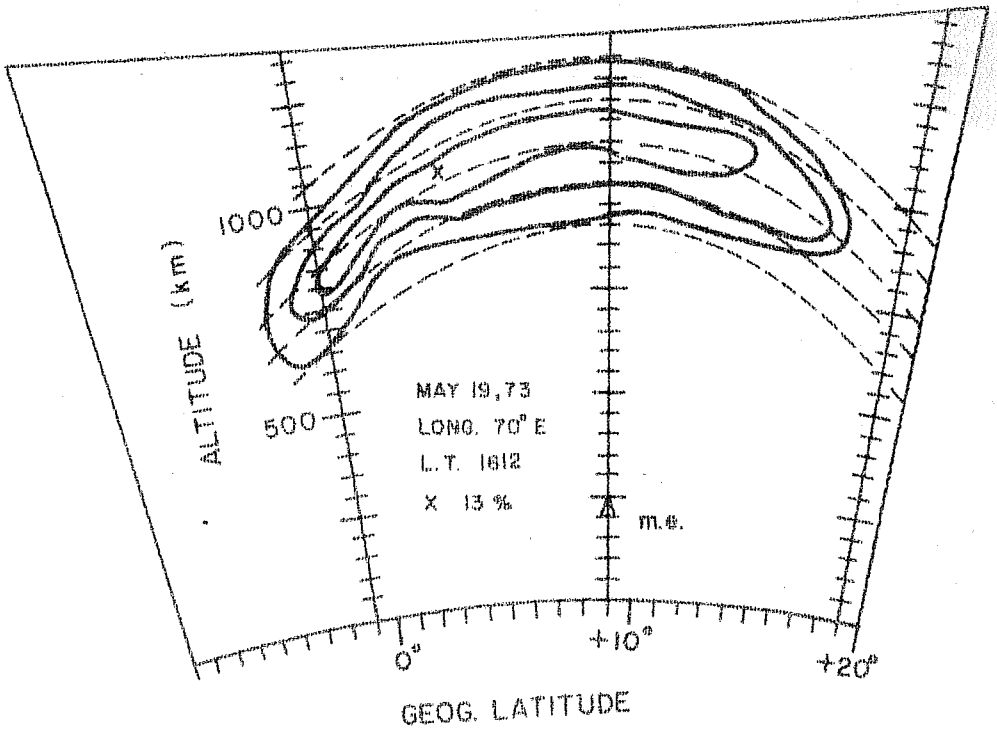


Fig. 4.7.- Spatial structure of the ledge on May 19, 1973 at 1612 hr

With the above assumption regarding the starting time of the cross-equatorial wind, its magnitude can be calculated from eq. (1). On substituting $\triangle L = 8^{o}.5$ latitude, $\triangle t = 7.7$ hrs and $I = 36^{o}$ for the ledge observation on Nov. 2, at 1842 hr LT shown in Fig. 4.3(a), one obtains the magnitude of the cross equatorial wind as 49 m/s, where $1^{o}$ geographic latitude has been taken as 130 km in the altitude region of the ledge. The wind speed thus obtained from the hemispherical displacement of ledge structure is of the same order as invoked by various authors to explain the observed solstice asymmetry of the IA.

We now present some more examples showing the displacement of the ledge into the winter hemisphere during solstitial months.

Fig. 4.7 shows the spatial structure of the ionisation ledge obtained from an ISIS-1 satellite at 1612 hr ($70^{o}$EMT) on May 19, 1973 (northern summer). The extremities of the latitudinal boundaries of the spatial structure in the two hemispheres are at $-3^{o}.0$ and $+17^{o}.0$ latitudes, thus giving the ledge lengths as $12^{o}$ and $8^{o}$ in the winter and the summer hemisphere respectively. The wind magnitude obtained from eq.(1), on substituting the observed values of the parameters $\triangle L$, $\triangle t$ and I, is 35 m/s.

Fig. 4.8 gives the ledge spatial structure on Dec. 7, 1973 at 1558 hr ($87^{\circ}$ EMT) obtained from an ISIS-2 pass. The ledge structure is almost completely displaced into the winter hemisphere. The magnitude of the cross-equatorial wind corresponding to the ledge displacement $\triangle L = 9^{\circ}.5$ latitude into the winter hemisphere, is found to be 71 m/s.

The spatial structures shown in Figs. 4.3 - 4.8 are typical of more than 50 examples, in which the ledge structure is found to be shifted into the winter hemisphere with no notable exception. It may be appropriate to point out that on rare occasions during equinoctial period also, the ledge is found to show small hemispherical displacements. An example of this kind is the spatial structure shown in Fig. 4.1(c) on March 19, 1974 at 2015 hr LT, in which the ledge length is $2^{\circ}$ more on the northern side of the magnetic equator than that on the southern side. The magnitude of the cross-equatorial wind calculated on this day, from eq.(1), is found to be about 9 m/s, which is much smaller than those found during solstitial period. Thus, it is likely that the cross-equatorial winds, small in magnitude though, might be present on occasion during equinoctial period.

It should be mentioned that the magnitude of the cross-equatorial wind, as obtained from the hemispherical shift of the ledge structure, represents the average wind prevailing between the time of the day at which significant cross-equatorial wind starts blowing and the time at which

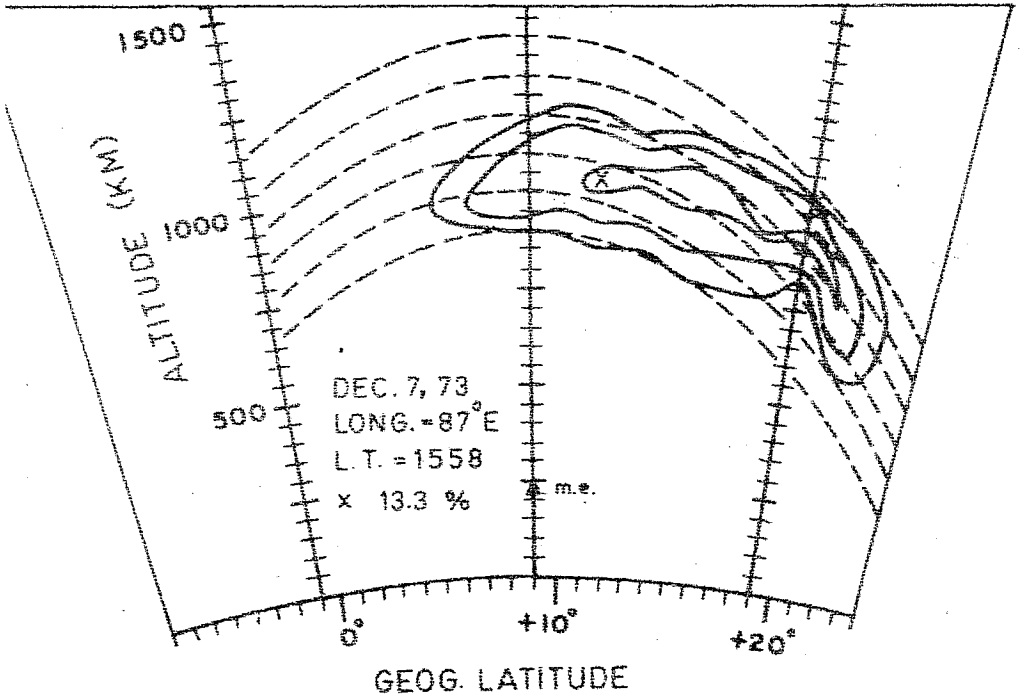


Fig.4.8

Fig.4.8:- Spatial structure of the ledge on Dec.7,1975 at 1558 hr (87°EMT) by means of ISIS-2 satellite.

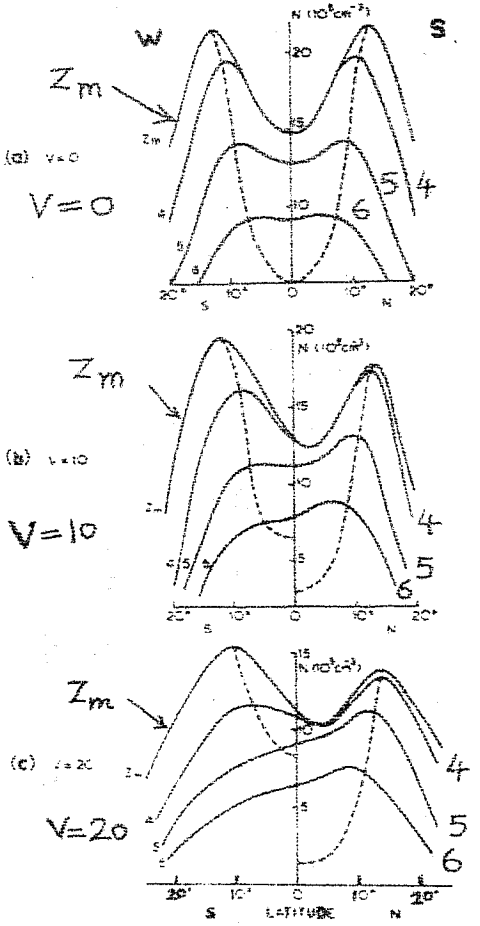


Fig.4.9

Fig.4.9:- Latitudinal variation of electron concentration at the height of the peak $Z_m$ and at three fixed heights in the topside ionosphere, Z = 4, 5, 6. The dashed lines are the anomaly field lines (a) wind speed V = 0, (b) V = 10 and (c) V = 20.
(After Bramley and Young, 1968)

The assumption regarding the time of the day at which significant cross-equatorial wind starts is perhaps the most critical in obtaining the wind speeds from the observed ledge displacements. It must be admitted that the starting hour for the wind has been estimated in the present work on the basis of scanty data of the ledge during the forenoon hours on different days having different magnetic activity conditions. It is likely that the starting hour of the wind has a day to day variation even on quiet days. The situation on magnetically disturbed days may be quite different and such days should be considered separately.

To ascertain how seriously the reckoning of the starting hour of the cross-equatorial wind affects its magnitude calculated from the ledge displacement, we recalculate the wind speeds on two of the occasions presented above by assuming the cross-equatorial wind to be operative at 1000 hr LT rather than at 1100 hr LT assumed previously. For the ledge observation on Nov. 2, 1973 at 1842 hr LT, shown in Fig. 4.3(a), the new value of the parameter $\Delta t$, by taking the starting hour of the wind at 1000 hr LT, is 8.7 hours. With this value of $\Delta t$, the magnitude of the wind, as estimated from eq.(1) is 44 m/s against the value 49 m/s obtained previously. For the ledge observation on Jan.18, 1974 at 1250 hr LT, shown in Fig. 4.6, the assumed starting time 1000 hr of the wind gives its magnitude as 47 m/s

against 73 m/s obtained earlier. From these two examples it is apparent that the evaluation of the cross-equatorial wind from the hemispherical displacement of the ledge, depends rather critically on the starting hour of the wind especially if the ledge observation is made in the early afternoon hours.

However, if one makes the observations of the ledge at close intervals of time on a single day, by means of two or more polar orbiting satellites, the starting time of the cross-equatorial wind can be ascertained fairly accurately and also the actual wind magnitudes at different local hours can be estimated.

It is interesting to compare the observed ledge displacement $\triangle$ L with the corresponding magnitude of the solstice asymmetry of the IA. We take the parameter R, the ratio of electron concentration at the summer peak and that at the winter peak at a fixed altitude in the topside ionosphere as a measure of the solstice asymmetry of the IA, on the basis of the work of Bramley and Young (1968) as discussed below.

Fig. 4.9 reproduced from Bramley and Young, shows the latitudinal distribution of electron concentration at the $h_{max}F2$ altitude and at three fixed altitudes in the topside (denoted by Z = 4, 5 and 6; where Z denotes the altitude above $h_{max}F2$ level in units of the electron density scale height).

The parameter V represents the cross-equatorial wind; V = 1 unit means wind speed of 4 m/s. It is apparent from Fig. 4.9 that the two anomaly peaks at any altitude for V = 0 are of equal strength. For V = 10, the anomaly peaks are asymmetric, the summer peaks being of higher strength than the corresponding winter peaks in the topside ionosphere. For V = 20 the asymmetry in the anomaly peaks in the topside ionosphere is seen to be more pronounced than for V = 10. For example, at the altitude Z = 4 the ratios of electron concentration at the summer peak to that at the winter peak (denoted by R) are 1.098 and 1.155 for V = 10 and V = 20 respectively. Thus the asymmetry of the ionisation anomaly becomes more pronounced for the higher cross-equatorial wind magnitude.

We have shown that the parameter $\triangle L$ representing the ledge displacement into the winter hemisphere is a measure of the cross equatorial wind. Fig. 4.10 shows a plot of $\triangle L$ against R, where the two parameters have been evaluated from the same satellite pass. R as defined above has been evaluated at 500 km altitude. The number of data points at the origin of the coordinates is five and thus the total number of data points is sixteen. The high correlation coefficient ($0.92 \pm 0.04$) obtained between the ledge displacement and the degree of solstice asymmetry of the ionisation anomaly provides further confirmation that the cross-equatorial wind velocities are measured by the hemispherical displacement of the ledge structure.

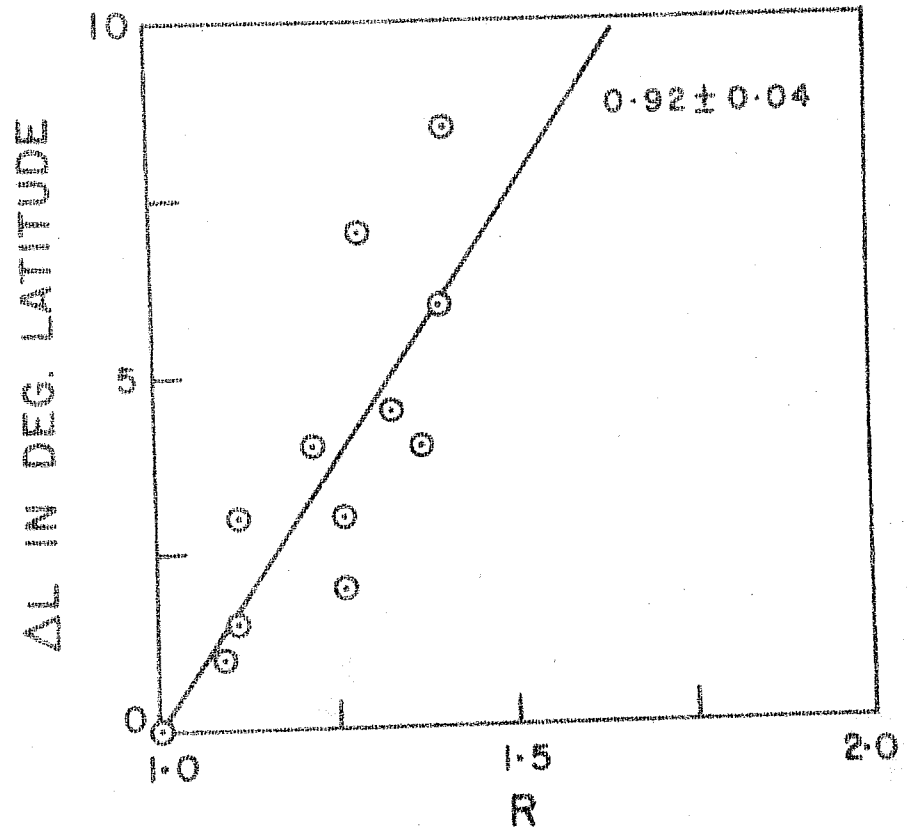


Fig.4.10:- Plot of the parameter $\Delta$ L of the ledge against the anomaly parameter R. The straight line represents the fitted regression line.

## IV.4 DISCUSSION AND CONCLUSION

The asymmetric ionisation anomaly (IA) peaks during solstice period, with the winter crest being of higher strength than the summer crest, would produce the corresponding asymmetry in the neutral anomaly (NA). This can be seen from the process of the NA formation described in Sec. I.3.3 of Chapter 1.

As the NA crest of higher magnitude forms on the winter side than on the summer side of the magnetic equator, the inhibition of plasma diffusion velocity along the field line passing through the crest becomes more severe in the winter hemisphere in proportion to the higher NA crest strength (see Sec. I.3.2 of Chapter 1 for ambipolar plasma diffusion). It appears that the magnetic field line tube containing the winter NA crest is heated up more than the field tube containing the summer crest, of course, each one in relation to its average hemispherical temperature. The plasma lifted up by the $\underline{E} \times \underline{B}$ force over the equator upto the ledge field line would then accrue essentially on the winter side to form the displaced ledge as evidenced by the examples presented in this chapter. To the extent that the asymmetry in the IA crest formation is dependent on the wind magnitude and its duration, the asymmetry of the spatial structure of the ledge would also be proportional to the wind magnitude and its duration. The dependence of the NA strength on the strength of IA is discussed in detail in Sec. III.5 of Chapter 3. Hence it is the average cross equatorial wind magnitude that is inferred from the asymmetrical distribution of the ledge spatial structures.

The author is wary about the limitation of the assumption regarding the local time at which significant cross equatorial wind starts. It is possible that the starting time is different on different days.

Although, the method of calculation adopted for the average wind may leave the impression on one that the ledge asymmetry is due to the shift of the ledge contours by the wind into the winter hemisphere; the purpose is essentially to evaluate the average wind. The physical process involved is that the wind causes the asymmetry in the IA which in turn causes asymmetry in heating the magnetic flux tube (during the time of NA formation) that results in higher concentration of ledge strength and also the longer length on the winter side as the asymmetry in the NA is expected to increase with the duration of the wind.

In conclusion, the spatial distribution of the ledge intensity provides observational evidence for the existence of the cross equatorial winds at the F region altitudes during solstitial period. The magnitude of the wind has been estimated from the observed displacement of the ledge into the winter hemisphere by making certain assumptions (based on our observations) regarding the local time of the day at which the wind becomes significant. The estimated

magnitudes of the cross equatorial wind are of the same order as required by theory to account for the observed solstice asymmetry of the ionisation anomaly. On this basis Raghavarao et.al. (1976 b) proposed that the ionisation ledge is a tracer for the cross equatorial winds at F region altitudes.

# C H A P T E R - V

## LUNAR EFFECT ON THE IONISATION LEDGES

### V.1 INTRODUCTION

Matsushita and Tarpley (1970) have discussed the electrostatic field distribution in the E region by examining dynamo actions due to various solar and lunar tidal modes. The equation governing the ionospheric dynamo action resulting in the current $\underline{j}$ is given by

$$\underline{j} = [\sigma].(\underline{V} \times \underline{B} + \underline{E})$$

where $[\sigma]$ is the electrical conductivity tensor, $\underline{v}$ is the neutral wind velocity, $\underline{B}$ is the main magnetic field of the earth and $\underline{E}$ is the electrostatic field. The wind field is primarily produced by the tidal forces due to the sun and the moon.

Matsushita (1969) and Tarpley (1970a,b) computed the current systems by taking the wind field corresponding to various modes of solar and lunar tides. It was shown that the solar diurnal (1, -1) tidal mode (mainly due to the solar heat input to the lower atmosphere) and the lunar semidiurnal (2, 2) tidal mode (mainly due to gravitational attraction of the moon) satisfactorily explain the experimentally deduced Sq and L variations in the geomagnetic H field, denoted by Sq(H) and L(H) respectively, on the ground.

These authors also calculated the electric fields S and L corresponding to the solar (1, -1) and lunar (2, 2) tidal modes respectively. They showed that at low latitudes both the S and the L electrostatic fields are mainly in the east-west direction, with very small north-south component. The S electric field has a magnitude of about 1 millivolt/m and is directed eastward during daylight hours and westward at night. The change of direction occurs around the sunrise and sunset times. The L field is semidiurnal with maximum amplitude of about 0.2 millivolt/m. The vertical $\underline{E} \times \underline{B}$ drift of the plasma in the equatorial F-region, due to the electric field generated in the dynamo region and communicated up along the earth's magnetic field lines, would be about 30 m/s and 6 m/s for S and L fields respectively (assuming B field as 0.3 gauss).

Rastogi (1961) found that the amplitude of the lunar tide in midday foF2 is abnormally large within a narrow belt around the magnetic equator. He showed that the amplitude of the predominant semi-monthly component of the lunar variation in foF2, when plotted against magnetic latitude has peaks at the equator and at about $\pm 20^{\circ}$ latitude. The phase distribution shows a sharp 6 hr shift in lunar time at about $\pm 10^{\circ}$ latitude. Later studies by Rastogi (1963, 1965) and Rush et al. (1968) showed that the lunar tidal variations in the F2 region vary with both latitude as well as solar time.

Anderson et al. (1973) and more recently Abur-Robb and Dunford (1975) have made theoretical evaluation of the lunar tidal variations in the F2 layer by solving the time dependent continuity equation for the electrons by including the vertical drift due to the S as well as the (S + L) electric field in the divergence term. The results obtained by these authors showed good agreement with the observations of Rastogi and Rush et al. mentioned above.

In this chapter the author presents the effect of the moon on the occurrence and the intensity of the ionisation ledges in the equatorial topside ionosphere.

## V.2 PARAMETERS OF THE LUNAR VARIATIONS IN THE IONOSPHERE

According to the phase law of lunar daily variation L(X) in any ionospheric parameter X, can be satisfactorily represented by the sum of four harmonic terms as (Chapman and Bartels, 1940 p. 248)

$$L(X) = \sum_{n=1}^{4} C_n \sin\{n\tau + (n-2)\nu + \alpha_n\} \qquad ----(1)$$

where $C_n$ and $\alpha_n$ denote the amplitude constants and the phase constants respectively. $\nu$, the lunar age and $\tau$, the lunar time are defined as follows.

The lunar age $\nu$ is defined as the position of the moon with respect to the mean sun and is reckoned either in angular measure or in hours ($15^{\circ}$ = 1 hr). The age of the moon completes a full cycle of 24 hours in the course of a synodic month; the value $\nu$ = 0 (or 24) hr refers to the

new moon and $\nu$ = 12 hr corresponds to the full moon. The value of $\nu$ increases by about 0.8 hr in the course of a mean solar day. The values of $\nu$ on individual days for the years 1850-2050 have been computed by Sugiura and Fanselau (1966). Some authors use the parameter lunar phase, $\mu$, which is related to the lunar age $\nu$ as $\mu = 24 - \nu$.

The lunar time $\tau$ is defined in anology with the mean solar time, t. Just as t is counted in 24 solar hours from midnight to midnight, $\tau$ is reckoned as zero for the lower transit of the mean moon and increases by 24 lunar hours up to the next lower transit. A mean lunar day equals 1.03505 solar days or $24^h\ 50.47^m$. The parameters t, $\tau$ and $\nu$ are related as

$$t = \tau + \nu \qquad \text{----(2).}$$

On substituting for $\nu$ from eq.(2) into eq.(1), one obtains

$$L(X) = \sum_{n=1}^{4} C_n \sin\{(n-2)t + 2\tau + \alpha_n\} \qquad \text{---(3)}$$

It is apparent from eq.(3) that the lunar semidiurnal (n = 2) component does not depend on solar time. The other components ($n \neq 2$) arise from solar modulation of the lunar semidiurnal oscillation. When eq.(3) is averaged in solar time, all the terms except the lunar semidiurnal component vanish. The solar modulation of L

is caused by local time variations in atmospheric and ionospheric parameters that, in turn, modify either the lunar tide or the resulting electromagnetic variations.

## V.3 RESULTS AND INTERPRETATION

The ISIS satellite data recorded at Ahmedabad during the period Feb.1972 - Mar. 1975 in the local time range 1000 - 2200 hr have been examined by the author for the presence of the ledge. During this period the ledge is found to be present on 216 days out of 577 days examined on which the data are available in the above local time range.

In Fig. 5.1, the histogram shown by short dashes gives the number of days on which the ionogram data are examined for the ledge formation for each lunar age ( $\lambda$ ). It is seen that the average number of days is about 24 at any lunar age, except at $\lambda$ = 4 and 8 hr for which the numbers are 20 and 21 respectively. The histogram shown by the solid line gives the distribution of the number of ledge occurrences. Two broad peaks in the occurrence of the ledges, around 01-05 hr and 13-15 hr lunar age, are apparent. The depression in the ledge occurrence distribution at $\lambda$ = 4 hr is probably due to the smaller number of data samples available for this lunar age and therefore we reckon the first peak to extend between 01-05 hr lunar ages.

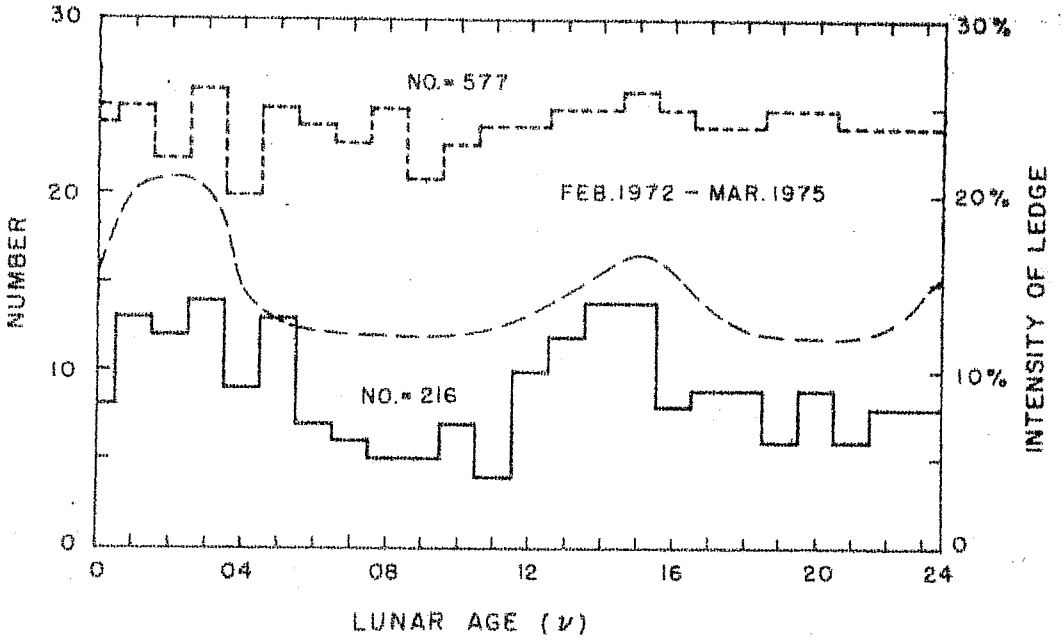


Fig.5.1:- The lunar age dependence of the occurrence (continuous histogram) and the intensity (smooth dashed curve) of the ionisation ledge. The dashed histogram gives the number of satellite passes examined for the ledge occurrence.

The average intensity distribution of the ledge is shown by the smooth curve drawn with long dashes and reveals two more defined peaks (than the occurrence distribution) around 01-03 and 14-15 hr lunar ages. The average intensity of the ledge is obtained by taking the arithmatic mean of the individual intensities for each lunar age.

We explain the observed dependence of the occurrence and intensity of the ionisation ledge on the basis of modulation of the diurnal solar electric field (S) by the semidiurnal lunar electric field (L). For certain lunar ages, L and S are in phase during the forenoon hours with the result that the resultant (S + L) electric field causes strong ionization anomaly (IA) formation around midday hours that, in turn, helps in building up the neutral anomaly (NA).

The modulation of the S field by the L field for three lunar ages, $\gamma$ = 0, 4 and 8 hr, is given by Anderson et al. (1973), and is reproduced in Fig. 5.2. The S and L fields were computed from the geomagnetic H field measured at Huancayo and the horizontal drift velocity of electrons at the E region altitude (by means of Jicamarca backscatter radar). Anderson et al. solved the time dependent continuity equation for electrons in the F2 region. The continuity equation was solved by including the appropriate $\underline{E} \times \underline{B}$ drifts corresponding to the electric fields S and (S + L) separately. By comparing the critical frequencies foF2,

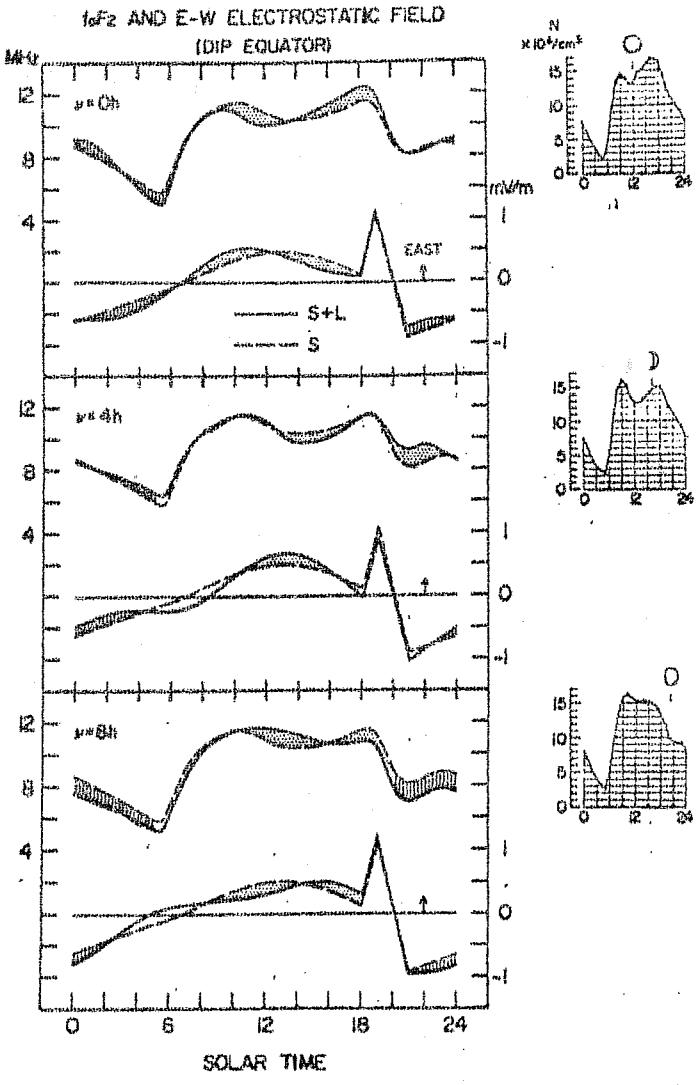


Fig.5.2:- Lunar variation of the solar diurnal E-W electric field for three lunar ages, 0, 4 and 8 hr, and the computed daily variation of foF2 at the dip equator. The right side of the figure shows Bartel's determinations for Huancayo at lunar ages corresponding to the computed foF2 curves (after Anderson et al, 1975).

obtained from the solution of the continuity equation corresponding to the (S + L) field with those corresponding to the S field, the lunar influence on the F2 layer was estimated. Fig. 5.2 is divided into three parts corresponding to $\gamma = 0$, 4 and 8 hr and in each part there are two sets of curves. The two curves in each lower set show the diurnal variation of S and (S + L) electric fields, represented by the dashed and the continuous lines respectively, and the two curves in the upper set represent the corresponding computed foF2.

In the case $\gamma = 0$ hr, the (S + L) field is higher than the S field between 0700 and 1215 hr LT. The midday bite-out in foF2 becomes more pronounced corresponding to the (S + L) field between 0830 and 1330 hr LT. It was shown by Rastogi (1959 ) that the midday bite-out in the daily variation of the foF2 near or at the dip equator is a manifestation of the strength of 'fountain effect' which produces the IA. The ionisation lifted up at the equator during daytime, because of the $\underline{E} \times \underline{B}$ effect, diffuses down the magnetic field lines thereby producing depletion at the equator (and hence the reduction in equatorial foF2) and enhancement at latitudes 15-20° away on either side of the dip equator. Thus it is clear from Fig. 5.2 that the strength of the IA, as depicted by the noon bite-out, for $\gamma = 0$ hr is higher between 0830 hr and 1330 hr LT for the (S + L) field than for the S field.

The condition for the NA formation, as discussed in Chapter 1, is that strong IA should be present around midday hours when the neutral speed is minimum before its reveral from westward to eastward direction. For the case $\gamma$ = 0 hr, the lunar modulation causes enhancement of the IA strength between 0830 and 1330 hr LT, and thus this lunar age should be favourable for the NA formation and hence for the ledge formation, on the basis of the mechanism given by Raghavarao and Sivaraman (1974).

For the case $\gamma$ = 4 hr, the (S + L) field is higher than the S field between 1045 hr and 1600 hr LT as seen from Fig. 5.2. The midday bite-out in foF2 is seen to be more pronounced between 1300 hr and 1800 hr LT for the curve corresponding to the (S + L) electric field than for the curve corresponding to the S electric field. Thus the enhancement of the IA for $\gamma$ = 4 hr occurs in the afternoon hours, later in local time than for $\gamma$ = 0 hr. The lunar age $\gamma$ = 4 hr is also favourable for the neutral anomaly formation on the basis of the arguments given for the case $\gamma$ = 0 hr.

From the lowermost part of Fig. 5.2 for the case $\gamma$ = 8 hr, it is seen that the (S + L) field is lower than the S field, thus revealing that the S and the L fields are in opposite phase, during the local time interval 0830-1430 hrs.

The reduction in the electric field during the forenoon hours for $\gamma$ = 8 hr causes the midday bite-out to be less pronounced between 1030 hr and 1600 hr LT, as is evident by comparing the foF2 daily variation profiles corresponding to the S and the (S + L) fields. Thus the IA in the afternoon hours between 1030 and 1600 hr LT is reduced for $\gamma$ = 8 hr and as a result, this lunar age would be less favourable for the NA formation than $\gamma$ = 0 or 4 hr .

From the work of Anderson et al. described above, it is apparent that the ionospheric electric field produced by the solar tide is modulated by the semidiurnal lunar tidal electric field. The modulation occurs in such a way that the period during which the two fields are in phase, shifts progressively to later local times with the progress of lunar age from $\gamma$ = 0 hr to $\gamma$ = 8 hr. The period during which the enhancement of the IA occurs, also shifts correspondingly to later local times. For $\gamma$ = 0 hr, the IA enhancement occurs between 0830 hr and 1330 hr LT and thus this lunar age is favourable for NA formation and hence for the ionisation ledge formation. For $\gamma$ = 4 hr the enhancement of the IA occurs between 1300 hr and 1800 hr LT. It is apparent from Fig. 5.2 that the noon bite-out in the daily variation of the foF2 curve corresponding to the (S + L) field for the case $\gamma$ = 4 hr is as prominent as that for the case $\gamma$ = 0 hr thus indicating that the electron concentration

enhancement at the crests of IA will be approximately same for either of these lunar ages, although it occurs at a later local time for $\lambda$ = 4 hr. It may be recalled here that the depression in the number of ledge occurrences for $\lambda$ = 4 hr as seen from Fig. 5.1 is an apparent effect caused by the smaller number of satellite passes available for this lunar age. However, the mean intensity of the ledge shows a significant decrease at $\lambda$ = 4 hr and is probably real. For $\lambda$ = 8 hr, the IA strength decreases significantly during midday hours and therefore this lunar age should be less favourable for the NA and hence the ledge formation. Indeed, Fig. 5.1 shows minima in the occurrence as well as intensity of the ledge for $\lambda$ = 8 hr.

Rastogi's work (1966) provides an observational evidence for the enhancement of the IA around midday hours for the lunar age $\lambda$ = 3 or 15 hr. Fig. 5.3 reproduced from his work gives latitudinal distribution of midday foF2 (averaged between 10-14 hr LT), for two lunar phases $\mu$ = 9 or 21 hr and $\mu$ = 3 or 15 hr, obtained from a chain of ground based ionosondes on either side of the magnetic equator. The parameter $\mu$ is related to the parameter $\lambda$ as $\mu = (24 - \lambda)$. This figure clearly shows that the crests of IA are of higher strength and the trough is deeper for $\lambda$ = 15 or 3 hr ($\mu$ = 9 or 21 hr) than for $\lambda$ = 21 or 09 hr ($\mu$ = 3 or 15 hr). For $\lambda$ = 15 or 3 hr, the ratios of crest to trough value of foF2 (representing the IA strength)

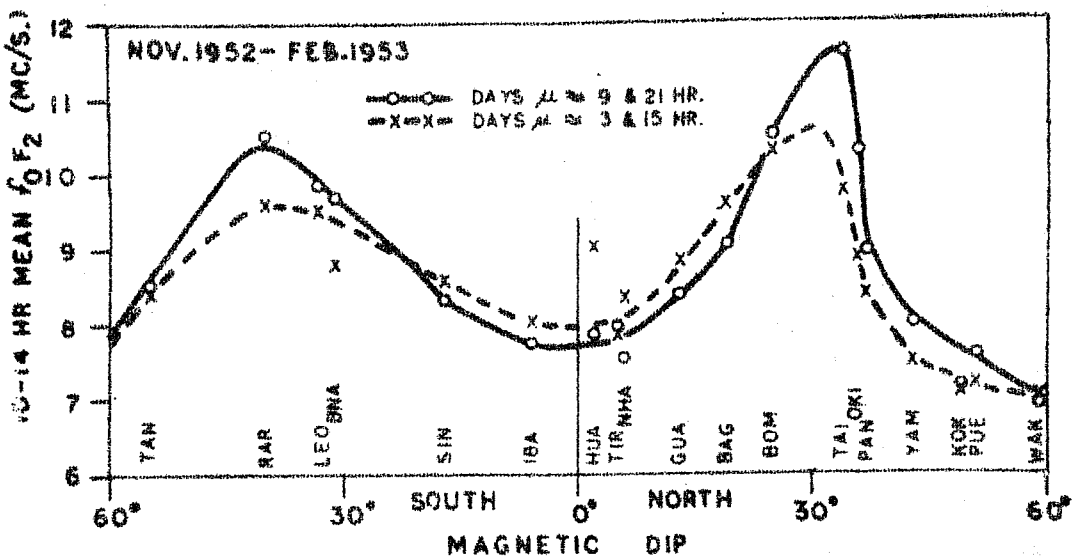


Fig. 5.3:- Latitudinal variation of foF2 averaged over 10-14 hr LT on days of lunar phase 9 or 21 hr and 3 or 15 hr for the period November 1952 to February 1953 (after Rastogi, 1966).

are 1.50 and 1.34 for the northern and the southern crests respectively whereas for the case $\lambda$ = 21 or 9 hr, the crest-to- trough ratios for the two crests are 1.32 and 1.19. Thus Rastogi's work confirms that the IA strength during the midday hours is higher for $\lambda$ = 03 or 15 hr than for $\lambda$ = 09 or 21 hr.

## V.4 DISCUSSION AND CONCLUSION

The lunar age dependence of the occurrence as well as intensity of the ionisation ledge is explained on the basis of the modulation of the diurnal solar electric field by the semidiurnal lunar electric field. The fact that a significant number of ledges occur even for those positions of the moon which seem to be unfavourable (on the basis of the work of Anderson et al. 1973 and Rastogi, 1966), shows that the moon has only a small modulating effect on this phenomenon caused primarily due to the sun. The lunar modulation in the occurrence as well as the intensity of the ionisation ledge is about 25-30%, which is of the same order as the lunar modulation in the S electric field around the noon hours, as may be noted from Fig. 5.2.

It should be mentioned that the explanation of the lunar effect on the ledges presented above is based on the model S and L field variations. In general, the relative magnitudes of these two electric fields could be different on different days. It is indeed shown by Onwumechilli (1967, p.448) that the mean Sq(H) as well as L(H) show considerable

day to day variation. On usual days, the L(H) is about 10-30% of the Sq(H). It is likely that the S field on the days around the lunar age $\psi$ = 8 or 20 hr, for which the ledge occurrence shows non-zero minima, might have been higher (or alternatively the L field might have been lower) than on usual days, with the result that the effect of the lunar electric field is comparatively small. On this basis it is possible to explain the formation of the ionisation ledges around the lunar age 8 or 20 hr.

It is interesting to note that the lunar age dependence of the counter-electrojet phenomenon in the E region also reveals maxima around $\psi$ = 02-03 hr and 14-15 hr as shown by the work of Sastry and Jayakar (1972) and Rastogi (1975 a ). On the basis of the similarity in the lunar age dependence of these two phenomena, together with the fact that both the phenomena occur more predominantly in solar minimum period than in solar maximum period, usually on a sequence of days in succession, it was felt desirable to make a comparative study of their occurrence on a day to day basis. The results of this study are presented in the next chapter.

# C H A P T E R - VI

## THE IONISATION LEDGE AND THE COUNTER ELECTROJET

### VI.1 INTRODUCTION

In this chapter the author presents a comparative study of the two phenomena : the ionisation ledge in the topside ionosphere and the counter electrojet in the E region. The similarities in the morphological features exhibited by the two phenomena are pointed out in Chapters3 and 5. Both the phenomena occur more frequently in sunspot minimum years, usually in a sequence of successive days. Both reveal the same lunar age dependence in their occurrence. On occasion both the phenomena occur in a narrow longitude zone ( $\sim 30^{\circ}$) and exhibit different intensities when they occur simultaneously at two longitudes about $30^{\circ}$ apart. On the basis of the above similarities in the morphological features of the ledge and the counter electrojet, it is desirable to compare the occurrence of the ledge and the afternoon counter electrojet on a day to day basis. The implications of these results are discussed and the significant role of the F region dynamics as a possible causative mechanism for the counter electrojet phenomenon for which no satisfactory explanation exists so far, is pointed out.

### VI.2 MORPHOLOGICAL FEATURES OF THE COUNTER ELECTROJET PHENOMENON

On a magnetically quiet day, the usual pattern of the daily variation of the H component of the geomagnetic field at an equatorial station consists of a steady increase in the

morning hours from about 0600 LT to about 1100-1200 LT followed by a smooth drop to nighttime zero level by about 1800 LT (Chapman and Bartels, 1940). However, on occasion the diurnal variation of the H field is found to deviate from its normal behaviour. It is known that the large diurnal variation in the amplitude of H field at an equatorial station is caused by a strong eastward current at the E-region altitudes called as the equatorial electrojet (Chapman, 1951 ), described in some detail in Sec. II.1, Chapter 2. Bartels and Johnston (1940) found large fluctuation and decrease in the geomagnetic horizontal (H) field daily variation at equatorial station Huancayo on occasion during daytime hours of magnetically quiet days. Gouin (1962) reported a considerable decrease of H field at equatorial station Adis Ababa on certain days around noon hours. Gouin and Mayaud (1967) found that the decrease in the H component was accompanied by an increase in the Z component. The phenomenon occurred more predominantly at 0700, 1200 and 1500 hrs. LT. Gouin and Mayaud examined the global extent of the phenomenon and concluded that it is due to the existence of a narrow current ribbon analogous to the equatorial electrojet but in the reverse direction, and named the phenomenon as "counter electrojet". Subsequently, this phenomenon was observed at other equations: Zaria and Ibadan (Hutton and Oyinloye, 1970), Kodaikanal and Trivandrum (Rastogi et al. 1971; Krishnamurthy and Sengupta, 1972; Rastogi, 1972 ), and a number of equatorial stations in American and African sectors (Kane, 1973a; Rastogi, 1974a).

Another feature which is associated with the counter-electrojet phenomenon is the sudden disappearance of q-type of sporadic E (Es-q) at the equatorial stations. The Es-q occurrence at the equatorial latitudes between 08 hr and 18 hr is a fairly regular phenomenon. However, on occasion Es-q disappears suddenly in the afternoon hours (hereafter called as SDEs-q event) and sometimes reappears for a short time before it finally disappears in the evening (Matsushita, 1957; Krishnamurthy and Sengupta, 1971, 1972; Rastogi et al. 1971; Rastogi, 1972 ). The SDEs-q event is shown to be associated with abnormal depression in the H field at equatorial stations. Rastogi et al. (1971) showed that the ionospheric E and F region horizontal drift velocity of electrons (as estimated by means of the spaced receiver technique) at the magnetic equator reverses from westward to eastward direction simultaneously with the SDEs-q event and the depression the equatorial H field. On the basis of these features, it was concluded by Rastogi et al. that the SDEs-q is due to a temporary reversal of the electrojet current which is caused by the imposition of an additional electrostatic field opposite in direction to that of the normal Sq electric field. Fambitakoye et al. (1973) showed that the condition for SDEs-q event is not necessarily the $\triangle$H at the magnetic equator becoming negative (relative to the nighttime zero level) but the latitudinal profiles of $\triangle$H and $\triangle$Z getting reversed. On a normal electrojet day at any local time during daylight hours $\triangle$H is maximum at equator (directly under the electrojet) and

decreases on either side. The normal $\triangle Z$ variation shows positive and negative values on the southern and northern side of the equator respectively; $\triangle Z$ at the equator itself being zero. At the time of counter-electrojet the latitudinal profiles of both $\triangle H$ and $\triangle Z$ become reversed. Fambitakoye et al. state that reversal in the latitudinal profiles of $\triangle H$ and $\triangle Z$ is better evidence for the occurrence of counter electrojet than $\triangle H_{equator}$ becoming negative. Rastogi (1974a) has shown examples of SDES-q event when the latitudinal profiles of $\triangle H$ and $\triangle Z$ show reversal, although $\triangle H$ field at an equatorial station is significantly positive (i.e., above the nighttime base level). Such events are called as "Partial counter electrojet" by Rastogi.

There is a marked effect of sunspot activity on the occurrence of the counter electrojet, the largest number of events occur in the sunspot minimum period (Gouin and Mayaud 1967; Hutton and Oyinloye 1970; Rastogi, 1973a; 1974a). In addition, Hutton and Oyinloye found the phenomenon to occur more frequently during times of low magnetic activity. However, Kane (1973c) showed that the counter electrojet occurs even during disturbed days and that its existence can be inferred from the diurnal variation of the quantity $\triangle Sd_I$, where $Sd_I$ is defined as $Sd_I = H_{equator} - H_{non\text{-}equator} + Sq_{non\text{-}equator}$. Chandra and Rastogi (1974 ) and Rastogi (1975b) showed that during disturbed periods the counter electrojet can be identified from the daily variation of the

parameter ($\triangle H_{equator} - \triangle H_{non\text{-}equator}$). Rastogi (1975 b) showed that the Es-q at Kodaikanal is absent precisely during the same time when the difference of $\triangle H$ at Kodaikanal and that at Alibag, ($\triangle H_{KOD} - \triangle H_{ALI}$) shows negative values; even a slightly positive value of the above parameter gives rise to fairly high values of foEs-q (the highest frequency at which Es-q is observed on the ionogram).

Gouin (1962) noted a remarkable depression of the H field at Adis Ababa on two consecutive days around noon hours. Rao and Rajarao (1963) reported that the H field, observed at the equatorial stations Trivandrum and Annamalainagar, did not show any noon depression on the same two days on which the counter electrojet was reported at Adis Ababa by Gouin (1962). It may be noted that the two stations Adis Ababa and Trivandrum (geographic longitudes $39^{\circ}$E and $77^{\circ}$E respectively) are separated by less than 3 hours in local time. Gouin and Mayaud (1967) also noted the occurrence of counter electrojet on some occasions in a restricted longitude range. Hutton and Oyinloye (1970), however, make a mention of a private communication with Mayaud in which the counter electrojet is reported to have occurred over a wide range of longitudes on the same day but with greatly varying amplitude at different longitudes. Kane (1973 a) and Rastogi (1973 a, 1974 a) presented a number of examples on the afternoon counter electrojet occurring in a narrow longitude zone.

Kane (1973 a) found an indication that the phenomenon is most prominent in the American zone, analogous to the normal equatorial electrojet which is known to have large amplitude in the American zone (Rastogi, 1962). Rastogi (1974 a), however, concluded that the evening counter electrojet events, although less prominent, are more frequent in Indian zone (where the electrojet current is weaker) than in the American zone.

A very conspicuous feature of the afternoon counter-electrojet phenomenon is its occurrence on a series of days in succession at a particular equatorial station. This behaviour was first reported by Hutton and Oyinloye (1970) and later by Kane (1973 a) and Rastogi (1973 a, 1974 a). Fig. 6.1 reproduced from the work of Kane (1973 a) clearly brings out both the featuresof the counter electrojet phenomena: a) the occurrence on a sequence of days (Dec. 18-21, 1964) and b) the narrow longitude range of its occurrence. The geographic longitudes of the three stations shown in Fig. 6.1 are $75^{o}$W (Huancayo), $39^{o}$E (Adis Ababa) and $77^{o}$E (Trivandrum). The afternoon depression in $\triangle Sd_I$ is seen on all the four days at Huancayo, only two days at Addis Ababa and none of the four days at Trivandrum. Thus, it is evident that the phenomenon does not occur at all longitudes on a particular day.

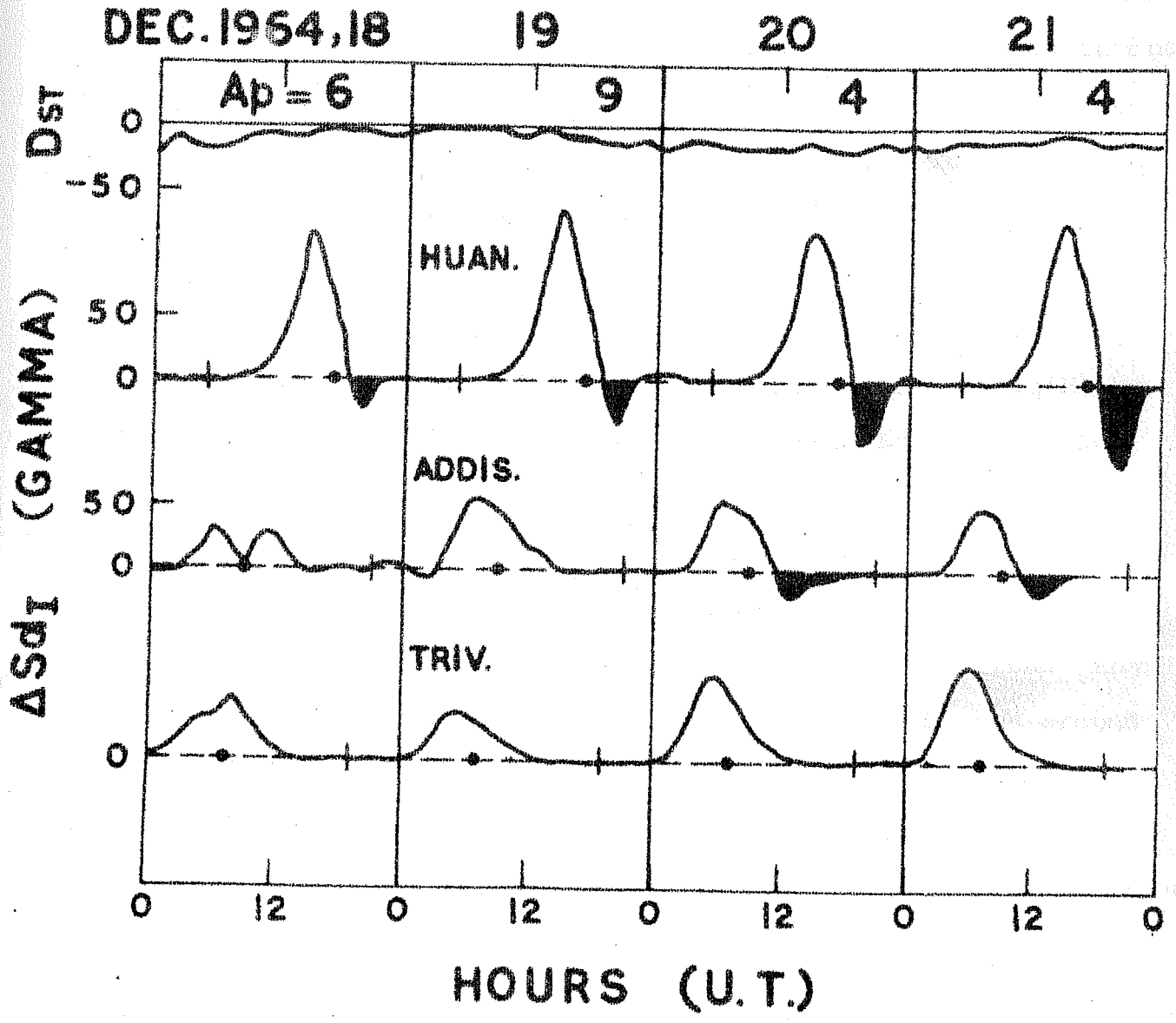


Fig. 6.1- Plots of hourly values (U.T.) of $\Delta Sd_I$ at Huancayo, Addis Ababa and Trivandrum for December 18-21, 1964. (after Kane, 1975 a)

SUMMARY OF THE EARLIER WORK ON COUNTER ELECTROJET

Bartels and Johnston (1940) suggested that the lunar modulation of the geomagnetic H field, L(H), is enhanced in the region of the equatorial electrojet similar to the enhancement of the solar variation of the H field, Sq (H). They suggested that L(H) is responsible for causing depressions in the H field. On some occasions (later called as 'Big L days' by Onwumechilli, 1963) L(H) could be comparable to Sq(H). Onwumechilli (1963, 1964) studied the modulation of Sq(H) by the L field and concluded that although the 'Big L days' do exist, the phases of Sq(H) and L(H) are found to be sometimes parallel and sometimes anti-parallel. Onwumechilli and Akasofu (1972) studied the days on which strong afternoon depression in the H field occurred at Huancayo and found that the depressions occurred most frequently in the months around December when L(H) is known to be greatest at the magnetic equator. However, they noted that the maximum depression in the H field does not always occur at minimum of L(H) indicating that the two are not really correlated.

Gouin and Mayaud (1967) suggested that the moon has no effect on the counter electrojet, as they found the phenomenon to occur at all times of the lunar day. Hutton and Oyinloye (1970) found that the distribution of its occurrence maximises around 0300 and 1500 lunar hours (thus coinciding with the centres of the intervals during which the L currents oppose the Sq currents), with two minima

around 0800 and 2000 lunar hours. The fact that counter electrojet occurred at all lunar hours, led Hutton and Oyinloye to reach the same conclusion, as that of Gouin and Mayaud (1967), that the moon has no effect on the counter electrojet.

Van Sabben (1968) concluded that the counter electrojet is associated with the solar flare current system but Hutton and Oyinloye found that on 14 occasions (out of 16) of solar flares observed during 1963, none was accompanied by any negative effect on the equatorial magnetograms. Hutton and Oyinloye also showed that the symmetric ring current ($D_{st}$ part) cannot cause the observed magnitude of depression in the afternoon.

Rastogi (1975c) described the SDEs-q events on the bottomside ionograms (obtained at Kodaikanal) on quiet days vis-a-vis the depressions in $\triangle H$ at Trivandrum, Kodaikanal and Annamalainagar (all stations within the belt of electrojet current), ($\triangle H_{KOD} - \triangle H_{ALI}$) and $\triangle Sd_I$. He observed the following three types of associations between these two phenomena :

Type 1 : - Occasions when Es-q disappears in the afternoon hours simultaneously with $\triangle H_{KOD}$ and $\triangle Sd_I$ becoming negative and the F-region horizontal drift is also found to reverse at the same time from westward to eastward direction. These observations indicate a reversal of the ionospheric currents in the E region almost simultaneously

with the SDEs-q event.

Type 2 :- On some occasions, at the time of SDEs-q event, $\triangle H_{KOD}$ and $\triangle Sd_I$ show positive values while the difference ( $\triangle H_{KOD} - \triangle H_{ALI}$) shows negative value. $\triangle H_{KOD}$ becomes negative typically 30-45 minutes later than the Es-q disappearance time.

Type 3 :- On some occasions $\triangle H$ at Trivandrum, Kodaikanal and Annamalainagar shows a strong depression in the afternoon hours but does not become negative. The $\triangle H$ variation at Alibag, which is outside the influence of the electrojet, remains normal; therefore ( $\triangle H_{KOD} - \triangle H_{ALI}$) as well as ( $\triangle H_{TRI} - \triangle H_{ALI}$) curves show negative values between the time interval when $\triangle H$ field at equatorial stations shows depression . Es-q was found to be absent on the equatorial ionograms and the ionospheric drift at F region was also reversed on such occassions. On the basis of such observations of partial counter electrojet, Rastogi suggested that there are two bands of current; one the normal eastward electrojet current at an altitude of about 107 km and the other at about 100 km altitude where the irregularities causing the Es-q are produced by the cross-field instability in the E region plasma. The fact that $\triangle H$ at equatorial stations remain significantly above the nighttime base level was interpreted due to the normal electrojet current which remains unaffected during the counter electrojet. The SDEs-q event during the counter electrojet was suggested to be due to

the reversal of the electric field (and hence the electric current) at 100 km level. The reverse current at 100 km altitude produces the depression in the H field observed at the ground. Rastogi also suggested that during strong counter electrojet events, the westward current may extend over the entire height range of the enhanced conductivity in the E region over the magnetic equator.

Rastogi's hypothesis of "two current-layers" to explain the observed counter electrojet effects can be best summarised in the following sentences reproduced from his paper : "during the first type of counter electrojet, the development of the westward current at 100 km is rather rapid and it more than balances the normal current at higher level causing the H field measured at ground to show a depression. During the second type of counter electrojet, the westward current at 100 km develops rather slowly such that the H field observed at ground decreases to nighttime level sometime after the disappearance of Es-q. During the third type of counter electrojet, westward current at 100 km is smaller in magnitude than the normal current at 107 km and is not able to cause a depression of the H field at ground below the nighttime level but the reversal of electrostatic field causes the disappearance of the Es-q layer".

Rastogi (1975c ) suggested three different sources for the three types of observed counter electrojet effects.

The counter electrojet of Type 1, exemplifying abrupt changes in the electrojet, have to be caused by sudden reversals of the E region electrostatic field. Patel and Rastogi (1974) had earlier associated the sudden disappearance of Es-q with the reversal of the interplanetary magnetic field component $B_z$ (z represents the direction perpendicular to the ecliptic plane) from the southward to northward direction. The electric field associated with the solar wind interacting with $B_z$ was shown to be responsible for causing the sudden changes in the equatorial ionosphere. On the basis of above work, Rastogi (1975c) suggested that the first type of counter electrojet is associated with the reversal of the $B_z$ component of the interplanetary magnetic field.

The counter electrojet of Type 2 which is characterised by slow reversal of the electrojet is attributed to the lunar current system on the basis of the fact that these currents have comparatively large periodicities. The control of the moon on the occurrence of the counter electrojet was clearly shown by Rastogi (1973a, 1974b). Rastogi (1975a) had earlier suggested the moon to be the source for causing the counter electrojet.

The counter electrojet of Type 3 which is described as partial, is associated with relatively short period of Es-q disappearance . Rastogi (1973b) discussed some events of Es-q disappearance at Huancayo and Kodaikanal to be associated with $DP_2$ type of polar substorms. The $DP_2$

fluctuations are found on a world wide scale and are more pronounced at the poles and at the equator as compared to other latitudes. The current directions are shown to be westward in the afternoon and eastward in the early morning hours by Nishida et al. (1966). The third type of counter electrojet was attributed to $DP_2$ substorm currents.

It appears unlikely that the counter electrojet phenomenon which occurs frequently during sunspot minimum period on a sequence of days, sometimes on eight or ten days in succession, should be caused by so many diverse mechanisms as suggested by Rastogi. However, the possibility that the individual events of counter electrojet could be caused by one or by the combined effect of the three mechanisms, cannot be ruled out.

Satya Prakash et al. (1971, 1976) studied the behaviour of the normal&counter electrojets by measuring the electron density and irregularities in the electron density by means of rocket borne Langmuir probe.

For the normal electrojet, the irregularities due to crossfield instability in the range of scale sizes 1-300 m with amplitudes of 10-20% of the ambient density for the scale sizes $\sim$ 30-300 m and 1-2% for the scale sizes $\lesssim$ 15 m are generated in 87-100 km region where the electron density gradient (being upwards) is in the same direction as the vertical polarisation field (Satya Prakash et al. 1971).

The Langmuir probe current during the normal electrojet shows saw-tooth structures, which represent the steepening of the waveforms in the vertical direction. The sawtooth structures are characteristic of the normal electrojet (Satya Prakash et al. 1971) and are interpreted as due to the nonlinear behaviour of the crossfield instability.

During the rocket experiment on August 17, 1972 at 1532 hr ($82^{o}.5$ EMT) which happened to be in the period of strong counter electrojet, positive electron density gradient was observed in the altitude range 86-94 km, with a sharp peak of electron concentration at 94 km altitude. Wavelike perturbations with wavelengths upto 200 m and with amplitudes upto 15% of the ambient density were observed. However, the shapes of Langmuir probe current waveforms did not appear like the characteristic sawtooth structures of the normal electrojet irregularities. On this basis Satya Prakash et al. (1976) concluded that the irregularities in the region of positive electron density gradient (below 94 km) are not due to crossfield instability mechanism.

In the altitude region 94-98 km the electron density showed a negative gradient and the irregularities having characteristic sawtooth structures were observed, with the direction of steepening downward, i.e. opposite to that observed for the normal electrojet. The scale sizes of the irregularities are a few tens of meters and the amplitudes are in the range 5-10% of the ambient density. This observation

shows that the electric field is reversed in the altitude range 94-98 km and also that the ionisation irregularities could be present during counter electrojet.

## VI.3 OBSERVATIONS AND RESULTS

The author has analysed the magnetic field (H component) data of the Indian stations, Trivandrum ($-0^{\circ}.3$ dip lat.) and Alibag ($+12^{\circ}.9$ dip lat.) on the days when the ledge was observed in the topside ionosphere. The ISIS satellite topside sounder data obtained at Ahmedabad during the period February 1972 to December 1974 recorded the ledge occurrence on 200 days, of which 168 days are magnetically undisturbed ($Ap < 15$). We have considered magnetically undisturbed days only for the present study. For determining whether counter electrojet on a particular day is present, the daily variation of the parameters $\triangle H_T$, $\triangle H_A$ and $(\triangle H_T - \triangle H_A)$ was plotted, where $\triangle H$ represents the increment from the nighttime base level (drawn by using the method of Rush and Richmond, 1973) in the H field and the suffixes 'T' and 'A' denote the stations Trivandrum and Alibag respectively. For the year 1972, the magnetic field data of Kodaikanal ($+1.7^{\circ}$ dip lat.) are also available. The daily variation profiles of $\triangle H_K$ and $(\triangle H_K - \triangle H_A)$ also reveal the counter electrojet, where the subscript 'K' represents Kodaikanal.

The days on which $\triangle H_T$ during afternoon hours goes below the nighttime base level and $(\triangle H_T - \triangle H_A)$

also becomes negative are called "full" counter electrojet days. On certain days $\triangle H_T$ in the afternoon does not go negative but the difference ($\triangle H_T - \triangle H_A$) is negative and such days are classified either "partial" or "full" counter electrojet depending on the strength of the negative depression. A depression of 10 gamma or more below the night level is taken as full counter electrojet. In addition, there are days on which a small afternoon depression is observed in $\triangle H_T$ and hence ($\triangle H_T - \triangle H_A$) shows a significant depression without crossing the nighttime base level; such days are categorised as partial counter electrojet days.

Fig. 6.2(a,b,c) shows the evidence for simultaneous occurrence of the ledge and the counter electrojet on Oct. 4, 1972; the part (a) gives the spatial structure of the ionisation ledge at 1250 hr ($62^{\circ}$ EMT), and the parts (b) and (c) give the evidence for the counter electrojet. The part (b) gives the diurnal variation of the $\triangle H$ field at Trivandrum, Kodaikanal, Alibag and the difference ($\triangle H_T - \triangle H_A$) and ($\triangle H_K - \triangle H_A$). The daily variation profiles of $\triangle H_T$ as well as $\triangle H_K$ show prominent depression in the afternoon hours going below the respective nighttime base levels. The daily variation profiles of ($\triangle H_T - \triangle H_A$) as well as ($\triangle H_K - \triangle H_A$) show the afternoon depression more prominently; the hatched portions denote the full counter electrojet. Fig. 6.2(c) shows the latitudinal profiles of $\triangle H$ at various fixed hours,

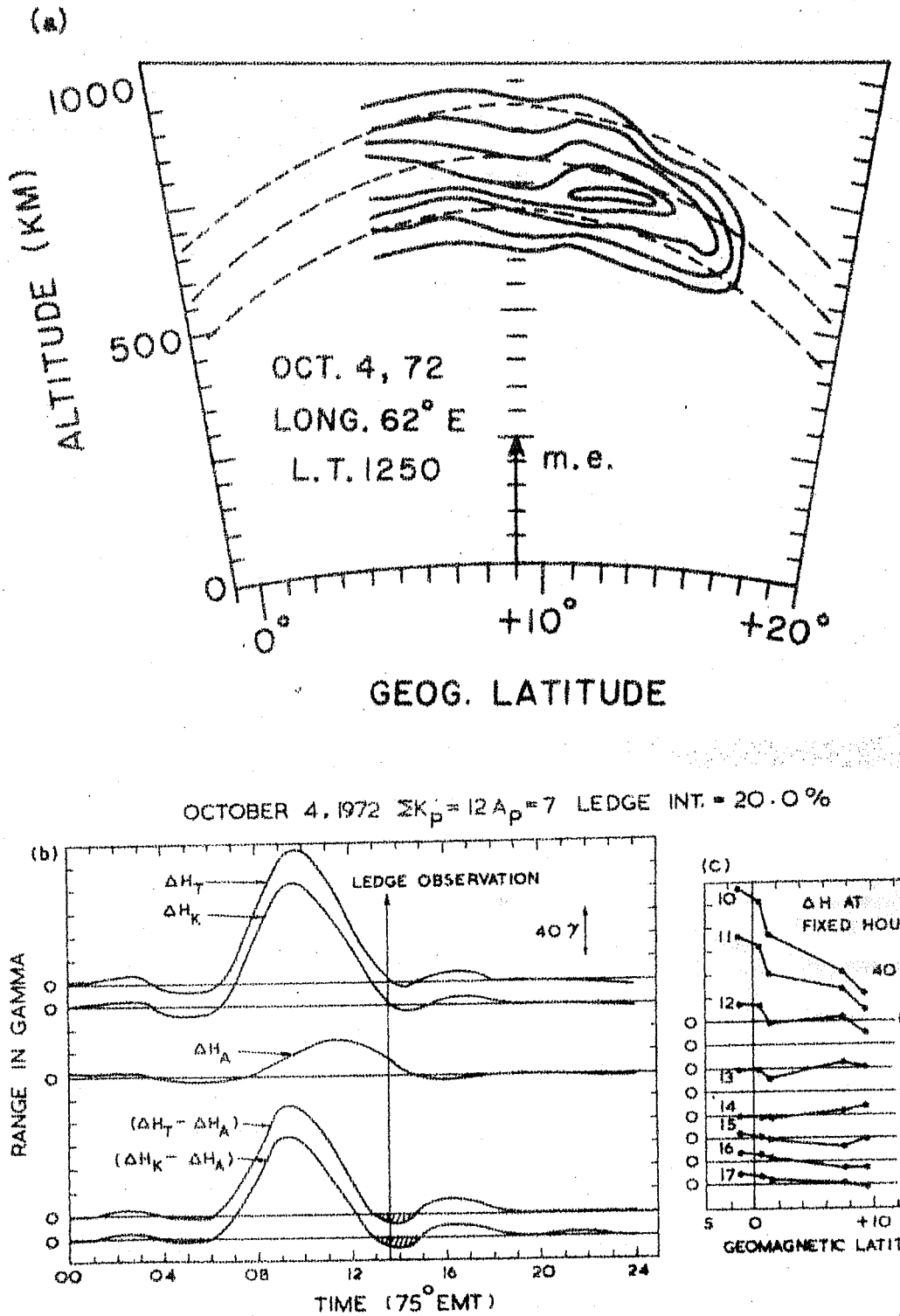


Fig. 6.2(a,b,c):- (a) The spatial structure of the ionisation ledge on October 4, 1972 at 1250 hr LT by means of ISIS-2 pass at 62°E longitude, (b) the daily variation of $\Delta H_T$, $\Delta H_K$, $(\Delta H_T - \Delta H_A)$, and $(\Delta H_K - \Delta H_A)$ on the same day and (c) the latitudinal profiles of $\Delta H$ at each one hour interval (between 1000 - 1700 hr LT).

1000 - 1700 LT, obtained from the published hourly magnetic data for the Indian stations Trivandrum, Kodaikanal, Annamalainagar, Hyderabad, and Alibag; the geomagnetic latitudes for these stations being -1.2, 0.6, 1.4, 7.6 and 9.5 degrees respectively. The latitudinal profiles at 10, 11 and 12 hrs. show that the $\triangle$ H at the equatorial stations Trivandrum and Kodaikanal is maximum and decreases steeply with increasing latitude. Such a behaviour of the latitudinal profile of $\triangle$ H is expected for normal electrojet current on theoretical grounds (e.g. Chapman, 1951 ) and is indeed observed. The latitudinal profiles at 13 and 14 hrs. are reversed; the equatorial stations Trivandrum and Kodaikanal showing lower value of $\triangle$ H than the non-equatorial station Alibag. Such reversals in the latitudinal profile of $\triangle$ H has been shown to be associated with the counter electrojet current by Fambitakoye et al. (1973). Thus Fig. 6.2(b,c) confirms the occurrence of the afternoon counter electrojet on Oct. 4, 1972 on which the ionisation ledge is observed at the local time shown by vertical arrow in Fig. 6.2(b). The latitudinal profile at 15 hr in Fig.6.2(c) shows the $\triangle$ H profile recovering from the effect of the reversed current and the profiles at 16 and 17 hrs show the normal profiles for an eastward electrojet current.

Figs. 6.3(a,b,c), 6.4(a,b,c), 6.5(a,b,c) and 6.6(a,b,c) show the simultaneous occurrence of the ledge and afternoon counter electrojet on Oct. 5, 6, 7 and 9 of the year 1972 respectively in the same manner as shown in Fig. 6.2(a,b,c). On Oct. 5 the afternoon counter electrojet

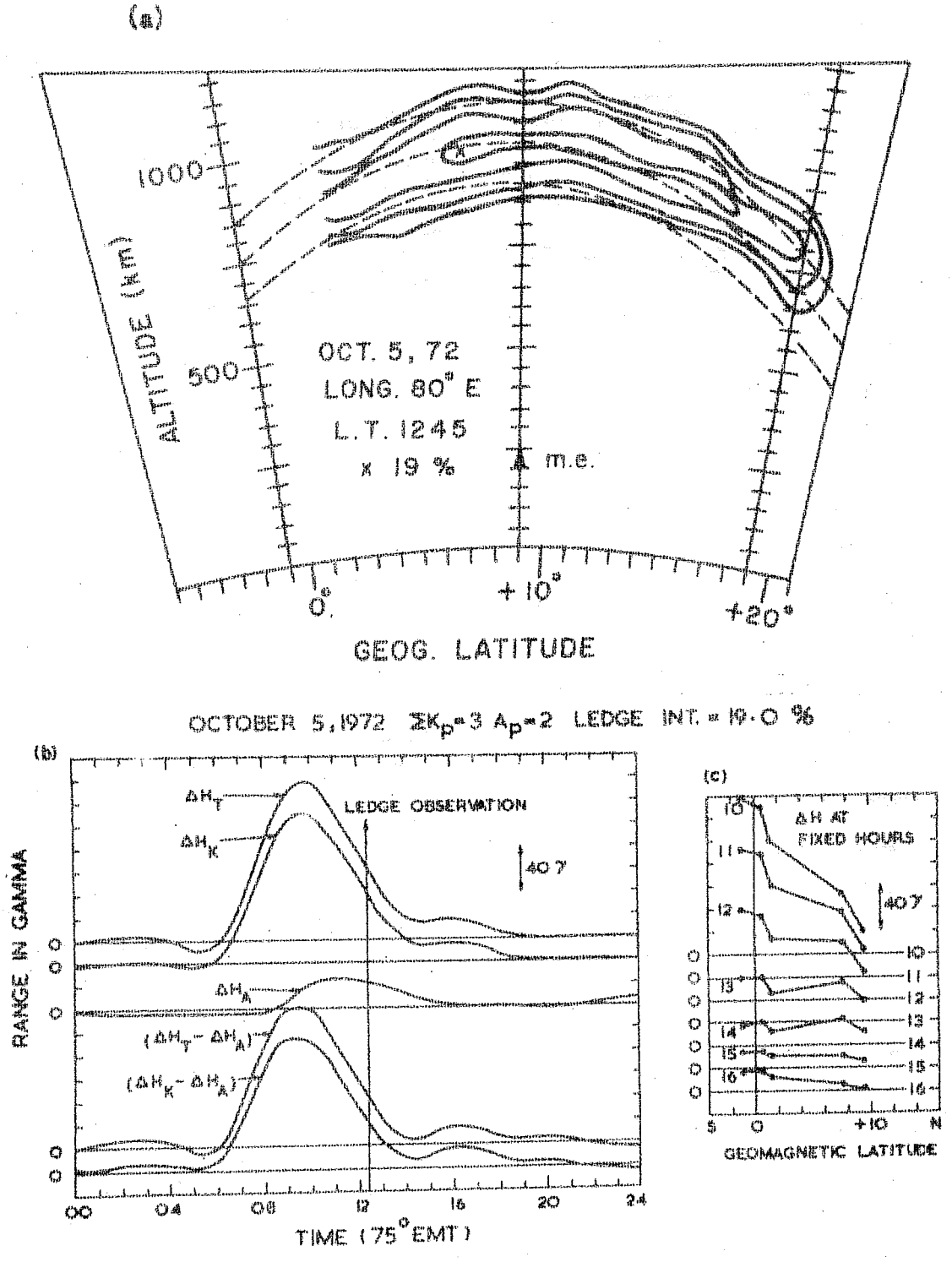


Fig. 6.5(a,b,c) :- Same as in Fig. 6.2(a,b,c) on October 5, 1972.

(a)

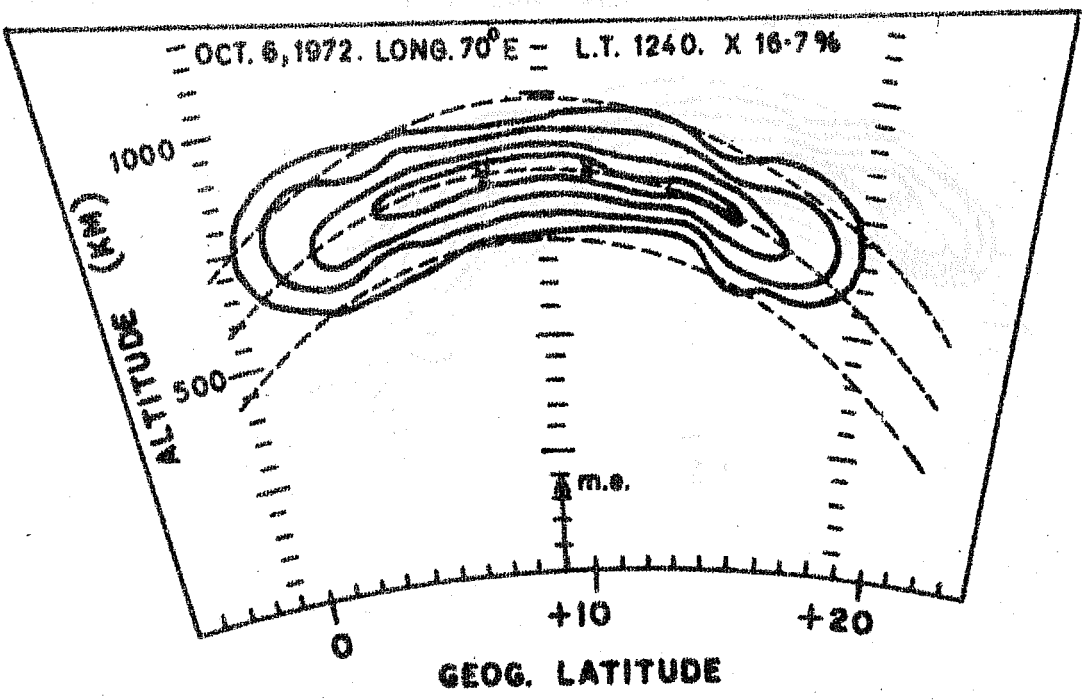


OCTOBER 6, 1972 $\Sigma K_p$=3 $A_p$=2 LEDGE INT. = 16.7%

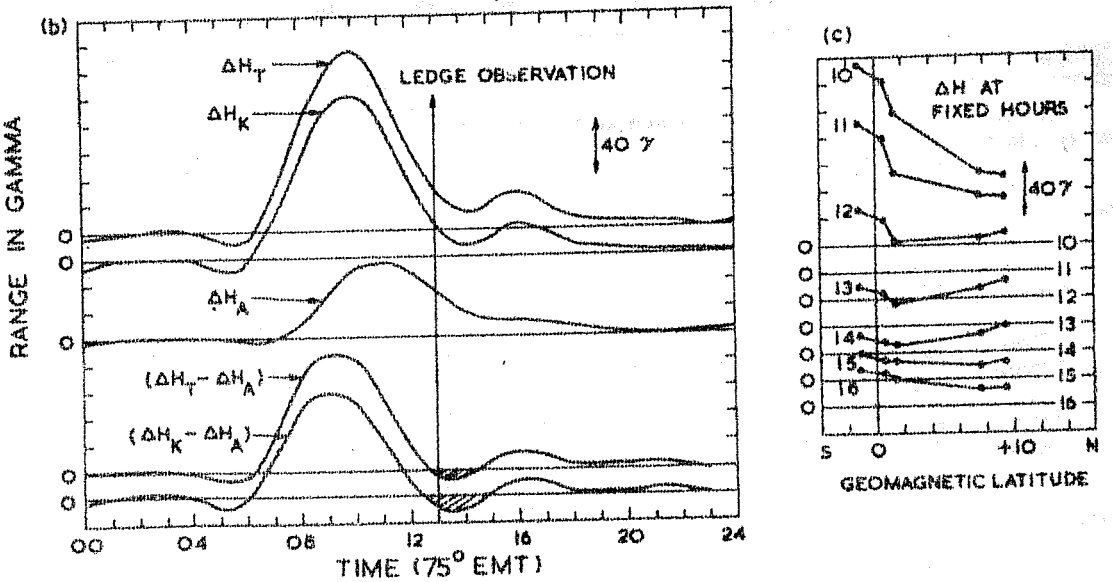


Fig. 6.4(a,b,c):- Same as in Fig. 6.2(a,b,c) on October 6, 1972.

(a)

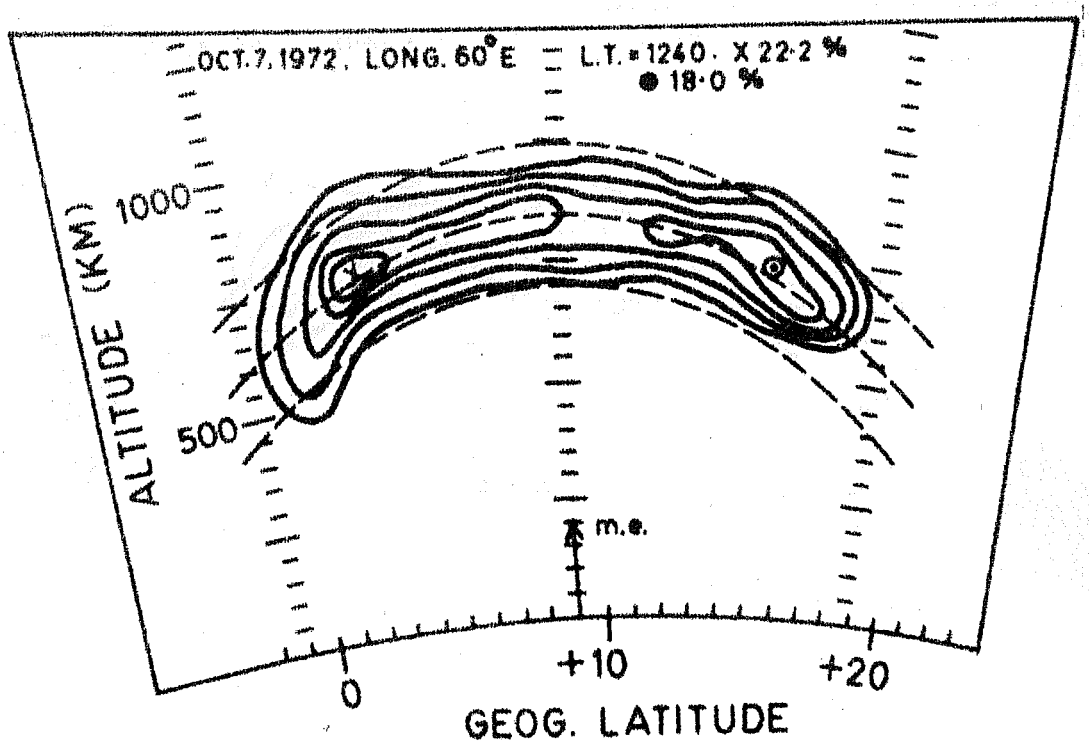


OCTOBER 7, 1972 $\Sigma K_p = 11+$ $A_p = 8$ LEDGE INT. = 22.2 %

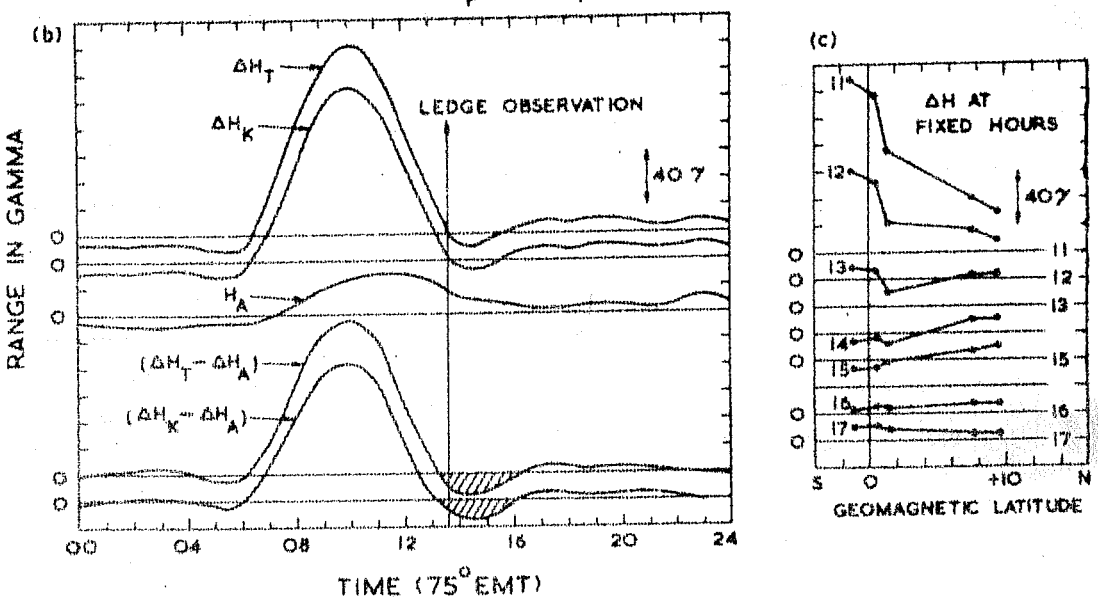


Fig. 6.5(a,b,c):- Same as in Fig. 6.2(a,b,c) on October 7, 1972.

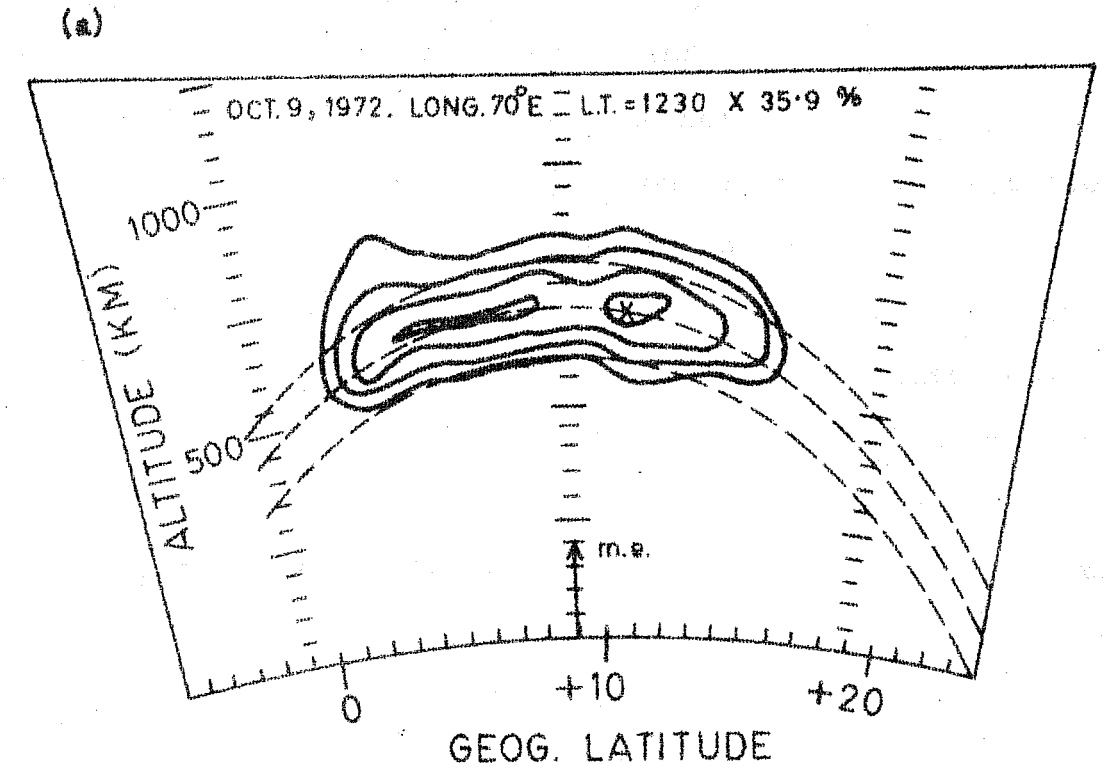


OCTOBER 9,1972 $\Sigma K_p = 8+$ $A_p = 4$ LEDGE INT. = 35·9 %

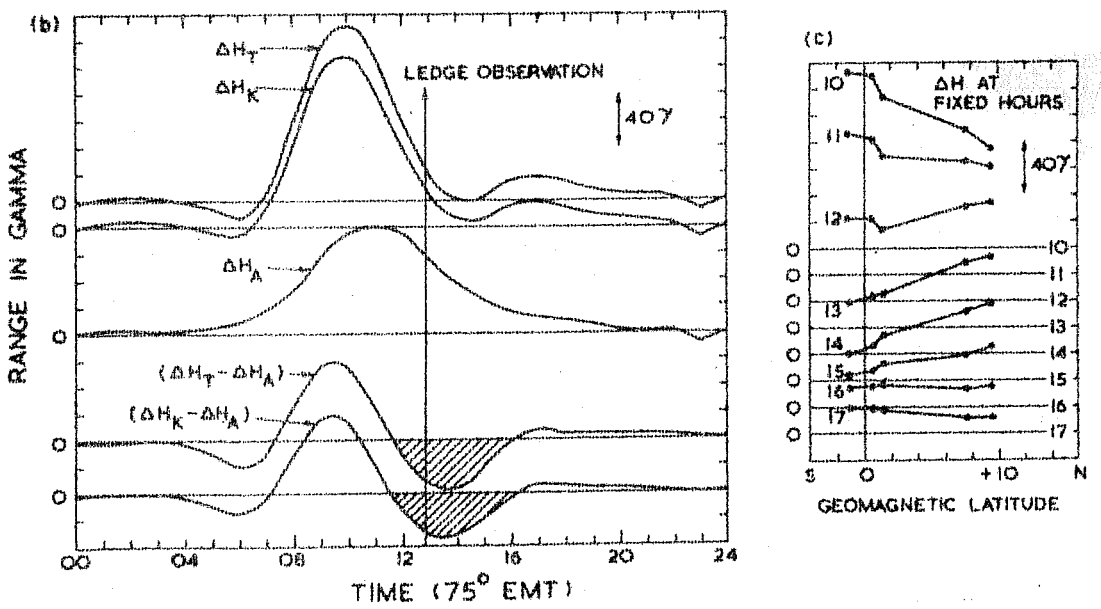


Fig. 6.6(a,b,c):- Same as in Fig. 6.2(a,b,c) on October 9, 1972.

is 'partial' whereas on the other three days, Oct. 6, 7 and 9 it is 'full'. It is important to note that the daily variation of $\triangle H_T$ as well as $\triangle H_K$ on all the five days (between Oct. 4-9, 1972) after reaching a minimum value attains a subsidiary maximum value before returning to the nighttime base level. The daily variation of $\triangle H_A$ curve also shows a slight oscillatory behaviour during the counter electrojet period. The daily variation profiles of $(\triangle H_T - \triangle H_A)$ as well as $(\triangle H_K - \triangle H_A)$ clearly show the oscillatory nature of the counter electrojet. On Oct. 6, 1972 the minimum in $(\triangle H_T - \triangle H_A)$ occurs at 1330 hr and the subsidiary maximum occurs at 1600 hr; the difference between these two times, viz. 2.5 hours, may be considered as the half period of the counter electrojet phenomenon. The $(\triangle H_K - \triangle H_A)$ daily variation profile also reveals the same half period as the $(\triangle H_T - \triangle H_A)$ profile. The period of the operative mechanism which is responsible for giving rise to the oscillatory behaviour of the counter electrojet is thus 5 hours. On different days, the period of the oscillatory nature of the counter electrojet is different; being in the range of 4.0 - 6.5 hours on Oct. 4-9, 1972.

The observations presented above represent one of the typical examples showing simultaneous occurrence of the ledge and the counter electrojet on a series of days in succession. The result of comparison on the simultaneous occurrence of the ledge and the counter electrojet on 168 magnetically undisturbed days of 1972-74 is shown in Table 1.

Table 1

| Year | No. of days studied | No. of days showing Full and Partial C-EJ |
|---|---|---|
| 1972 | 43 | 33 |
| 1973 | 70 | 53 |
| 1974 | 55 | 33 |
| Sum (1972 - 74) | 168 | 119 |

The counter electrojet either partial or full occurs on 119 days out of 168 days and thus the correlation in the occurrence of the two phenomena is about 70%. It should be pointed out that the ledge observations are made in a wide range of longitudes from $50^{\circ}$ - $105^{\circ}$E whereas the occurrence of the counter electrojet is examined at $75^{\circ}$E (corresponding to mean longitude of the stations Trivandrum, Kodaikanal and Alibag). In view of the limited longitude extent ($\sim 30^{\circ}$) of both the ledge and the counter electrojet phenomena, one should examine their simultaneous occurrence at the same longitude. From Table 1, it is seen that the counter electrojet is not present on 49 days corresponding to the ledge observations in 1972-74. An examination of the ledge observations on these 49 days revealed that the observations are made at longitudes which are more than the $\pm 20^{\circ}$ away from $75^{\circ}$E longitude at which the counter electrojet is examined. It is likely that the longitudinal extent of the counter electrojet on occasion

is as narrow as $20^{o}$. If so, the correlation in the occurrence would be greater than 70% obtained from Table 1.

The results presented above show that :

1) There is good correlation in the day to day occurrence of ionisation ledge and counter electrojet.

2) Both the phenomena occur more frequently during sunspot minimum period and also tend to occur on a series of days in succession.

3) Both the phenomena occasionally occur in a restricted longitude zone. The strengths of the ledge and the counter electrojet show different amplitudes at different longitudes when they are observed over a wide longitude range. These features of the ledge are shown in Sec. III.3 of Chapter 3 and those of the counter electrojet in the present chapter.

On the basis of these similarities in the morphological features of the two phenomena it is suggested by Raghavarao et al. (1976c ) and Raghavarao (1976) that both the phenomena are caused by the same agency. As the neutral anomaly is now known to be the cause for the ledge formation (Raghavarao and Sivaraman, 1974) it is suggested that the same neutral anomaly is also responsible for causing the reverse electrojet current.

## VI.4 A NEW MECHANISM OF THE COUNTER ELECTROJET

Raghavarao(1976) proposed a mechanism that can explain the formation of counter electrojet satisfactorily. He showed that the excess pressure bulges, associated with the neutral anomaly (NA), set up internal atmospheric gravity waves giving rise to vertically upward wind in the narrow zone of $\pm 2^{o}$ latitude around the dip equator. A brief description of this mechanism for explaining the counter electrojet on Oct. 6, 1972 (Fig. 6.4), is given below.

Fig. 6.7 gives the latitudinal distribution of $N_{max}F2$ (full line joining the open circles) and the computed exospheric gas temperature (dot dash curve) in the manner described in Sec. III.5 of Chapter 3. By using Jacchia (1970) model with the lower boundary at 90 km, the excess pressures of neutrals is computed. Fig. 6.8 gives the latitudinal distribution of pressure on one side of the magnetic equator at fixed altitudes upto 200 km. The maximum pressure bulge occurs between 100 to 160 km altitudes. The excess pressure at a particular altitude is calculated at each latitude with respect to the value at the magnetic equator. These pressure contours are shown in Fig. 6.9, where 1 unit denotes $1.3 \times 10^{-5}$ dynes/cm$^2$. The altitude is shown in units of $\log_{10}(Po/P)$, where Po is the gas pressure at 90 km and P at any altitude above it. The maximum value of the pressure, 100 units, occurs around 110 km. The horizontal arrows denote the force term $-\frac{1}{\rho}\frac{dp}{dx}$ that can generate winds.

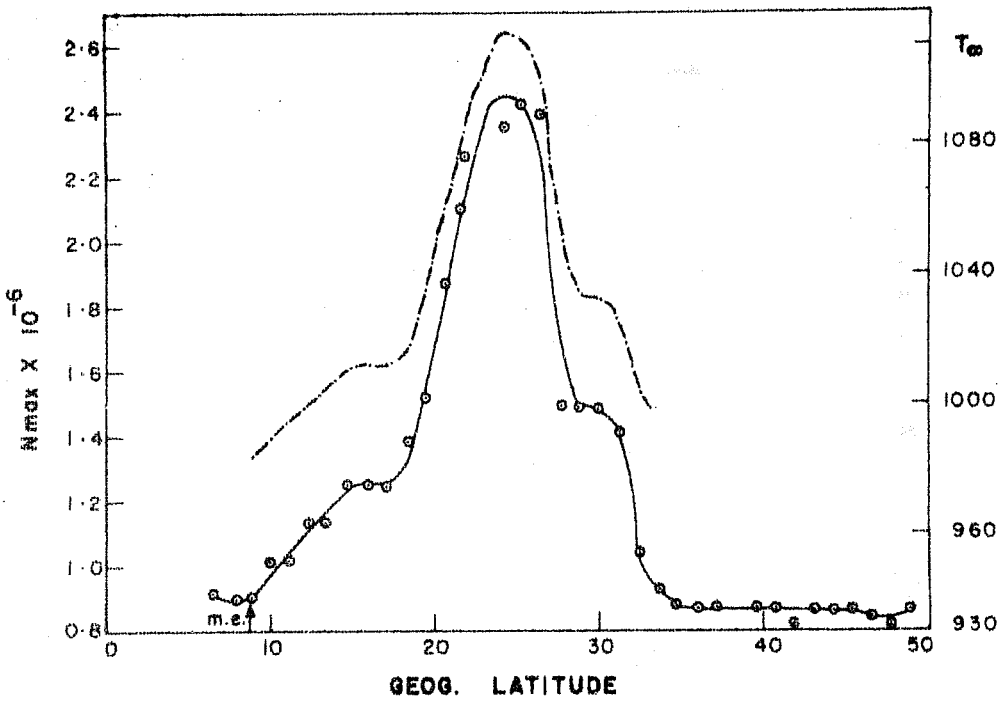


Fig.6.7:- Latitudinal distribution of $N_{max}F2$ (full line) obtained by means of ISIS-2 satellite on Oct. 6, 1972, 1240 hr LT and the calculated exospheric temperature (dot-dashed line).

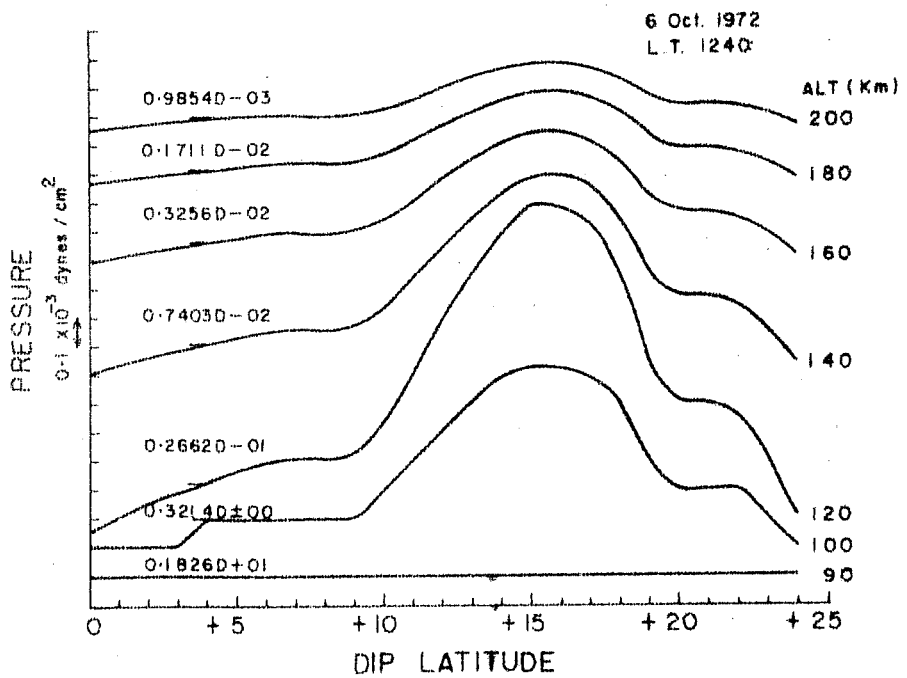

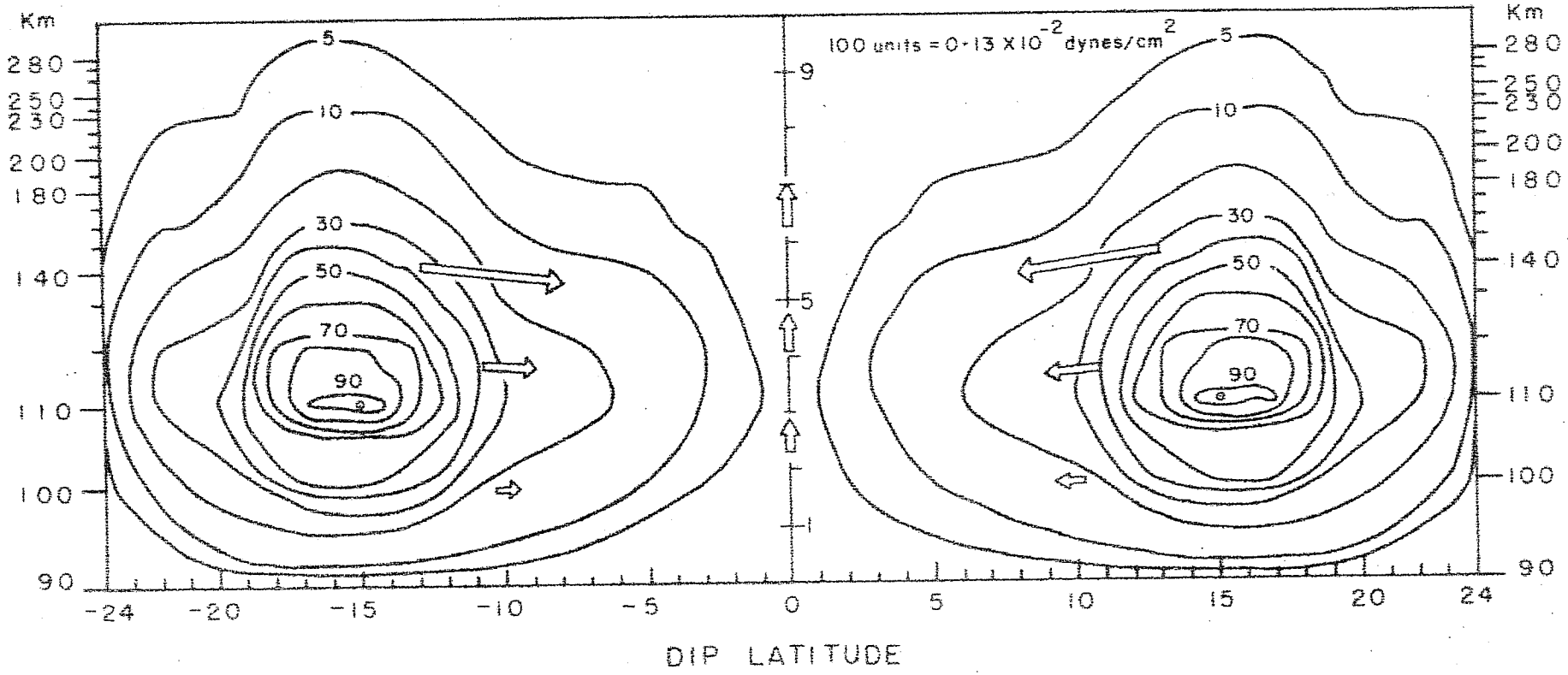


Fig.6.9:- Excess pressure contours obtained from the distribution shown in Fig. 6.8 as described in the text. The contours on the southern dip latitudes are drawn by assumed symmetry of the anomaly.

In the altitude region above 200 km, the neutral flow due to each ridge is essentially in the horizontal direction with two cells of meridional winds. The cell centered around 10-11° dip latitude gives rise to equatorward winds and the other centered around 19-20° dip latitudes gives rise to winds away from the equator. The wind speed and its variation with altitude and latitude are controlled by the pressure gradient force and the kinematic viscosity, $(\mu/\rho)$; the former drives the winds while the latter opposes the wind velocity gradients. The ion drag force prevents downward wind motion.

In the lower part of the thermosphere where the ion drag and kinematic viscosity terms are very small, the excess pressure ridges give rise to downward wind motion in addition to the meridional wind cells. As a consequence, the excess pressure ridges are likely to set up internal atmospheric gravity waves, with a period of 5 hours relevant to the case on Oct. 6, 1972. The neutral winds would flow towards the equator and downward in the latitude zone of 2°-14° dip latitude on both sides of the equator with maximum wind amplitude around 10° dip latitude. In the narrow zone of +2° to -2° dip latitudes vertically upwards winds are generated. For a large scale gravity wave, characterised by periodicity of 5 hours, $\omega = 2\pi/\tau = 3.5 \times 10^{-4}$ sec$^{-1}$. The distance between two pressure maxima is taken as one wavelength; in this case being 30° dip latitude which is equal to

$3.3 \times 10^6$ m, where $1^o$ latitude is taken as 110 km at about 100 km altitude. The wave number $k_x$ ( $= 2\pi/\lambda_x$) is $1.9 \times 10^{-6}$ $m^{-1}$. Hines (1960) has shown that corresponding to these wave parameters a spectrum of vertical wave numbers from $10^{-4}$ $m^{-1}$ to $10^{-3}$ $m^{-1}$ can exist.

The generation of gravity waves in a non isothermal atmosphere using WKB approximation is given by Einaudi and Hines (1970). The condition for generation of gravity waves requires $\alpha \gg \beta$, where the parameters $\alpha$ and $\beta$ are defined as

$$\alpha = \gamma H k_x$$
$$\beta = \omega^2 / (g k_x)$$

where H ( $= C^2/(\gamma g)$; C being the velocity of sound) is the neutral atmospheric scale height; g is the acceleration due to gravity and $\gamma$ is the ratio of specific heats ( = 1.4). At 110 km altitude the atmospheric parameters are : H = 12 km, g = 9.5 $ms^{-2}$ and therefore $\alpha = 3.19 \times 10^{-2}$ and $\beta = 6.79 \times 10^{-3}$ These values of $\alpha$ and $\beta$ satisfy the condition $\alpha \gg \beta$ required for gravity wave generation. As the scale height as well as the sound velocity C increases with altitude, the value of $\alpha$ calculated here is the smallest of a number of values corresponding to higher altitudes.

The spatial pressure variation, however, is not entirely sinusoidal but rather broad in latitudinal enhancements on either side of the dip equator. For the vertical wavelengths $\lambda_z$, although a spectrum is possible to exist,

one wavelength is likely to be predominant than the others under the circumstances of the pressure distribution shown in Figs. 6.8 and 6.9. In this particular case, for $k_x = 1.9 \times 10^{-6}$, any value(s) of the vertical wavenumber $k_z$ from about $2 \times 10^{-5}$ to $10^{-4}$ $m^{-1}$ is permissible at height above 100 km corresponding to 5 hour wave periodicity. For $\lambda_z$ = 200 km, $k_z$ is $3.14 \times 10^{-5}$ $m^{-1}$.

Applying the asymptotic relation between wavenumbers $k_x$, $k_z$ and the wind components $u_x$ and $u_z$ as given by Hines (1960), one obtains

$$\frac{k_x}{k_z} = \frac{u_z}{u_x} = \frac{1.9 \times 10^{-6}}{3.14 \times 10^{-5}} = \frac{1}{16.5}$$

If we put $u_x$ = 330 m/s, we obtain $u_z$ = 20 m/s. The asymptotic relation is not however valid for such small values of $k_z$ and therefore $u_z$ is likely to be larger than 20 m/s.

Alternatively, it can be visualised that the wind from the two excess pressure bulges, exerts its thrust downward while building up the momentum of the meridional flow. The column of air in between the pressure bulges is lifted up and the vertical velocity could be as large as 40 - 50 m/s. It may be mentioned that Anandarao et al. (1976) and Rieger (1974) found upward wind speeds of 19, 6 and 14 m/s at 93, 150 and 176 km altitudes respectively by barium spot releases over the equatorial station Thumba (near Trivandrum) during the evening twilight hours.

Raghavarao (1976) examined the effect of upward neutral wind on the vertical Hall polarisation electric field that drives the eastward electrojet current. He took the equation of motion for electrons and ions, neglecting their partial pressure and gravity terms at the E region altitudes where the neutral density is several orders of magnitude higher than the daytime plasma density. The equations of motion of an electron and an ion with these assumptions become

$$-e(\underline{E}+\underline{V}_e \times \underline{B}) - m_e \nu_e (\underline{V}_e - \underline{U}) = 0 \quad \text{------} \quad (1)$$

$$e(\underline{E}+\underline{V}_i \times \underline{B}) - m_i \nu_i (\underline{V}_i - \underline{U}) = 0 \quad \text{---} \quad (2)$$

where $\underline{E}$ and $\underline{B}$ are electric and magnetic fields respectively, $\underline{V}_e$ and $\underline{V}_i$ are the electron and the ion velocities, $m_e$ and $m_i$ are the masses and $\nu_e$ and $\nu_i$ are the collision frequencies of an electron and an ion with the neutrals respectively and $\underline{U}$ represents the neutral velocity. The ion electron collisions are negligible at E region altitudes.

From the equations (1) and (2), one can obtain $\underline{V}_e$ and $\underline{V}_i$ as

$$\underline{V}_e = \frac{1}{\Omega_e^2+\nu_e^2}\left[\frac{e}{m_e}(\underline{E}\times\underline{\Omega}_e) - \frac{e}{m_e}\nu_e \underline{E} + \nu_e^2 \underline{U} - \nu_e(\underline{U}\times\underline{\Omega}_e)\right] \quad \text{-------} \quad (3)$$

$$\underline{V}_i = \frac{1}{\Omega_i^2+\nu_i^2}\left[\frac{e}{m_i}(\underline{E}\times\underline{\Omega}_i) + \frac{e}{m_i}\nu_i \underline{E} + \nu_i^2 \underline{U} + \nu_i(\underline{U}\times\underline{\Omega}_i)\right] \quad \text{------} \quad (4)$$

where $\underline{\Omega}e = e\ B/m_e$ and $\underline{\Omega}i = e\ B/m_i$ are the electron and the ion cyclotron frequencies respectively.

With a coordinate system x, y, and z with x and y pointing magnetic south and east respectively and z in the upward direction, and assuming that $V_{ez} \approx V_{iz}$ (i.e. no vertical current over the magnetic equator), the value of the vertical electrostatic field is

$$E_z = \frac{\sigma_2}{\sigma_1} E_y - \frac{Ne}{\sigma_1} U_z \left[ \frac{1}{K_i^2 + 1} - \frac{1}{K_e^2 + 1} \right] - B U_y \quad \text{----- (5)}$$

where $\sigma_1$ and $\sigma_2$ are the Pedersen and the Hall conductivities and are given by

$$\sigma_1 = \frac{Ne}{B} \left[ K_e/(K_e^2+1) + K_i/(K_i^2+1) \right]$$

$$\sigma_2 = \frac{Ne}{B} \left[ K_e^2/(K_e^2+1) - K_i^2/(K_i^2+1) \right]$$

with $K_i = \Omega_i/\nu_i$ and $K_e = \Omega_e/\nu_e$

For the electrojet region (90-120 km) $K_i \ll 1$ and $K_e \gg 1$, and then eq.(5) can be simplified to

$$E_z \approx \frac{\sigma_2}{\sigma_1} (E_y - B U_z) - B U_y \quad \text{-----} \quad (6)$$

It is clear from eq.(6) that the upward wind $U_z$ is $\sigma_2/\sigma_1$ ($\approx 30$ at 100 km altitude) times more effective in reducing the vertical polarisation field than the eastward wind $U_y$ .

If we assume that $E_y$ = 1 mv/m, the magnitude of the upward wind, required to reduce $E_z$ to zero at the centre of the electrojet region which is at 106 km in the Indian zone

(Sastry, 1970), is $E_y/B = 10^{-3}/(0.38 \times 10^{-4}) = 26.3$ m/s, (B = .38 gauss at 106 km corresponding to $80^{\circ}$E longitude). Thus vertical wind speed of 26 m/s can annul the vertical polarisation field driving the electrojet and velocities $U_z$ greater than 26 m/s can reverse the $E_z$ field from upward to downward direction thus resulting in the reversal of the electrojet current. Eq.(6) can be interpreted physically in the following way:

The vertical polarisation field in the E region is caused as a result of the condition that the electrons are magnetised whereas the ions are collisional (see Sec. II.1, Chapter 2) and therefore the $\underline{E} \times \underline{B}$ force due to primary eastward electric field moves the electrons and not the ions. The vertical wind $U_z$ would move the ions as well, thus decreasing the Hall polarisation electrostatic field. A strong vertical wind would cause the ions to move faster than the $\underline{E} \times \underline{B}$ motion of electrons thereby giving rise to a downward vertical polarisation field that in turn gives rise to eastward motion of electrons because of $\underline{E} \times \underline{B}$ force and hence the current in the westward direction - the so called counter electrojet. The important criterion for the counter electrojet to occur is that the IA crest strength should attain a sufficient magnitude ($\geq$ 150%) by local noon hours when the zonal motion of the neutrals reverses from west to east and the ion drag force becomes effective in producing the neutral anomaly.

The above mechanism explains the more frequent occurrence of the afternoon counter electrojet in sunspot minimum period on the basis of the more frequent occurrence of the neutral anomaly in solar minimum period. The occurrence of the counter electrojet on occasion in a narrow longitude zone can be explained on the basis that the pressure bulges on either side of the magnetic equator associated with the neutral anomaly also occur in a narrow longitude zone (as is evident from the correlation of the counter electrojet with the ionisation ledge). The upward winds in the narrow latitude range in the vicinity of the magnetic equator would be generated in the narrow longitude zone of the neutral anomaly. On this basis the occurrence of the counter electrojet on occasion in a limited longitude zone can be explained.

## VI.5 CONCLUSION

The present study brings out many new features of the counter electrojet phenomenon. The significantly high correlation in the occurrence of the ionisation ledge and the counter electrojet points out the dynamical interaction between the E and F regions. The explanation of the counter electrojet on the basis of the vertical winds generated due to the neutral anomaly in the narrow latitude zone of $\pm 2^{o}$ dip latitude, provides a natural explanation of the morphological features, e.g. its more frequent occurrence in sunspot minimum period and occurrence in a narrow longitude zone on occasion. These features of the counter electrojet cannot be explained by the mechanism(s) of Rastogi (1975c)

# C H A P T E R - VII

## SOME NEW FEATURES OF EQUATORIAL SPREAD-F

### VII.1 INTRODUCTION

The term spread F describes a condition existing in the F region and topside ionosphere which gives rise to diffuse echo traces on the ionograms. The phenomenon was first observed on the bottomside ionograms by Booker and Wells (1938) and is being studied since then. The early work on spread F consisted of an analysis of the bottomside ionograms of the type shown in Fig. 7.1(a,b). The diffuse echoes, characteristic of the spread F phenomenon, are thought to be caused by electron density irregularities aligned to the earth's magnetic field lines. The field alignment of the irregularities, in the bottomside as well as topside, has been shown (e.g. Calvert and Cohen, 1961; Calvert and Schmid , 1964). Lockwood and Petrie (1963) by means of Alouette-1 ionograms, showed that not only the individual electron density irregularities but the whole patch of irregularities is aligned to a geomagnetic field line, when the spread F is formed below the satellite altitude.

In this chapter, the author presents evidence by means of ISIS-1 satellite to show that the upper boundary of the spread F irregularities does not form along a magnetic field line in the premidnight hours when the irregularities are just developing.

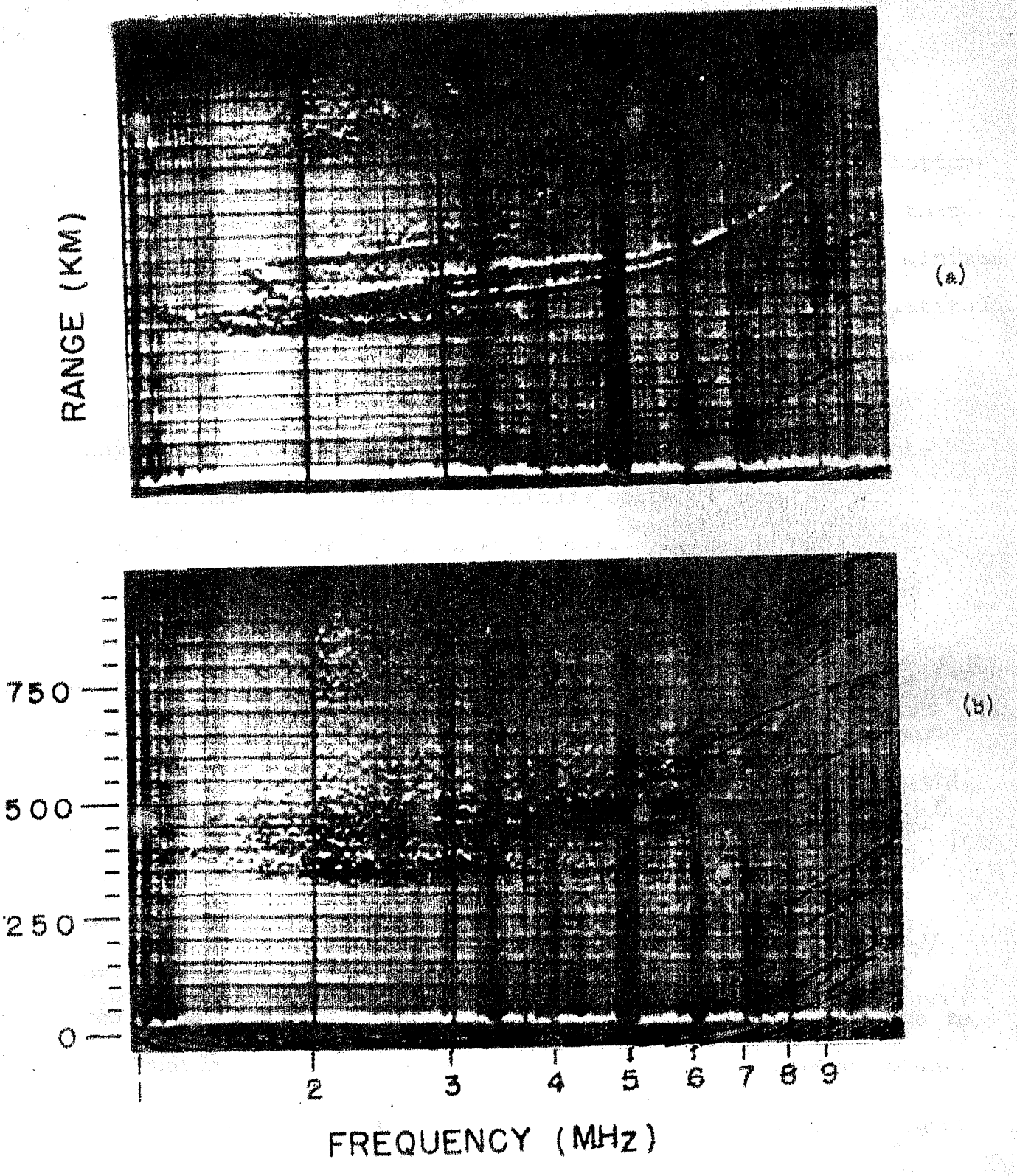


Fig.7.1(a,b):- Bottomside ionograms recorded at Trivandrum on Oct. 25, 1967 at 1835 hr and 1850 hr LT respectively.

## VII.2 SUMMARY OF PREVIOUS WORK

### VII.2.1 MORPHOLOGICAL FEATURES OF SPREAD F

The work of Singleton (1960) for the bottomside and Calvert and Schmid (1964) for the topside showed that the spread F occurs at both high and low latitudes, with a minimum probability of occurrence between $20^{o}$ and $40^{o}$ geomagnetic latitude. There is evidence of a statistical nature which suggests that high and low latitude spread F are distinct phenomena. For example, in the equatorial region spread F is mainly a nighttime phenomenon but the high latitude spread F occurs both during day and night (Shimazaki, 1959). The occurrence of spread F at high latitudes is positively correlated but the equatorial spread F is negatively correlated with magnetic activity (Lyon et al., 1958). The high latitude spread F is shown to be associated with particle precipitation (e.g. Dyson and Winnigham, 1974) that is absent at the equatorial latitudes. These evidences suggest that the equatorial and the non-equatorial spread F are two distinct phenomena. However, both involve field aligned irregularities of electron density in the F region but it seems likely that the irregularities are produced in different ways. We shall restrict the discussion to the equatorial spread F which is pertinent to the present study.

The early work, reviewed by Herman (1966), consisted mainly of analysis of bottomside ionograms. The launching of the satellite, Alouette-1, yielded information about the

occurrence and characteristics of spread F phenomenon in the topside. The range of irregularity scale sizes studied by the ionosonde technique are in the range of 15-150 meters. A major breakthrough in understanding the equatorial spread F phenomenon came from the powerful VHF radar observations at Jicamarca at 50 MHz operating frequency which detects irregularities having scale length $\lambda_{\perp}$ = 3 m. The radar also provides the measurement of electron concentration in the bottomside and topside just before and after the spread F. The doppler shift measurement provides the information about the F layer vertical drift velocity continuously with time, even when spread F irregularities are present. These observations, together with their implications are presented in the review paper by Farley et al. (1970).

The main features of the spread F phenomenon observed from the ionosonde (bottomside as well as topside) and the VHF radar observations, are summarised below:

1) The equatorial spread F can be broadly classified into three categories on the basis of its appearance on bottomside ionograms (McNicol et al., 1956; Chandra and Rastogi, 1972a).

a) When the diffuseness is mainly along the horizontal part of the trace giving rise to ambiguity in height but the critical frequencies are identifiable, the spread F is called as "range type". An example of this kind is

the ionogram shown in Fig. 7.1(a). Range type spread is mainly a premidnight phenomenon occurring more frequently in high sunspot years than in low sunspot years (Chandra and Rastogi, 1972b).

b) When the echo spreading is maximum at higher frequencies causing ambiguity in identifying the layer penetration frequencies while the trace is comparatively clear and sharp at lower frequencies, the spread F is called as "frequency type". At equatorial stations, frequency spreading occurs mostly during post midnight period. Frequency spreading is also called as "temperate latitude" spread F by some authors because of its resemblance to the commonly observed spread F at midlatitudes.

c) On some occasions the spreading of echo traces is seen to be equally prominent in the entire frequency range and is classified as "complete spread F". Such spread F is very intense, an example of which is the ionogram shown in Fig. 7.1(b).

2) The spread F commences typically around 1900 hr LT. Usually there is a bifurcation of the F region trace on the ionosondes which can extend into three or more "satellite traces" before the onset of spread F (Lyon et al. 1961). Fig. 7.1(a) shows the satellite traces at the time when spread F is just developing. In the evening hours the F layer rises up with velocity typically about 30 m/s but occasionally as large as 50-60 m/s (Farley et al. 1970). The upward velocity

is the sum of the true layer velocity caused by $\underline{E} \times \underline{B}$ effect and the apparent velocity, due to the loss of bottomside ionisation by recombination, which is less than 6 m/s (Krishnamurthy et al., 1976). Almost all the workers in this field have associated the occurrence of equatorial spread F with the postsunset rise of the F layer and with the vertical velocity of the layer. However, the results of Farley et al. (1970) and Krishnamurthy et al. (1976) clearly show that the first appearance of the spread F irregularities can occur in an upward as well as downward moving layer. Farley et al. suggested that the relation of the initial occurrence of spread F with layer height appears due to an altitude threshold for the bottom of the F layer ($h_{min}F \geqslant 300$ km), which implies that spread F favours low neutral densities. The initial appearance of spread F on the bottomside ionograms at the low frequency end suggests that spread F favours low plasma densities as well. However, the radar observations of 3 m irregularity scale sizes show that at times spread F can appear nearly simultaneously in the bottomside as well as topside and on occasion the disturbed region has been observed to extend from about 200 km to 800 km. It is likely that the temporal as well as spatial development of spread F irregularities in different scale sizes occurs differently.

3) The spread F density irregularities appear to have low phase velocities masked by the motion of the background ionosphere, except during strong spread F conditions

when turbulence may play a role (McClure and Woodman, 1972). Recently Krishnamurthy et al. (1976), using phase path measurements at 2.5 MHz frequency at equatorial station Thumba, noted that different echoing regions in the spread F patch show different motions, which are sometimes in opposite sense, confirming the existence of turbulence in the spread F region.

### VII.2.2 NATURE OF SPREAD F IRREGULARITIES

Earlier observations indicated that the spread F irregularities are highly field aligned (i.e., $\lambda_{\parallel} \ll \lambda_{\perp}$). For example, Cohen and Bowles (1961) estimated that irregularities are $\sim 1$ km in the direction of the magnetic field with transverse dimension of $\sim 10$ m. Radar measurements set a lower limit on $\lambda_{\parallel} / \lambda_{\perp} \sim 10^2$ at $\lambda_{\perp} = 3$ m. In situ rocket and satellite measurements of electron density or electrostatic potential fluctuations unfortunately do not determine either the ratio $\lambda_{\parallel} / \lambda_{\perp}$ or the orientation of $\lambda_{\perp}$. Recent electron and ion density fluctuation measurements range from 100 m to 5 km for irregularities with density enhancements in excess of a few percent of the background density (Kelley and Carlson, 1974). Thus the transverse scale sizes observed range from a few km ( $\lambda_{\perp} \gg \rho_i$ , the ion Larmous radius) down to a few meters ( $\lambda_{\perp} \lesssim \rho_i$ ). Ionospheric irregularities which cause radio wave ducting, observed on the topside ionograms (Calvert and Schmid , 1964), have been observed by rocket experiments (Knetch et al., 1961) and were found to be about 2 km in cross section and extending between 400-1000 km

The ground based ionosonde provides the information on the time development of spread F and especially the minimum height at which the spread F occurs during the course of a night. The topside sounder onboard the polar orbiting, Alouette and ISIS satellites, gives the spatial development of the spread F at the time of the satellite pass. It is possible to delineate the upper boundary of the spread F irregularities when it occurs below the satellite altitude. Lockwood and Petrie (1963) by means of Alouette-1 ionograms showed that the upper boundary of spread F irregularities in the topside ionosphere is aligned accurately to a geomagnetic field line.

In order to study the time development of spread F from topside sounder experiment one should have passes in close succession from two or three polar orbiting satellites. In the absence of such data, the author has made use of the characteristics of spread echoes observed on the bottomside ionograms to ascertain whether a particular echo reveals spread F in a developing or a well developed stage. These characteristics are the following:

1) An examination of the bottomside ionograms given by Chandra and Rastogi (1972a) at hourly intervals at equatorial station, Thumba, reveals that the spread F commences at the low frequency end ( 1-2 MHz) of the F region echo around 1900 hr LT. The high frequency end near the penetration frequencies shows clean O and X echoes. The two ionograms shown in Fig. 7.1(a,b) were obtained at Thumba on Oct. 25, 1967

at 15 min interval. The ionogram in Fig. 7.1(a) at 1835 hr LT shows the starting of the spread F phenomenon (the previous ionogram at 1820 hr showed clean echo traces). The doubling of echo trace, characteristic of the commencement of spread F phenomenon on the bottomside ionograms (Lyon et al., 1961), is clearly observed. The diffuse echoes appear below the main trace although some scatter above is also seen.

Fig. 7.1(b) gives the ionogram at 1850 hr LT on the same day and shows complete spreading. These examples reveal that the spread F develops at low frequencies showing that the larger scale sizes ($\sim$100 m) are generated first; within 15 minutes of the first appearance of spread echoes, the irregularities of all the scale sizes in the range 25-100 m (corresponding to the frequency range of 1.5 - 6 MHz) are formed. Another important feature which characterises the spread F development, as may be noted from Fig. 7.1(a), is that the spread echoes are observed below as well as above the normal O and X echoes, and also the 'clean' O and X traces are seen through the spread echoes. This shows that the irregularities are not very strong at the time when the ionogram is recorded. In the ionogram of Fig. 7.1(b), however, the normal O and X traces are completely suppressed by the spread echoes thus showing that the irregularities responsible for causing the latter are strong enough to cause multiple scattering of the probing radio waves so that no coherent ionospheric echo returns to the sounder receiver. The topside ionograms on which the spread echoes are very strong are also interpreted in the

The above characteristics of the spread echoes observed on the ionograms have been invoked by the author for distinguishing the well developed spread F irregularities from those just in the developing phase.

### VII.2.3 THEORIES OF SPREAD F

Several theories have been proposed to explain the formation of irregularities causing spread F. Some of the important theories are :

i) The drift instability theory (Martyn, 1959),

ii) The crossfield instability mechanism (Simon, 1963; Reid, 1968),

iii) The Rayleigh-Taylor instability mechanism (Dungey, 1956; Balsley et al. 1972),

iv) the drift mode instability (Hudson and Kennel, 1975; Chaturvedi and Kaw, 1976), and

v) The spatial resonance mechanism (Beer, 1974).

Farley et al. (1970) have criticised the theories (i) and (ii) mentioned above, in view of their own observations on 3 m scale size spread F irregularities. Their observation showing that the spread F occurs simultaneously in the bottomside and topside in the evening hours, argues against the Martyn's drift instability theory which requires upward drift of ionisation for irregularity formation in the bottomside and downward drift of ionisation for irregularity formation in the topside ionosphere.

The crossfield instability was first investigated by Simon (1963) for laboratory plasma and later applied to the ionospheric E region (Reid, 1968) where the Pedersen conductivity is the largest. This instability relies on ion-neutral collisions in an $\underline{E} \times \underline{B}$ field, and therefore it is much less effective at the F region altitudes. Reid (1968) suggested that this difficulty can be overcome if the instability is taken to be in the E region at the latitudes connected by the magnetic field lines to the equatorial F region. However, the problem with a mechanism involving the coupling between the E and F regions is that it is effective for wavelengths $\gtrsim 1$ km (Farley et al. 1970) and therefore the 3 m scale size irregularities cannot be explained by this mechanism.

Another important instability invoked for explaining the equatorial spread F irregularities is the Rayleigh-Taylor (R-T) instability, also known as the gravitational instability. The basic requirement for R-T mode to be operative is the presence of the electron density gradient antiparallel to $\underline{g}$, the earth's gravity. Dungey (1956) originally proposed the collisionless limit of the R-T mode as a source of equatorial spread F irregularities. Balsley et al. (1972) proposed that the long wavelength end of the spread F spectrum can be attributed to the collisional limit of the R-T instability which applies for ion-neutral collision frequencies $\nu_{in} \gg (g/L_\perp)^{\frac{1}{2}}$,

the collisionless R-T growth rate in a density gradient with scale length $L_{\perp} = (\triangle n/n)^{-1}$ . The R-T mode is not applicable to the topside spread F phenomenon because the primary density gradient, being downwards, is in the same direction as the earth's gravity $\underline{g}$ and thus does not satisfy the basic requirement for the R-T mode to be operative.

However, the most serious problem with the crossfield as well as the R-T instability, in their application to the spread F phenomenon, is that these modes are not applicable for irregularity scale sizes approaching the ion Larmor radius (being $\sim$ 20 m in the equatorial F region). Thus the 3 m scale sizes observed by the Jicamarca radar cannot be explained by these modes.

Hudson and Kennel (1975) showed that the spread F irregularities below a few hundred meters (and yet $\lambda_{\perp} \gg \rho_i$ ) can be explained by collisional drift wave instability. Earlier Hudson et al. (1973) proposed a two step mechanism for the generation of scale lengths $\lambda_{\perp} \lesssim \rho_i$ . Hudson et al. argued that long wavelength irregularities provide density gradients which in turn 'linearly' excite collisionless drift waves.

The drift mode belongs to a class of instabilities more generally known as the "universal instabilities". In contrast to the crossfield and the R-T modes which require an additional destabilizing force (electric field and the gravitational field respectively), the universal instabilities

do not require any additional driving force. The drift mode instability consists of waves, travelling with electron diamagnetic drift velocity (Chen, 1974, p. 196), which are destabilized solely by the plasma density gradient at short perpendicular wavelengths approaching the ion Larmor radius. The collisional drift mode growth rate, $\gamma \propto 1/(k_z^2 L_\perp^2)$, where $k_z$ represents the wavenumber parallel to the magnetic field, exceeds the collisionless growth rate, $(g/L_\perp)^{\frac{1}{2}}$, for a small enough density gradient scale length, $L_\perp$, at a given perpendicular wavelength.

Hudson and Kennel (1975) showed that the collisional drift mode can grow on topside as well as bottomside density gradients and thus this mode is applicable to the topside spread F phenomenon as well (cf. R-T mode). However, they concluded that for the bottomside spread-F, both the R-T and the drift modes can contribute to the total spectrum of spread F irregularities, the drift mode peaking at shorter perpendicular wavelengths.

Recently, Chaturvedi and Kaw (1976) showed that the two step process invoked by Hudson et al. (1973) cannot give rise to short wavelengths growing on long wavelength drift waves. This is because of the fact that in a drift wave the first order electron diamagnetic drift, which supports the secondary drift mode, is absent. They suggested that a drift wave can grow on the density gradients of a R-T mode or some other mode. As the long scale length irregularities increase

in amplitude, the gradient associated with them becomes sharper. When this gradient exceeds a critical value, the long wavelength mode becomes unstable to collisional as well as collisionless drift waves by a two step process.

The mechanism proposed by Chaturvedi and Kaw is applicable to short and long wavelength spread F irregularities in the bottomside ionosphere. However, if appropriate primary electron density gradients are present, the theory could be applicable to the topside spread F phenomenon as well (Chaturvedi, 1976, Private Communication).

Beer (1974) considered spread F as a multistage process. The first stage in the production of spread F occurs when the phase velocity of an atmospheric gravity wave matches the $\underline{E} \times \underline{B}$ ionization drift velocity in the direction of the wave's phase velocity, giving rise to the so called "spatial resonance effect". The gravity waves invoked for the spatial resonance mechanism were assumed to be launched by the equatorial electrojet. The physical mechanism leading to the spatial resonance has been explained by Beer in the following manner :

Atmospheric gravity waves are manifested by a wavelike perturbation in the neutral gas density and temperature. Wavelike perturbations of the ionisation then occur through collisions between the charged particles and the neutral particles and also from the changes induced by the gravity waves in the loss rate of the ionisation. The

loss coefficient $\beta$ in the F region is temperature dependent and thus the changes in the neutral temperature due to the passage of the gravity wave modify the loss rate. Beer shows that variations in the loss rate are far more effective in perturbing the ionisation density in the F region than the collisions with the neutral particles. The spatial resonance occurs if the velocity of the ionisation irregularity has a component which is the same as the phase velocity of the gravity wave and in the same direction. Under such circumstances the peaks of the ionisation perturbations will continue to stay in the same position relative to the wave. The ionisation perturbations will thus maintain the same phase relation to the wave and as the process continues the ionisation irregularity will continue to grow. The presence of a number of enhanced ionisation layers, one above the other, has been termed as 'pousse-cafe' effect. The spatial resonance cannot continue indefinitely and it will cease when the charged particle density of the ionisation irregularity has become so large that the system becomes unstable. The instability which is applicable for such a configuration is the collision dominated R-T instability. It is here that the instability is observed as spread F on the ionograms.

The time $\tau$ for the onset of instability after the start of spatial resonance is given as

$$\tau = \beta_0^{-1} \ln \left\{ 1 - \left( \frac{\beta_0 \nu_{in}}{g} - \frac{1}{n_0} \frac{dn_0}{dz} \right) \frac{C}{k_z U_{1x}} \right\}^{-1} \quad \text{---- (1)}$$

provided

$$0 < \left( \frac{\beta_0 \nu_{in}}{g} - \frac{1}{n_0} \frac{dn_0}{dz} \right) \frac{C}{k_z U_{1x}} < 1 \quad \text{------- (2)}$$

where n and $\beta$ denote the ionisation density and the loss rate, C and U denote the velocity of sound the ionisation irregularity respectively; the subscripts '0' and '1' refer to the unperturbed and the first order perturbed values of various parameters. 'x' and 'z' denote eastward and upward direction respectively and $k_z$ denotes the real part of the complex vertical wavenumber of the gravity wave.

The right hand inequality of (2) provides the lower limit for the occurrence of spread F. The lower limit of the instability depends on the upward ionisation gradient at the base of the ionosphere. However, since $(\beta_o / in/g)$ attains large values below 250 km, the lower limit will be close to this altitude. In the topside ionosphere, where $n_o^{-1}\, dn_o/dz$ is negative, there is an upper limit to the onset of instability. This occurs when $(\beta_o / in/g)$ is so small as to be negligible and

$$\frac{C}{k_z U_{1x}} > \left| n_o^{-1} \frac{dn_o}{dz} \right|^{-1} \quad \text{for} \quad n_o^{-1} \frac{dn_o}{dz} < 0$$

Indeed, Beer's mechanism explains some of the observed features of the equatorial spread F phenomenon; in particular the appearance of the "satellite traces" preceding the spread F onset observed on the bottomside ionograms. A number of spatially resonant ionization irregularities formed by the dominant atmospheric wave would produce the observed splitting of the ionogram traces. Beer evaluated

eq.(1) between 240 and 700 km by taking the appropriate values of the parameters for the nighttime conditions and showed that under the conditions encountered by Lyon et al. (1961), where the satellite traces occurred between altitudes of 450 and 500 km, the value of $\tau$ varies between 10 and 20 min. This is in agreement with the observations of Lyon et al. (1961) that the time of first appearance of spreading of echoes varies between 0 and 15 minutes.

However, the basic assumption in Beer's work is that the gravity waves required for producing the equatorial spread F are launched by the equatorial electrojet. Chimonas (1970) considered theoretically the effectiveness of the equatorial electrojet in launching gravity waves and concluded that it is not a very efficient source. He showed that the Lorentz coupling of the electrojet current ($\underline{J} \times \underline{B}$) on the neutrals is not very significant. On exceptionally disturbed days, however, when the joule heating caused by the current surges in the electrojet dominates over the Lorentz coupling, the electrojet can launch gravity waves. The observed anticorrelation of equatorial spread F with magnetic activity (e.g. Lyon et al. 1960), however, argues against the role of the equatorial electrojet in causing the spread F through spatial resonance mechanism.

Beer's mechanism for spread F is rather critically dependent on the gravity waves required for producing the irregularities through spatial resonance mechanism. Earlier, Beer (1973) proposed that the supersonic motion of the earth's

terminator generates gravity waves, but the expected westward phase speed of the waves so generated makes them unlikely contenders for the production of spread F irregularities which are in general observed to drift eastwards (e.g. Farley et al. 1970). The waves generated lower in the atmosphere, namely those generated by the weather disturbances in the troposphere are mostly reflected below the mesopause level due to the negative temperature gradient in the mesosphere. Although certain fraction of the wave energy leaks upward, it may not be sufficient in strength to trigger or maintain spread F for a considerable time. Thus the gravity waves relevant to the ionospheric F region will have to be generated in the altitude region above 100 km.

## VII.3 OBSERVATIONS AND THEIR IMPLICATIONS

A number of equatorial passes of ISIS-1 satellite at various longitudes during premidnight hours have been analysed to find out the presence of spread F and its boundary in the topside ionosphere.

Fig.7.2 shows a sequence of ionograms obtained on Feb. 11, 1969 at 03.37 UT at 86$^{o}$E mean longitude (LT 2158 hr). The three ionograms between 03.37.34 UT to 03.38.57 UT are seen to reveal a spread echo patch below the main X and O traces near the starting frequencies of the traces. On the basis of the development of spread F on the bottomside ionograms mentioned above, these three ionograms reveal developing spread F

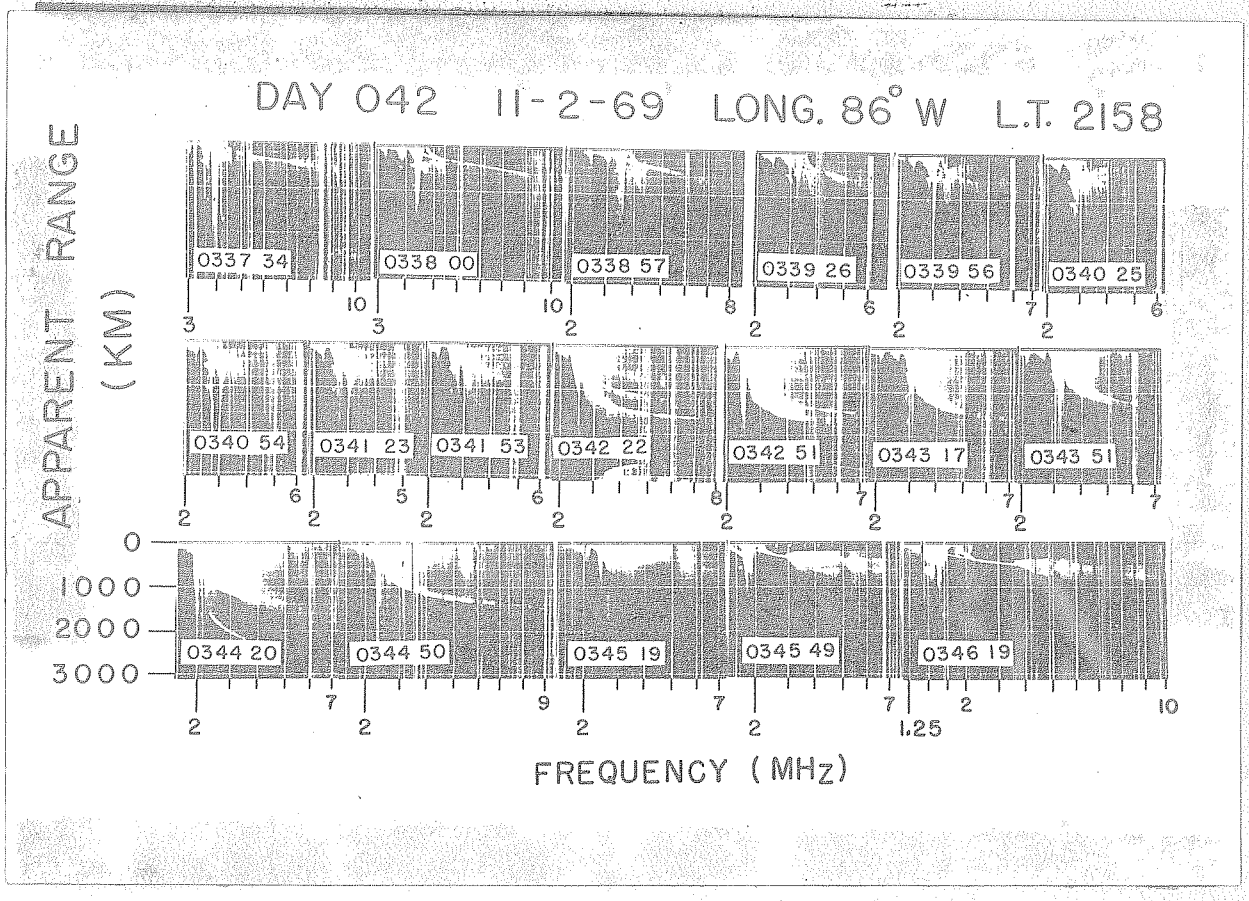


Fig. 7.2:- Sequence of ionograms obtained by means of ISIS-1 satellite on Feb. 11, 1969 at 2158 hr LT (86°WMT) showing spread echoes.

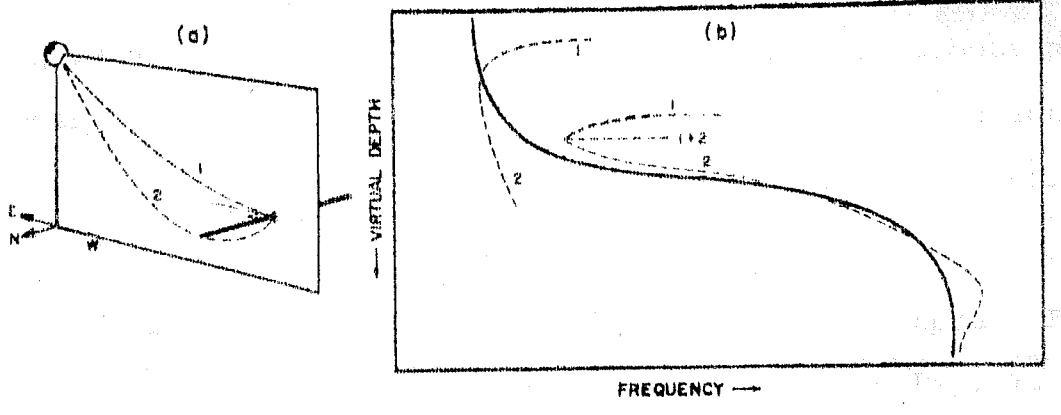


Fig.7.3(a,b):- The model for equatorial, aspect sensitive scattering (a) ray path geometry (b) sketch of the expected X mode echo configuration.
(After Calvert and Schmid , 1964)

The ionogram obtained at 03.39.56 UT shows the spread F at the low frequency end of the trace (the high frequency end shows clean echo) and thus reveals the irregularities in a developing stage. The four ionograms between 03.40.25 UT and 03.41.53 UT show the spread echoes through which clean O and X echo traces are seen, revealing that the irregularities are just in developing stage on the basis of the earlier discussion of the bottomside ionograms (Fig. 7.1). The two ionograms at 03.42.22 UT and 03.42.51 UT show conjugate ducted echoes caused by the ducting of radio wave energy when the satellite in inside a duct (Muldrew, 1963). The seven ionograms between 03.42.22 UT and 03.45.19 UT show that spread F irregularities extend upto the altitude of the satellite.

The last three ionograms in this pass between 03.45.49 UT and 03.46.49 UT (the last one not shown in the figure), reveal spread F 'brushes' under the conditions of fully developed spread F, as the normal ionospheric echoes are completely suppressed by the spread echoes. The word 'brush' will henceforth denote such spread F echoes, because of their appearance like a painter's brush.

The model for explaining the equatorial spread F configuration on topside ionograms such as shown in Fig. 7.2 is given by Calvert and Schmid (1964) and is reproduced in Fig. 7.3(a,b). The model is based on the aspect sensitive scattering caused by thin (compared to the wavelength of the probing radio wave) field aligned ionisation irregularities.

The irregularities represent slight deviations, either enhancements or depletions, in the ambient ionisation. The echoes caused by these irregularities are assumed to be the result of back-scattering normal to their long dimension. In Fig. 7.3(a) the thick solid line oriented in the N-S and horizontal direction shows the irregularity. Two ray paths from the sounder to the irregularity are shown in the east-west plane. The ray path 1 goes directly to the irregularity; raty path 2 reaches the irregularity after being reflected back upwards by the ionosphere. The expected extraordinary echo configurations produced by these ray paths are sketched in Fig.7.3(b). Those for ordinary wave propagation will be similar. When the satellite is at the magnetic equator the combination trace, (1 + 2), corresponding to the arrival at the irregularity by one ray path and return to the sounder by the other could also appear. In general, when the spread F is well developed a number of scattering irregularities are present thus giving rise to spread F echo to be a superposition of traces like those shown in Fig. 7.2(b).

Lockwood and Petrie (1963) showed that the true height of the upper boundary of the spread echo (irregularity) in the portion of the trace where the boundary shows constant depth below the satellite altitude, is the same as its apparent depth, to within 15-20 km. They showed that this upper boundary line, obtained as the true heights corresponding to the minimum range of the spread echoes at different latitudes, is field aligned. Thus the work of Lockwood and

Petrie shows that the individual scattering irregularities as well as the whole patch of irregularities causing the equatorial spread F are aligned to a single line of force of the earth's magnetic field.

However, an important point needs to be mentioned about the result of Lockwood and Petrie. The spread F echoes (shown in Fig.2 of their paper), from which the boundary line of the irregularities was found field aligned, reveal well developed spread echoes. The O and X ionospheric echo traces are completely suppressed by the spread echoes. On the basis of such observations, Calvert and Schmid (1964) inferred that the irregularities are strong enough to cause multiple scattering of the probing radio waves so that no coherent ionospheric echo returns to the sounder receiver. On the basis of these characteristics, the results of Lockwood and Petrie suggest that the upper boundary line of the fully developed spread F irregularities is aligned to a field line.

Fig. 7.4 gives the minimum range of the spread F irregularities derived from ionograms of Fig. 7.2, on an altitude versus latitude diagram. The smooth dashed curves represent the geomagnetic field lines and the thick line with the arrow indicates the path of the satellite. Position of the satellite at each one minute interval is indicated on the satellite path. The minimum range of the spread F echoes below the satellite altitude are shown by X's and the dashed line joining the crosses delineates the upper

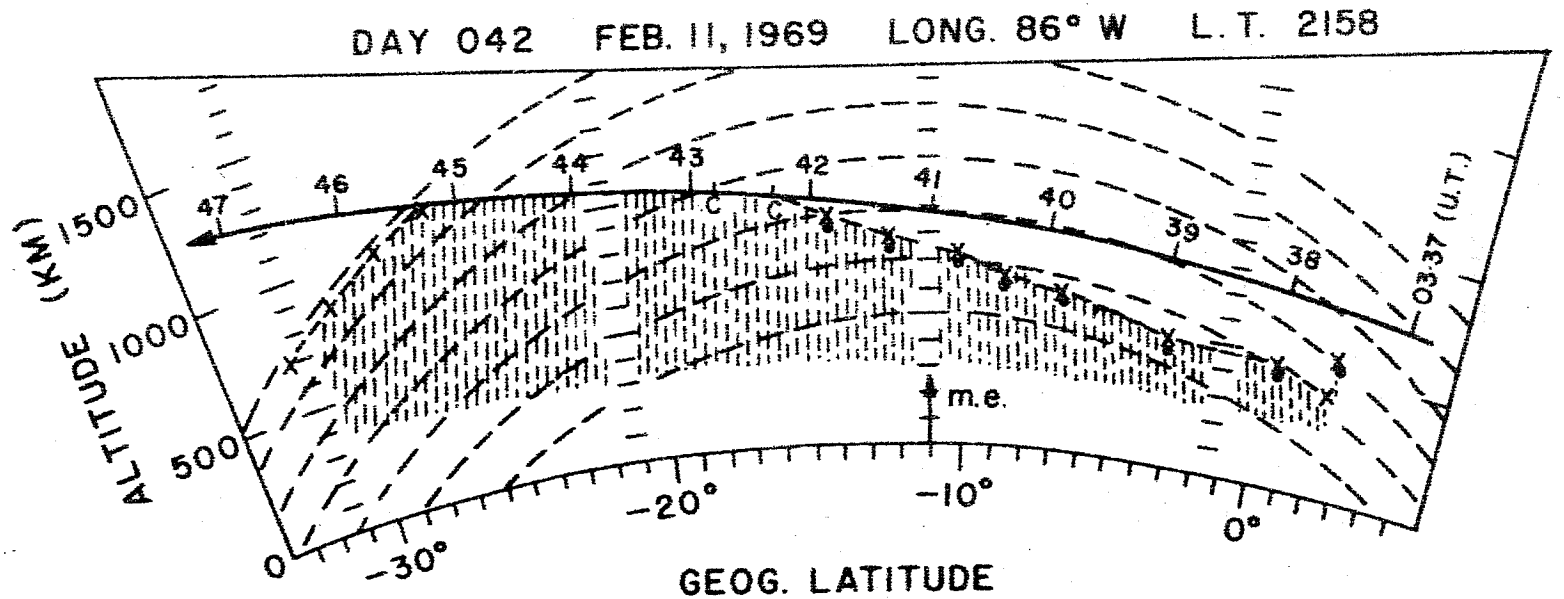


Fig. 7.4:- The upper boundary line of the spread-F irregularities, given by the dashed line joining the X's, on Feb. 11, 1969 obtained from the ionograms shown in Fig. 7.2. The X's with thick dots denote developing spread-F. The letter 'C' denotes a conjugate echo.

boundary of the spread F irregularities. The region below this boundary line is hatched with broken lines to show that spread F occurs below this boundary. It is seen that the portion of the upper boundary line between $+2^{\circ}.0$ and $-14^{\circ}.4$ latitudes, obtained by joining the X's with a thick dot underneath, corresponding to the ionograms between 03.37.34 UT and 03.41.53 UT (in Fig. 7.2) revealing the spread F in a developing stage, shows prominent deviation from the field alignment.

In the region between $-16^{\circ}.2$ latitude and $-26^{\circ}.7$ latitude (corresponding to the ionograms between 03.42.22 UT and 03.45.19 UT the spread F is present at the satellite altitude. The upper boundary line in that latitude zone is necessarily above the satellite altitude but could not be determined from the ionograms. The letter 'C' denotes the occurrence of conjugate ducted echoes. The portion of the boundary line between $-26^{\circ}.7$ latitude and $-31^{\circ}.9$ latitude, corresponding to ionograms between 03.45.19 UT and 03.46.49 UT (the last ionogram not shown in Fig. 7.2) revealing well developed sptead F, is seen to be accurately field aligned. Thus it is very clearly seen that the upper boundary line of fully developed spread F irregularities is field aligned while the boundary of spread F in the developing phase reveals prominent deviation from the field aligned nature.

Fig. 7.5(a,b) shows a sequence of ionograms on February 18, 1969 obtained on an ISIS-1 satellite pass at 1934 UT at $26^{\circ}$E longitude (2121 hr LT). The five ionograms between

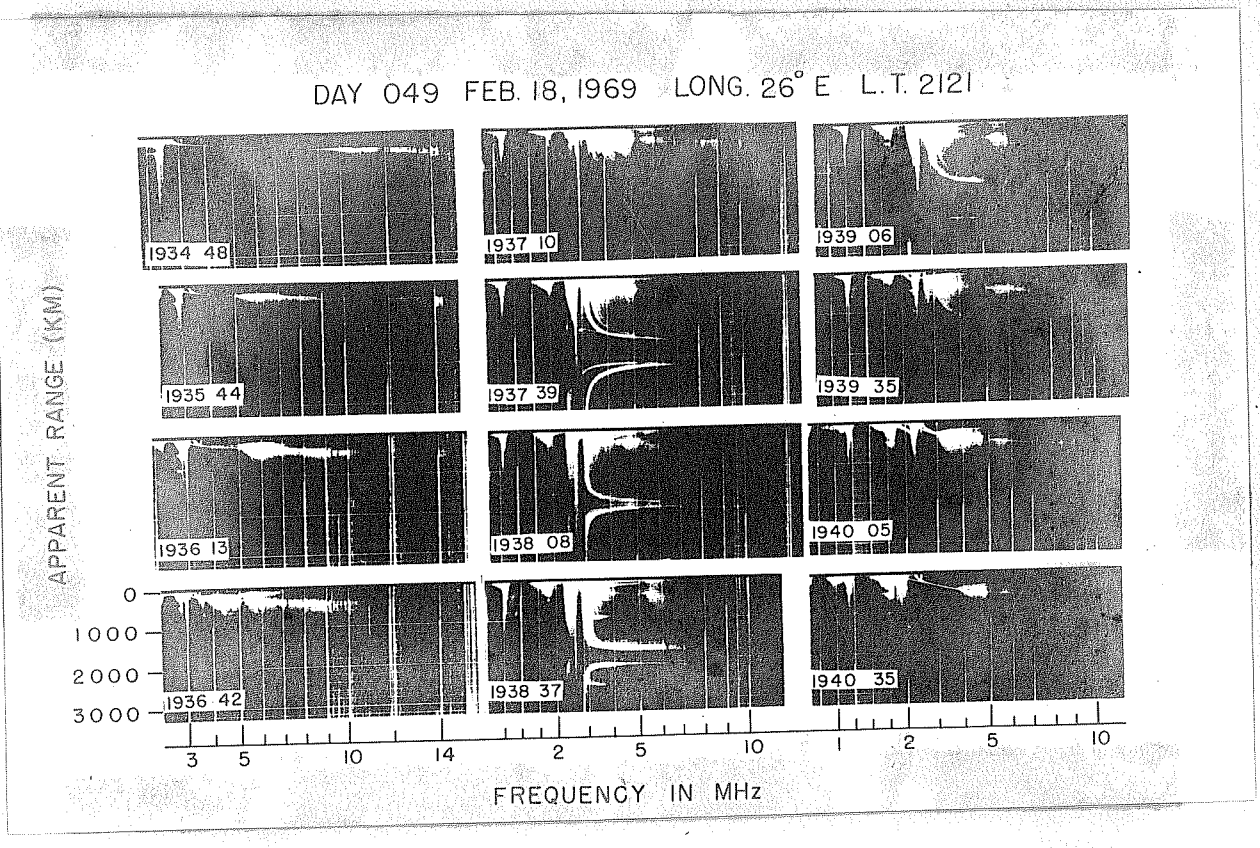


(a)

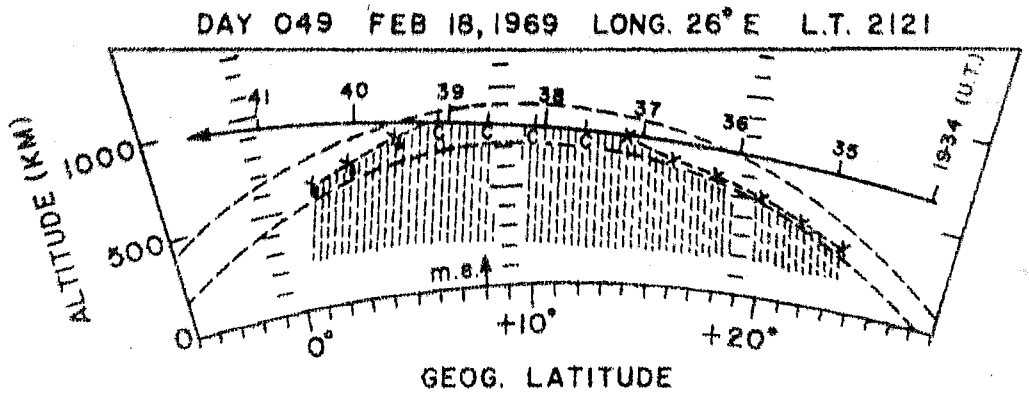


(b)

Fig.7.5(a,b):- (a) Sequence of ionograms obtained by means of ISIS-1 satellite on Feb. 18, 1969 at 1934 hr UT at 26°E long. (LT 2121 hr) and (b) the minimum range to the spread F irregularities from the satellite. The description is same as in Fig. 7.4.

19.34.48 UT and 19.37.10 UT are seen to reveal fully developed spread F brush type echo, the minimum range to these echoes giving the portion of the boundary line between $23^{o}.2$ latitude and $15^{o}.9$ latitude corresponding to the above ionograms is seen to be accurately field aligned. The four ionograms between 19.37.39 UT and 19.39.06 UT show conjugate ducted echoes denoted by 'C' at the latitudes between $12^{o}.2$ and $6^{o}.6$ in Fig.7.5(b). The last three ionograms at 19.39.35 UT, 19.40.05 UT and 19.40.35 UT show developing spread F; the spread is seen to occur at the low frequency end of the ionogram traces and clean ionospheric echo traces are seen at the high frequency end of the ionograms. The minimum range to these spread echoes being 75 km, 200 km, and 300 km, shown by crosses with a thick a dot underneath, at $4^{o}.8$ , $2^{o}.9$ , and $1^{o}.1$ latitude give the boundary line which is not field aligned.

Fig. 7.6 gives the upper boundary line of spread F irregularities obtained from the ISIS-1 pass on Feb. 18, 1969 at 2144 UT at $6.5^{o}$W longitude (2121 hr LT), being in succession to the pass shown in Fig.7.5. The two ionograms at 20.50.04 and 20.50.32 UT showed spread F brush type echoes which revealed the irregularities in developing phase at $-2^{o}.8$ and $-4^{o}.5$ latitude corresponding to these two ionograms. The portion of the boundary line shows prominent deviation from the field alignment between these latitudes.

Fig. 7.7(a) shows twelve ionograms from a sequence of twenty ionograms obtained from the topside sounder data recorded by ISIS-1 satellite on February 20, 1969 at 20.48 UT at

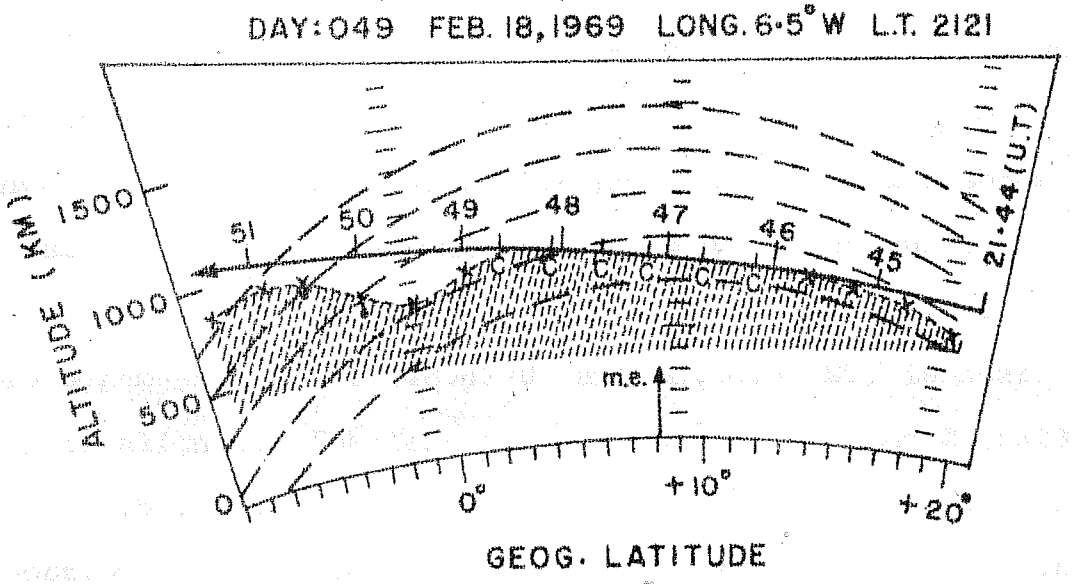


Fig. 7.6:- Same as in Fig. 7.5(b) on Feb. 18, 1969 at 2144 UT at 6°.5 W longitude (LT 2121 hr).

$5^{o}$E longitude (local time 2112 hr). Fig. 7.7(b) shows the upper boundary of spread F irregularities derived from these ionograms. The five ionograms between 20.50.36 UT and 20.52.31 UT show spread F in a developing stage, the brushes are seen at low frequency end of the ionogram and clean O and X traces are seen through the spread F. The portion of the boundary line of the spread F irregularities obtained from the minimum range of these five brush echoes, marked by crosses with dots underneath, at $13^{o}.5$ , $11^{o}.6$ , $9^{o}.8$ and $7^{o}.9$ latitude, shows distinct non field alignment. The portion of the boundary line between $20^{o}.3$ and $15^{o}.3$ latitudes, obtained from the ionograms between 20.48.42 UT and 20.50.08 UT, is nearly field aligned. The last three ionograms between 20.53.00 UT and 20.53.58 UT show well developed spread F brushes and the portion of the boundary line between $4^{o}.3$ and $0^{o}.8$ latitude, corresponding to these brushes is aligned accurately to the magnetic field line with its equatorial altitude as 950 km. The two crosses marked at $-0^{o}.9$ and $-2^{o}.8$ latitude obtained from spread F ionograms at 20.54.30 UT and 20.55.00 UT (not shown in Fig.7.7(a) ), are also found to be on the same magnetic field line.

Fig. 7.8(a) gives a series of 16 ionograms out of 21 ionograms obtained from the ISIS-1 pass on February 25, 1969 at 20.37 UT at $2^{o}$E mean longitude (local time 2050 hr) and Fig.7.8(b) gives the boundary line of spread F irregularities obtained from them. The five ionograms between 20.37.00 UT

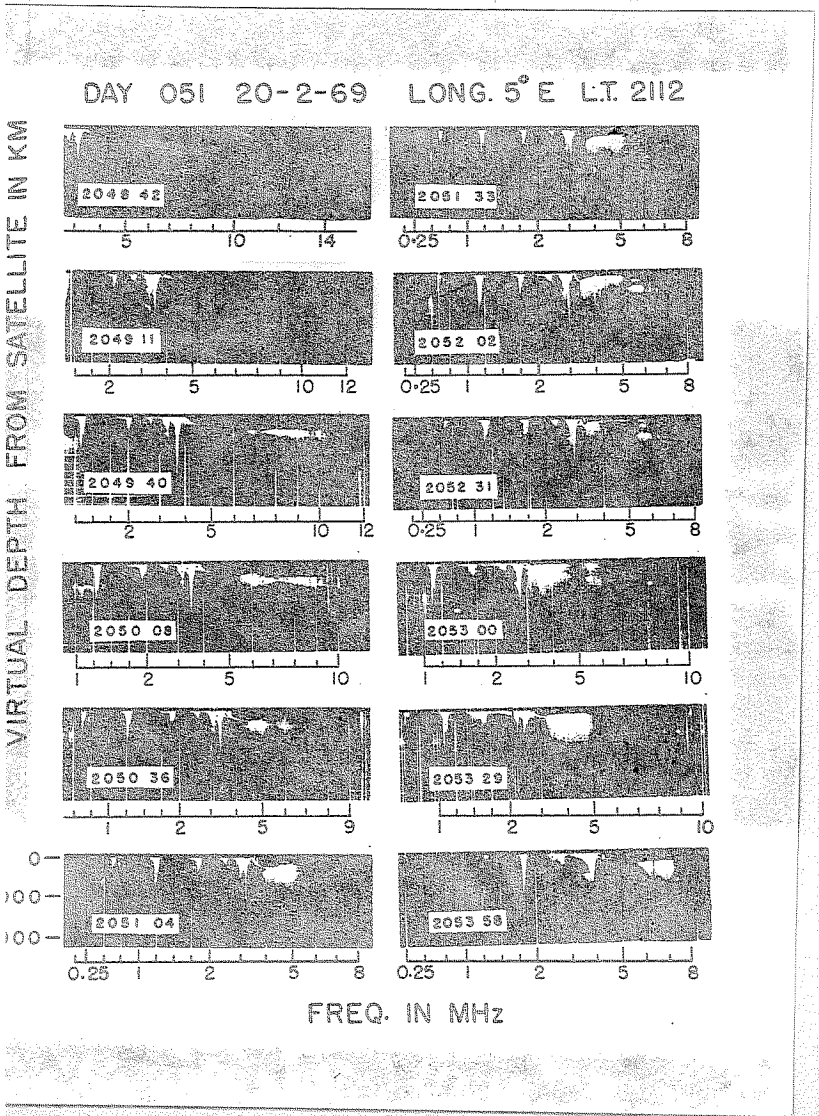


(a)

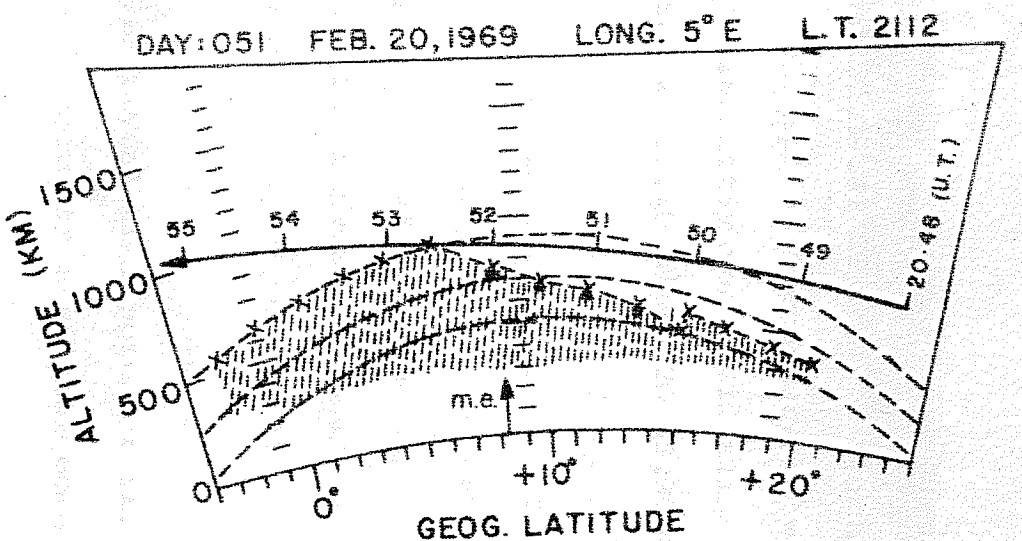


(b)

Fig.7.7(a,b):- Same as in Fig. 7.5(a,b) on Feb.20,1969 at 2048 UT at 5°E longitude (LT 2112 hr).

and 20.39.42 UT (out of which four are shown) give the portion of the spread F boundary between $30^{\circ}.5$ and $19^{\circ}.2$ latitude which is distinctly non field aligned. All the remaining ionograms from 20.40.10 UT to 20.45.30 UT, except the four ionograms between 20.41.37 and 20.43.03 UT for which the satellite is embedded in the spread F irregularities and therefore the upper boundary cannot be ascertained, reveal fairly well developed spread F brushes. The upper boundary of the spread F irregularities between $17^{\circ}.5$ and $-1^{\circ}.5$ latitude, plotted in Fig.7.8(b) is nearly field aligned.

The above five examples on days between Feb.11-25, 1969 reveal that spread F irregularities while developing are not aligned to a single geomagnetic field line.

None of the existing theories is able to explain the behaviour of non field aligned boundary of spread F irregularities at the time of their formation. The observations presented above suggest that any mechanism that invokes a plasma instability would be an unlikely contender in triggering the spread F phenomenon. This conclusion is based on the fact that a plasma instability generates field aligned boundary of the irregularity. We propose that the origin of spread F irregularities lies in a disturbance in the neutral atmosphere. This would explain the initial non field alignment of the spread F boundary line. Subsequently the disturbance might trigger a plasma instability that in turn gives rise to field aligned boundary line of irregularities when spread F is fully developed.

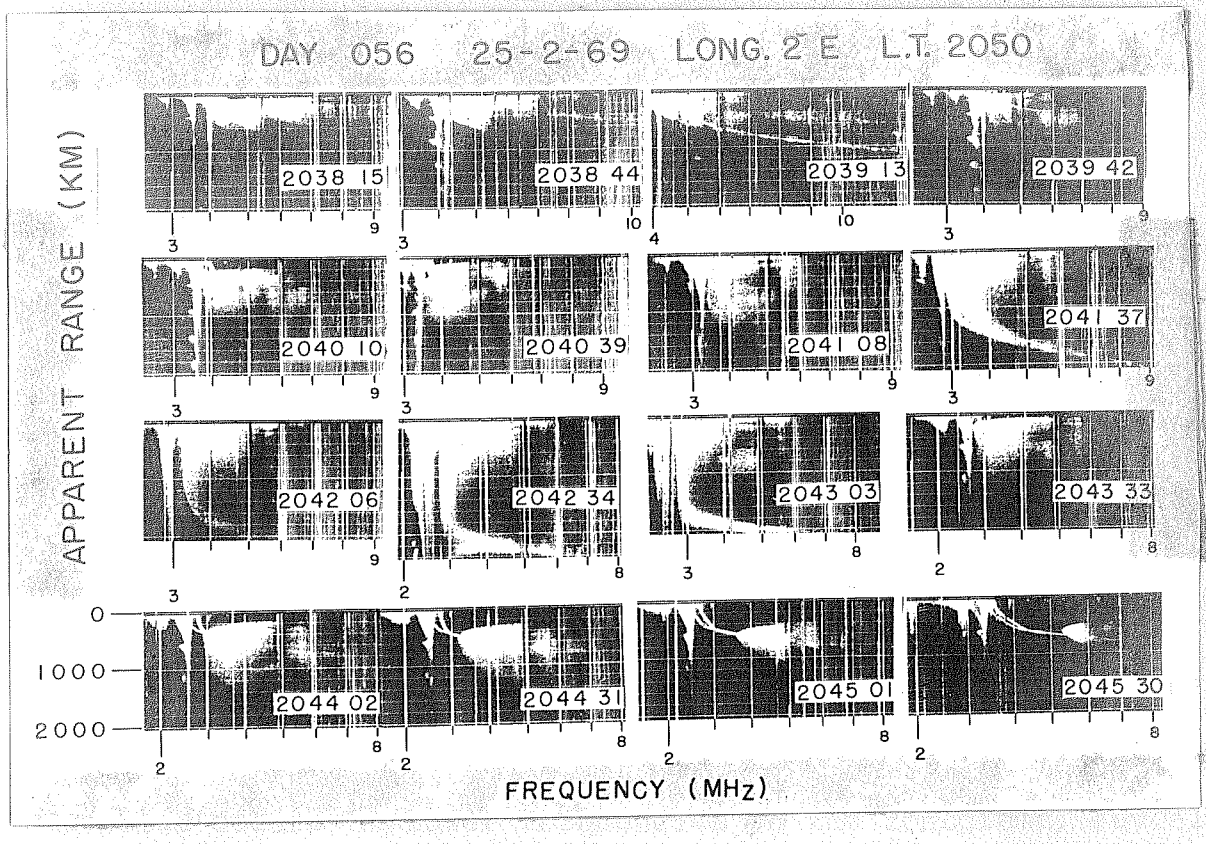


(a)

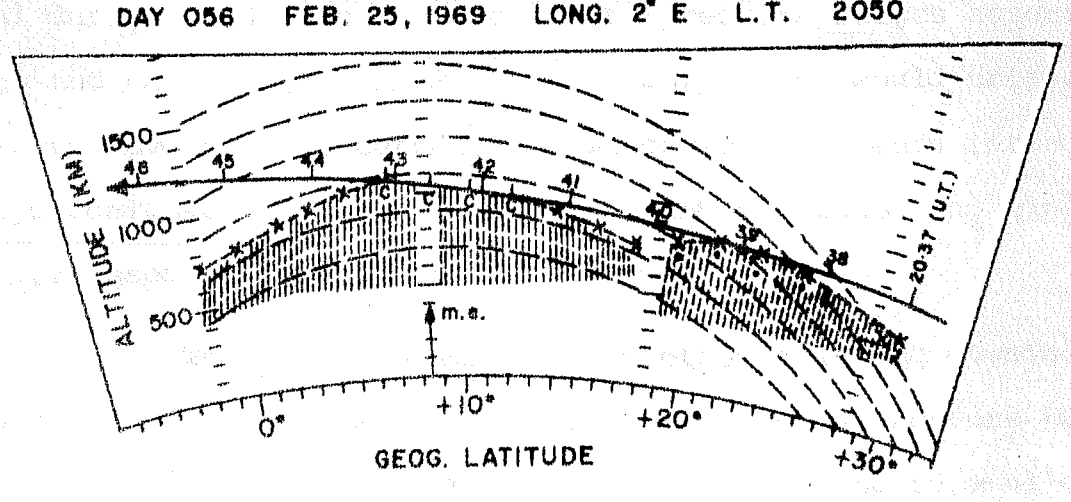


(b)

Fig.7.8(a,b):- Same as in Fig. 7.5(a,b) on Feb. 25, 1969 at 2037 UT at 2°E longitude (LT 2050 hr).

Recently Raghavarao (1976) proposed a new mechanism for explaining the premidnight spread F during the solar maximum ($S_{max}$) period. The salient features of his theory are the following:

During sunspot maximum period, the ionisation anomaly (IA) attains maximum strength around 1900-2000 hrs LT; the strength indicated by the excess percentage electron concentration at the IA crest over that at the trough being about 200-300% (see sec. I.3.2, Chapter 1). The spread F commences around the same hours. It is mentioned in Sec. VII.2 and VII.3, that the onset of the spread F both in the bottomside and the topside occurs at lower frequencies on the ionograms, revealing that the large scale size irregularities ($\sim$100 m) are generated in the initial stages of spread F development. The intense IA in the premidnight hours gives rise to strong neutral anomaly (NA) during these hours. The excess pressure bulges associated with the NA, as shown in Fig.6.9 of Chapter 6, would trigger gravity wave type perturbations, which would in turn introduce large scale vertical wavelengths and the corresponding winds as discussed in Sec.VI.4 of Chapter 6.

The neutral atmosphere contracts in the evening hours due to the postsunset cooling. The broad pressure bulges while collapsing due to the cooling can give rise to smaller wavelengths of gravity waves. The meriodional flow of the gas would then lead to accretions and depletions of ionisations providing the "Pousse-cafe" effect discussed by Beer (1974).

Thus, Raghavarao's mechanism essentially provides a source of gravity waves in the equatorial E and F regions to cause the spread F through the spatial resonance mechanism described in Sec. VII.2.3. The fact that the gravity waves have their origin in the neutral atmosphere, would explain the initial non field alignment of the large scale size irregularities generated by them. The Rayleigh-Taylor instability which follows the spatial resonance phenomenon would generate the small scale size irregularities for which the individual irregularities as well as the boundary along which the irregularities form, would lie along a magnetic field line.

The presence of wave motions in the equatorial F region during premidnight hours when the spread F was present is provided by the work of Crochet (1972) and Nielson and Crochet (1974). These authors have shown that the inhomogeneities in the postsunset F region lead to a scatter like propagation of HF and VHF frequencies used in the transequatorial propagation (TEP) experiments. Because of wide range of irregularity scale sizes and the plasma densities associated with them in the equatorial ionosphere, the reflections can occur for as high as 100 MHz frequency.

The field aligned irregularities in the equatorial ionosphere produce significant level of "off path" propagation at high frequencies. The identification of off-path modes is based on delay measurements of pulsed signals and direction finding with the help of highly directive transmitting and

the occurrence of equatorial spread F and thus the TEP technique provides a means of investigating the occurrence of irregularities over an extended area using only two stations located in different hemispheres.

Fig. 7.9(a,b) reproduced from Nielson and Crochet (1974) gives the contrast of signal strength at 11.24 MHz frequency on TEP path between Valensole, France and Grahamstown, South Africa on 9-10 March, 1970, the off path scatter signal shown by continuous curve in Fig.7.9(a) varies smoothly throughout the period of observation and spread F was found to be absent on the bottomside ionograms obtained at equatorial station, Ouagadougou. On March 13-14, 1970, in Fig.7.9(b), off-path scatter signal shows fluctuations in the signal strength between 2000-0200 GMT and the Ouagadougou ionograms revealed the presence of spread F. The fluctuations in the signal strength are interpreted as due to patches of irregularities moving in the antenna pattern (Crochet, 1972). They reveal periodicities of half an hour to 2 hours and thus suggest the presence of the internal atmospheric gravity waves. Thus Fig.7.9(a,b) shows the presence of such wave motions in the equatorial F region when spread F is present.

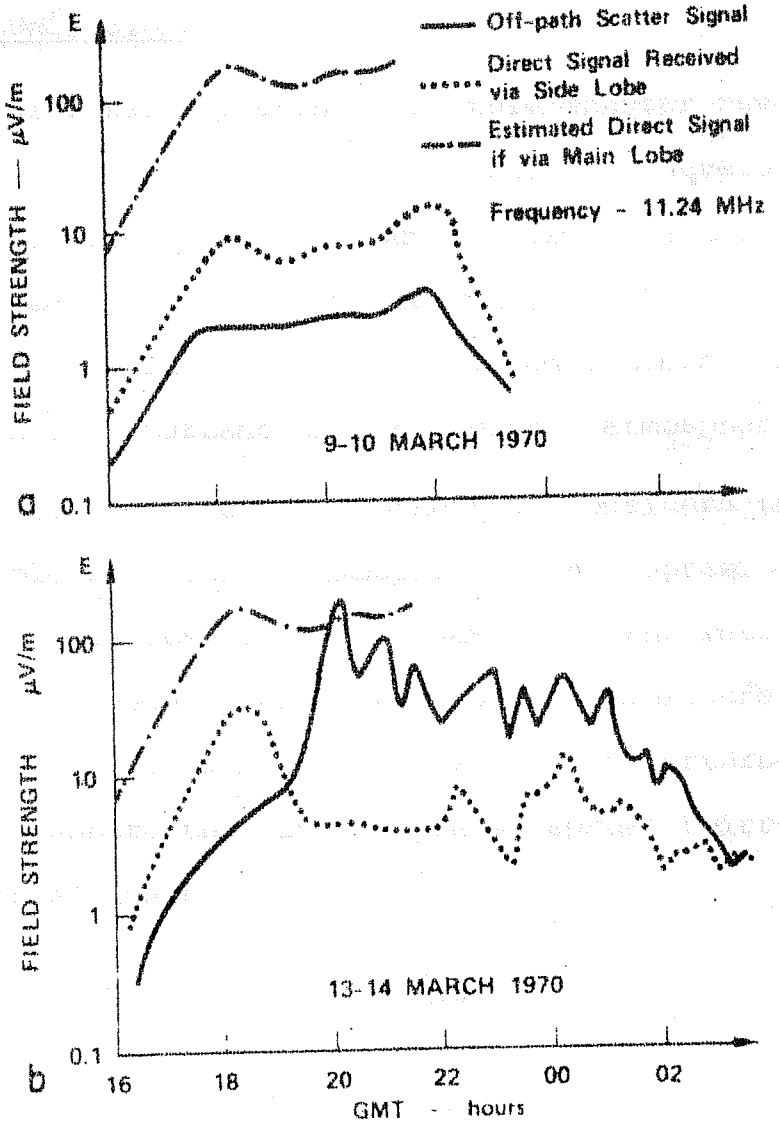


Fig.7.9(a,b):- Contrast of signal strengths between nights when spread F was (a) not present (b) present obtained by transequatorial radio propagation experiment. (After Nielson and Crochet, 1974)

## REFERENCES


Abur-Robb, M.F.K. & Dunford, E., 1975, Planet. Space Sci. 23, 1071.

Anandarao, B.G. et al., 1975, Presented at URSI Gen. Assembly, PERU.

Anandarao, B.G., 1976, Geophys. Res. Lett. (in press).

Anandarao, B.G., et al., 1976, Presented at COSPAR XIX Meeting, Philadelphia, USA.

Anderson, A.D., 1973, Planet. Space Sci., 21, 2049.

Anderson, D.N., 1973, Planet. Space., 21, 421

Anderson, D.N. et al., 1973, J. Atmos. Terr. Phys., 35, 753.

Appleton, E.V., 1946, Nature, 157, 691.

Appleton, E.V., 1954, J. Atmos. Terr. Phys. 5, 348.

Bailey, G.J. et al., 1973, J. Geophys. Res., 78, 5597.

Baker, W.G. & Martyn, D.F., 1952, Nature, 170, 1090.

Baker, W.G. & Martyn, D.F., 1953, Phil. Trans. R. Soc., A246, 281

Balsley, B.B. & Woodman, R.F., 1969, J. Atmos. Terr. Phys., 31, 865.

Balsley, B.B. et al., 1972, J. Geophys. Res., 77, 5625.

Bartels, J. & Johnston, H.F., 1940, Terr. Magn. Atmos. Electr., 45, 269.

Bauer, S.J., 1969, Proc. IEEE, 57, 1114.

Bauer, S.J. & Hartle, R.E., 1974, Geophys. Res. Lett., 1, 7.

Baxter, R.G. & Kendall, P.C., 1968, Proc. Roy. Soc., A304, 171.

Beer, T., 1973, Nature, 242, 34.

Beer, T., 1974, Aust. J. Phys., 27, 391.

Blum, P.W. & Harris, I. 1975a, J. Atmos. Terr. Phys., 37, 193.

Blum, P.W. & Harris, I., 1975b, J. Atmos. Terr. Phys., 37, 213.

Blumen, W. & Hendle, R.G., 1969, J. Atmos. Sci., 26, 210.

Booker, H.G. & Wells, H.W., 1938, Terr. Magn. Atmos. Electr. 43, 249.

Bramley, E.N. & Peart, M., 1965, J. Atmos. Terr. Phys., 27, 1201.

Bramley, E.N. & Young, M., 1968, J. Atmos. Terr. Phys., 30, 99.

Brown, G.M., 1973, Geophys. J. Roy. Astr. Soc., 33, 93.

Burge, J.D. et. al., 1973, J. Atmos. Terr. Phys. 35, 617.

Calvert, W. & Cohen, R., 1961, J. Geophys. Res., 66, 3125.

Calvert, W. & Schmid, C.W., 1964, J. Geophys. Res., 69, 1839.

Chandra, H. & Rastogi, R.G., 1972a, Ann. Geophys., 28, 37.

Chandra, H. & Rastogi, R.G., 1972b, Ann. Geophys., 28, 709.

Chandra, H. &Rastogi, R.G., 1974, Indian J.Radio Space Phys., 3, 332.
Chandra, S. &Goldberg, R.A., 1964, J.Geophys.Res., 69, 3187.
Chandra, S. et al., 1973, J.Geophys.Res., 78, 4630.
Chapman, S., 1931, Proc.Phys.Soc., 43, 26.
Chapman, S., 1951, Arch.Meteorol.Geophys.Bioklimatol., A4, 368.
Chapman, S., 1956, Nuovo Cimento Suppl., 4 (4), 1385.
Chapman, S. &Bartels, J., 1940, Geomagnetism, Oxford University Press, London
Chaturvedi, P.K. &Kaw, P.K., 1976, J.Geophys.Res., 81 (in press).
Chen, F.S., 1974, Introduction to Plasma Physics, Plenum Press New York&London.
Chimonas, G., 1970, Planet.Space.Sci., 18, 583
Chimonas, G. &Hines, C.O., 1970, Planet.Space Sci., 18, 565.
Cohen, R. &Bowles, K.L., 1961, J.Geophys.Res., 66, 1081.
Cole, K.D., 1974, J.Atmos.Terr.Phys., 36, 1099.
Crochet, M., 1972, Ann, Geophys., 28, 27.
Croom, S.A., et al., 1959, Nature, 184, 2003.
Duncan, R.A., 1960, J.Atmos.Terr.Phys., 18, 89
Dunford, E., 1967, J.Atmos.Terr.Phys., 29, 1489.
Dungey, J.W., 1956, J.Atmos.Terr.Phys., 9, 304.
Dyson, P.L. &Winningham, J.D., 1974, J.Geophys.Res., 79, 5219.
Eccles, D. &King, J.W., 1969, Proc.IEEE, 57, 1012.
Egedal, J., 1947, Terr.Magn.Atmos.Electr., 52, 449.
Egedal, J., 1948, Nature, 161, 443.
Einaudi, F. &Hines, C.O., 1970, Can.J.Phys., 48, 1458.
Evans, J.V., 1972, J.Atmos.Terr.Phys., 34, 175.
Fambitakoye, O. et al., 1973, J.Atmos.Terr.Phys., 35, 1119.
Farley, D.T. et al., 1967, J.Geophys.Res., 72, 5837.
Farley, D.T. et al., 1970, J.Geophys.Res., 75, 7199.
Fisher, R.A. &Yates, F., 1957, Statistical Tables for Biological, Agricultural and Medical Research, Oliver&Boyd, London.
Gerard, J.C. &Monfils, A., 1974, J.Geophys.Res., 79, 2544.
Gouin, P., 1962, Nature, 196, 1145.
Gouin, P. &Mayaud, P.N., 1967, Ann.Geophys., 23, 41.

Hanson, W.B. & Moffett, R.J., 1966, J.Geophys., Res., 71, 5559.

Hanson, W.B. et al., 1973, J.Geophys.Res., 78, 751.

Hedin, A.E. & Mayr, H.G., 1973, J.Geophys.Res., 78, 1688.

Herman, J.R., 1966, Rev.Geophys., 4, 255.

Hines, C.O., 1960, Can.J.Phys., 38, 1441.

Hirono, M. & Maeda, H., 1954, J.Geomag.Geoelectr., 6, 122.

Huang, C.M., 1960, J.Geophys.Res., 65, 897.

Huang, C.M., 1974, J.Atmos.Terr.Phys., 36, 43.

Hudson, M.K. et al., 1973, (Abstract) EOS Trans.AGU, 54, 1147.

Hudson, M.K. & Kennel, C.F., 1975, J.Geophys.Res., 80, 4581.

Hutton, R. & Oyinloye, J.O., 1970, Ann.Geophys., 26, 921.

Jacchia, L.G., 1965, Smithsonian Astrophys.Obs.Spec.Rep.NO. 184 Cambridge, Mass., USA

Jacchia, L.G., 1970, Smithsonian Astrophys.Obs.Rep.NO. 313 Cambridge, Mass., USA.

Jacchia, L.G., 1971, Smithsonian Astrophys.Obs.Rep.NO. 332 Cambridge, Mass., USA.

Jackson, J.E., 1969, Proc.IEEE, 57, 960.

Johnson, C.Y., 1969, Ann. IQSY, 5, 197.

Kane, R.P., 1973a, Scientific Report AER-73-08, PRL, Ahmedabad (PRL: Physical Research Laboratory).

Kane, R.P., 1973b, J.Atmos.Terr.Phys., 35, 1565.

Kane, R.P., 1973c, Scientific Report AER-73-01, PRL, Ahmedabad.

Kelly, M.C. & Carlson, C.W., (Abstract) EOS Trans.AGU, 55, 381.

King, J.W. et al., 1964, Proc.Roy.Soc., A281, 464.

King, J.W. & Kohl, H., 1965, Nature, 206, 699.

Klostermeyer, J., 1972, J.Atmos.Terr.Phys., 34, 1393.

Knetch, R.W. et al., 1961, J.Geophys.Res., 66, 3078.

Kohl, H. & King, J.W., 1967, J.Atmos.Terr.Phys., 29, 1045.

Krishnamurthy, B.V. & Sengupta, K., 1971, Paper presented at the Symp.on Ionosphere-Magnetosphere Interactions, New Delhi, India.

Krishnamurthy, B.V. & Sengupta, K., 1972, Planet.Space Sci., 20, 371.

* Hooke, W.H., 1968, J.Atmos.

Krishnamurthy, B.V., Raghava Reddi C.R., Subbarao, K.S.V., Raghavarao, R. &Sharma, P., 1976., J.Geophys.Res. 81, 705.

Lindzen, R.S., 1967, J.Geophys.Res., 72, 1591.

Lockwood, G.E.K. &Petrie, L., 1963, Planet.Space Sci., 11, 327.

Lockwood, G.E.K. &Nelms, G.L., 1964, J.Atmos.Terr.Phys., 26, 569.

Lyon, A.J. et al., 1958, Nature, 181, 1724.

Lyon, A.J. et al., 1960, J.Atmos.Terr.Phys., 19, 145.

Lyon, A.J. et al., 1961, J.Atmos.Terr.Phys., 21, 100.

Lyon, A.J. &Thomas, L., 1963, J.Atmos.Terr.Phys., 25, 373.

Maeda, H., 1955, Rep.Ionos.Res.Japan, 9, 59.

Mao, Fu Wu, 1970, J.Geophys.Res., 75, 5612.

Martyn, D.F., 1947, Proc.Roy.Soc., A189, 241.

Martyn, D.F., 1959, Proc.IRE, 47, 147.

Matsushita, S., 1957, J.Atmos.Terr.Phys., 10, 163.

Matsushita, S., 1969, Radio Sci., 4, 771.

Matsushita, S. &Tarpley, J.D., 1970, J.Geophys.Res., 75, 5433.

MC Clure, J.P. &Woodman, R.F., 1972, J.Geophys.Res., 77, 5617.

MC Nicol, R.W.E , 1956, Aust.J.Phys., 9, 247.

Mitra, S.K., 1946, Nature, 158, 668.

Muldrew, D.B., 1963, J.Geophys.Res., 68, 5355.

Nielson, D.L., &Crochet, M., 1974, Rev.Geophys.Space Phys. 12, 688.

Nishida, A. et al., 1966, Ann.Geophys., 22, 478.

Onwumechilli, A., 1963, J.Atmos.Terr.Phys., 25, 55.

Onwumechilli, A., 1964, J.Atmos.Terr.Phys., 26, 729.

Onwumechilli, A., 1967, in Physics of Geomagnetic Phenomena Vol.1 edited by S.Matsushita&W.H.Campbell, P.425, Academic Press, New York.

Onwumechilli, A. &Akasofu, S.I., 1972, J.Geomag.Geoelectr., 24, 161.

Patel, V.L. &Rastogi, R.G., 1974, (Abstract)EOS Trans.AGU, 55, 394.

Philbrick, C.R. & Mc Issac, J.P., 1972, Space Res., 12, 743.

Pramanik, S.K. &Hariharan, P.S., 1953, Indian J.Meteorol.Geophys., 4, 353.

Prolss, G.W. &Von Zahn, U., 1974, J.Geophys.Res., 79, 2535.

Raghavarao, R., 1976, (Review Talk) Proc. Solar Planetary Symp. held at PRL, Ahmedabad, India.

Raghavarao, R., Sharma, P, &Sivaraman, M.R., 1976a, Proc. Solar Planetary Symp. held at PRL, Ahmedabad, India.

Raghavarao, R., Sharma, P, &Sivaraman, M.R., 1976b, Paper presented at XIX COSPAR meeting, Philadelphia, USA, and submitted for publication to Space Research XVII.

Raghavarao, R., Sharma, P. &Jain, A.R., 1976c, Paper presented at XIX COSPAR meeting, Philadelphia, USA and submitted for publication to Space Research XVII.

Raghavarao, R. &Sivaraman, M.R., 1973, J. Atmos. Terr. Phys., 35, 2091.

Raghavarao, R. &Sivaraman, M.R., 1974, Nature, 249, 331.

Raghavarao, R. &Sivaraman, M.R., 1975, Space Res., 15, 385.

Rao, K.N. &Rajarao, K.S., 1963, Nature, 200, 460.

Rastogi, R.G., 1959, J. Geophys. Res., 64, 727.

Rastogi, R.G., 1961, J. Atmos. Terr. Phys., 22, 290.

Rastogi, R.G., 1962, J. Atmos. Terr. Phys., 24, 1031.

Rastogi, R.G., 1963, Proc. Indian Acad. Sci., 58, 38.

Rastogi, R.G., 1965, Z. Geophys., 31, 27.

Rastogi, R.G., 1966, J. Inst. Telecom. Engrs., 12, 245.

Rastogi, R.G., 1971, Nature Phys. Sci., 229, 240.

Rastogi, R.G., 1972, Ann. Geophys., 28, 717.

Rastogi, R.G., 1973a, Planet. Space Sci., 21, 1355.

Rastogi, R.G., 1973b, Proc. Indian Acad. Sci., 77, 130.

Rastogi, R.G., 1974a, J. Geophys. Res., 79, 1503.

Rastogi, R.G., 1974b, J. Atmos. Terr. Phys., 36, 167.

Rastogi, R.G., 1975a, Current Sci., 44, 251.

Rastogi, R.G., 1975b, Geophys. Res. Lett., 2, 142.

Rastogi, R.G., 1975c, Proc. Indian Acad. Sci., 81, 80

Rastogi, R.G., et al., 1971, Proc. Indian Acad. Sci. 74, 62.

Rastogi, R.G. &Rajaram, G., 1971, Indian J. Pure Appl. Phys., 9, 531

Ratcliff, J.A., 1956, J. Atmos. Terr. Phys., 8, 260.

Reber, C.A., 1975, (Abstract) Paper presented at XVI IUGG Gen. Assembly, Grenoble, France.

Reid, G.C., 1968, J.Geophys.Res., 73, 1627.

Rieger, E., 1974, J.Atmos.Terr.Phys., 36, 1377.

Rishbeth, H., 1966, J.Atmos.Terr.Phys., 28, 911.

Rishbeth, H., 1968, Rev.Geophys., 6, 33.

Rishbeth, H.&Barron, D.W., 1960, J.Atmos.Terr.Phys., 18, 234.

Rishbeth, H.et al., 1966, Ann.Geophys., 22, 538.

Rishbeth, H.&Garriott, O.K., 1969, Introduction to Ionospheric Physics, Academic Press, New York&London.

Rush, C.M.&Vekateswaran, S.V., 1968, J.Atmos.Terr.Phys., 30, 633.

Rush, C.M.et al., 1969, Radio Sci., 4, 829.

Rush, C.M.&Richmond, A.D., 1973, J.Atmos.Terr.Phys., 35, 1171.

Sastry, N.S., &Jayakar, R.W., 1972, Ann.Geophys., 28, 589.

Sastry, T.S.G., 1970, Space Res., 10, 778.

Sato, T., 1968, J.Geophys.Res., 73, 6225.

Satyaprakash et al., 1971, Nature Phys.Sci., 230, 170.

Satyaprakash et al., 1976, Space Res., 16, 401.

Shimazaki, T., 1959, J.Radio Res.Labs.Japan, 6, 688.

Simon, L., 1963, Phys.Fluids, 6, 382.

Singleton, D.G., 1960, J.Geophys.Res., 65, 3615.

Sivaraman, M.R., 1974, Topside ionosphere at low latitudes, Ph.D Thesis, Gujarat University, Ahmedabad, India.

Sivaraman, M.R.et al., 1976, Ind.J.Radio Space Phys. 5, 136.

Sterling, D.L.et al., 1969, Radio Sci., 4, 1005.

Sugiura, M.&Cain, J.C., 1966, J.Geophys.Res., 71, 1869.

Sugiura, M.&Fanselau, G., 1966, NASA Report X-612-66-401.

Tarpley, J.D., 1970a, Planet.Space Sci., 18, 1075.

Tarpley, J.D., 1970b, Planet.Space Sci., 18, 1091.

Tarpley, J.D., &Balsley, B.B., 1972, J.Geophys.Res., 77, 1951.

Taylor, H.A.Jr., 1971, Planet. Space Sci. 19, 77.

Titheridge, J.E., 1976, Planet.Space Sci., 24, 229.

Van Sabben, D, 1968, J.Atmos.Terr.Phys., 30, 1641.

Van Zandt, T.E.et al, 1972, Proc.IV International Symp.on Equatorial Aeronomy, Edited by Ebun Oni, P.646.

Woodman, R.F., 1970, J.Geophys.Res., 75, 6249.

Woodman, R.F., 1972, Space Res., 12, 969

Yeh, K.C. et al., 1975, Ann.Geophys., 31, 321.

Young, H.D., 1962, Statistical treatment of experimental data, MC Graw-Hill, New York.